frontiers | Research Topics

Fibrosis, inflammation, and cancers: Dangerous liaisons to be depicted and targeted

Edited by
Denisa Baci, Valentina Audrito, Manol Jovani and Antonino Bruno

Published in
Frontiers in Immunology

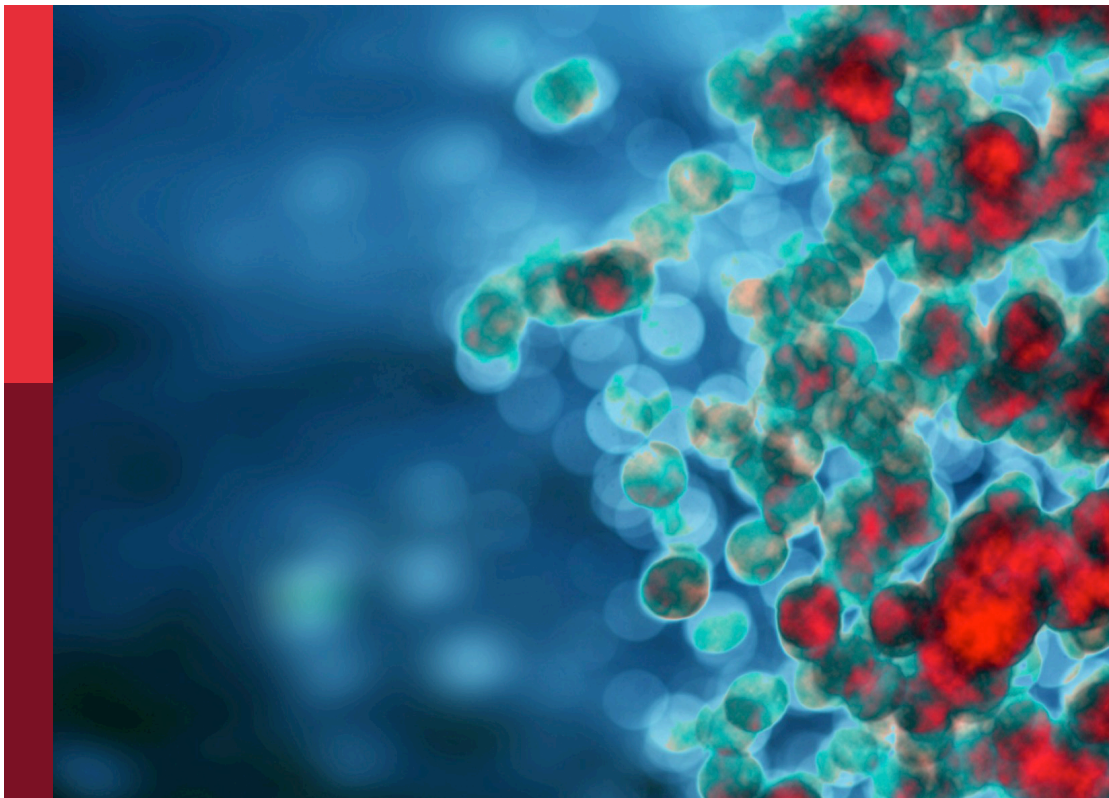

ISSN 1664-8714
ISBN 978-2-8325-3229-4
DOI 10.3389/978-2-8325-3229-4

About Frontiers

Frontiers is more than just an open access publisher of scholarly articles: it is a pioneering approach to the world of academia, radically improving the way scholarly research is managed. The grand vision of Frontiers is a world where all people have an equal opportunity to seek, share and generate knowledge. Frontiers provides immediate and permanent online open access to all its publications, but this alone is not enough to realize our grand goals.

Frontiers journal series

The Frontiers journal series is a multi-tier and interdisciplinary set of open-access, online journals, promising a paradigm shift from the current review, selection and dissemination processes in academic publishing. All Frontiers journals are driven by researchers for researchers; therefore, they constitute a service to the scholarly community. At the same time, the *Frontiers journal series* operates on a revolutionary invention, the tiered publishing system, initially addressing specific communities of scholars, and gradually climbing up to broader public understanding, thus serving the interests of the lay society, too.

Dedication to quality

Each Frontiers article is a landmark of the highest quality, thanks to genuinely collaborative interactions between authors and review editors, who include some of the world's best academicians. Research must be certified by peers before entering a stream of knowledge that may eventually reach the public - and shape society; therefore, Frontiers only applies the most rigorous and unbiased reviews. Frontiers revolutionizes research publishing by freely delivering the most outstanding research, evaluated with no bias from both the academic and social point of view. By applying the most advanced information technologies, Frontiers is catapulting scholarly publishing into a new generation.

What are Frontiers Research Topics?

Frontiers Research Topics are very popular trademarks of the *Frontiers journals series*: they are collections of at least ten articles, all centered on a particular subject. With their unique mix of varied contributions from Original Research to Review Articles, Frontiers Research Topics unify the most influential researchers, the latest key findings and historical advances in a hot research area.

Find out more on how to host your own Frontiers Research Topic or contribute to one as an author by contacting the Frontiers editorial office: frontiersin.org/about/contact

Fibrosis, inflammation, and cancers: Dangerous liaisons to be depicted and targeted

Topic editors

Denisa Baci — University of Insubria, Italy

Valentina Audrito — Dipartimento di Scienze e Innovazione Tecnologica, Università del Piemonte Orientale, Italy

Manol Jovani — Maimonides Medical Center, United States

Antonino Bruno — University of Insubria, Italy

Citation

Baci, D., Audrito, V., Jovani, M., Bruno, A., eds. (2023). *Fibrosis, inflammation, and cancers: Dangerous liaisons to be depicted and targeted*. Lausanne: Frontiers Media SA. doi: 10.3389/978-2-8325-3229-4

Table of contents

frontiers | Frontiers in Immunology

ORIGINAL RESEARCH
published: 17 May 2022
doi: 10.3389/fimmu.2022.875407

Single-Cell RNA-seq Analysis Reveals Cellular Functional Heterogeneity in Dermis Between Fibrotic and Regenerative Wound Healing Fates

Cao-Jie Chen[1], *Hiroki Kajita*[1], *Kento Takaya*[1], *Noriko Aramaki-Hattori*[1], *Shigeki Sakai*[1], *Toru Asou*[2*] and *Kazuo Kishi*[1*]

[1] Department of Plastic and Reconstructive Surgery, Keio University School of Medicine, Tokyo, Japan, [2] Department of Plastic Surgery, Tokyo Cosmetic Surgery Clinic, Tokyo, Japan

OPEN ACCESS

Edited by:
Tian Li,
Independent Researcher, Xi'an, China

Reviewed by:
Li-xin Tang,
Chongqing Public Health Medical Center, China
Zi-chao Li,
Fourth Military Medical University, China

***Correspondence:**
Kazuo Kishi
kkishi@a7.keio.jp
Toru Asou
mori@ideajapan.com

Specialty section:
This article was submitted to Cancer Immunity and Immunotherapy, a section of the journal Frontiers in Immunology

Received: 14 February 2022
Accepted: 04 April 2022
Published: 17 May 2022

Citation:
Chen C-J, Kajita H, Takaya K, Aramaki-Hattori N, Sakai S, Asou T and Kishi K (2022) Single-Cell RNA-seq Analysis Reveals Cellular Functional Heterogeneity in Dermis Between Fibrotic and Regenerative Wound Healing Fates. Front. Immunol. 13:875407. doi: 10.3389/fimmu.2022.875407

Background: Fibrotic scars are common in both human and mouse skin wounds. However, wound-induced hair neogenesis in the murine wounding models often results in regenerative repair response. Herein, we aimed to uncover cellular functional heterogeneity in dermis between fibrotic and regenerative wound healing fates.

Methods: The expression matrix of single-cell RNA sequencing (scRNA-seq) data of fibrotic and regenerative wound dermal cells was filtered, normalized, and scaled; underwent principal components analysis; and further analyzed by Uniform Manifold Approximation and Projection (UMAP) for dimension reduction with the Seurat package. Cell types were annotated, and cell–cell communications were analyzed. The core cell population myofibroblast was identified and the biological functions of ligand and receptor genes between myofibroblast and macrophage were evaluated. Specific genes between fibrotic and regenerative myofibroblast and macrophage were identified. Temporal dynamics of myofibroblast and macrophage were reconstructed with the Monocle tool.

Results: Across dermal cells, there were six cell types, namely, EN1-negative myofibroblasts, EN1-positive myofibroblasts, hematopoietic cells, macrophages, pericytes, and endothelial cells. Ligand and receptor genes between myofibroblasts and macrophages mainly modulated cell proliferation and migration, tube development, and the TGF-β pathway. Specific genes that were differentially expressed in fibrotic compared to regenerative myofibroblasts or macrophages were separately identified. Specific genes between fibrotic and regenerative myofibroblasts were involved in the mRNA metabolic process and organelle organization. Specific genes between fibrotic and regenerative macrophages participated in regulating immunity and phagocytosis. We then observed the underlying evolution of myofibroblasts or macrophages.

Conclusion: Collectively, our findings reveal that myofibroblasts and macrophages may alter the skin wound healing fate through modulating critical signaling pathways.

Keywords: skin wound healing, fibrosis, regeneration, myofibroblast, macrophage, single-cell RNA sequencing

INTRODUCTION

The skin is the organ with the largest surface area in the human body that provides an efficient protective barrier against mechanical injury, microbial pathogens, and trauma (1). The skin's immune system is divided into two structural compartments: epidermis and dermis, both of which contain a plethora of immunocompetent cell types (2). The epidermis is home to the main skin-resident immune cells, Langerhans cells, and melanocytes. Meanwhile, immune-specialized cells like dendritic cells, macrophages, and T cells reside in the dermis (3). The communications within immune populations and the skin environment are critical to the effectiveness of the skin immune system (4). Wound healing is a complex process in the human body, where numerous cell populations with different functions are involved in the stages of hemostasis, inflammatory response, growth, re-epithelialization, and remodeling (5). It is essential to repair the skin after damage (6). Skin wound healing involves three primary phases: inflammation, re-epithelialization, and tissue remodeling (7). Nevertheless, effective therapeutic strategies of accelerating healing and decreasing scarring remain lacking. Single-cell RNA sequencing (scRNA-seq) technology has emerged as an indispensable tool for elucidating cellular phenotype and functional heterogeneity (8). Deciphering the role of each cell type and interactions within cells is of importance to understand the mechanism of normal wound closure (9). Alterations in the microenvironment may influence cellular recruitment or activation, resulting in damaged states of wound healing. ScRNA-seq can be applied for deciphering the cellular changes in chronic wounds and hypertrophic scarring, thereby promoting the development of more effective therapeutic solutions for healing wounds (10). Moreover, in-depth understanding of the differences between fibrotic and regenerative wound healing fates is a prerequisite for developing more effective therapeutic interventions (2). Here, the purpose of this study was to reveal cellular functional heterogeneity in the dermis between fibrotic and regenerative wound healing fates.

MATERIALS AND METHODS

Acquisition of scRNA-seq Profiles

10× genomics scRNA-seq data of regenerative [GSM4213633; large full-thickness excision (1 cm^2) allows *de novo* follicle regeneration] and fibrotic (GSM4213632; large wounds lead to hairless scars) wound-induced hair neogenesis (WIHN) wounds of adult 6- or 7-week-old C57Bl/6j mice were curated from the Gene Expression Omnibus (GEO) repository (https://www.ncbi.nlm.nih.gov/gds/). The accession number was GSE141814 (11). Regenerative wounds were defined as hair neogenesis, decreased contraction, decreased Wnt and TGF-β signaling activity, and decreased collagen production, while fibrotic wounds were defined as decreased hair neogenesis, increased contraction, increased Wnt and TGF-β signaling activity, and increased collagen production. This dataset was based on the platform of GPL21103 Illumina HiSeq 4000 (*Mus musculus*).

Quality Control

The DropletUtils package (v 3.13) was adopted to read unique molecular identifiers (UMI) count matrix, identify cells from empty droplets, remove barcode-swapped pseudo-cells, and downsample the count matrix (12). The calculateQCMetrics function of the Scater package was used for counting the expression of genes in cells (13). Cells with proportions of mitochondrial genes ≤ 10% and ribosomal genes ≥ 10% were determined for further analysis.

Data Preprocessing and Principal Component Analysis

The expression matrix was normalized with the NormalizeData function of the Seurat package (14). The top 2,000 highly variable genes were screened by the FindVariableFeatures function. Then, expression data were linearly scaled utilizing the ScaleData function. Finally, principal component analysis (PCA) was performed with the RunPCA function based on the 2,000 genes.

Cell Cluster and Annotation

The principal components with large standard deviations were selected. Then, cell clustering analysis was performed using the FindNeighbors and FindClusters function of the Seurat package. With the RunUMAP function, Uniform Manifold Approximation and Projection (UMAP) was carried out for dimension reduction. Cell types were annotated on the basis of the known marker genes.

Identification of Novel Marker Genes

To calculate the differentially expressed genes between each cluster and all other cells, the FindAllMarkers function of the Seurat package was used and novel marker genes were identified according to the following criteria: |log fold change (FC)| ≥ 0.1, the minimum expression ratio of cell population = 0.25, and p-value ≤ 0.05.

Ligand–Receptor Network Analysis

Based on the ligand–receptor pairs from the previous literature (15), the relationship pairs of receptors and ligands were analyzed based on the marker genes of various cells. Then, a cell–cell communication network was conducted and visualized with the Cytoscape software (16). The core cell population was identified according to the largest number of receptor–ligand pairs in the network. Moreover, the receptor and ligand genes were extracted.

Function Enrichment Analysis

Function enrichment analysis of the indicated genes was carried out utilizing the clusterProfiler package, including Gene Ontology (GO) and Kyoto Encyclopedia of Genes and Genomes (KEGG) pathway analysis (17). GO categories contain biological process, cellular component, and molecular function. Terms with $p < 0.05$ were considered significantly enriched.

Protein–Protein Interaction Analysis

The Search Tool for the Retrieval of Interacting Genes (STRING) database (version 11.0; https://string-db.org/) was utilized for

exploring the functional interactions between marker gene-encoded proteins (18). Then, PPI networks were constructed and the top 20 hub genes were identified.

Pseudotime Analysis

Pseudotime analysis was carried out with the Monocle 3 tool (19). Firstly, genes that were expressed in at least 5% of the cells were selected. Then, the reduceDimension function was utilized to perform dimensionality reduction analysis, followed by cell cluster with the clusterCells function. Afterwards, the differentialGeneTest function was adopted to determine candidate genes with differences between the clusters with $p < 0.05$. The dimensionality reduction analysis of the cells was carried out using the DDRTree approach and the reduceDimension function based on the candidate genes. Through the orderCells function, the cells along the quasi-chronological trajectory were sorted and visualized.

Gene Set Variation Analysis

The single-sample gene set enrichment analysis (ssGSEA) function of the Gene Set Variation Analysis (GSVA) package was utilized for comparisons of the differences in GO and KEGG terms between groups (20).

Isolation and Culture of Fibroblasts

C57BL/6 male mice (8–10 weeks old; Sankyo) were used for fibroblast isolation. Briefly, mice were sacrificed by cervical dislocation. The trunk skin was separated in the ultra-clean bench, immersed in 75% ethanol for disinfection, and then cut into small pieces. Blood was removed by rinsing with PBS buffer and transferred evenly to cell culture dishes. DMEM complete medium (Wako) was added to submerge the tissue block that was placed in a constant temperature incubator to fully cultivate. After 24 h, DMEM complete medium was added, which was replaced every 3 days. The mouse skin fibroblasts were purified by the differential adhesion method and were used for subsequent experiments. Our study was approved by the Animal Ethics Committee of Keio University School of Medicine [12090(5)].

Transfection

Using the TransIT-TKO Transfection Reagent (Mirus), siRNA-Engrailed-1 (horizon) and siRNA-control were transfected into fibroblasts in a constant-temperature incubator. Forty-eight hours later, the knockdown effect of siRNA was confirmed by real-time quantitative polymerase-chain reaction (RT-qPCR).

RT-qPCR

Total RNA was extracted from fibroblasts using the Isogen reagent (Nippon Gene) following the manufacturer's instructions. cDNA synthesis was achieved based on the cDNA Synthesis System (Bio-Rad). RT-qPCR was carried out utilizing SYBR Qpcr Mix (Toyobo) on a 7500 Real-Time PCR system (Applied Biosystems). The primer sequences were as follows: EN1, 5'-ACACAACCCTGCGATCC TACT-3'(forward) and 5'-GGACGGTCCGAATAGCGTG-3' (reverse); ACTB, 5'-GGC TGTATTCCCCTCCATCG-3'(forward) and 5'-CCAGTTGGTAACAATGCCATGT-3' (reverse). The relative expressions were calculated with the $2^{-\Delta\Delta Ct}$ method.

Wound Healing Assay

Fibroblasts were plated onto a 6-well plate (about 3×10^5 cells/well). When the confluence reached 100%, the fibroblast monolayer was scratched with a 1000-μl pipette tip. Additionally, detached fibroblasts were removed with serum-free medium. At 0 h and 24 h, the wounded area was photographed.

Statistical Analysis

All statistical analysis was performed using the R language (version 3.6.1) and R Bioconductor packages. $p < 0.05$ indicated statistical significance.

RESULTS

Quality Control of scRNA-seq Data of Fibrotic and Regenerative Wound Dermal Cells

Herein, we collected scRNA data of dermal cells from large skin wounds on day 18 with two distinct healing fates (fibrosis: GSM4213632 or regeneration: GSM4213633) from the GSE141814 dataset. Before analysis, we presented quality control of scRNA data. Barcode rank plots separately depicted the distribution of barcodes in total UMI count for fibrotic and regenerative wound dermal cells (**Supplementary Figures 1A, B**). Knee and inflection points in the barcode rank plots indicated the transition of the total UMI count distribution, which reflected the difference between empty droplets and cell droplets. After filtrating empty droplets, we counted the expression of genes in each cell (**Supplementary Figures 1C, D**). Afterwards, we filtrated out cells with proportions of mitochondrial genes > 10% and ribosomal genes < 10% (**Supplementary Figures 1E, F**).

Cell Cluster of Fibrotic and Regenerative Wound Dermal Cells

After normalizing scRNA data, we screened the top 2,000 highly variable genes across fibrotic and regenerative wound dermal cells (**Figure 1A**). Then, scRNA data were linearly scaled and analyzed by dimensionality reduction with PCA. Here, we screened the top two principal components for subsequent analysis (**Figure 1B**). PCA results uncovered the prominent difference between fibrotic and regenerative wound dermal cells (**Figure 1C**). According to the elbow point, we identified the optimal principal components as 8 (**Figure 1D**). Heatmaps depicted the top 20 marker genes in each principal component (**Figure 1E**). With the UMAP method, dermal cells were clustered into 15 clusters (**Figure 1F**). The top ten marker genes of each cell cluster are presented in **Figure 1G**.

Identification of Cell Types and Their Marker Genes Across Fibrotic and Regenerative Wound Dermal Cells

This study attempted to identify cell types across fibrotic and regenerative wound dermal cells. Based on the known marker genes, six cell types were annotated, as follows: EN1-negative

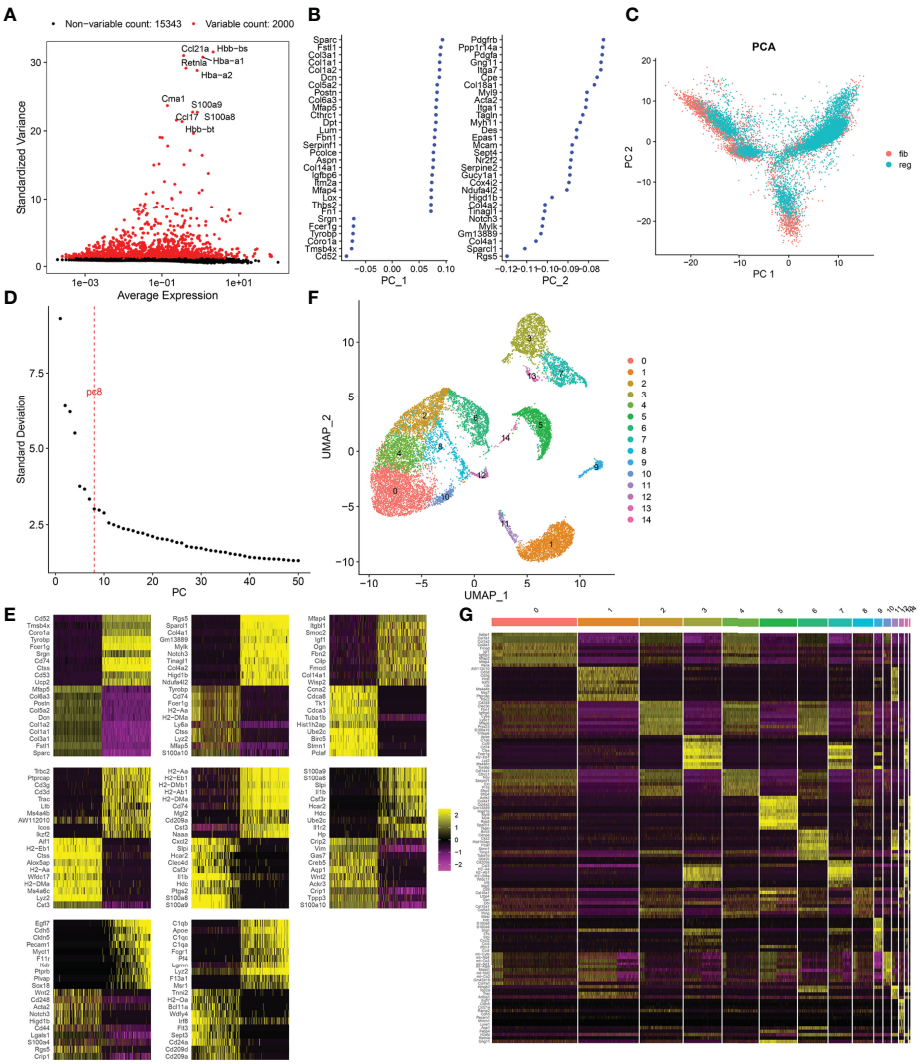

FIGURE 1 | Cell cluster of fibrotic and regenerative wound dermal cells. **(A)** The top 2,000 highly variable genes across fibrotic and regenerative wound dermal cells according to standard deviation. Red dots meant highly variable genes. The top ten highly variable genes were marked. **(B)** Two of the most principal components according to standard deviation. **(C)** PCA plots of wound dermal cells between fibrotic (fib) and regenerative (reg) conditions. Reference atlas was colored by tissue of origin (fibrotic and regenerative wounds). **(D)** Determination of the optimal principal components through elbow plot. **(E)** Heatmaps showing the top 20 marker genes in each principal component. **(F)** Cell cluster based on the screened principal components. **(G)** Heatmap showing the expression patterns of the top ten marker genes in each cell cluster.

myofibroblasts (n = 6,392), EN1-positive myofibroblasts (n = 2,219), hematopoietic cells (n = 3,774), macrophages (n = 1,461), pericytes (n = 1,493), and endothelial cells (n = 303; **Figure 2A**). **Table 1** lists the cell ratio of each cell type. In particular, we noticed the differences in ratios of EN1-negative and -positive myofibroblasts between fibrotic and regenerative wound dermal cells (**Figure 2B**). With $|\log FC| \geq 0.1$, the minimum expression ratio of cell population = 0.25, and p-value ≤ 0.05, we identified novel marker genes in each cell type (**Supplementary Table 1**). The top ten marker genes in each cell type were visualized, as follows: EN1-negative myofibroblasts (Aebp1, Col1a1, Col1a2, Col3a1, Col8a1, Dcn, Eln, Mfap2, Mfap4, and Sparc), hematopoietic cells (AW112010, Cd3d, Cd3g, Cd52, Hcst, Ltb, Ptprcap, Rac2, Srgn, and Trbc2), macrophages (Apoe, C1qb, Ccl9, Cd74, Ctss, Fcer1g, H2-Eb1, Lyz2, Ms4a6c, and Tyrobp), pericytes (Acta2, Col4a1, Col4a2, Gm13889, Higd1b, Myl9, Mylk, Rgs5, Sparcl1, and Tagln), EN1-positive myofibroblasts (Birc5, Pclaf, Stnm1, Ube2c, Hist1h2ap, Col5a3, Cks2, Aqp1, Tnfaip6, and Timp1), and endothelia cells (Egfl7, Cldn5, Cdh5, Ramp2, Ecscr, Pecam1, Cd200, Ltbp4, Aqp1, and Hist1h2ap) (**Figure 2C**). Furthermore, we detected the expression levels of the known marker genes that were used for annotating cell types, as follows: endothelial cells (Cldn5, Pecam1, and Cd74), EN1-negative and -positive myofibroblasts (En1, Col1a1, Dcn, Sfrp4,

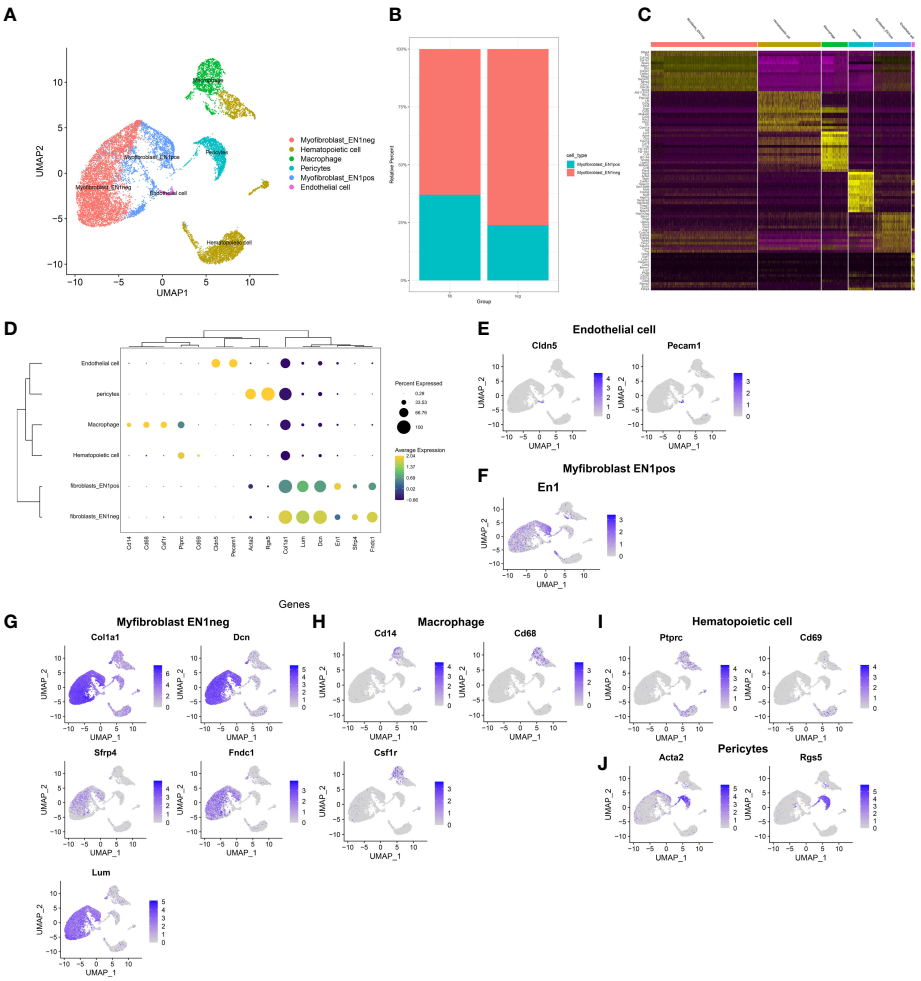

FIGURE 2 | Identification of cell types and their marker genes across fibrotic and regenerative wound dermal cells. **(A)** UMAP plots showing cell types identified by marker genes. Each cell type was colored by a unique color. **(B)** The cell ratio of EN1-negative and -positive myofibroblasts among fibrotic and regenerative wound dermal cells. **(C)** Heatmap visualizing cell-type-specific gene expression patterns. Each column represented the average expression after cells were grouped. **(D)** Integrated analysis showing marker genes across cell types. The size of each circle reflected the percentage of cells in each cell type where the gene was detected, and the color shadow reflected the average expression level within each cell type. **(E–J)** UMAP plots of expression of the marker genes for endothelial cells, EN1-negative and -positive myofibroblasts, macrophages, hematopoietic cells, and pericytes.

TABLE 1 | Cell ratio of each cell type.

Cell type	Group	Count	Total	Ratio
Endothelial cell	Fibrotic	76	5,130	0.014815
Endothelial cell	Regenerative	112	10,512	0.010654
EN1-negative myofibroblasts	Fibrotic	772	5,130	0.150487
EN1-negative myofibroblasts	Regenerative	5,620	10,512	0.534627
EN1-positive myofibroblasts	Fibrotic	454	5,130	0.088499
EN1-positive myofibroblasts	Regenerative	1,765	10,512	0.167903
Hematopoietic cell	Fibrotic	2,439	5,130	0.475439
Hematopoietic cell	Regenerative	1,335	10,512	0.126998
Macrophage	Fibrotic	725	5,130	0.141326
Macrophage	Regenerative	851	10,512	0.080955
Pericytes	Fibrotic	664	5,130	0.129435
Pericytes	Regenerative	829	10,512	0.078862

Fndc1, and Lum), macrophages (Cd14, Cd68, and Csf1r), and hematopoietic cells (Ptprc, Cd69, Acta2, and Rgs5) (**Figures 2D–J**).

Cell–Cell Interactions Based on Ligand–Receptor Interactions

Wound healing is a complex process that necessitates the collaborative efforts of diverse cell lineages (21). Cell-to-cell communications across diverse cell types thoroughly govern appropriate functions of metazoans as well as widely rely on interactions between secreted ligands and cell-surface receptors. Based on the marker genes, ligand–receptor interactions were matched. The number of ligands/receptors for myofibroblasts, pericytes, endothelial cells, macrophages, and hematopoietic cells was 114, 91, 32, 28 and 17, respectively (**Figure 3A**). According to the number of intercellular receptor–ligand pairs, we screened out myofibroblasts as the core cell population.

Biological Functions of Ligand and Receptor Genes Between Myofibroblasts and Macrophages

We further evaluated the biological functions of ligand and receptor genes between myofibroblasts and macrophages. Our results demonstrated that ligand and receptor genes between myofibroblasts and macrophages were mainly involved in tube morphogenesis and development, regulation of cell migration, and motility (**Figure 3B**). Moreover, we found that the TGF-β signaling pathway was markedly enriched by these

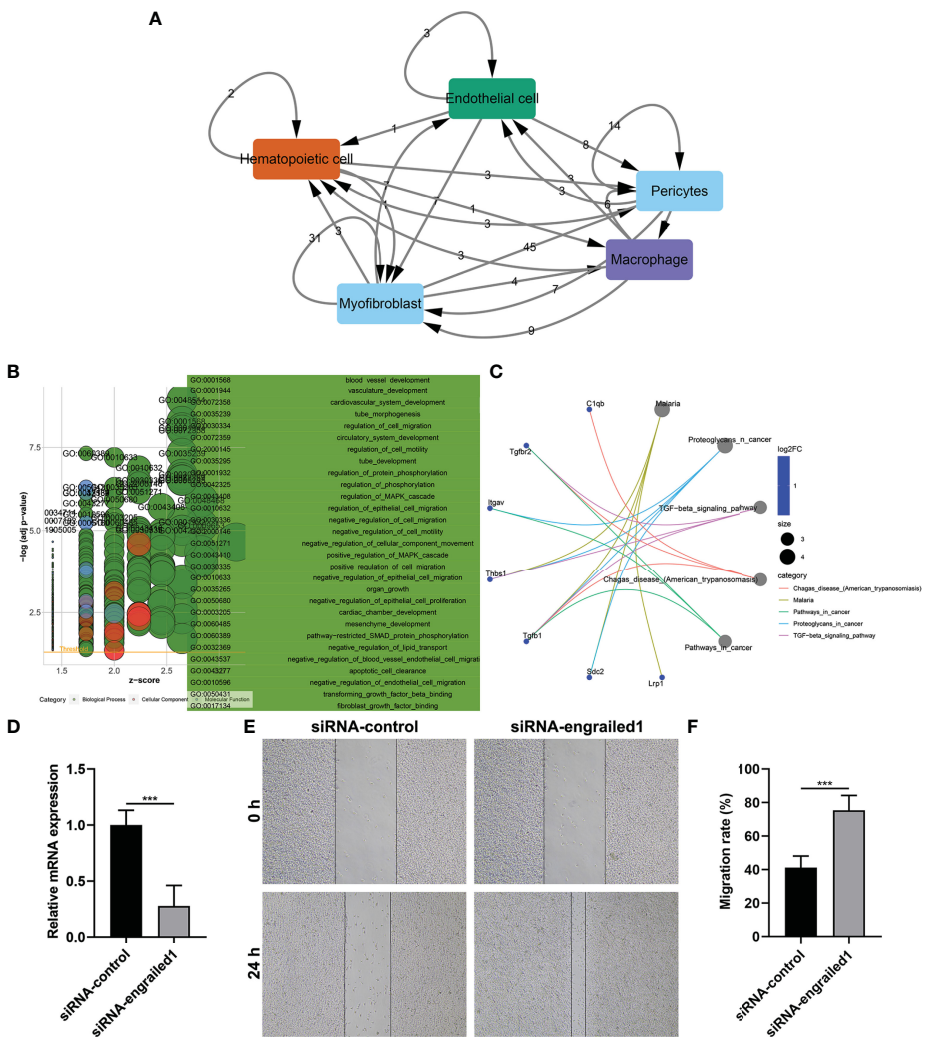

FIGURE 3 | Cell–cell interactions and biological functions of ligand and receptor genes between myofibroblasts and macrophages. **(A)** The network of ligand–receptor-mediated multicellular signaling. The arrow pointed to the recipient cell, and the number on the line indicated the number of receptor–ligand pairs. **(B)** GO enrichment results of ligand and receptor genes between myofibroblasts and macrophages. **(C)** KEGG pathways enriched by ligand and receptor genes between myofibroblasts and macrophages. **(D)** RT-qPCR for the mRNA expressions of EN1 in fibroblasts transfected with siRNA of EN1. **(E, F)** Wound healing assay for the migration of EN1-knockdown fibroblasts. Bar, 20 μm. ***$p < 0.001$.

ligand and receptor genes between myofibroblasts and macrophages (**Figure 3C**).

Knockdown of EN1 Facilitates Fibroblast Migration

We further verified the effects of EN1 on the migration of fibroblasts. Firstly, siRNA against EN1 was designed and transected into fibroblasts. RT-qPCR demonstrated that EN1 mRNA expression was distinctly reduced following siRNA-EN1 transfection (**Figure 3D**). According to wound healing results, EN1-knockout fibroblasts displayed significantly enhanced migration capacity (**Figures 3E, F**). Hence, EN1 suppression enabled to facilitate fibroblast migration.

Identification of Specific Genes Between Fibrotic and Regenerative Myofibroblasts and Their Biological Functions

With the cutoffs of |FC| > 1.2 and $p < 0.05$, we identified 546 up- and 481 downregulated specific genes in regenerative compared to fibrotic myofibroblasts (**Figures 4A–C**). **Table 2** lists the first 20 up- and downregulated specific genes between regenerative and fibrotic myofibroblasts. As depicted in **Figure 4D**, we observed that the specific genes markedly participated in collagen-containing extracellular matrix, posttranscriptional regulation of gene expression, positive regulation of cell migration, mRNA metabolic process, and apoptotic signaling pathway. Moreover, ribosome and thermogenesis were prominently enriched by the specific genes (**Figure 4E**).

Identification of Specific Genes Between Fibrotic and Regenerative Macrophages and Their Biological Functions

With the cutoffs of |FC| > 1.2 and $p < 0.05$, we found that 100 specific genes were significantly upregulated while 197 specific genes were significantly downregulated in regenerative compared to fibrotic macrophages (**Figures 5A–C**). **Table 3** lists the first 20 up- and downregulated specific genes between fibrotic and regenerative macrophages. GO enrichment analysis uncovered that the specific genes were markedly involved in the negative regulation of programmed cell death, the regulation of cell migration, innate immune response and apoptotic signaling pathway, collagen-containing extracellular matrix, the positive regulation of T cell activation, and response to interferon γ (**Figure 5D**). Moreover, we observed that antigen processing and presentation, pathways in cancer, phagosome, ribosome, and tuberculosis were prominently enriched by the specific genes (**Figure 5E**).

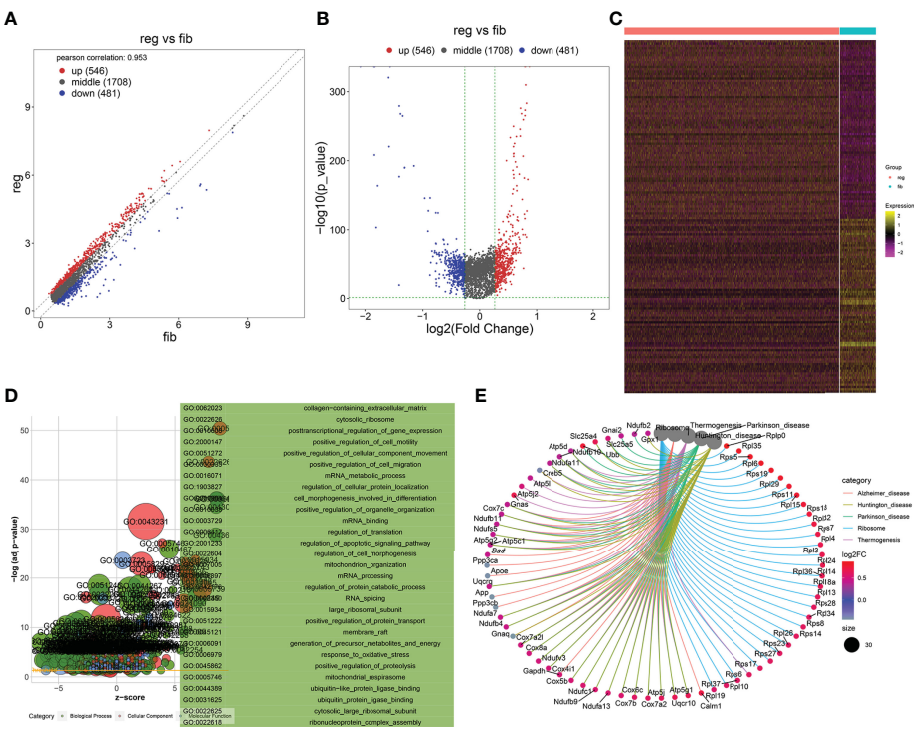

FIGURE 4 | Identification of specific genes between fibrotic and regenerative myofibroblasts and their biological functions. **(A, B)** Scatter plots and volcano diagram for the up- and downregulated specific genes in regenerative (reg) compared to fibrotic (fib) myofibroblasts. Red dots meant upregulated genes while blue dots meant downregulated genes. **(C)** Heatmap visualizing the expression patterns of the specific genes in fibrotic and regenerative myofibroblasts. Yellow represented upregulation and purple represented downregulation. **(D)** GO enrichment results of specific genes that were abnormally expressed between fibrotic and regenerative myofibroblasts. **(E)** KEGG pathways involved in specific genes that were abnormally expressed between fibrotic and regenerative myofibroblasts.

TABLE 2 | The first 20 up- and downregulated specific genes between fibrotic and regenerative myofibroblasts.

Gene	log2FC	*p*-value	*Q*-value	Regenerative	Fibrotic
Rplp0	0.870992	0	0	5.166991	4.295999
Ifitm2	0.843781	1.12E−173	1.94E−169	3.837826	2.994046
Mfap5	0.826158	5.93E−128	1.03E−123	4.591184	3.765026
Lgals1	0.820706	4.86E−284	8.43E−280	6.19352	5.372813
Hist1h2bc	0.81979	4.50E−90	7.81E−86	2.042755	1.222965
Serf2	0.805752	1.37E−310	2.39E−306	4.973459	4.167707
Rpl35	0.801322	0	0	5.164454	4.363133
Rps5	0.795055	5.07E−274	8.79E−270	4.725084	3.930029
Basp1	0.794315	1.55E−93	2.69E−89	2.268422	1.474106
Rpl6	0.792999	4.84E−266	8.40E−262	4.489802	3.696803
Ybx1	0.791379	6.39E−117	1.11E−112	2.98192	2.19054
Rps19	0.790084	0	0	5.198609	4.408525
Ost4	0.782118	2.55E−123	4.42E−119	3.079057	2.296939
Rpl29	0.780779	1.14E−175	1.98E−171	3.875578	3.094799
H19	0.767949	8.58E−45	1.49E−40	3.185378	2.417429
Rps11	0.763653	3.10E−260	5.37E−256	4.655295	3.891641
Rpl15	0.760256	2.28E−207	3.96E−203	4.262648	3.502392
Ift20	0.758	1.47E−93	2.55E−89	2.397842	1.639842
Ssr4	0.745387	2.11E−101	3.67E−97	2.89302	2.147633
Ubb	0.744921	1.14E−144	1.97E−140	4.529784	3.784862
mt-Nd4l	−2.08112	0	0	0.883721	2.964844
mt-Atp6	−1.85976	0	0	5.349053	7.20881
Hspa1b	−1.85125	4.49E−209	7.79E−205	0.611879	2.463132
mt-Co2	−1.84169	0	0	4.106449	5.948142
AC160336.1	−1.81875	4.98E−104	8.63E−100	0.763221	2.58197
Hspa1a	−1.79337	2.08E−164	3.61E−160	1.385872	3.179244
mt-Nd4	−1.60147	3.51E−321	6.08E−317	3.543676	5.145146
mt-Nd5	−1.59322	2.78E−221	4.83E−217	1.144946	2.738165
mt-Cytb	−1.57454	0	0	4.565919	6.140456
Igfbp2	−1.4162	1.28E−20	2.21E−16	2.045862	3.462061
mt-Nd3	−1.41514	1.13E−177	1.96E−173	1.403288	2.818428
mt-Nd1	−1.4142	4.61E−280	8.00E−276	4.509633	5.923829
mt-Co3	−1.39259	1.24E−268	2.15E−264	5.529273	6.921861
mt-Co1	−1.35374	1.30E−265	2.26E−261	5.598606	6.952347
mt-Nd2	−1.32088	1.81E−190	3.14E−186	2.765453	4.086338
Gm26917	−1.31863	7.03E−191	1.22E−186	0.653702	1.972335
Cd74	−1.15624	2.79E−193	4.84E−189	0.624805	1.781046
Lars2	−0.96874	2.21E−146	3.83E−142	0.232192	1.200933
Luc7l2	−0.91132	1.16E−98	2.01E−94	1.18695	2.098275
Hspg2	−0.90368	3.60E−128	6.24E−124	2.381196	3.284878

PPI Network Analysis of Specific Genes Between Fibrotic and Regenerative Myofibroblasts or Macrophages

With the STRING tool, we probed the interactions between myofibroblast- or macrophage-specific gene-encoded proteins. In **Figure 6A**, there were 616 nodes in the PPI network of myofibroblasts, reflecting the close interactions of myofibroblast-specific gene-encoded proteins. According to degree, the top 20 nodes were identified as hub genes, including Rps27a, Rps11, Rps23, Rps3, Rps5, Rps15a, Rps6, Rps9, Rps13, Rps14, Rps25, Rps3a1, Rps27, Rps8, Rps19, Rps28, Rps7, Rpl8, Rps18, Rpl26, Rpl32, and Rps16, indicating that the above genes were the core of the network. **Figure 6B** depicts the interactions between macrophage-specific gene-encoded proteins. The 20 hub genes were as follows: Uba52, Rps9, Gnb2l1, Rpl27, Rpl38, Rps13, Rps15a, Fau, Rpl18, Rpl30, Rpl35a, Rpl7, Rplp2, Rps24, Rpl13a, Rpl4, Rps10, Rps12, Rps27rt, and Rps2. The above genes deserve in-depth explorations.

Reconstruction of the Temporal Dynamics of Myofibroblast and Macrophage

To investigate the underlying evolution among myofibroblasts and macrophages, this study adopted the Monocle tool to reveal a pseudotemporal ordering for the similarity of cell clusters with developmental lineages. For myofibroblasts, the results clearly demonstrated the uniform development of myofibroblasts from cluster 6 to cluster 10 (**Figure 7A**). The trends of pseudotime-dependent genes along the pseudo-timeline were divided into six cell clusters of myofibroblasts with diverse expression dynamics. Furthermore, we observed that macrophage under fibrotic conditions was in the beginning position of the differentiation process and was sequentially transformed into macrophage under regenerative conditions (**Figure 7B**).

GSVA Between Clusters 6 and 10 of Fibrotic and Regenerative Myofibroblasts

According to the results of pseudotime analysis of myofibroblasts, we carried out GSVA between the initially differentiated cluster 6

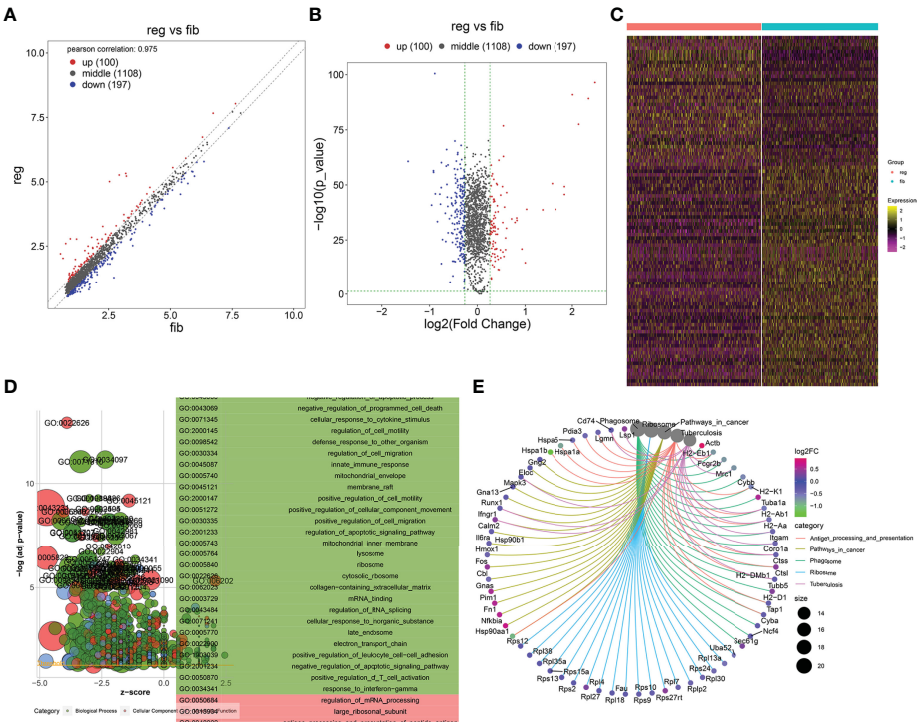

FIGURE 5 | Identification of specific genes between fibrotic and regenerative macrophages and their biological functions. **(A, B)** Scatter plots and volcano diagram showing the up- and downregulated specific genes in regenerative (reg) compared to fibrotic (fib) macrophages. Red dots meant upregulated genes while blue dots meant downregulated genes. **(C)** Heatmap visualizing the expression patterns of the specific genes in fibrotic and regenerative macrophages. Yellow represented upregulation and purple represented downregulation. **(D)** GO enrichment results of specific genes that were abnormally expressed between fibrotic and regenerative macrophages. **(E)** KEGG pathways involved in specific genes that were abnormally expressed between fibrotic and regenerative macrophages.

and the final differentiated cluster 10. Compared with cluster 10 of myofibroblasts in fibrotic and regenerative dermal cells, biological processes such as the metabolic process significantly activated cluster 6 of myofibroblasts in fibrotic and regenerative dermal cells (**Figure 8A**). As depicted in **Figure 8B**, we noticed the prominent activation of cellular components such as mitochondria in cluster 6 of fibrotic and regenerative myofibroblasts in comparison to those in cluster 10. Moreover, we observed that fibrotic and regenerative myofibroblasts in cluster 6 had significantly activated molecular functions like oxidoreductase activity compared with fibrotic and regenerative myofibroblasts in cluster 10 (**Figure 8C**). We also compared the differences in KEGG pathways between clusters. Diverse signaling pathways like metabolic pathways, RNA transport, spliceosome, thermogenesis, oxidative phosphorylation, carbon metabolism, ribosome, cell cycle, protein processing in the endoplasmic reticulum, and biosynthesis of amino acids were prominently activated in fibrotic and regenerative myofibroblasts in cluster 6 compared to those in cluster 10 (**Figure 8D**).

GSVA Between Fibrotic and Regenerative Macrophages

GSVA was also presented between fibrotic and regenerative macrophages. In **Figure 9A**, we determined that biological processes such as the metabolic process and immune response were markedly activated in fibrotic macrophages compared to regenerative macrophages. The significantly activated cellular components such as the spliceosomal complex, catalytic complex, ribonucleoprotein complex, nuclear lumen, nucleoplasm, nucleolus, cytosol, nucleus, catalytic step 2 spliceosome, chromosome, and protein-containing complex were found in fibrotic macrophages compared with regenerative macrophages (**Figure 9B**). As shown in **Figure 9C**, we investigated the marked activation of molecular functions like RNA binding, ATP binding, mRNA binding, adenyl ribonucleotide binding, adenyl nucleotide binding, drug binding, nucleic acid binding, heterocyclic compound binding, organic cyclic compound binding, and ATPase activity in fibrotic macrophages in comparison to regenerative macrophages. Moreover, our results showed that KEGG pathways such as spliceosome, NOD-like receptor signaling pathway, Fc gamma R-mediated phagocytosis, antigen processing and presentation, endocytosis, necroptosis, and natural killer cell-mediated cytotoxicity displayed marked activation in fibrotic macrophages compared to regenerative macrophages (**Figure 9D**).

DISCUSSION

Skin wound healing involves complicated coordinated interactions within cells. Through scRNA-seq data, this study identified six cell

TABLE 3 | The first 20 up- and downregulated specific genes between fibrotic and regenerative macrophages.

Gene name	log2FC	*p*-value	*Q*-value	Regenerative	Fibrotic
Sparc	2.474022	3.60E–97	6.24E–93	5.010571	2.536548
Col1a1	2.33817	6.49E–90	1.13E–85	5.266303	2.928133
Col1a2	2.13485	3.01E–78	5.21E–74	5.327119	3.192269
Col3a1	2.005563	1.16E–91	2.01E–87	5.223726	3.218163
Dcn	1.836106	2.30E–46	3.98E–42	2.785851	0.949745
Bgn	1.83586	5.99E–50	1.04E–45	2.600128	0.764269
Fstl1	1.648779	1.28E–39	2.22E–35	2.200177	0.551399
Postn	1.572566	2.54E–51	4.40E–47	2.775437	1.202871
Mfap5	1.370976	2.18E–39	3.79E–35	2.023966	0.65299
Hbb-bs	1.031846	1.21E–39	2.10E–35	2.844128	1.812282
Cxcl2	1.004274	2.60E–15	4.51E–11	3.268016	2.263742
Actb	0.934603	1.46E–21	2.53E–17	7.663418	6.728815
Klf2	0.828223	1.34E–34	2.33E–30	2.497856	1.669632
Timp2	0.824526	1.09E–35	1.89E–31	1.978589	1.154062
Neat1	0.789153	1.13E–33	1.96E–29	2.328203	1.53905
Nfkbia	0.718421	2.88E–35	4.99E–31	2.761737	2.043317
Lgals1	0.61418	3.23E–47	5.60E–43	4.783109	4.168928
Fn1	0.610899	5.21E–31	9.03E–27	3.726565	3.115666
Pim1	0.59329	1.34E–26	2.32E–22	2.966403	2.373113
Cd63	0.592092	2.84E–21	4.92E–17	2.447508	1.855417
Hspa1b	–1.44863	2.08E–61	3.60E–57	1.266466	2.715092
Hsp90aa1	–0.957	1.59E–41	2.76E–37	2.518111	3.475109
Gm26917	–0.91834	3.81E–57	6.61E–53	0.782974	1.701314
Gm42418	–0.91626	1.85E–56	3.20E–52	1.082872	1.999131
Tpt1	–0.89005	3.21E–101	5.57E–97	4.517284	5.40733
mt-Nd5	–0.87923	1.13E–46	1.96E–42	0.858755	1.737986
Hspa1a	–0.83491	4.80E–34	8.32E–30	3.320621	4.155527
mt-Co2	–0.78506	1.59E–46	2.76E–42	3.967573	4.752638
mt-Atp6	–0.77046	5.82E–42	1.01E–37	4.934988	5.70545
Mycbp2	–0.75645	1.65E–49	2.86E–45	0.967289	1.723739
H2-Eb1	–0.75235	6.73E–15	1.17E–10	5.220528	5.972878
Fcgr2b	–0.75221	7.44E–61	1.29E–56	1.801335	2.553547
Mrc1	–0.72837	6.62E–26	1.15E–21	1.012111	1.740482
mt-Nd4l	–0.67023	7.15E–38	1.24E–33	0.682842	1.35307
AC160336.1	–0.65981	5.00E–25	8.66E–21	1.805651	2.465465
Prkcd	–0.6507	2.95E–59	5.12E–55	1.387319	2.038016
Cybb	–0.64225	8.79E–67	1.52E–62	1.99459	2.636836
Tgfbi	–0.63629	6.10E–51	1.06E–46	2.746255	3.382547
H2-K1	–0.62809	3.72E–45	6.44E–41	2.787025	3.415118
Ier5	–0.61724	5.52E–41	9.58E–37	2.037704	2.654947

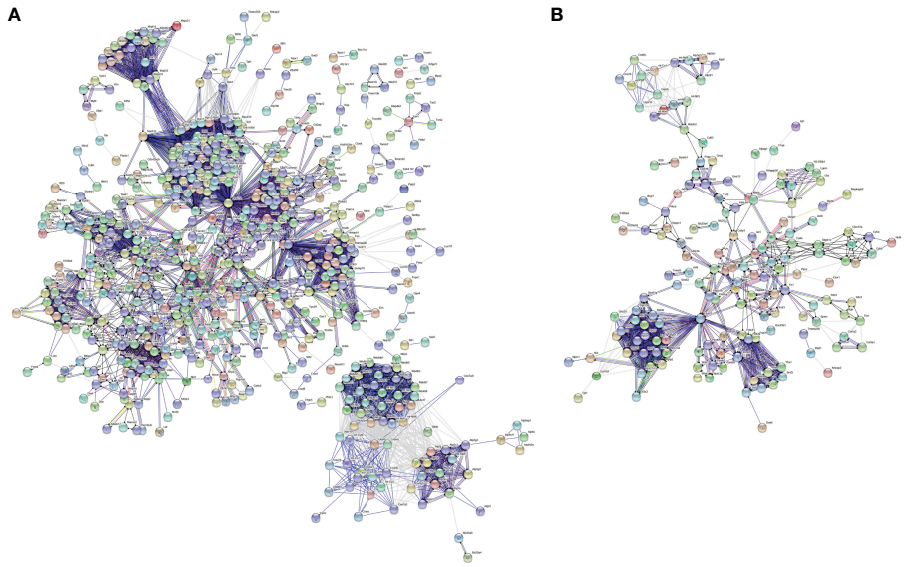

FIGURE 6 | PPI network analysis of specific genes between fibrotic and regenerative myofibroblasts or macrophages. **(A)** The PPI network of specific genes between fibrotic and regenerative myofibroblasts. **(B)** The PPI network of specific genes between fibrotic and regenerative macrophages.

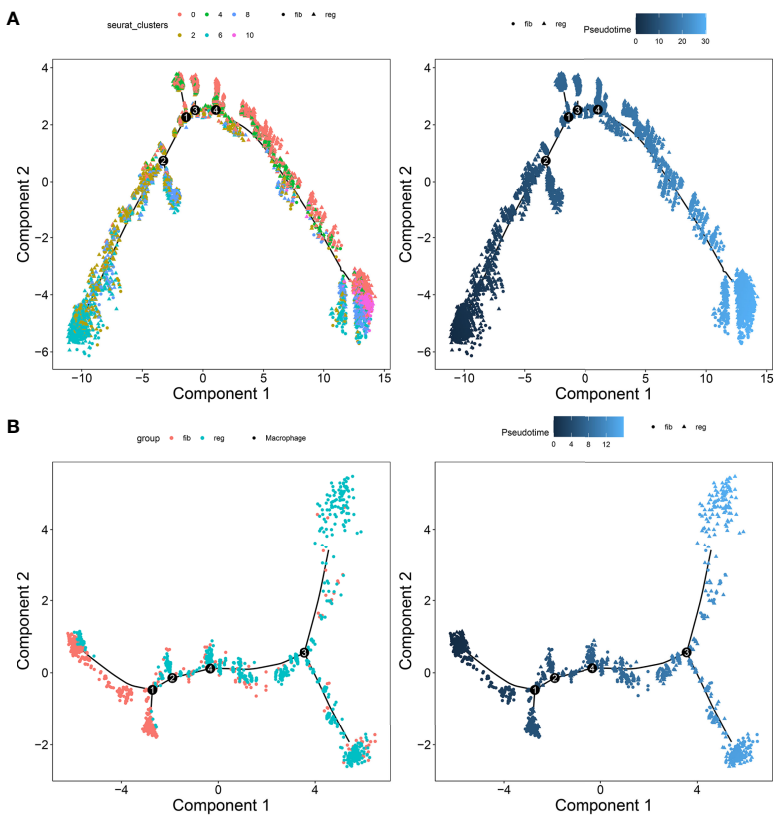

FIGURE 7 | Pseudotime ordering of myofibroblasts and macrophages. **(A)** Myofibroblasts and **(B)** macrophages. Each dot represented one cell and each branch represented one cell state. The left plot was labeled with cell states and the right plot was labeled with developmental time.

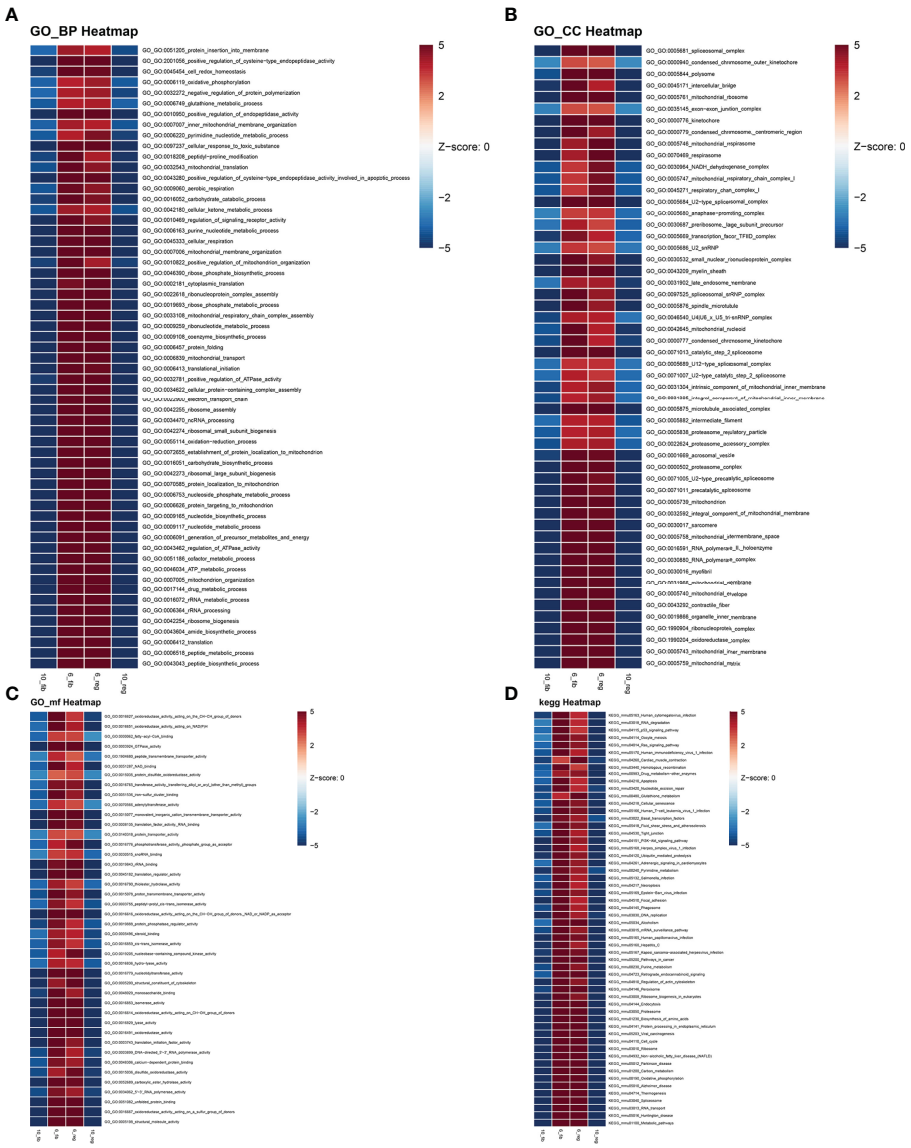

FIGURE 8 | GSVA between clusters 6 and 10 of fibrotic and regenerative myofibroblasts. **(A–D)** Heatmaps showing the differences in activation of biological processes, cellular components, molecular functions, and KEGG pathways between clusters 6 and 10 of fibrotic (fib) and regenerative (reg) myofibroblasts.

populations, namely, EN1-negative myofibroblasts, EN1-positive myofibroblasts, hematopoietic cells, macrophages, pericytes, and endothelial cells, across the dermis. Evidence suggests that EN1-positive fibroblasts are known to function in scarring, and EN1-negative fibroblasts yield wound regeneration. Thus, we used EN1 as a marker to divide the subgroups. Dynamic cellular events after skin injury rely on bidirectional cell–cell communications against effective wound healing (22). Our results demonstrated the cross-talks between myofibroblasts, hematopoietic cells, macrophages, pericytes, and endothelial cells in the dermis based on the ligand–receptor interactions. As per previous studies, CX3CR1 may mediate the recruitment of bone marrow-derived monocytes or macrophages in skin wound healing, thereby releasing profibrotic as well as angiogenic mediators (23). Moreover, macrophages support proliferation and heterogeneity of myofibroblasts in skin repair (24). Serum endothelial cell-derived extracellular vesicles facilitate diabetic wound healing *via* enhancing myofibroblast proliferation and decreasing senescence (25). Intradermal adipocytes modulate the recruitment of myofibroblasts in skin wound healing (26). Fibroblasts promote NG^{2+} pericyte populations in murine skin development as well as repair (27). On the basis of the above lines of evidence, there were remarkable interplays between diverse cell types during dermis progression. According to the number of ligands and receptors, we identified myofibroblasts as the core cell population. Our function enrichment analyses uncovered that the ligand and receptor

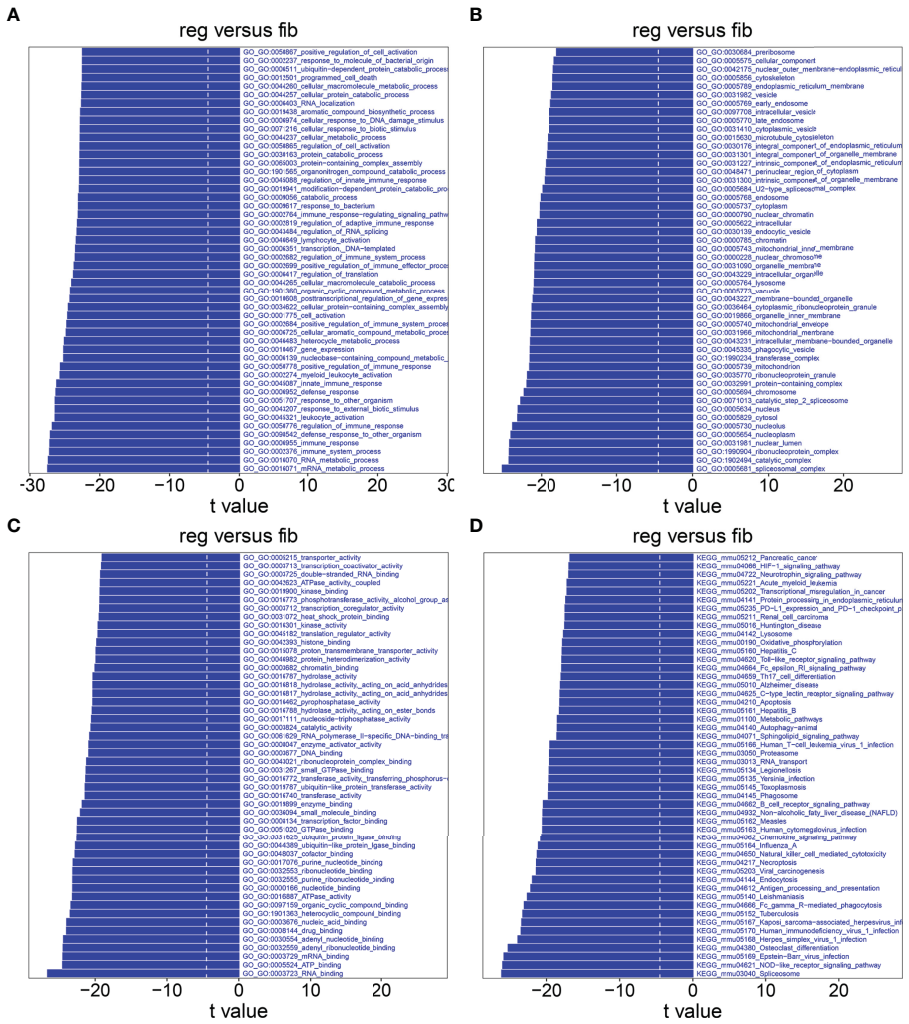

FIGURE 9 | GSVA between fibrotic and regenerative macrophages. **(A–D)** Heatmaps visualizing the differences in activation of biological processes, cellular components, molecular functions, and KEGG pathways between fibrotic (fib) and regenerative (reg) macrophages.

genes between myofibroblasts and macrophages were mainly involved in regulating cell proliferation and migration, tube development, and the TGF-β pathway. The TGF-β signaling pathway plays an important role in the formation of collagen in fibroblasts and myofibroblasts (28). Cytokine TGF-β may induce dermal dendritic cells to express IL-31, thereby activating sensory neurons as well as stimulating wound itching during skin would healing (29). Hence, targeting the TGF-β pathway is the promising therapeutic intervention to reduce abnormal skin scar formation.

To explore the differences in molecular mechanisms involving myofibroblasts between fibrotic and regenerative wound healing fates, we identified 546 up- and 481 downregulated specific genes in regenerative compared to fibrotic myofibroblasts. This revealed the heterogeneity of myofibroblasts between fibrotic and regenerative wound healing. Our GO and KEGG enrichment analysis uncovered the key biological functions involving the specific genes between fibrotic and regenerative myofibroblasts. As a result, these specific genes between fibrotic and regenerative myofibroblasts prominently participated in the mRNA metabolic process and organelle organization. Extracellular matrix of connective tissues is synthesized by myofibroblasts that play a critical role in sustaining the structural integrity of various tissues (30).

Skin wound macrophage is an important regulator of skin repair, and its dysfunction may cause chronic and non-healing skin wounds (31). Further analysis identified that 100 specific genes were significantly upregulated while 197 specific genes were significantly downregulated in regenerative compared to fibrotic macrophages. Functional enrichment analysis uncovered that these specific genes between fibrotic and regenerative macrophages primarily participated in regulating inflammatory response, immunity, and phagocytosis. Immunity is the most important function of the skin, which can prevent harmful exposure from the external and internal environment (32).

Furthermore, late wound macrophage phagocytosis of the Wnt inhibitor may induce chronic Wnt activity during fibrotic skin healing (11). Collectively, our findings revealed that the heterogeneity of myofibroblasts or macrophages might determine wound healing fate as regenerative or fibrotic.

CONCLUSION

Taken together, this study uncovered cellular functional heterogeneity in dermis between fibrotic and regenerative wound healing fates. Moreover, myofibroblasts and macrophages may change the skin wound healing fates by modulating critical signaling pathways. Therefore, our data provided an insight into the development of more effective therapeutic interventions for improving healing fates.

DATA AVAILABILITY STATEMENT

The datasets presented in this study can be found in online repositories. The names of the repository/repositories and accession number(s) can be found at: https://www.ncbi.nlm.nih.gov/, GSM4213633; https://www.ncbi.nlm.nih.gov/, GSM4213632; https://www.ncbi.nlm.nih.gov/, GSE141814.

ETHICS STATEMENT

Ethical review and approval were not required for the study on human participants in accordance with the local legislation and institutional requirements. Written informed consent for participation was not required for this study in accordance with the national legislation and the institutional requirements. The animal study was reviewed and approved by Keio University School of Medicine. Written informed consent was not obtained from the individual(s) for the publication of any potentially identifiable images or data included in this article.

AUTHOR CONTRIBUTIONS

C-JC, HK, and KT: conception or design of the work. C-JC, HK, KT, NA-H, SS, TA, and KK: acquisition, analysis, or interpretation of data. C-JC, HK, KT, NA-H, SS, TA, and KK: drafting the manuscript or revising it critically for important intellectual content. All authors contributed to the article and approved the submitted version.

FUNDING

This work was supported in part by Japan China Sasakawa Medical Fellowship (2017816).

SUPPLEMENTARY MATERIAL

The Supplementary Material for this article can be found online at: https://www.frontiersin.org/articles/10.3389/fimmu.2022.875407/full#supplementary-material

Supplementary Figure 1 | Quality control of scRNA-seq data of fibrotic and regenerative wound dermal cells. **(A, B)** Barcode rank plots separately showing the detected knee and inflection points for fibrotic and regenerative wound dermal cells. **(C, D)** The expression of all genes, ribosomal genes, and mitochondrial genes in each cell was shown for fibrotic and regenerative wound dermal cells. **(E, F)** The proportions of mitochondrial and ribosomal genes expressed in each cell were counted for fibrotic and regenerative wound dermal cells.

Supplementary Table 1 | The list of novel marker genes identified in each cell type.

REFERENCES

1. Rajesh A, Stuart G, Real N, Tschirley A, Ahn J, Wise L, et al. Skin Antigen-Presenting Cells and Wound Healing: New Knowledge Gained and Challenges Encountered Using Mouse Depletion Models. *Immunology* (2021) 163(1):98–104. doi: 10.1111/imm.13311
2. Griffin DR, Archang MM, Kuan C-H, Weaver WM, Weinstein JS, Feng AC, et al. Activating an Adaptive Immune Response From a Hydrogel Scaffold Imparts Regenerative Wound Healing. *Nat Mater* (2021) 20(4):560–9. doi: 10.1038/s41563-020-00844-w
3. Yamaguchi K, Kanno E, Tanno H, Sasaki A, Kitai Y, Miura T, et al. Distinct Roles for Dectin-1 and Dectin-2 in Skin Wound Healing and Neutrophilic Inflammatory Responses. *J Invest Dermatol* (2021) 141(1):164–76.e8. doi: 10.1016/j.jid.2020.04.030
4. Chen T-Y, Wen T-K, Dai N-T, Hsu S-H. Cryogel/hydrogel Biomaterials and Acupuncture Combined to Promote Diabetic Skin Wound Healing Through Immunomodulation. *Biomaterials* (2021) 269:120608. doi: 10.1016/j.biomaterials.2020.120608
5. Rodrigues M, Kosaric N, Bonham CA, Gurtner GC. Wound Healing: A Cellular Perspective. *Physiol Rev* (2019) 99(1):665–706. doi: 10.1152/physrev.00067.2017
6. Aragona M, Dekoninck S, Rulands S, Lenglez S, Mascré G, Simons BD, et al. Defining Stem Cell Dynamics and Migration During Wound Healing in Mouse Skin Epidermis. *Nat Commun* (2017) 8:14684. doi: 10.1038/ncomms14684
7. Govindaraju P, Todd L, Shetye S, Monslow J, Puré E. CD44-Dependent Inflammation, Fibrogenesis, and Collagenolysis Regulates Extracellular Matrix Remodeling and Tensile Strength During Cutaneous Wound Healing. *Matrix Biol* (2019) 75–6:314–30. doi: 10.1016/j.matbio.2018.06.004
8. Haensel D, Jin S, Sun P, Cinco R, Dragan M, Nguyen Q, et al. Defining Epidermal Basal Cell States During Skin Homeostasis and Wound Healing Using Single-Cell Transcriptomics. *Cell Rep* (2020) 30(11):3932–47.e6. doi: 10.1016/j.celrep.2020.02.091
9. Theocharidis G, Baltzis D, Roustit M, Tellechea A, Dangwal S, Khetani RS, et al. Integrated Skin Transcriptomics and Serum Multiplex Assays Reveal Novel Mechanisms of Wound Healing in Diabetic Foot Ulcers. *Diabetes* (2020) 69(10):2157–69. doi: 10.2337/db20-0188
10. Guerrero-Juarez CF, Dedhia PH, Jin S, Ruiz-Vega R, Ma D, Liu Y, et al. Single-Cell Analysis Reveals Fibroblast Heterogeneity and Myeloid-Derived Adipocyte Progenitors in Murine Skin Wounds. *Nat Commun* (2019) 10(1):650. doi: 10.1038/s41467-018-08247-x
11. Gay D, Ghinatti G, Guerrero-Juarez CF, Ferrer RA, Ferri F, Lim CH, et al. Phagocytosis of Wnt Inhibitor SFRP4 by Late Wound Macrophages Drives

Chronic Wnt Activity for Fibrotic Skin Healing. *Sci Adv* (2020) 6(12): eaay3704. doi: 10.1126/sciadv.aay3704
12. Lun ATL, Riesenfeld S, Andrews T, Dao TP, Gomes T, Marioni JC. EmptyDrops: Distinguishing Cells From Empty Droplets in Droplet-Based Single-Cell RNA Sequencing Data. *Genome Biol* (2019) 20(1):63. doi: 10.1186/s13059-019-1662-y
13. McCarthy DJ, Campbell KR, Lun ATL, Wills QF. Scater: Pre-Processing, Quality Control, Normalization and Visualization of Single-Cell RNA-Seq Data in R. *Bioinformatics* (2017) 33(8):1179–86. doi: 10.1093/bioinformatics/btw777
14. Butler A, Hoffman P, Smibert P, Papalexi E, Satija R. Integrating Single-Cell Transcriptomic Data Across Different Conditions, Technologies, and Species. *Nat Biotechnol* (2018) 36(5):411–20. doi: 10.1038/nbt.4096
15. Ramilowski JA, Goldberg T, Harshbarger J, Kloppmann E, Lizio M, Satagopam VP, et al. A Draft Network of Ligand-Receptor-Mediated Multicellular Signalling in Human. *Nat Commun* (2015) 6:7866. doi: 10.1038/ncomms8866
16. Doncheva NT, Morris JH, Gorodkin J, Jensen LJ. Cytoscape StringApp: Network Analysis and Visualization of Proteomics Data. *J Proteome Res* (2019) 18(2):623–32. doi: 10.1021/acs.jproteome.8b00702
17. Yu G, Wang L-G, Han Y, He Q-Y. Clusterprofiler: An R Package for Comparing Biological Themes Among Gene Clusters. *OMICS* (2012) 16 (5):284–7. doi: 10.1089/omi.2011.0118
18. Szklarczyk D, Gable AL, Lyon D, Junge A, Wyder S, Huerta-Cepas J, et al. STRING V11: Protein-Protein Association Networks With Increased Coverage, Supporting Functional Discovery in Genome-Wide Experimental Datasets. *Nucleic Acids Res* (2019) 47(D1):D607–13. doi: 10.1093/nar/gky1131
19. Cao J, Spielmann M, Qiu X, Huang X, Ibrahim DM, Hill AJ, et al. The Single-Cell Transcriptional Landscape of Mammalian Organogenesis. *Nature* (2019) 566(7745):496–502. doi: 10.1038/s41586-019-0969-x
20. Hänzelmann S, Castelo R, Guinney J. GSVA: Gene Set Variation Analysis for Microarray and RNA-Seq Data. *BMC Bioinf* (2013) 14:7. doi: 10.1186/1471-2105-14-7
21. Sorkin M, Huber AK, Hwang C, Carson WF4, Menon R, Li J, et al. Regulation of Heterotopic Ossification by Monocytes in a Mouse Model of Aberrant Wound Healing. *Nat Commun* (2020) 11(1):722. doi: 10.1038/s41467-019-14172-4
22. Zhou X, Brown BA, Siegel AP, El Masry MS, Zeng X, Song W, et al. Exosome-Mediated Crosstalk Between Keratinocytes and Macrophages in Cutaneous Wound Healing. *ACS Nano* (2020) 14(10):12732–48. doi: 10.1021/acsnano.0c03064
23. Ishida Y, Gao J-L, Murphy PM. Chemokine Receptor CX3CR1 Mediates Skin Wound Healing by Promoting Macrophage and Fibroblast Accumulation and Function. *J Immunol* (2008) 180(1):569–79. doi: 10.4049/jimmunol.180.1.569
24. Shook BA, Wasko RR, Rivera-Gonzalez GC, Salazar-Gatzimas E, López-Giráldez F, Dash BC, et al. Myofibroblast Proliferation and Heterogeneity are Supported by Macrophages During Skin Repair. *Science* (2018) 362(6417). doi: 10.1126/science.aar2971
25. Wei F, Wang A, Wang Q, Han W, Rong R, Wang L, et al. Plasma Endothelial Cells-Derived Extracellular Vesicles Promote Wound Healing in Diabetes Through YAP and the PI3K/Akt/mTOR Pathway. *Aging (Albany NY)* (2020) 12(12):12002–18. doi: 10.18632/aging.103366
26. Schmidt BA, Horsley V. Intradermal Adipocytes Mediate Fibroblast Recruitment During Skin Wound Healing. *Development* (2013) 140 (7):1517–27. doi: 10.1242/dev.087593
27. Goss G, Rognoni E, Salameti V, Watt FM. Distinct Fibroblast Lineages Give Rise to NG2+ Pericyte Populations in Mouse Skin Development and Repair. *Front Cell Dev Biol* (2021) 9:675080. doi: 10.3389/fcell.2021.675080
28. Zhang T, Wang X-F, Wang Z-C, Lou D, Fang Q-Q, Hu Y-Y, et al. Current Potential Therapeutic Strategies Targeting the TGF-β/Smad Signaling Pathway To Attenuate Keloid and Hypertrophic Scar Formation. *BioMed Pharmacother* (2020) 129:110287. doi: 10.1016/j.biopha.2020.110287
29. Xu J, Zanvit P, Hu L, Tseng P-Y, Liu N, Wang F, et al. The Cytokine TGF-β Induces Interleukin-31 Expression From Dermal Dendritic Cells to Activate Sensory Neurons and Stimulate Wound Itching. *Immunity* (2020) 53(2):371–83.e5. doi: 10.1016/j.immuni.2020.06.023
30. Lynch MD, Watt FM. Fibroblast Heterogeneity: Implications for Human Disease. *J Clin Invest* (2018) 128(1):26–35. doi: 10.1172/JCI93555
31. Chen H, Shi R, Luo B, Yang X, Qiu L, Xiong J, et al. Macrophage Peroxisome Proliferator-Activated Receptor γ Deficiency Delays Skin Wound Healing Through Impairing Apoptotic Cell Clearance in Mice. *Cell Death Dis* (2015) 6 (1):e1597. doi: 10.1038/cddis.2014.544
32. Matejuk A. Skin Immunity. *Arch Immunol Ther Exp (Warsz)* (2018) 66(1):45–54. doi: 10.1007/s00005-017-0477-3

Conflict of Interest: The authors declare that the research was conducted in the absence of any commercial or financial relationships that could be construed as a potential conflict of interest.

Publisher's Note: All claims expressed in this article are solely those of the authors and do not necessarily represent those of their affiliated organizations, or those of the publisher, the editors and the reviewers. Any product that may be evaluated in this article, or claim that may be made by its manufacturer, is not guaranteed or endorsed by the publisher.

frontiers | Frontiers in Immunology

TYPE Correction
PUBLISHED 31 March 2023
DOI 10.3389/fimmu.2023.1175360

OPEN ACCESS

EDITED AND REVIEWED BY
Tian Li,
Independent Researcher, Xi'an, China

*CORRESPONDENCE
Kazuo Kishi
kkishi@a7.keio.jp
Toru Asou
mori@ideajapan.com

SPECIALTY SECTION
This article was submitted to Cancer Immunity and Immunotherapy, a section of the journal Frontiers in Immunology

RECEIVED 27 February 2023
ACCEPTED 20 March 2023
PUBLISHED 31 March 2023

CITATION
Chen C-J, Kajita H, Takaya K, Aramaki-Hattori N, Sakai S, Asou T and Kishi K (2023) Corrigendum: Single-cell RNA-seq analysis reveals cellular functional heterogeneity in dermis between fibrotic and regenerative wound healing fates. *Front. Immunol.* 14:1175360. doi: 10.3389/fimmu.2023.1175360

Corrigendum: Single-cell RNA-seq analysis reveals cellular functional heterogeneity in dermis between fibrotic and regenerative wound healing fates

Cao-Jie Chen[1], Hiroki Kajita[1], Kento Takaya[1], Noriko Aramaki-Hattori[1], Shigeki Sakai[1], Toru Asou[2*] and Kazuo Kishi[1*]

[1]Department of Plastic and Reconstructive Surgery, Keio University School of Medicine, Tokyo, Japan, [2]Department of Plastic Surgery, Tokyo Cosmetic Surgery Clinic, Tokyo, Japan

KEYWORDS

skin wound healing, fibrosis, regeneration, myofibroblast, macrophage, single-cell RNA sequencing

A corrigendum on

Single-cell RNA-seq analysis reveals cellular functional heterogeneity in dermis between fibrotic and regenerative wound healing fates

by Chen C-J, Kajita H, Takaya K, Aramaki-Hattori N, Sakai S, Asou T and Kishi K (2022) *Front. Immunol.* 13:875407. doi: 10.3389/fimmu.2022.875407

In the published article, there was an error in Figures 2C, D and F as published. The dot size for EN1 gene in different cell types in Figure 2D was wrong because we mislabeled the gene name during the production of the picture. Due to the same reason, the Figure 2F was also wrongly placed. In addition, we want to replace Figure 2C to add more feature genes (top 15, previously was top 10) in the heatmap to better characterize cell-type-specific gene expression patterns. The corrected Figures 2C, D and F appear below.

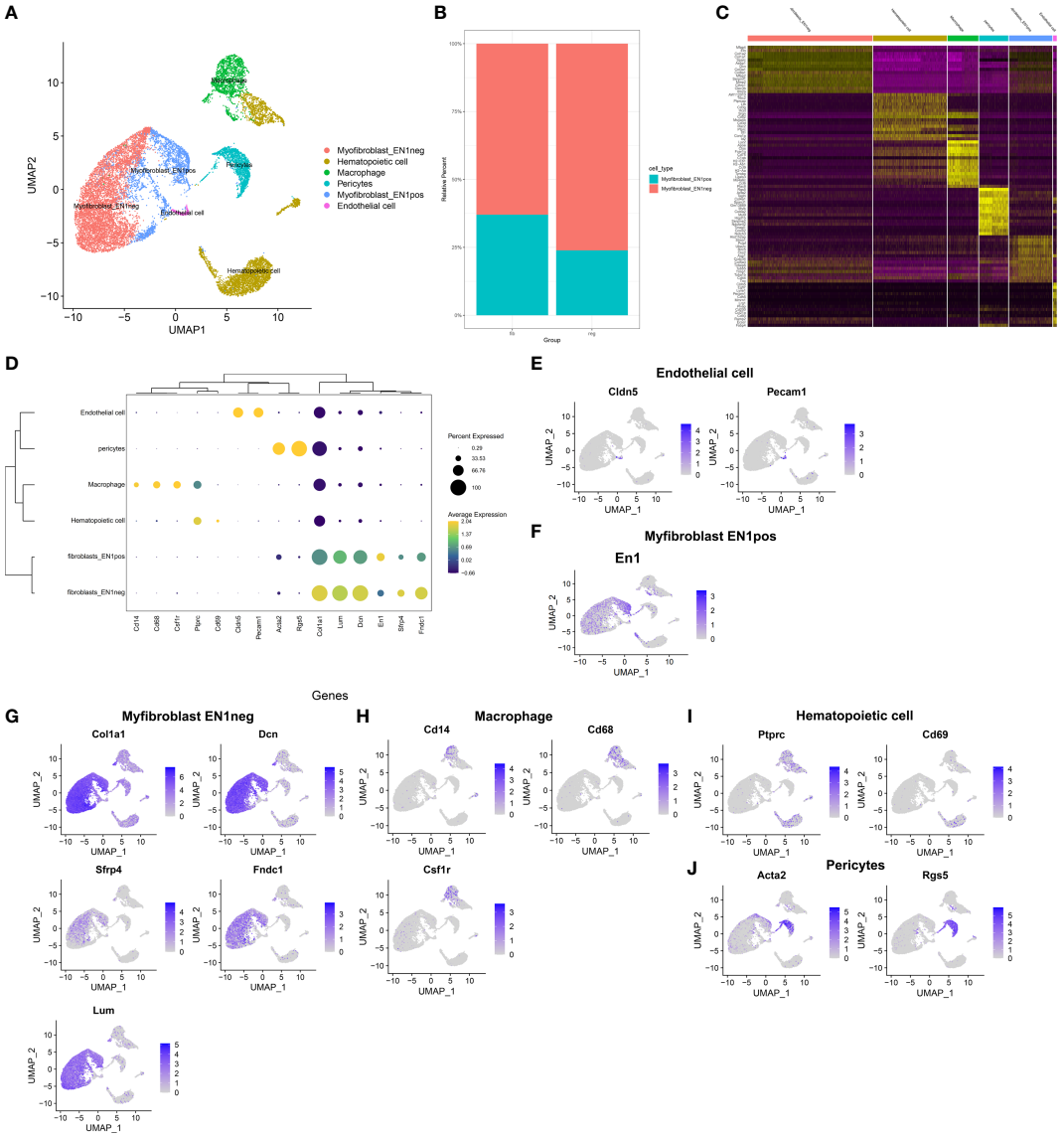

FIGURE 2
Identification of cell types and their marker genes across fibrotic and regenerative wound dermal cells. **(A)** UMAP plots showing cell types identified by marker genes. Each cell type was colored by a unique color. **(B)** The cell ratio of EN1-negative and -positive myofibroblasts among fibrotic and regenerative wound dermal cells. **(C)** Heatmap visualizing cell-type-specific gene expression patterns. Each column represented the average expression after cells were grouped. **(D)** Integrated analysis showing marker genes across cell types. The size of each circle reflected the percentage of cells in each cell type where the gene was detected, and the color shadow reflected the average expression level within each cell type. **(E–J)** UMAP plots of expression of the marker genes for endothelial cells, EN1-negative and -positive myofibroblasts, macrophages, hematopoietic cells, and pericytes.

The authors apologize for this error and state that this does not change the scientific conclusions of the article in any way. The original article has been updated.

Publisher's note

frontiers | Frontiers in Immunology

REVIEW
published: 31 May 2022
doi: 10.3389/fimmu.2022.876291

Understanding Tricky Cellular and Molecular Interactions in Pancreatic Tumor Microenvironment: New Food for Thought

Antonio Agostini[1,2†], *Arturo Orlacchio*[3†], *Carmine Carbone*[1*‡] *and Ilaria Guerriero*[4*‡]

[1] Medical Oncology, Department of Medical and Surgical Sciences, Fondazione Policlinico Universitario Agostino Gemelli IRCCS, Rome, Italy, [2] Medical Oncology, Department of Translational Medicine, Catholic University of the Sacred Heart, Rome, Italy, [3] NYU Grossman School of Medicine, NYU Langone Health, New York, NY, United States, [4] Biogem, Biology and Molecular Genetics Institute, Ariano Irpino, Italy

OPEN ACCESS

Edited by:
Valentina Audrito,
Dipartimento di Scienze e Innovazione Tecnologica, Università del Piemonte Orientale, Italy

Reviewed by:
Nune Markosyan,
University of Pennsylvania, United States
Direna Alonso Curbelo,
Institute for Research in Biomedicine, Spain

***Correspondence:**
Ilaria Guerriero
ilaria.guerriero@biogem.it
Carmine Carbone
carmine.carbone@policlinicogemelli.it

[†]These authors share first authorship

[‡]These authors share last authorship

Specialty section:
This article was submitted to Cancer Immunity and Immunotherapy, a section of the journal Frontiers in Immunology

Received: 15 February 2022
Accepted: 29 April 2022
Published: 31 May 2022

Citation:
Agostini A, Orlacchio A, Carbone C and Guerriero I (2022) Understanding Tricky Cellular and Molecular Interactions in Pancreatic Tumor Microenvironment: New Food for Thought. Front. Immunol. 13:876291. doi: 10.3389/fimmu.2022.876291

Pancreatic ductal adenocarcinoma (PDAC) represents 90% of all pancreatic cancer cases and shows a high mortality rate among all solid tumors. PDAC is often associated with poor prognosis, due to the late diagnosis that leads to metastasis development, and limited efficacy of available treatments. The tumor microenvironment (TME) represents a reliable source of novel targets for therapy, and even if many of the biological interactions among stromal, immune, and cancer cells that populate the TME have been studied, much more needs to be clarified. The great limitation in the efficacy of current standard chemoterapy is due to both the dense fibrotic inaccessible TME barrier surrounding cancer cells and the immunological evolution from a tumor-suppressor to an immunosuppressive environment. Nevertheless, combinatorial therapies may prove more effective at overcoming resistance mechanisms and achieving tumor cell killing. To achieve this result, a deeper understanding of the pathological mechanisms driving tumor progression and immune escape is required in order to design rationale-based therapeutic strategies. This review aims to summarize the present knowledge about cellular interactions in the TME, with much attention on immunosuppressive functioning and a specific focus on extracellular matrix (ECM) contribution.

Keywords: PDAC, TME, ECM, immune escape, immunotherapy

INTRODUCTION

Pancreatic ductal adenocarcinoma (PDAC) is a deadly disease with a 5-year overall survival of 10% (1). This solid tumor is characterized by a dense fibrotic tumor microenvironment (TME) constituted by connective tissue, fibroblasts, blood vessels, and immune cells. Notably, PDAC is fueled by the immunosuppressive TME (2), thus revealing that the relationship between cancer progression and immunological evolution of TME is a key point to improve therapies (3). Although several solid tumors show a good response to immunotherapies, PDAC lacks effective treatments due to the continuous changes in the immune TME, where immunosuppressive cells are recruited, such as tumor-associated macrophages (TAMs), regulatory T cells (Tregs), and bone marrow

myeloid-derived suppressor cells (MDSCs) (4), that all together help cancer cells to escape immunosurveillance (5). Since 1997, chemotherapy based on gemcitabine as a single agent had been a standard-of-care first-line treatment for more than two decades, but two important clinical trials had shown that combination regimens could guarantee stronger response and longer median overall survival. In detail, PRODIGE and MPACT analyzed the utility to combine several chemotherapeutic agents to increase the efficacy of metastatic PDAC treatment (6–9). FOLFIRINOX (5-fluorouracil, leucovorin, irinotecan, and oxaliplatin) and gemcitabine/nab-paclitaxel are current first-line treatment for PDAC patients with metastasis, but they have been associated with many side effects (10–12). Currently, few novel effective treatments are available for this cancer, despite the fact that patients diagnosed with other solid tumors can rely on several therapeutic strategies, highlighting the need to strengthen the research in this field. Future perspectives for PDAC treatment are looking at the combination of immunotherapeutic and chemotherapeutic agents, aiming to fight cancer progression by multiple approaches.

Despite numerous clinical trials recruiting PDAC patients to test novel therapeutic strategies, a deep understanding of pathological mechanisms driving carcinogenesis is needed. In this context, it is helpful to consider that a complex interaction among cells in the TME orchestrates PDAC progression and determines the scarce success rate of available therapies, due to the limited accessibility to cancer cells.

Recently, stromal, immune, and cancer cell interactions have received much attention, being involved in PDAC progression and immune response modulation. However, it is not completely clear how these cells interact in the TME.

This review aims to summarize lights and shadows of this complicated communication, considering critical mediators that are emerging as important players in pancreatic tumorigenesis and progression. Moreover, a specific focus on the recent therapeutic strategies is also provided, attesting that different combination treatments are entering clinic trials and seem to be promising approaches to improve personalized therapies.

MOLECULAR SUBTYPES OF PDAC: THE CONTRIBUTION OF TME CELLS

PDAC mainly develops from pancreatic intraepithelial neoplasia (PanIN) (13), which is denoted by microscopic precursor lesions undetectable with present diagnostic imaging techniques. A small percentage of PDAC originates from pancreatic cystic lesions, such as intraductal papillary mucinous neoplasms (IPMNs) and mucinous cystic neoplasms, and can have different aggressiveness depending on the specific site in the pancreas (13). Histopathological features of PDAC have been widely described over time (14, 15), but this classification does not correspond to precise indications for treatments.

Molecular subtyping of PDAC could be more informative, and the single gene mutations most commonly considered are *KRAS*, *TP53*, *SMAD4*, and *CDKN2A* with a prevalence of more than 50% in patients (16, 17). The progression from PanIN to PDAC is marked by the accumulation of several molecular events: *KRAS* mutations and telomerase shortening are early events that determine the transition from normal duct to PanIN-1; *CDKN2A* mutations are related to PanIN-2 stage; late events, such as *TP53, SMAD4*, and also *BRCA* mutations, lead from PanIN-3 to PDAC, with the consequent progression to metastatic disease (18, 19).

During the last decade, several studies have been published in which whole-genome sequencing and transcriptional profiling analysis were applied on large cohorts of PDAC samples with the aim of dissecting the molecular landscape of PDAC (20–24). This has been possible thanks to the advances in next-generation sequencing technologies and encouraged by the promising results achieved in other tumor types with therapeutic approaches based on a molecular stratification of the patients (25–27). In 2011, Collisson and colleagues performed a first array-based mRNA expression analysis of resected PDAC by epithelium microdissection with stroma exclusion. They proposed three subtypes, namely, classical, quasi-mesenchymal, and exocrine-like, with the quasi-mesenchymal subtype showing high tumor grade and poor survival (28).

In 2015, Moffitt and colleagues completed the molecular subtyping of PDAC samples and metastasis by hybridization arrays, and a subgroup of them by RNAseq. Transcripts derived from normal pancreas and from TME were excluded, defining two PDAC subtypes called basal-like and classical, and two stromal subtypes described as normal and activated, with the last one being associated with a worse prognosis (29).

In 2016, Bailey and colleagues profiled PDAC samples with a wide variety of cellularity by array-based hybridization, describing four subtypes, namely, squamous, pancreatic progenitor, immunogenic, and aberrantly differentiated endocrine exocrine (ADEX) (30). In comparison to Collisson classification, Bailey et al. added the immunogenic subtype by the profiling of the immune infiltrates in the TME, and this is extremely important to identify an ideal therapeutic strategy, especially for immunotherapeutic options.

Transcriptional profiling has been useful and informative for signature mutations in *KRAS, TP53, CDKN2A*, and *SMAD4* that have been confirmed, but, more importantly, new genes have been found mutated or transcriptionally altered, thus uncovering a considerable genetic heterogeneity among PDAC patients (22, 31). For instance, about 10% of pancreatic cancer cases are familiar and show germline inactivating mutations in genes associated with the DNA repair pathways (e.g., *BRCA1/2, ATM*, and *PALB2*) and a subgroup of these patients also have similar germline mutations in epigenetic regulators (e.g., *TET2, DNMT3A*, and *ASXL1*) (22, 32). This suggests that epigenetic changes are an important factor in predisposing individuals to pancreatic cancer.

Moreover, whole exome and genome sequencing exposed the presence of somatic mutations in epigenetic regulators and chromatin remodeling complexes (e.g., *ARID1A/B, PBRM1, MLL2/3/4, KDM6A*, and *SMARCA2/4*) in a significant percentage of PDAC patients (22, 31).

These results further highlight the deep heterogeneity (both molecular and epigenetic) of PDAC, made also evident by the identification of various PDAC subtypes with different molecular and phenotypic characteristics that reflect on prognosis and response to therapies (28–30, 33).

Classical subtype tumors are more differentiated and tend to respond better to chemotherapy and to have better prognosis. On the other hand, basal-like subtype is characterized by high tumor grade, strong chemoresistance and worse prognosis. From a molecular standpoint, these subtypes are associated with distinct gene signatures and epigenetic profiles. Specifically, the classical subtype is characterized by an epithelial differentiation gene signature, while the basal-like subtype shows a more mesenchymal expression profile (21–24, 28–30, 33, 34).

Moreover, the two subtypes show differences in the activity of specific superenhancers (SEs) and their upstream regulators (21). SEs are large clusters of transcriptional enhancers that drive gene expression to control cell identity (35, 36). The main transcription factors (TFs) involved in the regulation of subtype-specific SEs and transcription programs are *MET, MYC*, and the ΔN isoform of the transcription factor *TP63* (ΔNp63) for the basal-like subtype, and *GATA6, PDX1*, and *HNFs* for the classical one (37–41). There is evidence that the activity of these transcription factors is controlled by epigenetic regulators that can not only alter their expression, but also function as transcriptional co-regulators (41, 42).

Somerville et al. demonstrated that the ΔN isoform of the transcription factor *TP63* (ΔNp63) is a master regulator critical for establishing basal-like cell identity in PDAC through enhancer reprogramming, thus promoting tumor growth and metastatic potential (43). Mechanistically, ΔNp63 increases H3K27ac levels at the enhancers of basal-like lineage genes, thus leading to increased transcriptions of genes such as *KRT5/6*, *TRIM29*, and *PTHLH*, which promotes more aggressive PDAC phenotypes (43).

Enhancer reprogramming has also been described as the mechanism underlying *FOXA1*-driven tumor-to-metastasis transition (44). Roe et al. established 3D organoid culture from primary tumors derived from the KPC PDAC mouse model and used ChIP-seq analysis to assess H3K27ac occupancy. Their analysis, complemented with *in vitro* and *in vivo* overexpression experiments, revealed that *FOXA1* is responsible for increasing H3K27ac at specific enhancer regions, thus activating foregut developmental genes that promote anchorage-independent cell growth and invasion. Moreover, *FOXA1* gene transcription is enhanced in the presence of missense mutations of *p53* (p53R172H, p53R245W, and p53R270H) (45). Specifically, KRAS effectors phosphorylates cyclic AMP responsive element binding protein 1 (CREB1) and enable binding and hyperactivation by mutant p53. Consequently, FOXA1 is upregulated and, by promoting β-catenin stabilization, activates the canonical WNT pathway supporting proliferation and metastasis (45, 46).

Pancreatic cancer cells can also remodel the epigenetic landscape by repressing epigenetic modulators in order to upregulate TFs that drive squamous PDAC transcriptional programs. For instance, mutations in the histone H3K27me2/3-specific lysine demethylase 6A (*KDM6A*) are frequently found in the basal-like subtypes (47). Andricovich et al. found that loss of KDM6A in PDAC can directly induce the basal-like subtype by rewiring enhancer chromatin and activating SE regulating ΔNp63, MYC, and RUNX3 (47). Mechanistically, such rewiring is the consequence of the activity of histone type 2 lysine methyltransferases (KMT2), which, as a consequence of KDM6A loss, occupy and activate enhancers of genes supporting the basal-like subtype. KMT2 enzyme families are histone H3K4-specific methyltransferases that mark active gene enhancers with H3K4me1 (48, 49) and indeed increased H3K4me1, and KMT2D occupancies at basal-like supporting elements have been reported in the absence of KDM6A (47).

Taken together, these studies highlight the ability of pancreatic cancer cells to reprogram their epigenetic landscape and subsequent transcription programs to sustain their growth, differentiation, and metastasis.

In addition, recently, several studies have employed single-cell RNA sequencing (scRNA-seq) aiming at further elucidating the complexity of TME in PDAC (**Table 1**).

In a study from 2019, Elyada et al., using both PDAC patient samples and murine models, identified two main immune cell clusters: myeloid and lymphoid (52). Subsequent subclustering showed the presence of six distinct subpopulations within the first group, and five within the second. Specifically, for the myeloid cluster, resident macrophages, alternatively activated M2-like macrophages, classic monocytes, conventional type 1 dendritic cells (cDC1), and two types of Langerhans-like dendritic cells were identified. For the lymphoid cluster, the identified cell types were $CD8^+$ T cells, $CD4^+$ T cells, Tregs, proliferating Tregs, and natural killer (NK) cells.

ScRNA-seq analysis of the immune cells in the TME has also been employed to show differences between low-grade and high-grade tumors, as well as between primary versus metastatic lesions. In 2018, Bernard et al. performed a single-cell transcriptomic profiling of cystic precursor lesions of PDAC demonstrating that low-grade IPMNs are enriched for CTLs and $CD4^+$ effector T cells compared to high-grade IPMNs. At the same PDACs, when compared to IPNMs, show an increased presence of granulocytic MDSCs. This suggests a progressive shift of the microenvironment in a tumor-promoting direction (50). This modulation of the TME by the malignant cells seems to be supported by other studies as well. For instance, Peng et al. identified three PDAC patient clusters, with cluster 3 being characterized by proliferation markers and associated with worse survival compared with patients in the other two clusters. Moreover, differential gene expression analysis showed an enrichment of cell cycle, DNA replication, and DNA repair pathways and depletion in several immune/T-cell activation gene sets in cluster 3 in comparison to clusters 1 and 2 (51). They reported an inverse correlation between high expression of proliferative ductal markers and low expression of T-cell activation markers. This result was then confirmed by immunohistochemistry (IHC), which demonstrated that areas characterized by ductal cells expressing low levels of Ki67 were

TABLE 1 | scRNA-seq analyses to dissect the molecular complexity of TME in PDAC: a historical summary.

Year	Molecular analysis Samples	Resulting evidence	Reference
2018	scRNA-seq IPMN patients	Low-grade IPMNs are enriched for CTLs and $CD4^+$ effector T cells compared to high-grade IPMNs	Bernard et al. (50)
2019	scRNA-seq PDAC patients	Three patient clusters identified: cluster 3 vs. clusters 1 and 2 showed high expression of proliferation markers and worse survival; enrichment of cell cycle, DNA replication, and DNA repair pathways and depletion in several immune/T-cell activation gene sets	Peng et al. (51)
2019	scRNA-seq PDAC patients, murine models	Two immune clusters identified: 1. Myeloid cluster, composed of resident macrophages, M2 macrophages, classic monocytes, cDC1, and two types of Langerhans-like dendritic cells 2. Lymphoid cluster, composed of $CD8^+$ T cells, $CD4^+$ T cells, Tregs, proliferating Tregs, and NK cells	Elyada et al. (52)
2019	scRNA-seq Murine models of PDAC (KIC, KPC, KPfC)	Two immune clusters identified: 1. Expression of several genes associated with chemokines and inflammation 2. Enriched in MHC-II-associated genes	Hosein et al. (53)
2020	scRNA-seq Human primary tumors and metastatic lesions	Two tumor-infiltrating lymphocyte clusters identified, with no difference between primary tumors and metastases: 1. High levels of markers associated with activation and exhaustion 2. Antigen-inexperienced T cell Two macrophage clusters identified: 1. M2 polarization, expression of genes associated with extracellular matrix production and wound healing processes 2. Expression of genes associated with antigen presentation.	Lin et al. (54)

also characterized by high T-cell infiltration and *vice versa*, thus linking altered ductal cell proliferation and local immune response and suggesting that a combination of cell-cycle inhibitors and immunotherapy could be a valid therapeutic approach (55).

Two novel subtypes of macrophages were identified by Hossein et al. in advanced tumors by applying scRNA-seq to three mouse models of PDAC: $Kras^{LSL\text{-}G12D/+}$ $Ink4a^{fl/fl}$ $Ptf1a^{Cre/+}$ (KIC), $Kras^{LSL\text{-}G12D/+}$ $Trp53^{LSL\text{-}R172H/+}$ $Ptf1a^{Cre/+}$ (KPC), and $Kras^{LSL\text{-}G12D/+}$ $Trp53^{fl/fl}$ $Pdx1^{Cre/+}$ (KPfC) (53). Specifically, one subtype expressed several genes associated with chemokines and inflammation, while the other was enriched in major histocompatibility complex II (MHC II)–associated genes.

In regard to the differences in TME immune cells between primary tumors and metastatic lesions, using scRNA-seq, Lin and colleagues compared immune cell population from primary tumor resections with the ones obtained from metastatic biopsies (54). Two tumor-infiltrating lymphocyte (TIL) clusters were identified, showing no difference between primary tumors and metastases. One cluster was characterized by high levels of markers associated with activation and exhaustion, while the second one was representative of naive, antigen-inexperienced T cells. On the other hand, macrophages from primary tumors and metastases clustered separately. While the first displayed a gene signature typical of M2-like polarization (higher levels of genes associated with extracellular matrix production and wound healing processes), the second expressed genes associated with antigen presentation. However, it is worth mentioning that the analyzed metastases were mostly hepatic; therefore, the observed differences may be partially due to the distinct characteristic of liver-resident and pancreas-resident macrophages.

A downside of scRNA-seq is the loss of tissue architecture, which constitutes an obstacle to the study of intercellular interaction. For this reason, complementary approaches like multiplexed immunolabeling or RNA *in situ* hybridization (RNA-ISH) have been developed. Despite having significantly less molecular resolution, they provide spatial information at the single-cell level. One of the earlier attempts was reported by Carstens et al. who were able to simultaneously assess eight markers [Dapi, alpha-smooth muscle actin (α-SMA), collagen I, cytokeratin 8, Foxp3, CD3, CD4, and CD8] on tissue microarrays composed of tissue obtained upon pancreatectomy of 132 patients with PDAC without neoadjuvant therapy (56). Interestingly, they report an independent association between improved patient survival and high infiltration levels of total T cell, $CD8^+$ cytotoxic T cell, and $CD4^+$ effector T cell (56); however, such association became only significant for the seconds when taking into consideration only a 20-μm radius around each cytokeratin 8-positive cancer cell. Moreover, no correlation was found between α-SMA levels and T-cell infiltration, while collagen I deposition positively correlated with T-cell infiltration, suggesting that desmoplastic stroma does not negatively impact lymphocyte infiltration (57, 58).

A similar approach was employed with a focus on myeloid cells and macrophages by Väyrynen and colleagues (59). Using tissue microarrays generated from 305 primary PDAC specimens, the authors focused on four polarization markers to assess the macrophage polarization status (M1: CD86, IRF1; M2: CD163, CD206). They reported that M1-polarized macrophages were located in significantly closer proximity to cancer cells than M2-polarized macrophages and that a higher density of the latter as well as $CD15^+ARG1^+$ immunosuppressive granulocytic cells was associated with poor patient survival. Moreover, the authors reported interesting associations between myeloid cell densities and alterations in PDAC driver genes, thus further supporting the effect of cancer cell on immune cell modulation in the TME (59).

The integration of ISH techniques with scRNA-seq data has allowed mapping rare cellular subpopulations on a spatial context (60, 61). However, a throughput limitation persists in

ISH techniques, avoiding considering it the best spatial approach. Aiming to overcome this limit, recent spatial transcriptomics (ST) methods have been developed, in order to map any transcripts in whole tissue sections using ISH of spatially barcoded oligonuclotides (62). Very recently, Moncada et al. (2020) showed the potential of this breaktrough technology to study PDAC TME composition (63). They used an array-based ST novel approach to deconvolute scRNA-seq on whole tissue by dividing the PDAC samples into two portions: one to be used to obtain a single-cell suspension processed for scRNA-seq; on the second portion, ST was performed to map the expressed transcripts across the tissue. By the integration of the two resulting analyses output, from primary PDAC tumors from different patients, they were able to identify several specific cell types and subpopulations, such as M1 and M2 macrophages, enriched across spatially restricted areas of the tissue.

Keynote

Understanding molecular features of PDAC can reveal a source of novel targets to be exploited for important advances in PDAC therapy. The improvement of methods and the integration of different technologies can give a comprehensive overview of molecular landscape, during cancer progression and resistance to treatments. The knowledge of genetics, epigenetics, and transcriptomics behind PDAC is the key to targeting crucial pathological mechanisms.

IMMUNOSUPPRESSIVE CELLS IN THE TME OF PDAC

TAMs derive from the recruitment of $CCR2^+$ monocytes to the TME and usually represent the most abundant immune population (64–66). In general, macrophages have distinct states of polarization, which are commonly defined as M1 and M2. The M1 phenotype is associated with pro-inflammatory function and is activated through the classic pathway, by IFNγ or bacterial component stimulation; the M2 phenotype is related to anti-inflammatory function, and is activated by alternative pathways that lead to the suppression of Th1 immune response in favor of the Th2 one (67, 68). As part of the innate immune response, monocytes are recruited in the first phase of cancer onset and differentiate in macrophages able to phagocyte cancer cells, but their function is impaired by several mechanisms of immune escape. TAMs in TME show very heterogeneous features; however, most of them display an M2 polarization state, supporting angiogenesis and tumor growth (69, 70). Cancer cells can adopt mechanisms to evade immune surveillance; an example is to express high levels of the transmembrane protein CD47, which represents the classic signal "don't eat me", inducing an anti-phagocytic response (71). Several cancers exploit this immune evasion strategy, and some authors have considered the blockade of CD47 on cancer cells or signal regulatory protein α (SIRPα) on macrophages as a valid therapeutic option (72, 73), also for PDAC to target pancreatic cancer stem cells and as adjuvant immunotherapy for liver micrometastasis (74, 75). TAMs can also secrete in the TME a number of immunosuppressive cytokines, such as IL-6, TGF-β, and IL-10 that are able to suppress $CD8^+$ T-cell function (76). Specifically, IL-6 is expressed at high levels in PDAC, and its increasing circulating level is associated with advanced disease and poor prognosis (77). The inhibition of IL-6 signaling along with CD40 blockade is able to revert the TME to support an antitumor immune response, by reducing TGF-β activation and fibrosis deposition due to a decreased collagen type I production (78). Moreover, chemokines such as CCL2, CCL17, CCL20, and CCL22 induce the recruitment of Tregs to the tumor sites, activating their regulatory function by IL10 and TGFβ signaling, leading to the accumulation of Tregs and impairing the migration and activation of T cytotoxic effector cells (79–82). TAMs can also express arginase I that is involved in reducing L-arginine in the TME impairing T-cell function (83). TAMs are also responsible for a reduced NK cell function, due to the secretion of the above-mentioned cytokines resulting in a limited production of IFN-γ, perforin, and IL-12 by NK cells, which determines a lower cytotoxicity and proliferation in the TME (84). TAMs are able to reduce NK cell functioning also by direct cell–cell interactions, since PDL-1 expressed on TAMs can bind to PD-1 on NK cells, avoiding the activation of their cytotoxic receptors (85).

Similarly to TAMs, neutrophils can also show heterogeneity in the TME, showing a different state of activation and consequent function. Neutrophils take part in early inflammatory response, being able to produce and secrete many cytotoxic compounds and also reactive oxygen species (ROS), in order to kill stromal cells in the TME (86). By secreting a high number of chemokines, such as CCL2, CCL3, CCL19, and CCL20, neutrophils can drive the immune response, recruiting monocytes and DCs, NK cells, and T-helper type 1 (Th1) and type 17 (Th17) cells to the inflamed tissues (87, 88). Despite a clear pro-inflammatory function, neutrophils can change to a pro-tumor profile. Thus, the population of tumor-associated neutrophils (TANs) can be considered dichotomous, showing an N1 or N2 profile, comparably to TAMs. The N2 profile sustains tumor growth by the activation of TGF-β signaling (89). Moreover, pancreatic cancer cells can recruit TANs by secreting chemokines of the CXC family, specifically CXCL6 and CXCL8 or CXCL1–3 and CXCL5–8 that are recognized by CXCR1 or CXCR2 receptors expressed on neutrophils (90). High levels of CXCR2 have been associated with tumor size in PDAC (91), and a high number of TAN infiltrates can be considered an indication of higher malignancy and worse prognosis in PDAC, considering the expression of the CD177 neutrophil marker (92). A very recent study has demonstrated that lorlatinib, an FDA-approved ATP-competitive small-molecule tyrosine kinase inhibitor, is able to inhibit the growth of PDAC at primary and metastatic sites, through the regulation of neutrophil development and recruitment and by constraining neutrophil-induced tumor growth in the TME, in preclinical murine models of PDAC (93).

Myeloid-derived suppressor cells (MDSCs) are immature myeloid cells with heterogeneous features; in fact, they can be phenotypically similar to monocytes defining the subpopulation

of mononuclear or monocytic (M-MDSCs or Mo-MDSCs), or they can be more like neutrophils and are called polymorphonuclear (PMN-MDSCs) or granulocytic (G-MDSCs or Gr-MDSCs) (94, 95). MDSCs can exploit their strongly immunosuppressive functions by several mechanisms. One of them is to reduce T-cell proliferation through the increased PD-L1 expression that binds to the PD-1 receptor on T cells inhibiting their activation and self-tolerance (96, 97). Moreover, MDSCs may positively regulate the expansion of immunosuppressive Tregs by IL-10-induced TGF-β and IFNγ production (98) or by the secretion of reactive oxygen species, such as ROS, Arg1, and iNOS (99). MDSCs can proliferate and accumulate in the TME through the stimulation received by some cytokines and chemokines produced after Yap signaling activation (100). High levels of MDSCs, both in peripheral blood and as tumor infiltrates, have been associated with low overall survival and metastasis development in patients, even if their immunosuppressive function is not common for all PDAC patients. Specifically, a detailed gene signature has revealed that immunosuppressive MDSCs can be defined as circulating STAT3/arginase1-expressing $CD14^+$ cells (101). MDSCs can also directly promote tumor growth and angiogenesis by MMP9 and VEGF secretion; in fact, they can produce high levels of matrix metalloproteinases that are able to dissolve extracellular matrix (ECM) and allow cancer cells to migrate and invade other tissues (102). In addition, through the secretion of high levels of VEGF and basic fibroblast growth factor (bFGF), they can sustain angiogenesis (103).

Tregs represent an immune subset population of T lymphocytes $CD4^+CD25^+FOXP3^+$ with an immunosuppressive function that is present in the TME of both PanIN and PDAC (104). A high number of Treg infiltrates in the tumor has been correlated to poor prognosis and metastasis development (105, 106). Tregs can interact with $CD11c^+$ DCs determining their reduced expression of MHC II, co-stimulatory molecules (CD40 and CD86), and indoleamine 2,3-dioxygenase (IDO), suppressing IFN-γ production and finally T-cell activation (107). Moreover, PDAC patients have shown an imbalance in the number of Tregs and Th17 cells, with a notable increase in their ratio, determining important changes in cytokine production, such as higher levels of IL-10 and TGFβ, and lower levels of IL-23, INF-γ, and IL-17, with a consequent T-cell inactivation (108).

On the other side, very recently, Tregs have been correlated to an antitumorigenic effect by immune response stimulation during pancreatic carcinogenesis. The depletion of Tregs in mouse models of spontaneous tumorigenesis both before and after the onset of PanIN determined a strong tumor progression, and in murine models of invasive tumors, the depletion of Tregs was not able to control cancer growth. A compensatory mechanism to increase other $CD4^+$ T cells and also immunosuppressive myeloid cells has been demonstrated as a consequence of Treg depletion (109, 110).

Besides immune cells, stromal cells in the TME can also influence cancer progression and immune response. A scheme of stroma-mediated interaction in PDAC is proposed in **Figure 1**. Cancer-associated fibroblasts (CAFs) play a crucial role in this context, since they are responsible for ECM deposition and remodeling. They are the most abundant population representing up to 85% of all stromal cells, and are also involved in a complex crosstalk with cancer and immune cells (111). Fibroblasts do not show a characteristic expression of specific surface markers; thus, it is very difficult to give a precise definition of their origin and whether they convert in CAFs during tumor progression. In a human cancer biopsy, CAFs can be identified for exclusion due to the absence of epithelial, endothelial, and leukocyte markers; the lack of molecular mutations by cancer cells; and the characteristic elongated morphology (112). A common consensus is that CAFs have a tumor-suppressive function at the early state of tumorigenesis, since depletion of an αSMA^+ subset of fibroblasts in a PDAC mouse model led to undifferentiated tumors with enhanced hypoxia, increased tumor invasion, and decreased animal survival (113), but during tumor progression, they can dynamically change their role. CAFs are able to produce fibrotic compounds, such as collagens, hyaluronic acid, and fibronectin, contributing to ECM deposition (114) (better discussed below). In addition, CAFs can secrete chemokines, cytokines, growth factors, miRNAs, extracellular vesicles, and metabolites to communicate with cancer cells and other TME players to promote tumor progression (115). Over time, different CAF subpopulations have been defined: myofibroblastic CAFs (myCAFs) that express α-SMA and are responsible of TGFβ production; inflammatory CAFs (iCAFs) that produce inflammatory mediators, such as cytokines, chemokines, and complement complex; and antigen-presenting CAFs (apCAFs) that express CD74 and MHC class II and interact with $CD4^+$ T cells. This apCAF subpopulation, however, lacks the necessary co-stimulatory molecules to activate T cells, and is, therefore, supposed to have an immunosuppressive role by acting as a decoy tilting the ratio of $CD8^+$ to Tregs.

Many authors have confirmed this classification by scRNA-seq, in both mouse and human tissues (50, 52, 53, 116, 117). iCAFs are associated with an activity of immune modulation, which is crucial during PDAC progression, and are activated in a paracrine manner by cancer cells through the secretion of stimulating factors, but they are located distant from cancer cells and myCAFs. Once activated, iCAFs can produce inflammatory mediators, such as IL-6, IL-8, IL-11, CXCL1, CXCL2, CXCL12, and leukemia inhibitory factor (LIF). Moreover, they show an activation of several inflammatory pathways, such as IFN-γ response, TNF/NF-κB, IL-2/STAT5, and IL-6/JAK/STAT3 signaling in humans (118). iCAFs can modulate the immune response at different levels, inducing M2 polarization of TAMs, accumulating MDSCs, TANs, regulatory B-cells (Bregs), and Th17 cells in the tumors, but also directly decreasing $CD8^+$ T cells through the production of the βig-h3 stromal protein in a TGF-β-dependent manner (119). Recently, an additional subtype has been identified in loose-type stromal PDAC compared to dense-type stromal PDAC and named meCAFs, representing a highly activated metabolic state and associated with a poor prognosis but a better response to

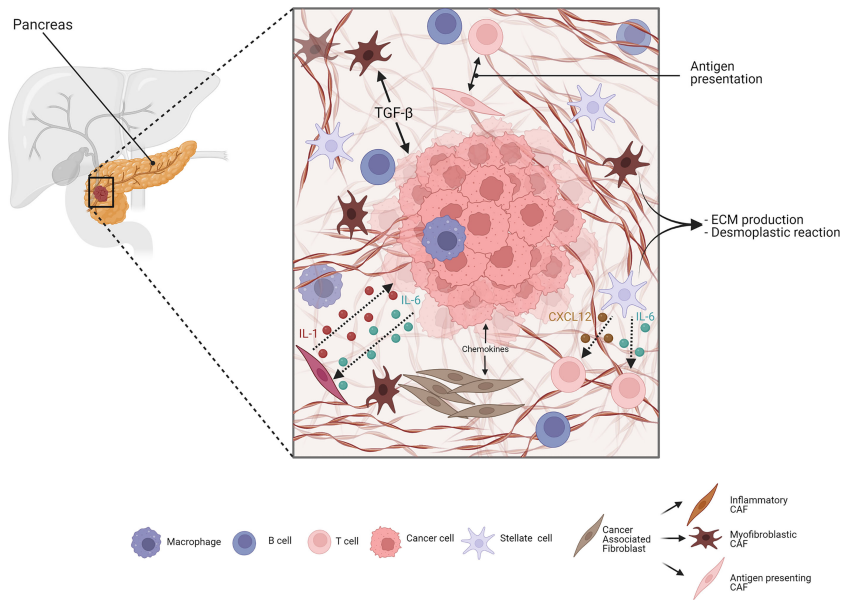

FIGURE 1 | Simplified scheme of stroma-mediated interaction in PDAC. Cancer-associated fibroblasts (CAFs) are crucial elements of the pancreatic ductal adenocarcinoma (PDAC) stroma. They include different subtypes: myofibroblastic, inflammatory, and antigen-presenting subtypes. Both cell–cell and paracrine interaction CAFs and PDAC cells are involved in manipulating the stroma. The cancer cells can induce, through transforming growth factor-β (TGFβ) signaling, the surrounding CAFs to adopt a myfibroblastic phenotype. Similarly, cancer cells produce IL-1, reprogramming CAFs to inflammatory CAFs, which, in turn, produce chemokines like IL-6 and sustain cancer growth. Antigen-presenting CAFs, expressing MHC class II molecules, modulate the immune cells in the stroma. Pancreatic stellate cells (PSCs) are mainly responsible for ECM deposition during PDAC, and are also able to modulate the immune response through the production and secretion of cytokines, such as CXCL12 and IL-6, negatively affecting T-cell activity and migration. Adapted from "PDAC histology" by BioRender.com (2022). Retrieved from https://app.biorender.com/biorender-templates.

immunotherapeutic inhibition of PD-1 (120). In addition, a new CAFs subset, named complement-secreting CAFs (cs-CAFs), has been identified in early PDAC by scRNA-seq, showing high enrichment for the components of the complement system, such as C3, C7, CFB, CFD, CFH, and CFI, and being able to modulate the immune response in the tumor (121).

Interestingly, these CAF subpopulations show a level of plasticity being able to shift among the different phenotypes (52), thus suggesting that TME modulation to improve therapies based on immunological agents is theoretically possible.

Pancreatic stellate cells (PSCs) are resident cells in the pancreas and are mainly responsible for fibrosis deposition during PDAC (122), and their crucial role in pancreatic cancer progression has been investigated more deeply in recent years. PSCs were isolated for the first time in 1982 by Watari and colleagues who identified, in murine pancreas, cells containing vitamin A droplets after an excess of retinoid administration (123). In addition to several physiological functions, such as pancreatic architecture maintenance, tissue homeostasis, induction of amylase secretion, phagocytosis, and ECM turnover (124), their contribution to pathological mechanisms has also been elucidated, leading to the confirmation that PSCs can influence the dense desmoplastic reaction, tumor progression, metastasis, and resistance to therapies (125). They are in a quiescent state and can respond to different stimuli, such as cytokines/transcription factors, non-coding RNAs, oxidative stress-related factors, hyperglycemia, and ion channels and calcium signaling, to perform their activities (126). Activated PSCs (aPSCs) acquire a myofibroblast-like phenotype and produce ECM. In addition to many physiological functions, aPSCs can play important roles also in pathological conditions, such as PDAC, being responsible for the abundant desmoplastic reaction that surrounds cancer cells reducing accessibility to drugs. During early tumorigenesis, an intense communication between stromal and cancer cells induces the reprogramming of mesenchymal cells, and aPSCs can represent a valid cellular source of CAFs (127). Despite these two populations expressing similar markers, nowadays they are considered as separate cellular entities; in fact, in experiments of three-dimensional co-culture systems that reproduce the interactions between CAFs and cancer cells, two spatially separated, mutually exclusive, dynamic, and phenotypically distinct CAF subtypes have been identified, but the difference between aPSCs and CAFs still represents an important topic of discussion (116). Besides the fibrotic activity, aPSCs are also able to regulate the immune response during PDAC progression through the production and secretion of cytokines, such as CXCL12, impairing the migration of $CD8^+$ and $CD4^+$ T cells, NK cells, and Tregs to the juxtatumoral compartment in proximity of the tumor site (57). By several mechanisms, aPSCs can suppress T-cell activity through IL-6 secretion, i.e., inhibiting T effector cell migration, activating Tregs and TAMs, and impairing the balance in the Tregs/T effectors ratio (128).

During the last few years, many authors have contributed to describe the cellular heterogeneity in PDAC, but much is to be learned about how stromal cells, such as CAFs, are able to modulate cancer cells. Recently, Ligorio et al. identified a single-cell population that can switch towards invasive and proliferative phenotypes, marked by MAPK and STAT3 activation (129). This elegant work combined scRNA-seq and proteomics to highlight that CAFs play an important role in modulating cancer cell heterogeneity, and findings obtained in model systems were then translated to primary human tumors, in order to contextualize these cellular populations in the architecture of PDAC tissue. Around 2015, some authors had demonstrated that PDAC is the result of a mosaic in which cancer cells are "tumor islands" and CAFs represent the "sea" all around them. This nice view led to the convincement that the interaction between PDAC cells and CAFs are not strictly defined as stimulatory or inhibitory, but modulations of stromal content can determine a different behavior in specific tumor areas (130–132). Very recently, Grünwald and colleagues defined subTMEs as functional units with specific epithelial and immune phenotypes that are able to influence the progression of PDAC (133). SubTMEs can be classified into "deserted" regions (regions characterized by the presence of spindle-shaped fibroblasts), "reactive" regions (regions with plump fibroblasts containing enlarged nuclei), and "intermediate" regions (with mixed features and an intermediate level of both characteristics). Molecular and immune features are different in the three types of subTMEs, but the key message of this study is the involvement of stroma in influencing the response to chemotherapy as well. The authors showed that the deserted subTME has a chemoprotective role, associated with a poor response, leading to the conclusion that future approaches aimed to attenuate the deserted TME state could be able to improve therapy outcome.

Keynote

Intratumoral heterogeneity is the major obstacle for effective PDAC therapies. Tricky cellular interactions support tumor progression and resistance to current treatments. The intuition of different types of communication of cancer cells with stromal and immune compartments, in several spatial architecture contexts, is the starting point to understand that PDAC needs a novel approach. Taking into consideration the multiple faces of the disease, opposing pro-tumor behaviors and enhancing tumor-suppressive ones, could be a valuable strategy to fight PDAC.

THE EMERGING ROLE OF ECM COMPONENTS IN IMMUNE ESCAPING

A desmoplastic reaction is the deposition of a dense layer of fibrotic ECM that happens as a response to an insult of different nature such as tissue damage or neoplastic growth. Desmoplasia is in fact a hallmark of PDAC, where it probably originates as an attempt to restrain neoplastic cells (134). In fact, several studies showed that impairing the stroma deposition lead to a more aggressive disease (113, 135, 136). PDAC cells, however, remodel ECM to escape the confinement and interact with many ECM proteins to support its growth. It is well known that the protein-rich and collagen-based ECM plays an important role in PDAC oncogenesis (137). This dense matrix is composed of type I, type III, and type IV collagens, glycoproteins, proteoglycans, and glycoaminoglycans that altogether support tumor progression, metastatization, and therapy resistance (138, 139).

Recently, several studies also showed that ECM components also play a role in immune regulation.

In PDAC, collagens are the most abundant ECM proteins where they form the main scaffold for the TME. The binding of ECM collagens with integrins and receptors such as DDR-1 expressed on the surface of neoplastic cell promotes proliferation and migration of PDAC (137). Collagen overproduction and consequent fibrosis seems to be inversely correlated with immune infiltration in PDAC, mainly by providing a barrier for immune cells and activating signaling that promotes immune escape. Focal adhesion kinase (FAK) is the main driver of collagen production in PDAC where it is hyperactivated. The expression of this protein in PDAC correlates with fibrosis and immune suppression (140). Loss of FAK in PDAC caused not only a decrease in collagen deposition but also an increase in effector T-cell infiltration in PDAC models (140). Sharma et al. (141) targeted the hexosamine biosynthesis pathway (HBP), a shunt pathway of glycolysis with 6-diazo-5-oxo-l-norleucine to disrupt collagen deposition in the TME, causing an increase in immune infiltration and an enhancement of immune checkpoint inhibitory (ICI) therapy, such as anti-PD1. Deng et al. (142) showed that the binding of collagen I to DDR1 promoted PDAC growth, and it was also the major stimulus for CXCL5 production mediated by a DDR1/PKCθ/SYK/NF-κB signaling cascade. CXCL5 production and secretion resulted in the recruitment of TANs, which not only favored immune suppression but also supported cancer cell invasion and metastasis by formation of neutrophil extracellular traps. These traps are web-like extracellular fibers formed by neutrophils in the ECM, consisting of chromatin DNA filaments, lactoferrin, myeloperoxidase (MPO), histones, and elastase that are able to activate PDAC invasion and also cause apoptosis of cytotoxic T cells (142).

In addition to collagen, the TME also contains high levels of glycoproteins that confer an immunosuppressive status.

Galectins are small glycoproteins that actively support cancer growth and also immune escaping. These proteins are potent negative regulators of the immune cell functions, and they are highly expressed in cancer where they favor immune escaping mainly by inducing $CD8^+$ T-cell death (143). Galectin-1 has been found to be upregulated in the PDAC, and is lowly expressed in long-term (≥10 years) survivors (144). Orozco et al. showed that loss of Galectin-1 in Ela-KrasG12Vp53$^{-/-}$Lgals1$^{-/-}$ murine models leads to a reduced stromal activation and favored a transition in an immune permissive TME causing an effector T-cell infiltration (145). Moreover, Galectin-1 can be secreted by aPSCs mediating the immunosuppression of $CD8^+$ T cells and promoting T-cell apoptosis, contributing to the

immunosuppressive TME (146). Galectin-3 is also secreted by PDAC in the TME, where it inhibits T-cell proliferation (147). Zhao et al. (148) demonstrated that Galectin-3 released by PDAC stimulates the production of the M2 macrophages inducer IL-8 on PSCs *via* ITGB1/NF-κB signaling. Daley et al. (149) showed that Galectin-9 is also present in PDAC TME where it promotes tumor progression with its ligand Dectin-1. This Galectin ligand is a member of the C-type lectin family of pattern recognition receptors and is present on the surface of myeloid-monocytic lineage cells, especially in macrophages. Dectin-1 is highly expressed in PDAC TAMs, where it promotes the M2 phenotype upon activation by ligation with Galectin-9. Daley et al. showed that anti-Galectin-9 immunotherapy triggered an immune reprogramming in TAMs favoring the M1 phenotype and also provoked an increase in immune infiltration and consequent tumor reduction. This finding paves the way for the development of new treatment strategies for PDAC. In fact, Galectin-9 is also known to be a potent stimulator of T-cell exhaustion and a major cause for immunotherapy failure. Yang et al. (150) showed that Galectin-9 binds both PD-1 and TIM-3 causing both cell apoptosis and T-cell exhaustion in several types of tumors, and they also demonstrated that anti-Galectin-9 immunotherapy was an effective treatment.

Mucins are a family heavily glycosylated proteins that are involved in many physiological mechanisms (151, 152). Mucin secretion is the main characteristic of PDAC precursor lesions (IPMNs) (153). Mucins are also highly expressed in PDAC TME; in fact, most of the recent studies that utilized scRNA-seq to characterize PDAC samples identified a cluster of mucin-producing cells especially in the patients with a more aggressive disease (51, 154, 155). This evidence suggests that mucins play a major role in PDAC carcinogenesis, not only supporting PDAC development by activating several oncogenic pathways, but also sustaining cancer cells to escape the immune surveillance by multiple mechanisms.

MUC1 has been associated with a decreased interaction of the NK cell receptor (NKG2D) with the tumor-associated ligand MICA (major histocompatibility complex class I-related chain A) by the involvement of Galectin-3, which is differentially expressed in pancreatic cancer (156, 157). In detail, Galectin-3 can bind the NKG2D-binding site of MICA through modified core 2 O-glycans of MUC1, thus inactivating NK cells and inhibiting TNF-mediated apoptosis of cancer cells, promoting the development of distant metastasis (158, 159). Moreover, the purification of glycosylated MUC1 from ascitic fluid of pancreatic patients have demonstrated that this mucin can influence DC maturation, due to the limited processing and presentation that retains MUC1 into the early endosomes (160). DCs can also express MUC1 on their surface, impairing Toll-like receptor (TLR) activation (161); in fact, the deletion of *MUC1* gene induces DC response through the activation of TLR4 and TLR5 and the production of co-stimulatory molecules, such as CD40, CD80, and CD86, in addition to the secretion of pro-inflammatory cytokines, such as TNF-α and VEGF (162). Also, MUC2 is able to regulate DC response by decreasing pro-inflammatory cytokines and increasing the secretion of IL-10 and TGFβ1, leading to an increased Treg recruitment (163). On the other side, MUC4 expressed by pancreatic cancer cells induces the apoptosis of cytotoxic T cells in a Fas-independent manner, reducing immune response (164).

Mucins have also been related to metastasis development, due to their deregulated glycosylation that leads to the expression of specific structures on their surface, named T, sTn, sLea, and sLex structures (165). MUC1, MUC2, MUC4, and MUC16 can express these structures functioning as ligands for selectins that are expressed on the surface of leukocytes and platelets, inducing the formation of aggregates and metastasis (166, 167).

MUC5AC determines the suppression of antitumor function of neutrophils, enhancing tumor progression and metastasis. Since IL-8 produced by cancer cells induces neutrophil migration, it has been demonstrated that MUC5AC silencing is able to increase IL-8 production and neutrophil activation in pancreatic cancer cells, showing the important role of this mucin in modulating immune response (168). On the other hand, MUC16 has been associated with long-term survival of pancreatic cancer patients, inducing the activation of T cells reactive to MUC16 neoantigens in response to primary tumors, which are progressively lost during metastasis development (169), attesting that mucin activities are very complex and are strictly related to specific cancer contexts showing different interactions among stromal, cancer, and immune cells.

Furthermore, TME in pancreatic cancer is strongly hypoxic, and PSCs are mainly responsible for pH and oxygen level modulation. In an acidic pH and hypoxic environment, PSCs, in turn, increase the secretion of HGF that can activate MET signaling in PDAC cells. MUC20 can contribute to cancer progression since hypoxia and low pH upregulate MUC20 expression that is able to physically interact with the MET receptor, being a crucial mediator between PSCs and cancer cell communication (170). In addition, hypoxia impairs immune cell function modulating both innate and adaptive immune response, by transcriptional regulation *via* hypoxia-inducible factors (HIFs) (171) and MUC1 is able to stabilize HIF-1α by reducing the intracellular levels of α-ketoglutarate (172).

In the last decade, the perspective about ECM in PDAC changes from an inert material to a key regulator of tumor progression. It is clear now that ECM components' ratios and quality are finely regulated by PDAC, which uses these molecules to communicate with TME cells and keep immunity at bay. The general view now is that ECM provides a barrier that not only protects PDAC cells physically, but also provides a plethora of immunesuppressive signals. A huge effort has been made to develop new strategies to disrupt these ECM tumor-promoting functions; some of these sound promising, while many failed. Probably, the main reason is that we are still missing many pieces of knowledge about the complex interactions happening in the ECM. New technologies may help us in the near future in this context. The arising technologies of ST and proteomics will give us an unprecedented look into PDAC. The two main spatial technologies Visium (10X Genomics) and GeoMx (Nanostring) are able to map on a histological image the entire transcriptome and the expression of hundreds of proteins simultaneously at a

resolution of few dozens of microns, helping researchers to precisely identify and characterize the myriad of interactions that happen in PDAC TME. Moreover, in 2022, two new spatial technologies have been presented, the Xenium (10X Genomics) and CosMx Spatial Molecular Imager (Nanostring) that will move the ST and proteomics at a single-cell and even sub-cellular level resolution, increasing exponentially the understanding and knowledge of PDAC ECM interactome in the years to come.

Keynote

The hypothesis of a crucial role played by ECM in PDAC progression is a well-demonstrated thesis. Exploiting the ECM, with all the signals supporting tumor growth and helping cancer cells in immune evasion, is a successful approach. However, we need a deeper understanding of specific mechanisms and interactions in the TME. Many studies are focusing on this aspect and future directions are all aimed to compose the puzzle, piece by piece.

THERAPEUTIC STRATEGIES: HOW CAN WE HARNESS OUR KNOWLEDGE ABOUT TME TO IMPROVE PDAC TREATMENT?

Current treatment options for PDAC are very limited in their efficacy. Chemotherapy with gemcitabine as a single agent has been used for many years (6), but the overall survival of patients remained extremely low; thus, the combination therapy with different chemotherapeutic agents became more effective and entered the clinical practice. Gemcitabine/nab-paclitaxel and FOLFIRINOX (5-fluorouracil, leucovorin, irinotecan, and oxaliplatin) are still valid options, but they are associated with many side effects (10, 12). Recently, a novel second-line treatment based on nanoliposomal Irinotecan (Nal-IRI) proved to be effective. The NAPOLI1 trial (173, 174) showed the efficacy of Nal-IRI in combination with 5-fluorouracil and leucovorin to increase both overall survival and progression-free survival (PFS) in both non-metastatic and metastatic patients. The HOLIPANC trial (175) proved that neoadjuvant combination of Nal-IRI, oxaliplatin, 5-fluouracil, and folinic acid (NAPOX) had a considerable antitumor effect and increased overall survival of patients with a metastatic disease.

Immunotherapy has received much consideration in PDAC, but without reaching high success rate, due to the complex and not fully understood relationship between immune and cancer cells in the TME, as largely described above. Once activated, T cells express PD-1, a transmembrane glycoprotein type I belonging to the immunoglobulin superfamily CD28 that is bound by its ligands, PD-L1 and PD-L2, expressed on antigen-presenting cells (APCs) and cancer cells, resulting in T-cell suppression and exhaustion (176). PD-1 expression is transient and can decrease in the absence of signaling through the T-cell receptor (TCR); otherwise, it is chronically activated in the presence of an epitope target, such as in chronic viral infections and in cancer (177). Less is known about PD-L1 expression on T cells, but recently, it has been demonstrated that its ligation stimulates intracellular signaling with a suppressive activity, similar to PD-1 (178). Moreover, PD-L1 on T cells is able to induce the M2-like macrophage differentiation *via* STAT6 signaling and to suppress neighboring effector T cells (178). Cytotoxic T lymphocyte antigen 4 (CTLA-4) is another important inhibitory checkpoint that determines the suppression of the T cells' response by binding CD80/CD86 on APCs (179). However, the function of CTLA-4 is not completely understood, and some authors have proposed that the CTLA-4 cytoplasmic domain could not be directly involved in the transmission of inhibitory signals, but could be mainly responsible in regulating the access of CD28 receptors to their shared ligands (180). The aberrant overexpression of PD-1, PD-L1, and CTLA-4 is very common in the TME of PDAC, and they still represent good targets for immunotherapy, but targeting one of them as monotherapy approach (immune checkpoint inhibitors ICIs) has not granted good response in PDAC patients as occurred for other types of cancer (181–184). However, recent studies showed that the modulation of the complex cell intrinsic and extrinsic of TME may effectively increase immunotherapy efficacy. Carbone et al. (185) showed that intratumoral injection of the Toll-like receptor 9 agonist IMO-2125 in combination with anti-PD1 activated an immune-suppressive to immune-permissive transition of the TME in PDAC models with both high and low immunogenic potential. Toll-like receptor 9 (TLR-9) is a pattern recognition receptor that is predominantly located in the cytoplasm of DCs, macrophages, NK cells, and other APCs. IMO-2125 activates TLR-9 signals that ignite the immune response with the production of cytokines such as IFNγ, IL-6, and IL-12. The combination of this drug with anti-PD1 not only provoked a relevant reduction of the tumor in the primary site, but also showed an abscopal effect on distant sites as a result of the peculiar efficacy of IMO-2125 to prime the adaptive immune response.

A phase II clinical trial tested the efficacy of the combination of PD-1 inhibition (pembrolizumab) with a CXCR4 antagonist (BL-8040 also known as motixafortide) in patients with metastatic disease refractory to one or more previous lines of chemotherapy (186). BL-8040 is a small synthetic peptide that binds to and inhibits CXCR4 (187, 188). CXCR4 binds to its ligand CXCL12/SDF1, which is constitutively expressed in the bone marrow, and inhibits the mobilization of CXCR4 expressing immune progenitor cells. Indeed, numerous preclinical studies have shown that CXCR4 blockade through BL-8040 treatment stimulated mobilization of T, B, and NK cells from lymph nodes and bone marrow into the periphery (188, 189). Moreover, in murine models of lung cancer, BL-8040 also promoted selective reduction of Tregs (190).

BL-8040 monotherapy and in combination with pembrolizumab promoted an increase in the density of T cells ($CD3^+$, $CD4^+$, and $CD8^+$) and activated cytotoxic T cells ($CD8^+$ granzyme B^+) and a decrease in immunosuppressive elements such as MDSCs in the TME.

This is in line with the results from a recent study demonstrating that the chemokine CXCL12 derived from CAFs

impairs the trafficking of multiple immune cell types within the TME, thus favoring an immunosuppressive environment (191). The authors reported that BL-8040 in combination with pembrolizumab led to disease control in nearly a third of the patients with heavily pretreated pancreatic cancer (186). Successively, an expansion cohort of the study integrating BL-8040 and pembrolizumab with the NAPOLI-1 chemotherapy regimen was initiated (192). Enrolled patients had *de novo* metastatic PDAC and disease progression following first-line gemcitabine-based treatment. BL-8040 and pembrolizumab in combination with nanoliposomal irinotecan, fluorouracil, and folinic acid showed a potential for higher responses without added toxicity. Currently, the effects of BL-8040 and the anti-PD1 cemiplimab in combination with gemcitabine and nab-paclitaxel for the first-line treatment of metastatic PDAC have been tested in a phase II study (NCT04543071).

Another approach is targeting the CD40 member of the tumor necrosis factor family. CD40 is expressed on immune cells, and its stimulation through the use of agonists has been shown to increase anticancer activity (193, 194) by improving T-cell-dependent and -independent immune responses. Although preliminary, some encouraging data on the feasibility of the use of CD40 agonists are starting to be available. The phase I study NCT00711191 tested the therapeutic effect of the agonist CD40 monoclonal antibody (mAb) CP-870,893 in combination with gemcitabine in patients with advanced PDAC (195). Twenty-two patients with advanced chemotherapy-naïve PDAC, twenty of which with metastatic disease, were enrolled in the study. The results showed that combination of CP-870,893 with gemcitabine was well tolerated and provided some encouraging, although preliminary, evidence of efficacy. Following treatment, a systemic immune response was detected, characterized by leukocyte trafficking, cytokine production, and cellular activation. Moreover, thanks to metabolic imaging, the authors showed that many patients presented an overall decrease in the metabolic activity of the primary pancreatic lesion. Nevertheless, the responses of metastatic lesions to treatment were heterogeneous. These findings suggest that the CD40 agonist can potentially improve the efficacy of conventional therapies in PDAC treatment, but further studies are required (195).

Another phase I study (NCT03214250) tested the agonist CD40 mAb sotigalimab with gemcitabine and nab-paclitaxel, with or without anti-PD1 mAb nivolumab (196). The results of this study showed that this combination had clinical promise and a clinically manageable safety profile in patients with metastatic PDAC. Objective responses were documented in 14 of 24 dose-limiting toxicity-evaluable patients. Median PFS was 11.7 months (95% CI, 7.1 to 17.8), and median overall survival was 20.1 months (95% CI, 10.5 to not estimable). Moreover, systemic modulation of dendritic cells and B cells was detected, together with activation of $CD4^+$ and $CD8^+$ T cells. These data support the hypothesis that the addition of a CD40 agonist to chemotherapy activates innate and adaptive immune response in PDAC patients. This is also in line with observation from studies utilizing CD40 mAb in murine models of PDAC (197, 198). This approach is now being tested in a randomized phase II clinical trial (NCT03214250).

The modulating effect of CD40 agonists on TME is also confirmed by another clinical trial (NCT02588443). Specifically, the results showed decreased density of tumor stroma, increased DC activation, shift of TAM polarization from M2-like to M1-like, as well as increased T-cell infiltration, proliferation, and activation status (199).

Overall, these results suggest that CD40 agonists can potentially benefit patients by improving response to chemotherapy or immunotherapy and, since they act through distinct mechanisms compared to ICIs, may even provide an alternative for cancers refractory to ICIs.

Some of the possible strategies to overcome immunosuppression are presented in **Figure 2**.

The introduction of cellular immunotherapy has been a paradigm shift in cancer treatment.

Cell therapy based on chimeric antigen receptor (CAR) is one of the most studied approaches. CAR-T are genetically engineered T cells expressing specialized receptors that recognize and attack cancer cells (200), which are typically infused systemically. Although CAR-T therapy has shown promise in the treatment of hematological malignancies, its application in solid tumors has been hampered by a number of factors, such as immunosuppressive TME, sub-optimal survival, and ability of T cells to reach the tumor site, insufficient tumor infiltration, and limited choice of antigens (201, 202).

As previously described, the unique PDAC TME presents multiple challenges for the current therapeutic alternatives. CAR T cells are also affected by the numerous cellular components and extracellular matrix, which translates in a physical barrier impairing their detection and infiltration ability (203). Moreover, TME immune cells directly suppress T-cell activation through the release and the expression of a variety of factors that limit T-cell antitumor response (204). Another limit is represented by the deep heterogeneity observed in PDAC, both among the tumor cells as well as within the TME. This has drastically held up the identification of target antigens in PDAC (129). Despite these limitations, a number of targetable antigens suitable for cellular immunotherapy are currently being tested in both preclinical and clinical studies and include CEA, CD24, HER2, PSCA, MUC1, and MSLN (205, 206). Given the complexity of PDAC and its TME, and generally, to expand the use of CAR T cell therapy to solid cancers, cellular immunotherapies are also being explored in combination with other therapeutic approaches (207, 208). Recent studies have shown that chemotherapeutic drugs can be utilized in PDAC as priming agents before CAR T therapy in order to counteract the action of immunesuppressive cells, reduce autoimmunity, reduce tumor burden, sensitize cancer cells to immunotherapy, and improve CAR T cell survival rate *in vivo* (207).

In a phase I trial (NCT02159716), aimed at investigating the safety and efficacy of lentiviral-transduced CARs (209), subjects affected by solid cancers resistant to chemotherapy (PDAC, mesothelioma, and ovarian cancer) were administered anti-MSLN CAR T cells intravenously with and without cyclophosphamide pre-

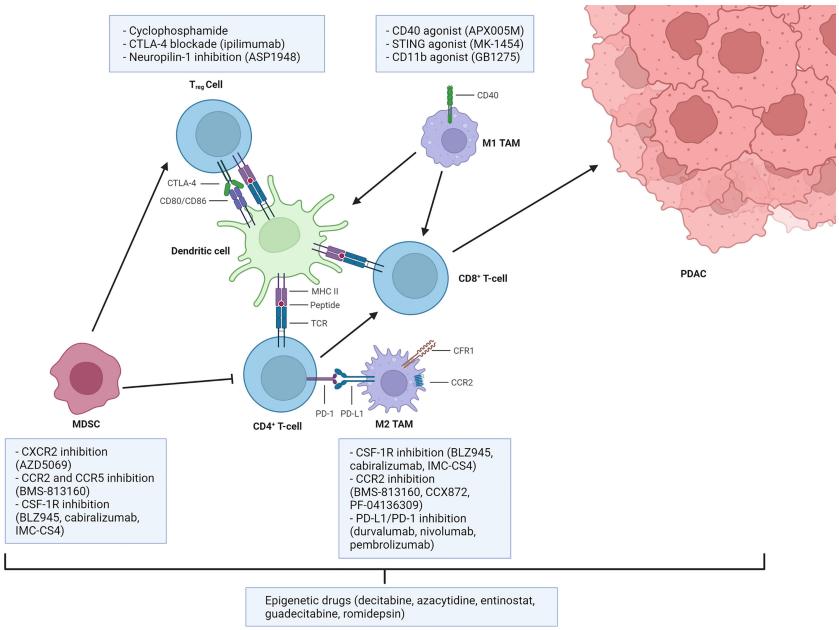

FIGURE 2 | Main strategies to overcome myeloid and Treg-mediated immunosuppression. Dendritic cells or inflammatory macrophages (TAMs M1) sustain the antitumor immune response through antigen presentation. Myeloid-derived suppressor cells (MDSCs), anti-inflammatory tumor-associated macrophages (TAMs M2), and regulatory T (Treg) cells regulate these processes by exploiting inhibitory pathways, thus establishing an immunosuppressive tumor microenvironment. Some of the most clinically relevant therapeutic strategies available to target those pathways are reported. Created with BioRender.com.

treatment. Indeed, the priming with chemotherapy was associated with an increase in CAR T cell expansion in peripheral blood, which peaked at day 14 after administration, but became undetectable after 6 months. Immune escape operated by tumors though upregulation of immune checkpoint receptors can also lead to CAR T cell inhibition (210).

The FDA has approved for solid tumors different checkpoint inhibitors, including mAbs against PD-1 and PD-L1 (211, 212). In the context of PDAC, CAR T cells against immune checkpoint inhibitors PD-1/PD-L1 were tested in PD-L1-overexpressing PDAC cells and in PDAC mouse models. Both CAR T cells induced tumor regression and reduced T-cell exhaustion (213). To overcome some of the limitations connected with the use of autologous CAR T cells, the implementation of allogeneic CAR T cells is being explored, as well as CAR NK cells and TIL therapy. Allogenic CAR T cells may offer a cheaper and more standardized alternative, which does not require individual-specific manufacturing. T cells can be collected from healthy donors, expanded, and stored, thus reducing time, cost, and variability for each treatment (214, 215). The main limitation with allogenic CAR T therapy is the potential risk for graft-versus-host disease (GvHD). Lack of compatibility between donor and recipient human leukocyte antigen (HLA) can lead to an immune response that will result in the elimination of the allogenic CAR T cells (216). Given its increased availability, next-generation sequencing is now being progressively more used to determine HLA compatibility; at the same time, gene editing technologies can be used to "hide" allogeneic CAR T cells from the host immune system by eliminating TCR expression (217).

CAR NK cells are also being evaluated as an alternative to allogenic CAR T cells (218). NK cells are components of the innate immune system that can recognize targets without prior sensitization, making them ideal candidates to deploy for therapeutic use against cancer (219). NK cells that recognize self-cells inhibit their own cytotoxic functions; therefore, more encouraging progresses have been made with allogeneic NK cell therapy in preclinical models and clinical trials. Indeed, it has been shown that autologous NK cells derived from cancer patients display less cytotoxicity compared to allogeneic NK cells, derived from healthy individuals (220, 221). In a recent study, Teng et al. employed, in a metastatic humanized pancreatic cancer mouse model, NK cells isolated from umbilical cord blood engineered to express a CAR construct recognizing prostate stem cell antigen (PSCA) and soluble IL-15 to improve antitumor response (222). The authors report an increase in cytotoxic function and survival, as well as reduced tumor growth and prolonged persistence of NK cells within the TME (up to 48 days).

Currently, two clinical trials (NCT02839954 and NCT03941457) are investigating the use of allogeneic NK cell infusions in PDAC, but no result has been published so far besides a case report from NCT03941457 showing that ROBO1-targeting NK cell infusions did not lead to serious toxicity (223). ROBO1 (Roundabout Guidance Receptor 1) mediates cellular responses to molecular guidance cues in cellular migration including neural axon guidance during development and has been found to be overexpressed in PDAC. While allogenic NK cells are a promising approach, one of the main limitations is the

limited number of cells that a single donor can provide. Therefore, the use of NK cell lines is also being investigated (224). In a phase I clinical trial, CAR NK-92 cells directed against MUC1 and PD-1 were tested on a variety of cancers expressing both proteins (225). No severe adverse effects were observed, and out of 13 subjects, 9 presented stable disease, one presented progressive disease, while the other 3 were withdrawn from the study. In an orthotopic PDAC model, treatment with anti-ROBO1 CAR NK-92 cells was reported to synergize in combination with brachytherapy (226); moreover, CAR NK-92 cells were well tolerated when administered as a case study in an individual with metastatic pancreatic cancer, and the patient achieved stable disease for 5 months (223). In a recent study, Da et al. have investigated the antitumor efficacy of stimulator of interferon gene (STING) agonist cyclic GMP-AMP (cGAMP) in combination with CAR NK-92 cells targeting mesothelin in a preclinical mouse model of pancreatic cancer (227). The authors demonstrate that cGAMP can directly activate NK cells and enhance the sensitivity of pancreatic cancer cells to the cytotoxicity of NK cells. Moreover, the combination of cGAMP with CAR NK-92 cells targeting mesothelin improved antitumor efficacy (227).

Currently, three phase I/II clinical trials (NCT03941457, NCT03940820, and NCT03931720) are ongoing to evaluate the safety and efficacy of anti-ROBO1 CAR NK-92 cell therapy in PDAC and other solid tumors. In a more recent approach, CAR NK cells are manufactured from induced pluripotent stem cells (iPSCs). CAR iPSC NK cells are derived from triple-homozygous HLA donors, thus reducing the risk of rejection over multiple infusions, and with the advantage of working with a cell population that can grow indefinitely in an undifferentiated state *via* self-renewal (228, 229). Moreover, this approach also allows the increase of NK cell cytotoxicity through genetic engineering (230–236). Clinical and preclinical studies are still ongoing; however, CAR iPSC-NK cells could possibly provide a way for consistent production of NK cells with an identical phenotype.

TILs are a heterogeneous population of lymphocytes that naturally infiltrate solid tumors during the initial immune response (237). Briefly, TILs are isolated from a tumor biopsy and expanded *ex vivo*. The patient is then admitted to the hospital, to receive preconditioning non-myeloablative lymphodepletion, autologous TILs, and interleukin-2 (IL-2) infusion. Currently, the efficacy of TIL therapy in PDAC is being assessed in phase I and phase II clinical trials (NCT05098197, NCT03935893, and NCT03610490); however, TIL therapy has achieved positive clinical results in clinical trials for other cancers. The adverse effects reported are connected to the high dose of IL-2 required after infusion and to the lymphodepletion (238–241). Despite the limited clinical efficacy of cellular immunotherapy in PDAC, this field of research is still promising. Several strategies are being tested in order to overcome the challenges posed by the unique TME and heterogeneity of pancreatic cancer. Eventually, the development of off-the-shelf cellular immunotherapies will reduce manufacturing costs and time to treatment administration and result in overall less variability of the product.

Also, immunotherapy in combination with epigenetic therapy has recently been shown to be a promising approach (242, 243). Epigenetic alterations are prominent in PDAC (21) and may be involved in primary and acquired resistance to treatment by conferring fitness advantage to tumor cells (244). The first epigenetic drugs to be approved by the Food and Drug Administration (FDA) and European Medicines Agency (EMA) for certain hematological malignancies were inhibitors of histone demethyltransferases (DNMTis) and histone deacetylases (HDACis). However, first-generation epigenetic drugs like the DNMTis azacytidine and decitabine and the HDACis vorinostat and romidepsin have shown limited efficacy in the treatment of solid tumors (245). Second-generation compound drugs (the DNMTis zebularine and guadecitabine and the HDACis belinostat, panobinostat, tucidinostat, and valproic acid), while showing increased selectivity (245), have also shown considerable side effects. Recently, a new generation of epigenetic drugs is being developed and is entering clinical testing.

Epigenetic drugs have been tested in combination with other anticancer therapies, in order to overcome resistance and sensitize cancer cells to treatment.

In the context of immunotherapy of PDAC, it has been recently shown using the KPC mouse model that low-dose treatment with the hypomethylating drug decitabine (DAC) can potentiate the response to ICI therapy. The authors reported increased tumor necrosis, slowing of tumor growth, and increased numbers of $CD4^+$, $CD8^+$, $PD\text{-}1^+$ TILs. However, the authors also reported a potentially unfavorable increase of M2 macrophages, following DAC treatment, that are predicted to antagonize ICI antitumor effects (243), thus suggesting that combination therapy using epigenetic drugs and immunotherapy can be further optimized.

In the future, new approaches will be developed involving a combination of next-generation epigenetic drugs and novel immunotherapy modalities, like vaccine-based and adoptive T-cell therapies (246, 247). The success of PDAC treatment will depend on the successful integration of genomic, epigenomic, and transcriptomic data in order to identify precise biomarkers for patient stratification and subsequent implementation of personalized strategies.

Precision medicine approaches have been nicely discussed in a very recent review. Hosein and colleagues have focused on current preclinical and clinical evidence to show promising combinatorial approaches, with the important conclusive message of future directions that could take into account side effects of PDAC treatments, with the aim to improve the quality of life for many patients (248).

Keynote

PDAC is not completely strong and much vulnerability has been unveiled. Current research shows much more integrated approaches, to understand the disease from different points of view, but finally considering the unique context and unifying the huge efforts that many researchers are doing in the world. Last but not least, there is an urgent need for biomarkers to stratify patients and monitor therapies' efficacy. Circulating cancer cells

interact with immune cells influencing their function. The consideration of a systemic immune involvement should be a key point of view to understand surprising interactions.

CONCLUSION

Despite the existence of a number of therapeutic options, PDAC remains among the diseases with the most urgent and prevalent medical need. The principal reason is the limited success of current treatments, which can be attributed to both late diagnosis and trouble in reaching and killing cancer cells. The challenging improvement of present therapeutic opportunities also harbors the necessity to identify targets for early diagnosis and novel drugs. To this aim, translational research focused in understanding the complicated connections among cells in the TME is more and more valuable to hypothesize novel treatment approaches. In closing, a strong prevention campaign for patients with high-risk factors and familiar predisposition for this cancer could be useful to avoid advanced disease.

AUTHOR CONTRIBUTIONS

AA, AO, CC, and IG wrote the first draft of the paper. AO prepared the figures. CC and IG supervised the work. All the authors contributed to revise and approve the final version submitted.

FUNDING

The publication fee was funded by Biogem.

REFERENCES

1. Siegel RL, Miller KD, Fuchs HE, Jemal A. Cancer Statistics, 2021. *CA Cancer J Clin* (2021) 71(1):7–33. doi: 10.3322/caac.21654
2. Karamitopoulou E. Tumour Microenvironment of Pancreatic Cancer: Immune Landscape Is Dictated by Molecular and Histopathological Features. *Br J Cancer* (2019) 121(1):5–14. doi: 10.1038/s41416-019-0479-5
3. Ho WJ, Jaffee EM, Zheng L. The Tumour Microenvironment in Pancreatic Cancer - Clinical Challenges and Opportunities. *Nat Rev Clin Oncol* (2020) 17(9):527–40. doi: 10.1038/s41571-020-0363-5
4. Porembka MR, Mitchem JB, Belt BA, Hsieh CS, Lee HM, Herndon J, et al. Pancreatic Adenocarcinoma Induces Bone Marrow Mobilization of Myeloid-Derived Suppressor Cells Which Promote Primary Tumor Growth. *Cancer Immunol Immunother* (2012) 61(9):1373–85. doi: 10.1007/s00262-011-1178-0
5. Banerjee K, Kumar S, Ross KA, Gautam S, Poelaert B, Nasser MW, et al. Emerging Trends in the Immunotherapy of Pancreatic Cancer. *Cancer Lett* (2018) 417:35–46. doi: 10.1016/j.canlet.2017.12.012
6. Burris HA3rd, Moore MJ, Andersen J, Green MR, Rothenberg ML, Modiano MR, et al. Improvements in Survival and Clinical Benefit With Gemcitabine as First-Line Therapy for Patients With Advanced Pancreas Cancer: A Randomized Trial. *J Clin Oncol* (1997) 15(6):2403–13. doi: 10.1200/JCO.1997.15.6.2403
7. Vaccaro V, Sperduti I, Milella M. Folfirinox Versus Gemcitabine for Metastatic Pancreatic Cancer. *N Engl J Med* (2011) 365(8):768–9. doi: 10.1056/NEJMc1107627
8. Conroy T, Desseigne F, Ychou M, Bouche O, Guimbaud R, Becouarn Y, et al. Folfirinox Versus Gemcitabine for Metastatic Pancreatic Cancer. *N Engl J Med* (2011) 364(19):1817–25. doi: 10.1056/NEJMoa1011923
9. Von Hoff DD, Ervin T, Arena FP, Chiorean EG, Infante J, Moore M, et al. Increased Survival in Pancreatic Cancer With Nab-Paclitaxel Plus Gemcitabine. *N Engl J Med* (2013) 369(18):1691–703. doi: 10.1056/NEJMoa1304369
10. Tong H, Fan Z, Liu B, Lu T. The Benefits of Modified Folfirinox for Advanced Pancreatic Cancer and Its Induced Adverse Events: A Systematic Review and Meta-Analysis. *Sci Rep* (2018) 8(1):8666. doi: 10.1038/s41598-018-26811-9
11. Principe DR, Underwood PW, Korc M, Trevino JG, Munshi HG, Rana A. The Current Treatment Paradigm for Pancreatic Ductal Adenocarcinoma and Barriers to Therapeutic Efficacy. *Front Oncol* (2021) 11:688377. doi: 10.3389/fonc.2021.688377
12. Saung MT, Zheng L. Current Standards of Chemotherapy for Pancreatic Cancer. *Clin Ther* (2017) 39(11):2125–34. doi: 10.1016/j.clinthera.2017.08.015
13. Basturk O, Hong SM, Wood LD, Adsay NV, Albores-Saavedra J, Biankin AV, et al. A Revised Classification System and Recommendations From the Baltimore Consensus Meeting for Neoplastic Precursor Lesions in the Pancreas. *Am J Surg Pathol* (2015) 39(12):1730–41. doi: 10.1097/PAS.0000000000000533
14. Furukawa T. Pathology of the Pancreatic Cancer. *Nihon Rinsho* (2015) 73 Suppl 3:22–5. doi: 10.21037/tgh.2019.06.02
15. Haeberle L, Esposito I. Pathology of Pancreatic Cancer. *Transl Gastroenterol Hepatol* (2019) 4:50. doi: 10.21037/tgh.2019.06.02
16. Aguirre AJ, Nowak JA, Camarda ND, Moffitt RA, Ghazani AA, Hazar-Rethinam M, et al. Real-Time Genomic Characterization of Advanced Pancreatic Cancer to Enable Precision Medicine. *Cancer Discovery* (2018) 8(9):1096–111. doi: 10.1158/2159-8290.CD-18-0275
17. Qian ZR, Rubinson DA, Nowak JA, Morales-Oyarvide V, Dunne RF, Kozak MM, et al. Association of Alterations in Main Driver Genes With Outcomes of Patients With Resected Pancreatic Ductal Adenocarcinoma. *JAMA Oncol* (2018) 4(3):e173420. doi: 10.1001/jamaoncol.2017.3420
18. Dunne RF, Hezel AF. Genetics and Biology of Pancreatic Ductal Adenocarcinoma. *Hematol Oncol Clin North Am* (2015) 29(4):595–608. doi: 10.1016/j.hoc.2015.04.003
19. Fokas E, O'Neill E, Gordon-Weeks A, Mukherjee S, McKenna WG, Muschel RJ. Pancreatic Ductal Adenocarcinoma: From Genetics to Biology to Radiobiology to Oncoimmunology and All the Way Back to the Clinic. *Biochim Biophys Acta* (2015) 1855(1):61–82. doi: 10.1016/j.bbcan.2014.12.001
20. Biankin AV, Waddell N, Kassahn KS, Gingras MC, Muthuswamy LB, Johns AL, et al. Pancreatic Cancer Genomes Reveal Aberrations in Axon Guidance Pathway Genes. *Nature* (2012) 491(7424):399–405. doi: 10.1038/nature11547
21. Lomberk G, Blum Y, Nicolle R, Nair A, Gaonkar KS, Marisa L, et al. Distinct Epigenetic Landscapes Underlie the Pathobiology of Pancreatic Cancer Subtypes. *Nat Commun* (2018) 9(1):1978. doi: 10.1038/s41467-018-04383-6
22. Cancer Genome Atlas Research Network, Electronic address aadhe and Cancer Genome Atlas Research N. Integrated Genomic Characterization of Pancreatic Ductal Adenocarcinoma. *Cancer Cell* (2017) 32(2):185–203.e13. doi: 10.1016/j.ccell.2017.07.007
23. Puleo F, Nicolle R, Blum Y, Cros J, Marisa L, Demetter P, et al. Stratification of Pancreatic Ductal Adenocarcinomas Based on Tumor and Microenvironment Features. *Gastroenterology* (2018) 155(6):1999–2013.e3. doi: 10.1053/j.gastro.2018.08.033
24. Chan-Seng-Yue M, Kim JC, Wilson GW, Ng K, Figueroa EF, O'Kane GM, et al. Transcription Phenotypes of Pancreatic Cancer Are Driven by Genomic Events During Tumor Evolution. *Nat Genet* (2020) 52(2):231–40. doi: 10.1038/s41588-019-0566-9

25. Alexandrov LB, Nik-Zainal S, Siu HC, Leung SY, Stratton MR. A Mutational Signature in Gastric Cancer Suggests Therapeutic Strategies. *Nat Commun* (2015) 6:8683. doi: 10.1038/ncomms9683
26. Bettaieb A, Paul C, Plenchette S, Shan J, Chouchane L, Ghiringhelli F. Precision Medicine in Breast Cancer: Reality or Utopia? *J Transl Med* (2017) 15(1):139. doi: 10.1186/s12967-017-1239-z
27. Politi K, Herbst RS. Lung Cancer in the Era of Precision Medicine. *Clin Cancer Res* (2015) 21(10):2213–20. doi: 10.1158/1078-0432.CCR-14-2748
28. Collisson EA, Sadanandam A, Olson P, Gibb WJ, Truitt M, Gu S, et al. Subtypes of Pancreatic Ductal Adenocarcinoma and Their Differing Responses to Therapy. *Nat Med* (2011) 17(4):500–3. doi: 10.1038/nm.2344
29. Moffitt RA, Marayati R, Flate EL, Volmar KE, Loeza SG, Hoadley KA, et al. Virtual Microdissection Identifies Distinct Tumor- and Stroma-Specific Subtypes of Pancreatic Ductal Adenocarcinoma. *Nat Genet* (2015) 47 (10):1168–78. doi: 10.1038/ng.3398
30. Bailey P, Chang DK, Nones K, Johns AL, Patch AM, Gingras MC, et al. Genomic Analyses Identify Molecular Subtypes of Pancreatic Cancer. *Nature* (2016) 531(7592):47–52. doi: 10.1038/nature16965
31. Waddell N, Pajic M, Patch AM, Chang DK, Kassahn KS, Bailey P, et al. Whole Genomes Redefine the Mutational Landscape of Pancreatic Cancer. *Nature* (2015) 518(7540):495–501. doi: 10.1038/nature14169
32. Roberts NJ, Norris AL, Petersen GM, Bondy ML, Brand R, Gallinger S, et al. Whole Genome Sequencing Defines the Genetic Heterogeneity of Familial Pancreatic Cancer. *Cancer Discovery* (2016) 6(2):166–75. doi: 10.1158/2159-8290.CD-15-0402
33. Aung KL, Fischer SE, Denroche RE, Jang GH, Dodd A, Creighton S, et al. Genomics-Driven Precision Medicine for Advanced Pancreatic Cancer: Early Results From the Compass Trial. *Clin Cancer Res* (2018) 24 (6):1344–54. doi: 10.1158/1078-0432.CCR-17-2994
34. Lomberk G, Dusetti N, Iovanna J, Urrutia R. Emerging Epigenomic Landscapes of Pancreatic Cancer in the Era of Precision Medicine. *Nat Commun* (2019) 10(1):3875. doi: 10.1038/s41467-019-11812-7
35. Whyte WA, Orlando DA, Hnisz D, Abraham BJ, Lin CY, Kagey MH, et al. Master Transcription Factors and Mediator Establish Super-Enhancers at Key Cell Identity Genes. *Cell* (2013) 153(2):307–19. doi: 10.1016/j.cell.2013.03.035
36. Tang F, Yang Z, Tan Y, Li Y. Super-Enhancer Function and Its Application in Cancer Targeted Therapy. *NPJ Precis Oncol* (2020) 4:2. doi: 10.1038/s41698-020-0108-z
37. Baylin SB, Jones PA. Epigenetic Determinants of Cancer. *Cold Spring Harb Perspect Biol* (2016) 8(9):a019505. doi: 10.1101/cshperspect.a019505
38. Dhara S, Chhangawala S, Chintalapudi H, Askan G, Aveson V, Massa AL, et al. Pancreatic Cancer Prognosis Is Predicted by an Atac-Array Technology for Assessing Chromatin Accessibility. *Nat Commun* (2021) 12(1):3044. doi: 10.1038/s41467-021-23237-2
39. Sato N, Parker AR, Fukushima N, Miyagi Y, Iacobuzio-Donahue CA, Eshleman JR, et al. Epigenetic Inactivation of Tfpi-2 as a Common Mechanism Associated With Growth and Invasion of Pancreatic Ductal Adenocarcinoma. *Oncogene* (2005) 24(5):850–8. doi: 10.1038/sj.onc.1208050
40. Sato N, Fukushima N, Chang R, Matsubayashi H, Goggins M. Differential and Epigenetic Gene Expression Profiling Identifies Frequent Disruption of the Reln Pathway in Pancreatic Cancers. *Gastroenterology* (2006) 130 (2):548–65. doi: 10.1053/j.gastro.2005.11.008
41. Nones K, Waddell N, Song S, Patch AM, Miller D, Johns A, et al. Genome-Wide DNA Methylation Patterns in Pancreatic Ductal Adenocarcinoma Reveal Epigenetic Deregulation of Slit-Robo, Itga2 and Met Signaling. *Int J Cancer* (2014) 135(5):1110–8. doi: 10.1002/ijc.28765
42. Campbell PJ, Yachida S, Mudie LJ, Stephens PJ, Pleasance ED, Stebbings LA, et al. The Patterns and Dynamics of Genomic Instability in Metastatic Pancreatic Cancer. *Nature* (2010) 467(7319):1109–13. doi: 10.1038/nature09460
43. Somerville TDD, Xu Y, Miyabayashi K, Tiriac H, Cleary CR, Maia-Silva D, et al. Tp63-Mediated Enhancer Reprogramming Drives the Squamous Subtype of Pancreatic Ductal Adenocarcinoma. *Cell Rep* (2018) 25 (7):1741–55.e7. doi: 10.1016/j.celrep.2018.10.051
44. Roe JS, Hwang CI, Somerville TDD, Milazzo JP, Lee EJ, Da Silva B, et al. Enhancer Reprogramming Promotes Pancreatic Cancer Metastasis. *Cell* (2017) 170(5):875–88.e20. doi: 10.1016/j.cell.2017.07.007
45. Kim MP, Li X, Deng J, Zhang Y, Dai B, Allton KL, et al. Oncogenic Kras Recruits an Expansive Transcriptional Network Through Mutant P53 to Drive Pancreatic Cancer Metastasis. *Cancer Discovery* (2021) 11(8):2094–111. doi: 10.1158/2159-8290.CD-20-1228
46. Zhan T, Rindtorff N, Boutros M. Wnt Signaling in Cancer. *Oncogene* (2017) 36(11):1461–73. doi: 10.1038/onc.2016.304
47. Andricovich J, Perkail S, Kai Y, Casasanta N, Peng W, Tzatsos A. Loss of Kdm6a Activates Super-Enhancers to Induce Gender-Specific Squamous-Like Pancreatic Cancer and Confers Sensitivity to Bet Inhibitors. *Cancer Cell* (2018) 33(3):512–26.e8. doi: 10.1016/j.ccell.2018.02.003
48. Hyun K, Jeon J, Park K, Kim J. Writing, Erasing and Reading Histone Lysine Methylations. *Exp Mol Med* (2017) 49(4):e324. doi: 10.1038/emm.2017.11
49. Lavery WJ, Barski A, Wiley S, Schorry EK, Lindsley AW. Kmt2c/D Compass Complex-Associated Diseases [Kcdcom-Ads]: An Emerging Class of Congenital Regulopathies. *Clin Epigenet* (2020) 12(1):10. doi: 10.1186/s13148-019-0802-2
50. Bernard V, Semaan A, Huang J, San Lucas FA, Mulu FC, Stephens BM, et al. Single-Cell Transcriptomics of Pancreatic Cancer Precursors Demonstrates Epithelial and Microenvironmental Heterogeneity as an Early Event in Neoplastic Progression. *Clin Cancer Res* (2019) 25(7):2194–205. doi: 10.1158/1078-0432.CCR-18-1955
51. Peng J, Sun BF, Chen CY, Zhou JY, Chen YS, Chen H, et al. Single-Cell Rna-Seq Highlights Intra-Tumoral Heterogeneity and Malignant Progression in Pancreatic Ductal Adenocarcinoma. *Cell Res* (2019) 29(9):725–38. doi: 10.1038/s41422-019-0195-y
52. Elyada E, Bolisetty M, Laise P, Flynn WF, Courtois ET, Burkhart RA, et al. Cross-Species Single-Cell Analysis of Pancreatic Ductal Adenocarcinoma Reveals Antigen-Presenting Cancer-Associated Fibroblasts. *Cancer Discovery* (2019) 9(8):1102–23. doi: 10.1158/2159-8290.CD-19-0094
53. Hosein AN, Huang H, Wang Z, Parmar K, Du W, Huang J, et al. Cellular Heterogeneity During Mouse Pancreatic Ductal Adenocarcinoma Progression at Single-Cell Resolution. *JCI Insight* (2019) 4(16):e12912. doi: 10.1172/jci.insight.129212
54. Lin W, Noel P, Borazanci EH, Lee J, Amini A, Han IW, et al. Single-Cell Transcriptome Analysis of Tumor and Stromal Compartments of Pancreatic Ductal Adenocarcinoma Primary Tumors and Metastatic Lesions. *Genome Med* (2020) 12(1):80. doi: 10.1186/s13073-020-00776-9
55. Goel S, DeCristo MJ, Watt AC, BrinJones H, Sceneay J, Li BB, et al. Cdk4/6 Inhibition Triggers Anti-Tumour Immunity. *Nature* (2017) 548(7668):471–5. doi: 10.1038/nature23465
56. Carstens JL, Correa de Sampaio P, Yang D, Barua S, Wang H, Rao A, et al. Spatial Computation of Intratumoral T Cells Correlates With Survival of Patients With Pancreatic Cancer. *Nat Commun* (2017) 8:15095. doi: 10.1038/ncomms15095
57. Ene-Obong A, Clear AJ, Watt J, Wang J, Fatah R, Riches JC, et al. Activated Pancreatic Stellate Cells Sequester Cd8+ T Cells to Reduce Their Infiltration of the Juxtatumoral Compartment of Pancreatic Ductal Adenocarcinoma. *Gastroenterology* (2013) 145(5):1121–32. doi: 10.1053/j.gastro.2013.07.025
58. Feig C, Jones JO, Kraman M, Wells RJ, Deonarine A, Chan DS, et al. Targeting Cxcl12 From Fap-Expressing Carcinoma-Associated Fibroblasts Synergizes With Anti-Pd-L1 Immunotherapy in Pancreatic Cancer. *Proc Natl Acad Sci USA* (2013) 110(50):20212–7. doi: 10.1073/pnas.1320318110
59. Vayrynen JP, Lau MC, Haruki K, Vayrynen SA, Dias Costa A, Borowsky J, et al. Prognostic Significance of Immune Cell Populations Identified by Machine Learning in Colorectal Cancer Using Routine Hematoxylin and Eosin-Stained Sections. *Clin Cancer Res* (2020) 26(16):4326–38. doi: 10.1158/1078-0432.CCR-20-0071
60. Achim K, Pettit JB, Saraiva LR, Gavriouchkina D, Larsson T, Arendt D, et al. High-Throughput Spatial Mapping of Single-Cell Rna-Seq Data to Tissue of Origin. *Nat Biotechnol* (2015) 33(5):503–9. doi: 10.1038/nbt.3209
61. Satija R, Farrell JA, Gennert D, Schier AF, Regev A. Spatial Reconstruction of Single-Cell Gene Expression Data. *Nat Biotechnol* (2015) 33(5):495–502. doi: 10.1038/nbt.3192
62. Stahl PL, Salmen F, Vickovic S, Lundmark A, Navarro JF, Magnusson J, et al. Visualization and Analysis of Gene Expression in Tissue Sections by Spatial Transcriptomics. *Science* (2016) 353(6294):78–82. doi: 10.1126/science.aaf2403
63. Moncada R, Barkley D, Wagner F, Chiodin M, Devlin JC, Baron M, et al. Integrating Microarray-Based Spatial Transcriptomics and Single-Cell Rna-

Seq Reveals Tissue Architecture in Pancreatic Ductal Adenocarcinomas. *Nat Biotechnol* (2020) 38(3):333–42. doi: 10.1038/s41587-019-0392-8
64. Mantovani A, Marchesi F, Malesci A, Laghi L, Allavena P. Tumour-Associated Macrophages as Treatment Targets in Oncology. *Nat Rev Clin Oncol* (2017) 14(7):399–416. doi: 10.1038/nrclinonc.2016.217
65. Perrotta C, Cervia D, Di Renzo I, Moscheni C, Bassi MT, Campana L, et al. Nitric Oxide Generated by Tumor-Associated Macrophages Is Responsible for Cancer Resistance to Cisplatin and Correlated With Syntaxin 4 and Acid Sphingomyelinase Inhibition. *Front Immunol* (2018) 9:1186. doi: 10.3389/fimmu.2018.01186
66. Najafi M, Goradel NH, Farhood B, Salehi E, Solhjoo S, Toolee H, et al. Tumor Microenvironment: Interactions and Therapy. *J Cell Physiol* (2019) 234(5):5700–21. doi: 10.1002/jcp.27425
67. Mosser DM, Edwards JP. Exploring the Full Spectrum of Macrophage Activation. *Nat Rev Immunol* (2008) 8(12):958–69. doi: 10.1038/nri2448
68. Biswas SK, Mantovani A. Macrophage Plasticity and Interaction With Lymphocyte Subsets: Cancer as a Paradigm. *Nat Immunol* (2010) 11 (10):889–96. doi: 10.1038/ni.1937
69. Belgiovine C, Digifico E, Anfray C, Ummarino A, Torres Andon F. Targeting Tumor-Associated Macrophages in Anti-Cancer Therapies: Convincing the Traitors to Do the Right Thing. *J Clin Med* (2020) 9(10):3226. doi: 10.3390/jcm9103226
70. Allavena P, Anfray C, Ummarino A, Andon FT. Therapeutic Manipulation of Tumor-Associated Macrophages: Facts and Hopes From a Clinical and Translational Perspective. *Clin Cancer Res* (2021) 27(12):3291–7. doi: 10.1158/1078-0432.CCR-20-1679
71. Sick E, Jeanne A, Schneider C, Dedieu S, Takeda K, Martiny L. Cd47 Update: A Multifaceted Actor in the Tumour Microenvironment of Potential Therapeutic Interest. *Br J Pharmacol* (2012) 167(7):1415–30. doi: 10.1111/j.1476-5381.2012.02099.x
72. Jaiswal S, Jamieson CH, Pang WW, Park CY, Chao MP, Majeti R, et al. Cd47 Is Upregulated on Circulating Hematopoietic Stem Cells and Leukemia Cells to Avoid Phagocytosis. *Cell* (2009) 138(2):271–85. doi: 10.1016/j.cell.2009.05.046
73. Murata Y, Saito Y, Kotani T, Matozaki T. Blockade of Cd47 or Sirpalpha: A New Cancer Immunotherapy. *Expert Opin Ther Targets* (2020) 24(10):945–51. doi: 10.1080/14728222.2020.1811855
74. Cioffi M, Trabulo S, Hidalgo M, Costello E, Greenhalf W, Erkan M, et al. Inhibition of Cd47 Effectively Targets Pancreatic Cancer Stem Cells *Via* Dual Mechanisms. *Clin Cancer Res* (2015) 21(10):2325–37. doi: 10.1158/1078-0432.CCR-14-1399
75. Michaels AD, Newhook TE, Adair SJ, Morioka S, Goudreau BJ, Nagdas S, et al. Cd47 Blockade as an Adjuvant Immunotherapy for Resectable Pancreatic Cancer. *Clin Cancer Res* (2018) 24(6):1415–25. doi: 10.1158/1078-0432.CCR-17-2283
76. Principe DR, DeCant B, Mascarinas E, Wayne EA, Diaz AM, Akagi N, et al. Tgfbeta Signaling in the Pancreatic Tumor Microenvironment Promotes Fibrosis and Immune Evasion to Facilitate Tumorigenesis. *Cancer Res* (2016) 76(9):2525–39. doi: 10.1158/0008-5472.CAN-15-1293
77. Miura T, Mitsunaga S, Ikeda M, Shimizu S, Ohno I, Takahashi H, et al. Characterization of Patients With Advanced Pancreatic Cancer and High Serum Interleukin-6 Levels. *Pancreas* (2015) 44(5):756–63. doi: 10.1097/MPA.0000000000000335
78. Eriksson E, Milenova I, Wenthe J, Moreno R, Alemany R, Loskog A. Il-6 Signaling Blockade During Cd40-Mediated Immune Activation Favors Antitumor Factors by Reducing Tgf-Beta, Collagen Type I, and Pd-L1/Pd-1. *J Immunol* (2019) 202(3):787–98. doi: 10.4049/jimmunol.1800717
79. Kulbe H, Levinson NR, Balkwill F, Wilson JL. The Chemokine Network in Cancer–Much More Than Directing Cell Movement. *Int J Dev Biol* (2004) 48 (5-6):489–96. doi: 10.1387/ijdb.041814hk
80. Balkwill F. Cancer and the Chemokine Network. *Nat Rev Cancer* (2004) 4 (7):540–50. doi: 10.1038/nrc1388
81. Savage ND, de Boer T, Walburg KV, Joosten SA, van Meijgaarden K, Geluk A, et al. Human Anti-Inflammatory Macrophages Induce Foxp3+ Gitr+ Cd25+ Regulatory T Cells, Which Suppress *Via* Membrane-Bound Tgfbeta-1. *J Immunol* (2008) 181(3):2220–6. doi: 10.4049/jimmunol.181.3.2220
82. Yang S, Liu Q, Liao Q. Tumor-Associated Macrophages in Pancreatic Ductal Adenocarcinoma: Origin, Polarization, Function, and Reprogramming. *Front Cell Dev Biol* (2021) 8:607209. doi: 10.3389/fcell.2020.607209
83. Kusmartsev S, Gabrilovich DI. Stat1 Signaling Regulates Tumor-Associated Macrophage-Mediated T Cell Deletion. *J Immunol* (2005) 174(8):4880–91. doi: 10.4049/jimmunol.174.8.4880
84. Konjevic GM, Vuletic AM, Mirjacic Martinovic KM, Larsen AK, Jurisic VB. The Role of Cytokines in the Regulation of Nk Cells in the Tumor Environment. *Cytokine* (2019) 117:30–40. doi: 10.1016/j.cyto.2019.02.001
85. Bassani B, Baci D, Gallazzi M, Poggi A, Bruno A, Mortara L. Natural Killer Cells as Key Players of Tumor Progression and Angiogenesis: Old and Novel Tools to Divert Their Pro-Tumor Activities Into Potent Anti-Tumor Effects. *Cancers (Basel)* (2019) 11(4):461. doi: 10.3390/cancers11040461
86. Tecchio C, Scapini P, Pizzolo G, Cassatella MA. On the Cytokines Produced by Human Neutrophils in Tumors. *Semin Cancer Biol* (2013) 23(3):159–70. doi: 10.1016/j.semcancer.2013.02.004
87. Sadik CD, Kim ND, Luster AD. Neutrophils Cascading Their Way to Inflammation. *Trends Immunol* (2011) 32(10):452–60. doi: 10.1016/j.it.2011.06.008
88. Tecchio C, Micheletti A, Cassatella MA. Neutrophil-Derived Cytokines: Facts Beyond Expression. *Front Immunol* (2014) 5:508. doi: 10.3389/fimmu.2014.00508
89. Fridlender ZG, Sun J, Kim S, Kapoor V, Cheng G, Ling L, et al. Polarization of Tumor-Associated Neutrophil Phenotype by Tgf-Beta: "N1" Versus "N2" Tan. *Cancer Cell* (2009) 16(3):183–94. doi: 10.1016/j.ccr.2009.06.017
90. Felix K, Gaida MM. Neutrophil-Derived Proteases in the Microenvironment of Pancreatic Cancer -Active Players in Tumor Progression. *Int J Biol Sci* (2016) 12(3):302–13. doi: 10.7150/ijbs.14996
91. Qiao B, Luo W, Liu Y, Wang J, Liu C, Liu Z, et al. The Prognostic Value of Cxc Chemokine Receptor 2 (Cxcr2) in Cancers: A Meta-Analysis. *Oncotarget* (2018) 9(19):15068–76. doi: 10.18632/oncotarget.23492
92. Wang Y, Fang T, Huang L, Wang H, Zhang L, Wang Z, et al. Neutrophils Infiltrating Pancreatic Ductal Adenocarcinoma Indicate Higher Malignancy and Worse Prognosis. *Biochem Biophys Res Commun* (2018) 501(1):313–9. doi: 10.1016/j.bbrc.2018.05.024
93. Nielsen SR, Strobech JE, Horton ER, Jackstadt R, Laitala A, Bravo MC, et al. Suppression of Tumor-Associated Neutrophils by Lorlatinib Attenuates Pancreatic Cancer Growth and Improves Treatment With Immune Checkpoint Blockade. *Nat Commun* (2021) 12(1):3414. doi: 10.1038/s41467-021-23731-7
94. Youn JI, Collazo M, Shalova IN, Biswas SK, Gabrilovich DI. Characterization of the Nature of Granulocytic Myeloid-Derived Suppressor Cells in Tumor-Bearing Mice. *J Leukoc Biol* (2012) 91(1):167–81. doi: 10.1189/jlb.0311177
95. Bronte V, Brandau S, Chen SH, Colombo MP, Frey AB, Greten TF, et al. Recommendations for Myeloid-Derived Suppressor Cell Nomenclature and Characterization Standards. *Nat Commun* (2016) 7:12150. doi: 10.1038/ncomms12150
96. Qu P, Wang LZ, Lin PC. Expansion and Functions of Myeloid-Derived Suppressor Cells in the Tumor Microenvironment. *Cancer Lett* (2016) 380 (1):253–6. doi: 10.1016/j.canlet.2015.10.022
97. Pinton L, Solito S, Damuzzo V, Francescato S, Pozzuoli A, Berizzi A, et al. Activated T Cells Sustain Myeloid-Derived Suppressor Cell-Mediated Immune Suppression. *Oncotarget* (2016) 7(2):1168–84. doi: 10.18632/oncotarget.6662
98. Huang B, Pan PY, Li Q, Sato AI, Levy DE, Bromberg J, et al. Gr-1+Cd115 + Immature Myeloid Suppressor Cells Mediate the Development of Tumor-Induced T Regulatory Cells and T-Cell Anergy in Tumor-Bearing Host. *Cancer Res* (2006) 66(2):1123–31. doi: 10.1158/0008-5472.CAN-05-1299
99. Kusmartsev S, Nefedova Y, Yoder D, Gabrilovich DI. Antigen-Specific Inhibition of Cd8+ T Cell Response by Immature Myeloid Cells in Cancer Is Mediated by Reactive Oxygen Species. *J Immunol* (2004) 172(2):989–99. doi: 10.4049/jimmunol.172.2.989
100. Murakami S, Shahbazian D, Surana R, Zhang W, Chen H, Graham GT, et al. Yes-Associated Protein Mediates Immune Reprogramming in Pancreatic Ductal Adenocarcinoma. *Oncogene* (2017) 36(9):1232–44. doi: 10.1038/onc.2016.288
101. Trovato R, Fiore A, Sartori S, Cane S, Giugno R, Cascione L, et al. Immunosuppression by Monocytic Myeloid-Derived Suppressor Cells in Patients With Pancreatic Ductal Carcinoma Is Orchestrated by Stat3. *J Immunother Cancer* (2019) 7(1):255. doi: 10.1186/s40425-019-0734-6

102. Jacob A, Prekeris R. The Regulation of Mmp Targeting to Invadopodia During Cancer Metastasis. *Front Cell Dev Biol* (2015) 3:4. doi: 10.3389/fcell.2015.00004
103. Shen P, Wang A, He M, Wang Q, Zheng S. Increased Circulating Lin(-/Low) Cd33(+) Hla-Dr(-) Myeloid-Derived Suppressor Cells in Hepatocellular Carcinoma Patients. *Hepatol Res* (2014) 44(6):639–50. doi: 10.1111/hepr.12167
104. Clark CE, Hingorani SR, Mick R, Combs C, Tuveson DA, Vonderheide RH. Dynamics of the Immune Reaction to Pancreatic Cancer From Inception to Invasion. *Cancer Res* (2007) 67(19):9518–27. doi: 10.1158/0008-5472.CAN-07-0175
105. Hiraoka N, Onozato K, Kosuge T, Hirohashi S. Prevalence of Foxp3+ Regulatory T Cells Increases During the Progression of Pancreatic Ductal Adenocarcinoma and Its Premalignant Lesions. *Clin Cancer Res* (2006) 12 (18):5423–34. doi: 10.1158/1078-0432.CCR-06-0369
106. Tang Y, Xu X, Guo S, Zhang C, Tang Y, Tian Y, et al. An Increased Abundance of Tumor-Infiltrating Regulatory T Cells Is Correlated With the Progression and Prognosis of Pancreatic Ductal Adenocarcinoma. *PloS One* (2014) 9(3):e91551. doi: 10.1371/journal.pone.0091551
107. Jang JE, Hajdu CH, Liot C, Miller G, Dustin ML, Bar-Sagi D. Crosstalk Between Regulatory T Cells and Tumor-Associated Dendritic Cells Negates Anti-Tumor Immunity in Pancreatic Cancer. *Cell Rep* (2017) 20(3):558–71. doi: 10.1016/j.celrep.2017.06.062
108. Wang X, Wang L, Mo Q, Dong Y, Wang G, Ji A. Changes of Th17/Treg Cell and Related Cytokines in Pancreatic Cancer Patients. *Int J Clin Exp Pathol* (2015) 8(5):5702–8.
109. Zhang Y, Lazarus J, Steele NG, Yan W, Lee HJ, Nwosu ZC, et al. Regulatory T-Cell Depletion Alters the Tumor Microenvironment and Accelerates Pancreatic Carcinogenesis. *Cancer Discovery* (2020) 10(3):422–39. doi: 10.1158/2159-8290.CD-19-0958
110. Aykut B, Chen R, Miller G. Regulatory T Cells Keep Pancreatic Cancer at Bay. *Cancer Discovery* (2020) 10(3):345–7. doi: 10.1158/2159-8290.CD-20-0002
111. Kota J, Hancock J, Kwon J, Korc M. Pancreatic Cancer: Stroma and Its Current and Emerging Targeted Therapies. *Cancer Lett* (2017) 391:38–49. doi: 10.1016/j.canlet.2016.12.035
112. Sahai E, Astsaturov I, Cukierman E, DeNardo DG, Egeblad M, Evans RM, et al. A Framework for Advancing Our Understanding of Cancer-Associated Fibroblasts. *Nat Rev Cancer* (2020) 20(3):174–86. doi: 10.1038/s41568-019-0238-1
113. Ozdemir BC, Pentcheva-Hoang T, Carstens JL, Zheng X, Wu CC, Simpson TR, et al. Depletion of Carcinoma-Associated Fibroblasts and Fibrosis Induces Immunosuppression and Accelerates Pancreas Cancer With Reduced Survival. *Cancer Cell* (2014) 25(6):719–34. doi: 10.1016/j.ccr.2014.04.005
114. Tian C, Clauser KR, Ohlund D, Rickelt S, Huang Y, Gupta M, et al. Proteomic Analyses of Ecm During Pancreatic Ductal Adenocarcinoma Progression Reveal Different Contributions by Tumor and Stromal Cells. *Proc Natl Acad Sci USA* (2019) 116(39):19609–18. doi: 10.1073/pnas.1908626116
115. Vennin C, Murphy KJ, Morton JP, Cox TR, Pajic M, Timpson P. Reshaping the Tumor Stroma for Treatment of Pancreatic Cancer. *Gastroenterology* (2018) 154(4):820–38. doi: 10.1053/j.gastro.2017.11.280
116. Ohlund D, Handly-Santana A, Biffi G, Elyada E, Almeida AS, Ponz-Sarvise M, et al. Distinct Populations of Inflammatory Fibroblasts and Myofibroblasts in Pancreatic Cancer. *J Exp Med* (2017) 214(3):579–96. doi: 10.1084/jem.20162024
117. Dominguez CX, Muller S, Keerthivasan S, Koeppen H, Hung J, Gierke S, et al. Single-Cell Rna Sequencing Reveals Stromal Evolution Into Lrrc15(+) Myofibroblasts as a Determinant of Patient Response to Cancer Immunotherapy. *Cancer Discovery* (2020) 10(2):232–53. doi: 10.1158/2159-8290.CD-19-0644
118. Geng X, Chen H, Zhao L, Hu J, Yang W, Li G, et al. Cancer-Associated Fibroblast (Caf) Heterogeneity and Targeting Therapy of Cafs in Pancreatic Cancer. *Front Cell Dev Biol* (2021) 9:655152. doi: 10.3389/fcell.2021.655152
119. Goehrig D, Nigri J, Samain R, Wu Z, Cappello P, Gabiane G, et al. Stromal Protein Betaig-H3 Reprogrammes Tumour Microenvironment in Pancreatic Cancer. *Gut* (2019) 68(4):693–707. doi: 10.1136/gutjnl-2018-317570
120. Wang Y, Liang Y, Xu H, Zhang X, Mao T, Cui J, et al. Single-Cell Analysis of Pancreatic Ductal Adenocarcinoma Identifies a Novel Fibroblast Subtype Associated With Poor Prognosis But Better Immunotherapy Response. *Cell Discovery* (2021) 7(1):36. doi: 10.1038/s41421-021-00271-4
121. Chen K, Wang Q, Li M, Guo H, Liu W, Wang F, et al. Single-Cell Rna-Seq Reveals Dynamic Change in Tumor Microenvironment During Pancreatic Ductal Adenocarcinoma Malignant Progression. *EBioMedicine* (2021) 66:103315. doi: 10.1016/j.ebiom.2021.103315
122. Apte MV, Park S, Phillips PA, Santucci N, Goldstein D, Kumar RK, et al. Desmoplastic Reaction in Pancreatic Cancer: Role of Pancreatic Stellate Cells. *Pancreas* (2004) 29(3):179–87. doi: 10.1097/00006676-200410000-00002
123. Watari N, Hotta Y, Mabuchi Y. Morphological Studies on a Vitamin a-Storing Cell and Its Complex With Macrophage Observed in Mouse Pancreatic Tissues Following Excess Vitamin a Administration. *Okajimas Folia Anat Jpn* (1982) 58(4-6):837–58. doi: 10.2535/ofaj1936.58.4-6_837
124. Apte MV, Haber PS, Applegate TL, Norton ID, McCaughan GW, Korsten MA, et al. Periacinar Stellate Shaped Cells in Rat Pancreas: Identification, Isolation, and Culture. *Gut* (1998) 43(1):128–33. doi: 10.1136/gut.43.1.128
125. Allam A, Thomsen AR, Gothwal M, Saha D, Maurer J, Brunner TB. Pancreatic Stellate Cells in Pancreatic Cancer: In Focus. *Pancreatology* (2017) 17(4):514–22. doi: 10.1016/j.pan.2017.05.390
126. Jin G, Hong W, Guo Y, Bai Y, Chen B. Molecular Mechanism of Pancreatic Stellate Cells Activation in Chronic Pancreatitis and Pancreatic Cancer. *J Cancer* (2020) 11(6):1505–15. doi: 10.7150/jca.38616
127. Tape CJ, Ling S, Dimitriadi M, McMahon KM, Worboys JD, Leong HS, et al. Oncogenic Kras Regulates Tumor Cell Signaling *Via* Stromal Reciprocation. *Cell* (2016) 165(7):1818. doi: 10.1016/j.cell.2016.05.079
128. Tsukamoto H, Nishikata R, Senju S, Nishimura Y. Myeloid-Derived Suppressor Cells Attenuate Th1 Development Through Il-6 Production to Promote Tumor Progression. *Cancer Immunol Res* (2013) 1(1):64–76. doi: 10.1158/2326-6066.CIR-13-0030
129. Ligorio M, Sil S, Malagon-Lopez J, Nieman LT, Misale S, Di Pilato M, et al. Stromal Microenvironment Shapes the Intratumoral Architecture of Pancreatic Cancer. *Cell* (2019) 178(1):160–75.e27. doi: 10.1016/j.cell.2019.05.012
130. Gore J, Korc M. Pancreatic Cancer Stroma: Friend or Foe? *Cancer Cell* (2014) 25(6):711–2. doi: 10.1016/j.ccr.2014.05.026
131. Laklai H, Miroshnikova YA, Pickup MW, Collisson EA, Kim GE, Barrett AS, et al. Genotype Tunes Pancreatic Ductal Adenocarcinoma Tissue Tension to Induce Matricellular Fibrosis and Tumor Progression. *Nat Med* (2016) 22 (5):497–505. doi: 10.1038/nm.4082
132. Neesse A, Algul H, Tuveson DA, Gress TM. Stromal Biology and Therapy in Pancreatic Cancer: A Changing Paradigm. *Gut* (2015) 64(9):1476–84. doi: 10.1136/gutjnl-2015-309304
133. Grunwald BT, Devisme A, Andrieux G, Vyas F, Aliar K, McCloskey CW, et al. Spatially Confined Sub-Tumor Microenvironments in Pancreatic Cancer. *Cell* (2021) 184(22):5577–92.e18. doi: 10.1016/j.cell.2021.09.022
134. Jiang H, Torphy RJ, Steiger K, Hongo H, Ritchie AJ, Kriegsmann M, et al. Pancreatic Ductal Adenocarcinoma Progression Is Restrained by Stromal Matrix. *J Clin Invest* (2020) 130(9):4704–9. doi: 10.1172/JCI136760
135. Lee JJ, Perera RM, Wang H, Wu DC, Liu XS, Han S, et al. Stromal Response to Hedgehog Signaling Restrains Pancreatic Cancer Progression. *Proc Natl Acad Sci USA* (2014) 111(30):E3091–100. doi: 10.1073/pnas.1411679111
136. Ko AH, LoConte N, Tempero MA, Walker EJ, Kate Kelley R, Lewis S, et al. A Phase I Study of Folfirinox Plus Ipi-926, a Hedgehog Pathway Inhibitor, for Advanced Pancreatic Adenocarcinoma. *Pancreas* (2016) 45(3):370–5. doi: 10.1097/MPA.0000000000000458
137. Perez VM, Kearney JF, Yeh JJ. The Pdac Extracellular Matrix: A Review of the Ecm Protein Composition, Tumor Cell Interaction, and Therapeutic Strategies. *Front Oncol* (2021) 11:751311. doi: 10.3389/fonc.2021.751311
138. Olivares O, Mayers JR, Gouirand V, Torrence ME, Gicquel T, Borge L, et al. Collagen-Derived Proline Promotes Pancreatic Ductal Adenocarcinoma Cell Survival Under Nutrient Limited Conditions. *Nat Commun* (2017) 8:16031. doi: 10.1038/ncomms16031
139. Xavier CPR, Castro I, Caires HR, Ferreira D, Cavadas B, Pereira L, et al. Chitinase 3-Like-1 and Fibronectin in the Cargo of Extracellular Vesicles Shed by Human Macrophages Influence Pancreatic Cancer Cellular Response to Gemcitabine. *Cancer Lett* (2021) 501:210–23. doi: 10.1016/j.canlet.2020.11.013
140. Jiang H, Hegde S, Knolhoff BL, Zhu Y, Herndon JM, Meyer MA, et al. Targeting Focal Adhesion Kinase Renders Pancreatic Cancers Responsive to Checkpoint Immunotherapy. *Nat Med* (2016) 22(8):851–60. doi: 10.1038/nm.4123

141. Sharma NS, Gupta VK, Garrido VT, Hadad R, Durden BC, Kesh K, et al. Targeting Tumor-Intrinsic Hexosamine Biosynthesis Sensitizes Pancreatic Cancer to Anti-Pd1 Therapy. *J Clin Invest* (2020) 130(1):451–65. doi: 10.1172/JCI127515
142. Deng J, Kang Y, Cheng CC, Li X, Dai B, Katz MH, et al. Ddr1-Induced Neutrophil Extracellular Traps Drive Pancreatic Cancer Metastasis. *JCI Insight* (2021) 6(16):e146133. doi: 10.1172/jci.insight.146133
143. Compagno D, Tiraboschi C, Garcia JD, Rondon Y, Corapi E, Velazquez C, et al. Galectins as Checkpoints of the Immune System in Cancers, Their Clinical Relevance, and Implication in Clinical Trials. *Biomolecules* (2020) 10 (5):750. doi: 10.3390/biom10050750
144. Chen R, Dawson DW, Pan S, Ottenhof NA, de Wilde RF, Wolfgang CL, et al. Proteins Associated With Pancreatic Cancer Survival in Patients With Resectable Pancreatic Ductal Adenocarcinoma. *Lab Invest* (2015) 95 (1):43–55. doi: 10.1038/labinvest.2014.128
145. Orozco CA, Martinez-Bosch N, Guerrero PE, Vinaixa J, Dalotto-Moreno T, Iglesias M, et al. Targeting Galectin-1 Inhibits Pancreatic Cancer Progression by Modulating Tumor-Stroma Crosstalk. *Proc Natl Acad Sci USA* (2018) 115 (16):E3769–E78. doi: 10.1073/pnas.1722434115
146. Tang D, Yuan Z, Xue X, Lu Z, Zhang Y, Wang H, et al. High Expression of Galectin-1 in Pancreatic Stellate Cells Plays a Role in the Development and Maintenance of an Immunosuppressive Microenvironment in Pancreatic Cancer. *Int J Cancer* (2012) 130(10):2337–48. doi: 10.1002/ijc.26290
147. Gonnermann D, Oberg HH, Lettau M, Peipp M, Bauerschlag D, Sebens S, et al. Galectin-3 Released by Pancreatic Ductal Adenocarcinoma Suppresses Gammadelta T Cell Proliferation But Not Their Cytotoxicity. *Front Immunol* (2020) 11:1328. doi: 10.3389/fimmu.2020.01328
148. Zhao W, Ajani JA, Sushovan G, Ochi N, Hwang R, Hafley M, et al. Galectin-3 Mediates Tumor Cell-Stroma Interactions by Activating Pancreatic Stellate Cells to Produce Cytokines *Via* Integrin Signaling. *Gastroenterology* (2018) 154(5):1524–37.e6. doi: 10.1053/j.gastro.2017.12.014
149. Daley D, Mani VR, Mohan N, Akkad N, Ochi A, Heindel DW, et al. Dectin 1 Activation on Macrophages by Galectin 9 Promotes Pancreatic Carcinoma and Peritumoral Immune Tolerance. *Nat Med* (2017) 23(5):556–67. doi: 10.1038/nm.4314
150. Yang R, Sun L, Li CF, Wang YH, Yao J, Li H, et al. Galectin-9 Interacts With Pd-1 and Tim-3 to Regulate T Cell Death and Is a Target for Cancer Immunotherapy. *Nat Commun* (2021) 12(1):832. doi: 10.1038/s41467-021-21099-2
151. Moniaux N, Escande F, Porchet N, Aubert JP, Batra SK. Structural Organization and Classification of the Human Mucin Genes. *Front Biosci* (2001) 6:D1192–206. doi: 10.2741/moniaux
152. Andrianifahanana M, Moniaux N, Batra SK. Regulation of Mucin Expression: Mechanistic Aspects and Implications for Cancer and Inflammatory Diseases. *Biochim Biophys Acta* (2006) 1765(2):189–222. doi: 10.1016/j.bbcan.2006.01.002
153. Nakanuma Y, Uesaka K, Kakuda Y, Sugino T, Kubota K, Furukawa T, et al. Intraductal Papillary Neoplasm of Bile Duct: Updated Clinicopathological Characteristics and Molecular and Genetic Alterations. *J Clin Med* (2020) 9 (12):3991. doi: 10.3390/jcm9123991
154. Krieger TG, Le Blanc S, Jabs J, Ten FW, Ishaque N, Jechow K, et al. Single-Cell Analysis of Patient-Derived Pdac Organoids Reveals Cell State Heterogeneity and a Conserved Developmental Hierarchy. *Nat Commun* (2021) 12(1):5826. doi: 10.1038/s41467-021-26059-4
155. Xu Q, Chen S, Hu Y, Huang W. Single-Cell Rna Transcriptome Reveals the Intra-Tumoral Heterogeneity and Regulators Underlying Tumor Progression in Metastatic Pancreatic Ductal Adenocarcinoma. *Cell Death Discovery* (2021) 7(1):331. doi: 10.1038/s41420-021-00663-1
156. Tsuboi S, Sutoh M, Hatakeyama S, Hiraoka N, Habuchi T, Horikawa Y, et al. A Novel Strategy for Evasion of Nk Cell Immunity by Tumours Expressing Core2 O-Glycans. *EMBO J* (2011) 30(15):3173–85. doi: 10.1038/emboj.2011.215
157. Senapati S, Chaturvedi P, Chaney WG, Chakraborty S, Gnanapragassam VS, Sasson AR, et al. Novel Interaction of Muc4 and Galectin: Potential Pathobiological Implications for Metastasis in Lethal Pancreatic Cancer. *Clin Cancer Res* (2011) 17(2):267–74. doi: 10.1158/1078-0432.CCR-10-1937
158. Okamoto T, Yoneyama MS, Hatakeyama S, Mori K, Yamamoto H, Koie T, et al. Core2 O-Glycan-Expressing Prostate Cancer Cells Are Resistant to Nk Cell Immunity. *Mol Med Rep* (2013) 7(2):359–64. doi: 10.3892/mmr.2012.1189
159. Suzuki Y, Sutoh M, Hatakeyama S, Mori K, Yamamoto H, Koie T, et al. Muc1 Carrying Core 2 O-Glycans Functions as a Molecular Shield Against Nk Cell Attack, Promoting Bladder Tumor Metastasis. *Int J Oncol* (2012) 40 (6):1831–8. doi: 10.3892/ijo.2012.1411
160. Hiltbold EM, Vlad AM, Ciborowski P, Watkins SC, Finn OJ. The Mechanism of Unresponsiveness to Circulating Tumor Antigen Muc1 Is a Block in Intracellular Sorting and Processing by Dendritic Cells. *J Immunol* (2000) 165(7):3730–41. doi: 10.4049/jimmunol.165.7.3730
161. Wykes M, MacDonald KP, Tran M, Quin RJ, Xing PX, Gendler SJ, et al. Muc1 Epithelial Mucin (Cd227) Is Expressed by Activated Dendritic Cells. *J Leukoc Biol* (2002) 72(4):692–701. doi: 10.1189/jlb.72.4.692
162. Williams MA, Bauer S, Lu W, Guo J, Walter S, Bushnell TP, et al. Deletion of the Mucin-Like Molecule Muc1 Enhances Dendritic Cell Activation in Response to Toll-Like Receptor Ligands. *J Innate Immun* (2010) 2(2):123–43. doi: 10.1159/000254790
163. Shan M, Gentile M, Yeiser JR, Walland AC, Bornstein VU, Chen K, et al. Mucus Enhances Gut Homeostasis and Oral Tolerance by Delivering Immunoregulatory Signals. *Science* (2013) 342(6157):447–53. doi: 10.1126/science.1237910
164. Zhu Y, Zhang JJ, Liang WB, Zhu R, Wang B, Miao Y, et al. Pancreatic Cancer Counterattack: Muc4 Mediates Fas-Independent Apoptosis of Antigen-Specific Cytotoxic T Lymphocyte. *Oncol Rep* (2014) 31(4):1768–76. doi: 10.3892/or.2014.3016
165. Bhatia R, Gautam SK, Cannon A, Thompson C, Hall BR, Aithal A, et al. Cancer-Associated Mucins: Role in Immune Modulation and Metastasis. *Cancer Metastasis Rev* (2019) 38(1-2):223–36. doi: 10.1007/s10555-018-09775-0
166. McEver RP. Selectins: Initiators of Leucocyte Adhesion and Signalling at the Vascular Wall. *Cardiovasc Res* (2015) 107(3):331–9. doi: 10.1093/cvr/cvv154
167. Chen SH, Dallas MR, Balzer EM, Konstantopoulos K. Mucin 16 Is a Functional Selectin Ligand on Pancreatic Cancer Cells. *FASEB J* (2012) 26 (3):1349–59. doi: 10.1096/fj.11-195669
168. Hoshi H, Sawada T, Uchida M, Iijima H, Kimura K, Hirakawa K, et al. Muc5ac Protects Pancreatic Cancer Cells From Trail-Induced Death Pathways. *Int J Oncol* (2013) 42(3):887–93. doi: 10.3892/ijo.2013.1760
169. Balachandran VP, Luksza M, Zhao JN, Makarov V, Moral JA, Remark R, et al. Identification of Unique Neoantigen Qualities in Long-Term Survivors of Pancreatic Cancer. *Nature* (2017) 551(7681):512–6. doi: 10.1038/nature24462
170. Chen ST, Kuo TC, Liao YY, Lin MC, Tien YW, Huang MC. Silencing of Muc20 Suppresses the Malignant Character of Pancreatic Ductal Adenocarcinoma Cells Through Inhibition of the Hgf/Met Pathway. *Oncogene* (2018) 37(46):6041–53. doi: 10.1038/s41388-018-0403-0
171. Chen Y, Gaber T. Hypoxia/Hif Modulates Immune Responses. *Biomedicines* (2021) 9(3):260. doi: 10.3390/biomedicines9030260
172. Chaika NV, Gebregiworgis T, Lewallen ME, Purohit V, Radhakrishnan P, Liu X, et al. Muc1 Mucin Stabilizes and Activates Hypoxia-Inducible Factor 1 Alpha to Regulate Metabolism in Pancreatic Cancer. *Proc Natl Acad Sci USA* (2012) 109(34):13787–92. doi: 10.1073/pnas.1203339109
173. Wang-Gillam A, Hubner RA, Siveke JT, Von Hoff DD, Belanger B, de Jong FA, et al. Napoli-1 Phase 3 Study of Liposomal Irinotecan in Metastatic Pancreatic Cancer: Final Overall Survival Analysis and Characteristics of Long-Term Survivors. *Eur J Cancer* (2019) 108:78–87. doi: 10.1016/j.ejca.2018.12.007
174. Wang-Gillam A, Li CP, Bodoky G, Dean A, Shan YS, Jameson G, et al. Nanoliposomal Irinotecan With Fluorouracil and Folinic Acid in Metastatic Pancreatic Cancer After Previous Gemcitabine-Based Therapy (Napoli-1): A Global, Randomised, Open-Label, Phase 3 Trial. *Lancet* (2016) 387 (10018):545–57. doi: 10.1016/S0140-6736(15)00986-1
175. Gebauer F, Damanakis AI, Popp F, Quaas A, Kutting F, Lutz K, et al. Study Protocol of an Open-Label, Single Arm Phase Ii Trial Investigating the Efficacy, Safety and Quality of Life of Neoadjuvant Chemotherapy With Liposomal Irinotecan Combined With Oxaliplatin and 5-Fluorouracil/Folinic Acid Followed by Curative Surgical Resection in Patients With Hepatic Oligometastatic Adenocarcinoma of the Pancreas (Holipanc). *BMC Cancer* (2021) 21(1):1239. doi: 10.1186/s12885-021-08966-3
176. Chikuma S, Terawaki S, Hayashi T, Nabeshima R, Yoshida T, Shibayama S, et al. Pd-1-Mediated Suppression of Il-2 Production Induces Cd8+ T Cell Anergy in Vivo. *J Immunol* (2009) 182(11):6682–9. doi: 10.4049/jimmunol.0900080
177. Youngblood B, Oestreich KJ, Ha SJ, Duraiswamy J, Akondy RS, West EE, et al. Chronic Virus Infection Enforces Demethylation of the Locus That

Encodes Pd-1 in Antigen-Specific Cd8(+) T Cells. *Immunity* (2011) 35 (3):400–12. doi: 10.1016/j.immuni.2011.06.015
178. Diskin B, Adam S, Cassini MF, Sanchez G, Liria M, Aykut B, et al. Pd-L1 Engagement on T Cells Promotes Self-Tolerance and Suppression of Neighboring Macrophages and Effector T Cells in Cancer. *Nat Immunol* (2020) 21(4):442–54. doi: 10.1038/s41590-020-0620-x
179. Vandenborre K, Van Gool SW, Kasran A, Ceuppens JL, Boogaerts MA, Vandenberghe P. Interaction of Ctla-4 (Cd152) With Cd80 or Cd86 Inhibits Human T-Cell Activation. *Immunology* (1999) 98(3):413–21. doi: 10.1046/j.1365-2567.1999.00888.x
180. Walker LS, Sansom DM. Confusing Signals: Recent Progress in Ctla-4 Biology. *Trends Immunol* (2015) 36(2):63–70. doi: 10.1016/j.it.2014.12.001
181. Brahmer JR, Tykodi SS, Chow LQ, Hwu WJ, Topalian SL, Hwu P, et al. Safety and Activity of Anti-Pd-L1 Antibody in Patients With Advanced Cancer. *N Engl J Med* (2012) 366(26):2455–65. doi: 10.1056/NEJMoa1200694
182. Royal RE, Levy C, Turner K, Mathur A, Hughes M, Kammula US, et al. Phase 2 Trial of Single Agent Ipilimumab (Anti-Ctla-4) for Locally Advanced or Metastatic Pancreatic Adenocarcinoma. *J Immunother* (2010) 33(8):828–33. doi: 10.1097/CJI.0b013e3181eec14c
183. Herbst RS, Soria JC, Kowanetz M, Fine GD, Hamid O, Gordon MS, et al. Predictive Correlates of Response to the Anti-Pd-L1 Antibody Mpdl3280a in Cancer Patients. *Nature* (2014) 515(7528):563–7. doi: 10.1038/nature14011
184. Patnaik A, Kang SP, Rasco D, Papadopoulos KP, Elassaiss-Schaap J, Beeram M, et al. Phase I Study of Pembrolizumab (Mk-3475; Anti-Pd-1 Monoclonal Antibody) in Patients With Advanced Solid Tumors. *Clin Cancer Res* (2015) 21(19):4286–93. doi: 10.1158/1078-0432.CCR-14-2607
185. Carbone C, Piro G, Agostini A, Delfino P, De Sanctis F, Nasca V, et al. Intratumoral Injection of Tlr9 Agonist Promotes an Immunopermissive Microenvironment Transition and Causes Cooperative Antitumor Activity in Combination With Anti-Pd1 in Pancreatic Cancer. *J Immunother Cancer* (2021) 9(9):e002876. doi: 10.1136/jitc-2021-002876
186. Bockorny B, Semenisty V, Macarulla T, Borazanci E, Wolpin BM, Stemmer SM, et al. Bl-8040, a Cxcr4 Antagonist, in Combination With Pembrolizumab and Chemotherapy for Pancreatic Cancer: The Combat Trial. *Nat Med* (2020) 26(6):878–85. doi: 10.1038/s41591-020-0880-x
187. Tamamura H, Hiramatsu K, Kusano a S, Terakubo S, Yamamoto N, Trent JO, et al. Synthesis of Potent Cxcr4 Inhibitors Possessing Low Cytotoxicity and Improved Biostability Based on T140 Derivatives. *Org Biomol Chem* (2003) 1(21):3656–62. doi: 10.1039/b306473p
188. Klein S, Abraham M, Bulvik B, Dery E, Weiss ID, Barashi N, et al. Cxcr4 Promotes Neuroblastoma Growth and Therapeutic Resistance Through Mir-15a/16-1-Mediated Erk and Bcl2/Cyclin D1 Pathways. *Cancer Res* (2018) 78 (6):1471–83. doi: 10.1158/0008-5472.CAN-17-0454
189. Fahham D, Weiss ID, Abraham M, Beider K, Hanna W, Shlomai Z, et al. *In Vitro* and in Vivo Therapeutic Efficacy of Cxcr4 Antagonist Bkt140 Against Human Non-Small Cell Lung Cancer. *J Thorac Cardiovasc Surg* (2012) 144 (5):1167–75 e1. doi: 10.1016/j.jtcvs.2012.07.031
190. Gaur P, Verma V, Gupta S, Sorani E, Haras A, Oberkovitz G, et al. Cxcr4 Antagonist (Bl-8040) to Enhance Antitumor Effects by Increasing Tumor Infiltration of Antigen-Specific Effector T-Cells. *J Clin Oncol* (2018) 36:no. 5_suppl (February 10, 2018) 73-73. doi: 10.1200/JCO.2018.36.5_suppl.73
191. Biasci D, Smoragiewicz M, Connell CM, Wang Z, Gao Y, Thaventhiran JED, et al. Cxcr4 Inhibition in Human Pancreatic and Colorectal Cancers Induces an Integrated Immune Response. *Proc Natl Acad Sci USA* (2020) 117 (46):28960–70. doi: 10.1073/pnas.2013644117
192. Bockorny B, Macarulla T, Semenisty V, Borazanci E, Feliu J, Ponz-Sarvise M, et al. Motixafortide and Pembrolizumab Combined to Nanoliposomal Irinotecan, Fluorouracil, and Folinic Acid in Metastatic Pancreatic Cancer: The Combat/Keynote-202 Trial. *Clin Cancer Res* (2021) 27(18):5020–7. doi: 10.1158/1078-0432.CCR-21-0929
193. Loskog AS, Eliopoulos AG. The Janus Faces of Cd40 in Cancer. *Semin Immunol* (2009) 21(5):301–7. doi: 10.1016/j.smim.2009.07.001
194. Vonderheide RH, Bajor DL, Winograd R, Evans RA, Bayne LJ, Beatty GL. Cd40 Immunotherapy for Pancreatic Cancer. *Cancer Immunol Immunother* (2013) 62(5):949–54. doi: 10.1007/s00262-013-1427-5
195. Beatty GL, Torigian DA, Chiorean EG, Saboury B, Brothers A, Alavi A, et al. A Phase I Study of an Agonist Cd40 Monoclonal Antibody (Cp-870,893) in Combination With Gemcitabine in Patients With Advanced Pancreatic Ductal Adenocarcinoma. *Clin Cancer Res* (2013) 19(22):6286–95. doi: 10.1158/1078-0432.CCR-13-1320
196. O'Hara MH, O'Reilly EM, Varadhachary G, Wolff RA, Wainberg ZA, Ko AH, et al. Cd40 Agonistic Monoclonal Antibody Apx005m (Sotigalimab) and Chemotherapy, With or Without Nivolumab, for the Treatment of Metastatic Pancreatic Adenocarcinoma: An Open-Label, Multicentre, Phase 1b Study. *Lancet Oncol* (2021) 22(1):118–31. doi: 10.1016/S1470-2045(20)30532-5
197. Byrne KT, Vonderheide RH. Cd40 Stimulation Obviates Innate Sensors and Drives T Cell Immunity in Cancer. *Cell Rep* (2016) 15(12):2719–32. doi: 10.1016/j.celrep.2016.05.058
198. Li DK, Wang W. Characteristics and Clinical Trial Results of Agonistic Anti-Cd40 Antibodies in the Treatment of Malignancies. *Oncol Lett* (2020) 20 (5):176. doi: 10.3892/ol.2020.12037
199. Byrne KT, Betts CB, Mick R, Sivagnanam S, Bajor DL, Laheru DA, et al. Neoadjuvant Selicrelumab, an Agonist Cd40 Antibody, Induces Changes in the Tumor Microenvironment in Patients With Resectable Pancreatic Cancer. *Clin Cancer Res* (2021) 27(16):4574–86. doi: 10.1158/1078-0432.CCR-21-1047
200. Porter DL, Levine BL, Kalos M, Bagg A, June CH. Chimeric Antigen Receptor-Modified T Cells in Chronic Lymphoid Leukemia. *N Engl J Med* (2011) 365(8):725–33. doi: 10.1056/NEJMoa1103849
201. Wagner J, Wickman E, DeRenzo C, Gottschalk S. Car T Cell Therapy for Solid Tumors: Bright Future or Dark Reality? *Mol Ther* (2020) 28(11):2320–39. doi: 10.1016/j.ymthe.2020.09.015
202. Walker AJ, Majzner RG, Zhang L, Wanhainen K, Long AH, Nguyen SM, et al. Tumor Antigen and Receptor Densities Regulate Efficacy of a Chimeric Antigen Receptor Targeting Anaplastic Lymphoma Kinase. *Mol Ther* (2017) 25(9):2189–201. doi: 10.1016/j.ymthe.2017.06.008
203. Li KY, Yuan JL, Trafton D, Wang JX, Niu N, Yuan CH, et al. Pancreatic Ductal Adenocarcinoma Immune Microenvironment and Immunotherapy Prospects. *Chronic Dis Transl Med* (2020) 6(1):6–17. doi: 10.1016/j.cdtm.2020.01.002
204. Bailey P, Chang DK, Forget MA, Lucas FA, Alvarez HA, Haymaker C, et al. Exploiting the Neoantigen Landscape for Immunotherapy of Pancreatic Ductal Adenocarcinoma. *Sci Rep* (2016) 6:35848. doi: 10.1038/srep35848
205. Raj D, Nikolaidi M, Garces I, Lorizio D, Castro NM, Caiafa SG, et al. Ceacam7 Is an Effective Target for Car T-Cell Therapy of Pancreatic Ductal Adenocarcinoma. *Clin Cancer Res* (2021) 27(5):1538–52. doi: 10.1158/1078-0432.CCR-19-2163
206. Yeo D, Giardina C, Saxena P, Rasko JEJ. The Next Wave of Cellular Immunotherapies in Pancreatic Cancer. *Mol Ther Oncolytics* (2022) 24:561–76. doi: 10.1016/j.omto.2022.01.010
207. Xu J, Wang Y, Shi J, Liu J, Li Q, Chen L. Combination Therapy: A Feasibility Strategy for Car-T Cell Therapy in the Treatment of Solid Tumors. *Oncol Lett* (2018) 16(2):2063–70. doi: 10.3892/ol.2018.8946
208. Moon EK, Wang LC, Dolfi DV, Wilson CB, Ranganathan R, Sun J, et al. Multifactorial T-Cell Hypofunction That Is Reversible Can Limit the Efficacy of Chimeric Antigen Receptor-Transduced Human T Cells in Solid Tumors. *Clin Cancer Res* (2014) 20(16):4262–73. doi: 10.1158/1078-0432.CCR-13-2627
209. Haas AR, Tanyi JL, O'Hara MH, Gladney WL, Lacey SF, Torigian DA, et al. Phase I Study of Lentiviral-Transduced Chimeric Antigen Receptor-Modified T Cells Recognizing Mesothelin in Advanced Solid Cancers. *Mol Ther* (2019) 27(11):1919–29. doi: 10.1016/j.ymthe.2019.07.015
210. Kalos M, June CH. Adoptive T Cell Transfer for Cancer Immunotherapy in the Era of Synthetic Biology. *Immunity* (2013) 39(1):49–60. doi: 10.1016/j.immuni.2013.07.002
211. Henick BS, Herbst RS, Goldberg SB. The Pd-1 Pathway as a Therapeutic Target to Overcome Immune Escape Mechanisms in Cancer. *Expert Opin Ther Targets* (2014) 18(12):1407–20. doi: 10.1517/14728222.2014.955794
212. Grosser R, Cherkassky L, Chintala N, Adusumilli PS. Combination Immunotherapy With Car T Cells and Checkpoint Blockade for the Treatment of Solid Tumors. *Cancer Cell* (2019) 36(5):471–82. doi: 10.1016/j.ccell.2019.09.006
213. Yang CY, Fan MH, Miao CH, Liao YJ, Yuan RH, Liu CL. Engineering Chimeric Antigen Receptor T Cells Against Immune Checkpoint Inhibitors

Pd-1/Pd-L1 for Treating Pancreatic Cancer. *Mol Ther Oncolytics* (2020) 17:571–85. doi: 10.1016/j.omto.2020.05.009
214. Depil S, Duchateau P, Grupp SA, Mufti G, Poirot L. 'Off-The-Shelf' Allogeneic Car T Cells: Development and Challenges. *Nat Rev Drug Discovery* (2020) 19(3):185–99. doi: 10.1038/s41573-019-0051-2
215. Aftab B, Sasu B, Krishnamurthy J, Gschweng E, Alcazer V, Depil S. Toward "Off-The-Shelf" Allogeneic Car T Cells. *Adv Cell Gene Ther* (2020) 3:e86. doi: 10.1002/acg2.86
216. Zeiser R, Blazar BR. Acute Graft-Versus-Host Disease - Biologic Process, Prevention, and Therapy. *N Engl J Med* (2017) 377(22):2167–79. doi: 10.1056/NEJMra1609337
217. Liu P, Liu M, Lyu C, Lu W, Cui R, Wang J, et al. Acute Graft-Versus-Host Disease After Humanized Anti-Cd19-Car T Therapy in Relapsed B-All Patients After Allogeneic Hematopoietic Stem Cell Transplant. *Front Oncol* (2020) 10:573822. doi: 10.3389/fonc.2020.573822
218. Siegler EL, Zhu Y, Wang P, Yang L. Off-The-Shelf Car-Nk Cells for Cancer Immunotherapy. *Cell Stem Cell* (2018) 23(2):160–1. doi: 10.1016/j.stem.2018.07.007
219. Daher M, Rezvani K. Next Generation Natural Killer Cells for Cancer Immunotherapy: The Promise of Genetic Engineering. *Curr Opin Immunol* (2018) 51:146–53. doi: 10.1016/j.coi.2018.03.013
220. Geller MA, Cooley S, Judson PL, Ghebre R, Carson LF, Argenta PA, et al. A Phase Ii Study of Allogeneic Natural Killer Cell Therapy to Treat Patients With Recurrent Ovarian and Breast Cancer. *Cytotherapy* (2011) 13(1):98–107. doi: 10.3109/14653249.2010.515582
221. Geller MA, Miller JS. Use of Allogeneic Nk Cells for Cancer Immunotherapy. *Immunotherapy* (2011) 3(12):1445–59. doi: 10.2217/imt.11.131
222. Teng KY, Mansour AG, Zhu Z, Li Z, Tian L, Ma S, et al. Off-The-Shelf Prostate Stem Cell Antigen-Directed Chimeric Antigen Receptor Natural Killer Cell Therapy to Treat Pancreatic Cancer. *Gastroenterology* (2022) 162(4):1319–33. doi: 10.1053/j.gastro.2021.12.281
223. Li C, Yang N, Li H, Wang Z. Robo1-Specific Chimeric Antigen Receptor Natural Killer Cell Therapy for Pancreatic Ductal Adenocarcinoma With Liver Metastasis. *J Cancer Res Ther* (2020) 16(2):393–6. doi: 10.4103/jcrt.JCRT_190_20
224. Bergman H, Sissala N H, Lindqvist C. Human Nk-92 Cells Function as Target Cells for Human Nk Cells - Implications for Car Nk-92 Therapies. *Anticancer Res* (2020) 40(10):5355–9. doi: 10.21873/anticanres.14543
225. Li Q, Wang Y, Lin M, Xia L, Bao Y, Sun X, et al. Phase I Clinical Trial With Pd-1/Muc1 Car-Pnk92 Immunotherapy. *Cancer Immunol Res* (2019) 3(2Suppl):34. doi: 10.1158/2326-6074.CRICIMTEATIAACR18-A014
226. Xia N, Haopeng P, Gong JU, Lu J, Chen Z, Zheng Y, et al. Robo1-Specific Car-Nk Immunotherapy Enhances Efficacy of (125)I Seed Brachytherapy in an Orthotopic Mouse Model of Human Pancreatic Carcinoma. *Anticancer Res* (2019) 39(11):5919–25. doi: 10.21873/anticanres.13796
227. Da Y, Liu Y, Hu Y, Liu W, Ma J, Lu N, et al. Sting Agonist Cgamp Enhances Anti-Tumor Activity of Car-Nk Cells Against Pancreatic Cancer. *Oncoimmunology* (2022) 11(1):2054105. doi: 10.1080/2162402X.2022.2054105
228. Nagata S, Toyoda M, Yamaguchi S, Hirano K, Makino H, Nishino K, et al. Efficient Reprogramming of Human and Mouse Primary Extra-Embryonic Cells to Pluripotent Stem Cells. *Genes Cells* (2009) 14(12):1395–404. doi: 10.1111/j.1365-2443.2009.01356.x
229. Takahashi K, Yamanaka S. Induction of Pluripotent Stem Cells From Mouse Embryonic and Adult Fibroblast Cultures by Defined Factors. *Cell* (2006) 126(4):663–76. doi: 10.1016/j.cell.2006.07.024
230. Wilber A, Linehan JL, Tian X, Woll PS, Morris JK, Belur LR, et al. Efficient and Stable Transgene Expression in Human Embryonic Stem Cells Using Transposon-Mediated Gene Transfer. *Stem Cells* (2007) 25(11):2919–27. doi: 10.1634/stemcells.2007-0026
231. Ma Y, Ramezani A, Lewis R, Hawley RG, Thomson JA. High-Level Sustained Transgene Expression in Human Embryonic Stem Cells Using Lentiviral Vectors. *Stem Cells* (2003) 21(1):111–7. doi: 10.1634/stemcells.21-1-111
232. Navarro-Guerrero E, Tay C, Whalley JP, Cowley SA, Davies B, Knight JC, et al. Genome-Wide Crispr/Cas9-Knockout in Human Induced Pluripotent Stem Cell (Ipsc)-Derived Macrophages. *Sci Rep* (2021) 11(1):4245. doi: 10.1038/s41598-021-82137-z
233. De Masi C, Spitalieri P, Murdocca M, Novelli G, Sangiuolo F. Application of Crispr/Cas9 to Human-Induced Pluripotent Stem Cells: From Gene Editing to Drug Discovery. *Hum Genomics* (2020) 14(1):25. doi: 10.1186/s40246-020-00276-2
234. Jackow J, Guo Z, Hansen C, Abaci HE, Doucet YS, Shin JU, et al. Crispr/Cas9-Based Targeted Genome Editing for Correction of Recessive Dystrophic Epidermolysis Bullosa Using Ips Cells. *Proc Natl Acad Sci USA* (2019) 116(52):26846–52. doi: 10.1073/pnas.1907081116
235. Gropp M, Itsykson P, Singer O, Ben-Hur T, Reinhartz E, Galun E, et al. Stable Genetic Modification of Human Embryonic Stem Cells by Lentiviral Vectors. *Mol Ther* (2003) 7(2):281–7. doi: 10.1016/s1525-0016(02)00047-3
236. Ramalingam S, Annaluru N, Kandavelou K, Chandrasegaran S. Talen-Mediated Generation and Genetic Correction of Disease-Specific Human Induced Pluripotent Stem Cells. *Curr Gene Ther* (2014) 14(6):461–72. doi: 10.2174/1566523214666140918101725
237. Miksch RC, Schoenberg MB, Weniger M, Bosch F, Ormanns S, Mayer B, et al. Prognostic Impact of Tumor-Infiltrating Lymphocytes and Neutrophils on Survival of Patients With Upfront Resection of Pancreatic Cancer. *Cancers (Basel)* (2019) 11(1):39. doi: 10.3390/cancers11010039
238. Nguyen LT, Saibil SD, Sotov V, Le MX, Khoja L, Ghazarian D, et al. Phase Ii Clinical Trial of Adoptive Cell Therapy for Patients With Metastatic Melanoma With Autologous Tumor-Infiltrating Lymphocytes and Low-Dose Interleukin-2. *Cancer Immunol Immunother* (2019) 68(5):773–85. doi: 10.1007/s00262-019-02307-x
239. Andersen R, Donia M, Ellebaek E, Borch TH, Kongsted P, Iversen TZ, et al. Long-Lasting Complete Responses in Patients With Metastatic Melanoma After Adoptive Cell Therapy With Tumor-Infiltrating Lymphocytes and an Attenuated Il2 Regimen. *Clin Cancer Res* (2016) 22(15):3734–45. doi: 10.1158/1078-0432.CCR-15-1879
240. Yang CJ, McSherry F, Mayne NR, Wang X, Berry MF, Tong B, et al. Surgical Outcomes After Neoadjuvant Chemotherapy and Ipilimumab for Non-Small Cell Lung Cancer. *Ann Thorac Surg* (2018) 105(3):924–9. doi: 10.1016/j.athoracsur.2017.09.030
241. Stevanovic S, Draper LM, Langhan MM, Campbell TE, Kwong ML, Wunderlich JR, et al. Complete Regression of Metastatic Cervical Cancer After Treatment With Human Papillomavirus-Targeted Tumor-Infiltrating T Cells. *J Clin Oncol* (2015) 33(14):1543–50. doi: 10.1200/JCO.2014.58.9093
242. Topper MJ, Vaz M, Marrone KA, Brahmer JR, Baylin SB. The Emerging Role of Epigenetic Therapeutics in Immuno-Oncology. *Nat Rev Clin Oncol* (2020) 17(2):75–90. doi: 10.1038/s41571-019-0266-5
243. Gonda TA, Fang J, Salas M, Do C, Hsu E, Zhukovskaya A, et al. A DNA Hypomethylating Drug Alters the Tumor Microenvironment and Improves the Effectiveness of Immune Checkpoint Inhibitors in a Mouse Model of Pancreatic Cancer. *Cancer Res* (2020) 80(21):4754–67. doi: 10.1158/0008-5472.CAN-20-0285
244. Stoica AF, Chang CH, Pauklin S. Molecular Therapeutics of Pancreatic Ductal Adenocarcinoma: Targeted Pathways and the Role of Cancer Stem Cells. *Trends Pharmacol Sci* (2020) 41(12):977–93. doi: 10.1016/j.tips.2020.09.008
245. Morel D, Jeffery D, Aspeslagh S, Almouzni G, Postel-Vinay S. Combining Epigenetic Drugs With Other Therapies for Solid Tumours - Past Lessons and Future Promise. *Nat Rev Clin Oncol* (2020) 17(2):91–107. doi: 10.1038/s41571-019-0267-4
246. Lu D, Hoory T, Monie A, Wu A, Wang MC, Hung CF. Treatment With Demethylating Agent, 5-Aza-2'-Deoxycytidine Enhances Therapeutic Hpv DNA Vaccine Potency. *Vaccine* (2009) 27(32):4363–9. doi: 10.1016/j.vaccine.2009.02.041
247. Vo DD, Prins RM, Begley JL, Donahue TR, Morris LF, Bruhn KW, et al. Enhanced Antitumor Activity Induced by Adoptive T-Cell Transfer and Adjunctive Use of the Histone Deacetylase Inhibitor Laq824. *Cancer Res* (2009) 69(22):8693–9. doi: 10.1158/0008-5472.CAN-09-1456
248. Hosein AN, Dougan SK, Aguirre AJ, Maitra A. Translational Advances in Pancreatic Ductal Adenocarcinoma Therapy. *Nat Cancer* (2022) 3(3):272–86. doi: 10.1038/s43018-022-00349-2

Conflict of Interest: The authors declare that the research was conducted in the absence of any commercial or financial relationships that could be construed as a potential conflict of interest.

this article, or claim that may be made by its manufacturer, is not guaranteed or endorsed by the publisher.

frontiers | Frontiers in Immunology

TYPE Original Research
PUBLISHED 22 July 2022
DOI 10.3389/fimmu.2022.916915

OPEN ACCESS

EDITED BY
Nabiha Yusuf,
University of Alabama at Birmingham, United States

REVIEWED BY
Ishtiaque Ahammad,
National Institute of Biotechnology, Bangladesh
Emilia Mira,
Spanish National Research Council (CSIC), Spain

*CORRESPONDENCE
Tao Xiao
xiaotaoxyl@csu.edu.cn
Hui Li
lihuix@csu.edu.cn

SPECIALTY SECTION
This article was submitted to Cancer Immunity and Immunotherapy, a section of the journal Frontiers in Immunology

RECEIVED 10 April 2022
ACCEPTED 27 June 2022
PUBLISHED 22 July 2022

CITATION
Zhao Z-Y, Chen Z-Y, Yu B, Xiao B, Liu L-Y, Xia Y, Li A-Y, Wang P-X, Xiang C, Liu C, Yang H-Q, Li H and Xiao T (2022) Characterization of the immune cell infiltration landscape in myxofibrosarcoma to aid immunotherapy.
Front. Immunol. 13:916915.
doi: 10.3389/fimmu.2022.916915

Characterization of the immune cell infiltration landscape in myxofibrosarcoma to aid immunotherapy

Zi-Yue Zhao[1,2], Zhuo-Yuan Chen[1,2], Bin Yu[1,2], Bo Xiao[1,2], Li-Yan Liu[1,2], Yu Xia[1,2], Ao-Yu Li[1,2], Ping-Xiao Wang[1,2], Cheng Xiang[1,2], Chao Liu[1,2], Hui-Qin Yang[1,2,3], Hui Li[1,2]* and Tao Xiao[1,2]*

[1]Department of Orthopedics, Second Xiangya Hospital, Central South University, Changsha, China, [2]Orthopedic Biomedical Materials Engineering Laboratory of Hunan Province, Changsha, China, [3]Department of Orthopedics, The Affiliated yanan Hospital of Kunming Medical University, Kunming, China

Myxofibrosarcoma (MFS) is a highly malignant subtype of soft tissue sarcoma, accounting for 5% of cases. Immunotherapy guided by immune cell infiltration (ICI) is reportedly a promising treatment strategy. Here, MFS samples (n = 104) from two independent databases were classified as ICI clusters A/B/C and gene clusters A/B/C. Then, a close relationship between ICI and gene clusters was established. We found that the features of these clusters were consistent with the characteristics of immune-inflamed tumors (cluster C), immune-desert tumors (cluster B), and immune-excluded tumors (cluster A). Moreover, cluster C was sensitive to immunotherapy. Finally, an independent ICI score was established to predict the therapeutic effect, which has prospects for application in guiding immunotherapy during clinical practice.

KEYWORDS

MFS, ICI, TME, prognosis, immunotherapy

Introduction

Myxofibrosarcoma (MFS) is an important subtype of soft tissue sarcoma, accounting for 5% of soft tissue sarcomas and predominantly occurring in the limbs of elderly men (1, 2). The pathological feature of MFS is pleomorphic tumor cells exhibiting nodular morphology in the myxoid stroma with an infiltrative growth pattern (3–5). Recently, surgery has become the mainstay of treatment for MFS (6). In low-grade MFS, the infiltration and growth characteristics lead to deceptive tumor tissue boundaries (highly malignant but with a low cellular appearance). The risk of metastasis is inevitable with

high-grade MFS malignancy. Regrettably, the rate of *in situ* recurrence after the MFS resection remains high (7). Consequently, although the overall prognosis of MFS is better than that of soft tissue sarcoma, given its unique pathological characteristics, individualized and accurate treatment is still helpful in improving the prognosis and survival expectation (8). Accordingly, it is essential to construct a novel immune cell infiltration (ICI) prognosis signature for predicting the prognosis and guiding the personalized treatment of MFS patients.

It has been established that immune cell infiltration is an important feature of the tumor microenvironment (TME) (9). Research on ICI is essential for researchers to better understand the TME, with mounting evidence that the efficacy of immunotherapy can be improved by increasing the degree of ICI in TME (10). Indeed, research on ICI in tumor tissue undoubtedly contributes to developing treatment plans. Immune checkpoint inhibitors (ICIs) represent a relatively new treatment scheme and have been the subject of a series of studies to assess their efficacy in various tumors (11–13), with satisfactory results being achieved in the clinic (14, 15).

Compared with traditional treatments, ICIs play a crucial role in inducing a long-term immune response (16). In particular, researchers have conducted clinical experiments to evaluate the efficacy of pembrolizumab, nivolumab (anti-PD-1) and ipilimumab (anti-CTLA) alone or in combination for sarcoma treatment (17). A study showed that after immunotyping of soft tissue sarcoma according to the composition of TME, there were B-cell-rich tertiary lymphoid structures in the two subtypes of the immune-high group, which showed a high response rate to PD-1 blockade with pembrolizumab in a phase 2 clinical trial (18). A study showed that although PD-L1 can predict the clinical outcome of pazopanib (a type of tyrosine kinase inhibitor, TKI) for treatingsoft tissue sarcoma, predictive models are still warranted to determine which patient population will benefit from pazopanib (19).

A recent retrospective study of ICIs in sarcoma treatment by You et al. analyzed the treatment-related indicators of 61 sarcoma patients treated with ICIs. It was suggested that alveolar soft part sarcoma (ASPS), undifferentiated pleomorphic sarcoma (UPS), and myxofibrosarcoma (MFS) were sensitive to immunotherapy (20). Notwithstanding that ICIs represent a new type of immunotherapy different from traditional anti-tumor therapy, the drug toxicity and efficacy remain relatively unknown during treatment, and prediction methods to investigate the treatment reaction are quite limited; it can be challenging to determine and optimize the pseudo-progression (PP) and hyper-progression (HP) of ICI treatment in time (21). For the immunotherapy of various tumors, although monotherapy with ICIs yields a good prognosis, it is widely thought that the combination of ICIs and other targeted drugs yields a better curative effect. Accordingly, the combination of drugs has gradually become a new direction for immunotherapy: A study analyzed the data of 1,769 cases of metabolic renal cell carcinoma (MRCC) routinely collected in randomized controlled trials and found that ICIs combined with TKIs significantly improved the prognosis of MRCC patients (22). In a retrospective study on the prognosis of immunotherapy with ICIs for hepatocellular carcinoma (HCC), the researchers found that the identification of predictive biomarkers of response (such as TMB and PD-L1) could effectively help patients during immunotherapy, suggesting that the targeted study of prognostic biomarkers of immunotherapy has broad prospects (23). Therefore, our study substantiates that the prognosis prediction index of immunotherapy for MFS based on ICI score has clinical significance for guiding the optimization of immunotherapy.

Abbreviations: MFS, myxofibrosarcoma;ICI, immune cell infiltration; GO, Gene Ontology; GSEA, Gene Set Enrichment Analysis; TME, tumor microenvironment; ICIs, immune checkpoint inhibitors; ASPS, alveolar soft part sarcoma; UPS, undifferentiated pleomorphic sarcoma; PP, pseudo-progression; HP, hyper-progression; mrcc, metabolic renal cell carcinoma; HCC, hepatocellular carcinoma; tkis, tyrosine kinase inhibitors; TCGA, The Cancer Genome Atlas; GEO, Gene Expression Omnibus database; FPKM, fragments per kilobase per million; DEGs, differentially expressed genes; TMB, tumor mutational burden; OS, overall survival time; BP, biological process; CC, cellular component; MF, molecular function.

Methods

Myxofibrosarcoma data collection

Clinical information and transcriptomic data of MFS patients were obtained from The Cancer Genome Atlas (TCGA) and Gene Expression Omnibus (GEO) databases. The TCGA-SARC was designated the "CASE" type by the TCGA, and the data were downloaded in fragments per kilobase per million (FPKM) format. The MFS survival data were searched in GEO, and the data which met the research requirements (n ≥30) were selected and downloaded based on the integrity of survival information and the sample size of the dataset. There were 40 samples from the TCGA and 64 samples from GEO (Dataset GSE 72545).

Consensus clustering for the landscape of immune cell infiltration

To quantify the degree of infiltration of 22 different immune cell subsets in MFS tissue samples, the R package "CIBERSORT" was used to conduct immune cell infiltration typing and the most appropriate grouping number was selected for follow-up research. To ensure the stability of the classification, 1,000

iterations were performed. The immune/stromal cell content of every sample was assessed by the ESTIMATE algorithm to determine the purity of tumor samples. Additionally, the unsupervised clustering "PAM" method was used in the analysis based on EUCLIDEAN and WARD's linkage. To explore the possible relationship between MFS-related genes and the ICI pattern at the genetic level, the differentially expressed genes (DEGs) involved in MFS samples were classified by the same method.

ICI-related DEGs enrichment analysis and establishment of the ICI score

After genotyping MFS patients through unsupervised clustering, the "Boruta" algorithm and "PCA" were used to translate each sample and obtain various scores for the main characteristics. The difference between the ICI scores of the two main marker genes of each sample was the exact ICI score of this scheme: ICI score = $\sum PCI_A - \sum PCI_B$. Then, Gene Set Enrichment Analysis (GSEA) enrichment analysis of the related pathways of the ICI high group and ICI low group was conducted. The ICI-related genes (DEGs) were classified by the "limma" R package according to the ICI in MFS samples. The appropriate number of genotypes was calculated according to the previous results to further explore the pattern of ICI. After preliminary processing, the data were corrected, and significant DEGs were screened based on the criteria: $p < 0.05$ and absolute fold change >1. Then, Gene Ontology (GO) functional enrichment analysis was conducted.

Independent verification of ICI score

MFS-related somatic mutation data were obtained from the TCGA. It is well-established that TMB is the number of mutations in the coding region of an exome (number of mutations detected in exon/mb length) (24). TMB is a validated scoring criterion for predicting tumor immunotherapy. Therefore, we used TMB as the standard to conduct differential expression analysis on MFS samples to confirm the sample composition, and then used the combination of ICI score and TMB score to conduct a stratified test to verify the independence of the ICI score.

Data statistics and visualization

The Wilcoxon test analyzed the difference between the two groups, while the Kruskal–Wallis test was used for more than two groups. Kaplan–Meier survival curves were generated. Various R packages were used to visualize the results, including: "limma, e1071, estimate, corrplot, ConsensusClusterPlus, survival, survminer, pheatmap, reshape2, ggpubr, ggplot2, and Boruta." Violin plots were generated by an online tool (http://vip.sangerbox.com/login.html).

Results

The immune cell infiltration landscape in the TME of MFS

CIBERSORT and ESTIMATE algorithms were used to analyze the MFS tumor tissue samples and quantify immune cells in MFS. The 104 tumor samples of MFS from the TCGA and GEO were divided into three subtypes by unsupervised clustering according to the pattern of ICI and the stability of the results (Figure 1). After cluster analysis, 100 of 104 samples with meaningful data were retained and classified as follows: ICI cluster A (n = 47), ICI cluster B (n = 22), and ICI cluster C (n = 31). There were significant differences in the prognosis and outcome among the three ICI types (log-rank test, $p < 0.001$). We found that the overall survival (OS) of ICI cluster B was significantly lower than the other two sub-types (Figure 2A). As seen in the heatmap, significant differences in clinical characteristics were found among the three ICI clusters, while the box plot showed the differences in expression of 22 immune cell subtypes and the Stromal/Immune Score. Significantly higher infiltration levels of resting memory CD4 T cells ($p < 0.001$), activated NK cells ($p < 0.01$), monocytes ($p < 0.001$), M2 macrophages ($p < 0.001$), and resting mast cells ($p < 0.001$) were found in ICI cluster A compared with the other 2 clusters. Memory B cells ($p < 0.05$), resting NK cells ($p < 0.01$), and M0 macrophages ($p < 0.001$) exhibited significantly higher infiltration levels in ICI cluster B. Finally, CD8 T cells ($p < 0.001$), follicular helper T cells ($p < 0.001$), gamma delta T cells ($p < 0.001$), and M1 macrophages ($p < 0.001$) exhibited higher infiltration levels in ICI cluster C, with the higher results in the Stromal/Immune Score (Figure 2B). We used a correlation coefficient matrix heat map to show the interaction among the immune infiltration characteristics. A negative correlation was found between M2 macrophage and follicular helper T cells, M2 macrophage and CD8 T cells, M2 macrophage and gamma delta T cells, resting memory CD4 and CD8 T cells, and immune score and resting memory CD4 T cells. A positive correlation was found between gamma delta and CD8 T cells, Immune Score and CD8 T cells, Immune Score and gamma delta T cells, eosinophils and activated CD4 memory T cells, and M1 macrophage and CD8 T cells (Figures 2C, D).

To further explore the feasibility of immunotherapy in MFS, the expression differences in common immune checkpoint-related genes in ICI typing were reflected by a violin plot, in which CTLA4, LAG3, PD-1, and PD-L2 were significantly different in three ICI sub-types ($p < 0.01$). CTLA4,

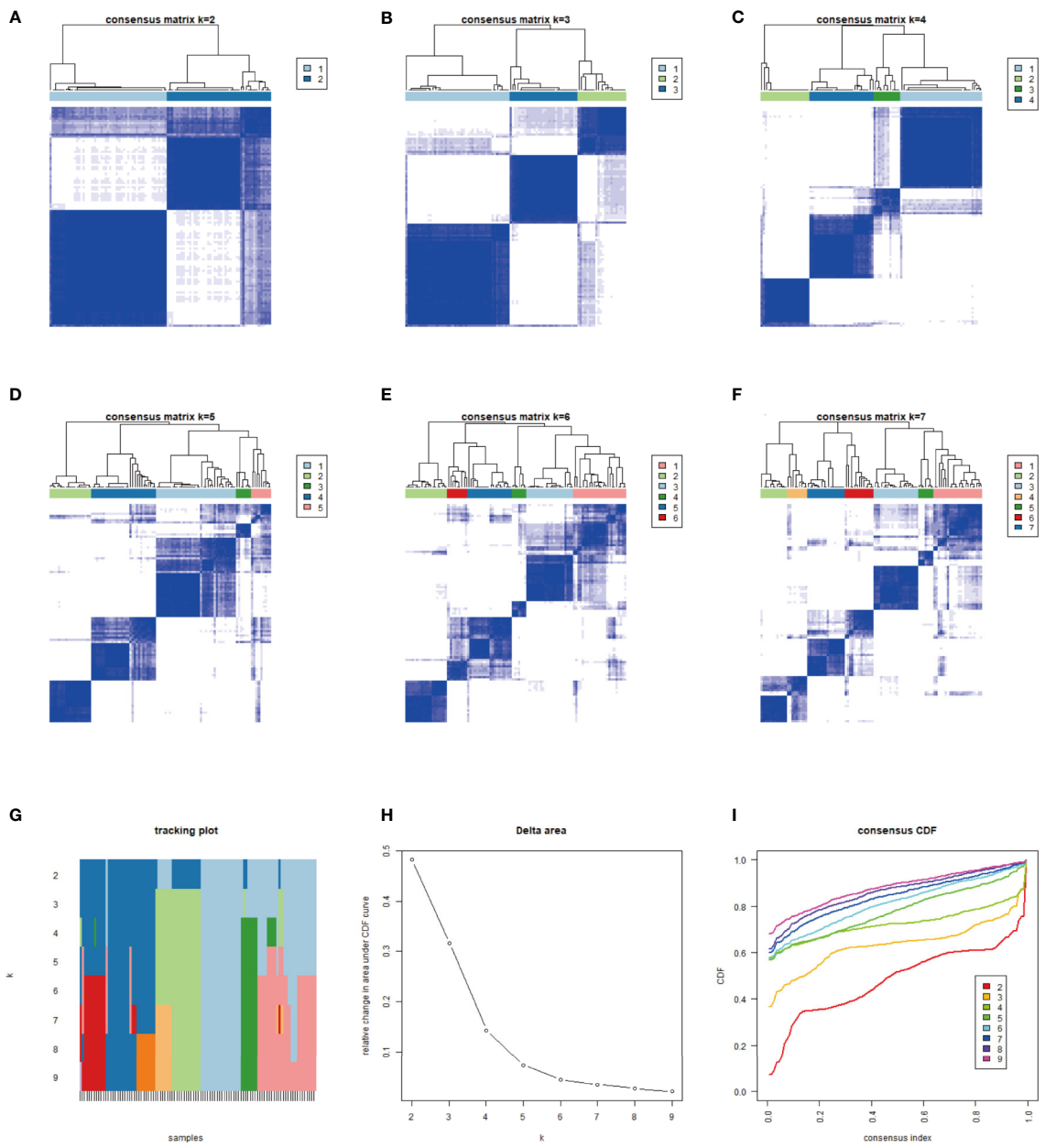

FIGURE 1
We typed 104 samples from the TCGA-MFS and GEO (GSM 72545) through CIBERSORT analysis. The samples were finally divided into 3 independent subtypes according to the stability of typing results. **(A–F)** represent the sample purity when the typing was 2–7: The blue square in the figure represents different classification aggregations. The darker the color and the smaller the number of blanks, the lower the difference in the aggregated samples and the higher the purity of typing. **(G–I)** reflect the purity of typing and the stability in the samples: **(G)** The abscissa is the sample, and the ordinate is the different classification, reflecting the stability between samples after different classification; **(H)** Cumulative Distribution Function (CDF) curve showing the sampling error in different classifications; **(I)** Explanation of CDF curve, although the results of both analyses were better, we still chose 3 types in combination with **(A–F)**.

LAG3, PD-1, and PD-L2 expression in ICI cluster C was significantly higher than in clusters A and B, and there were significant differences among the three ICI subtypes of these four genes (Figure 3).

Genotyping and difference analysis of ICI-related genes

The gene expression of all samples was analyzed by ICI typing and the R package "limma." After three repetitions, 689 DEGs were

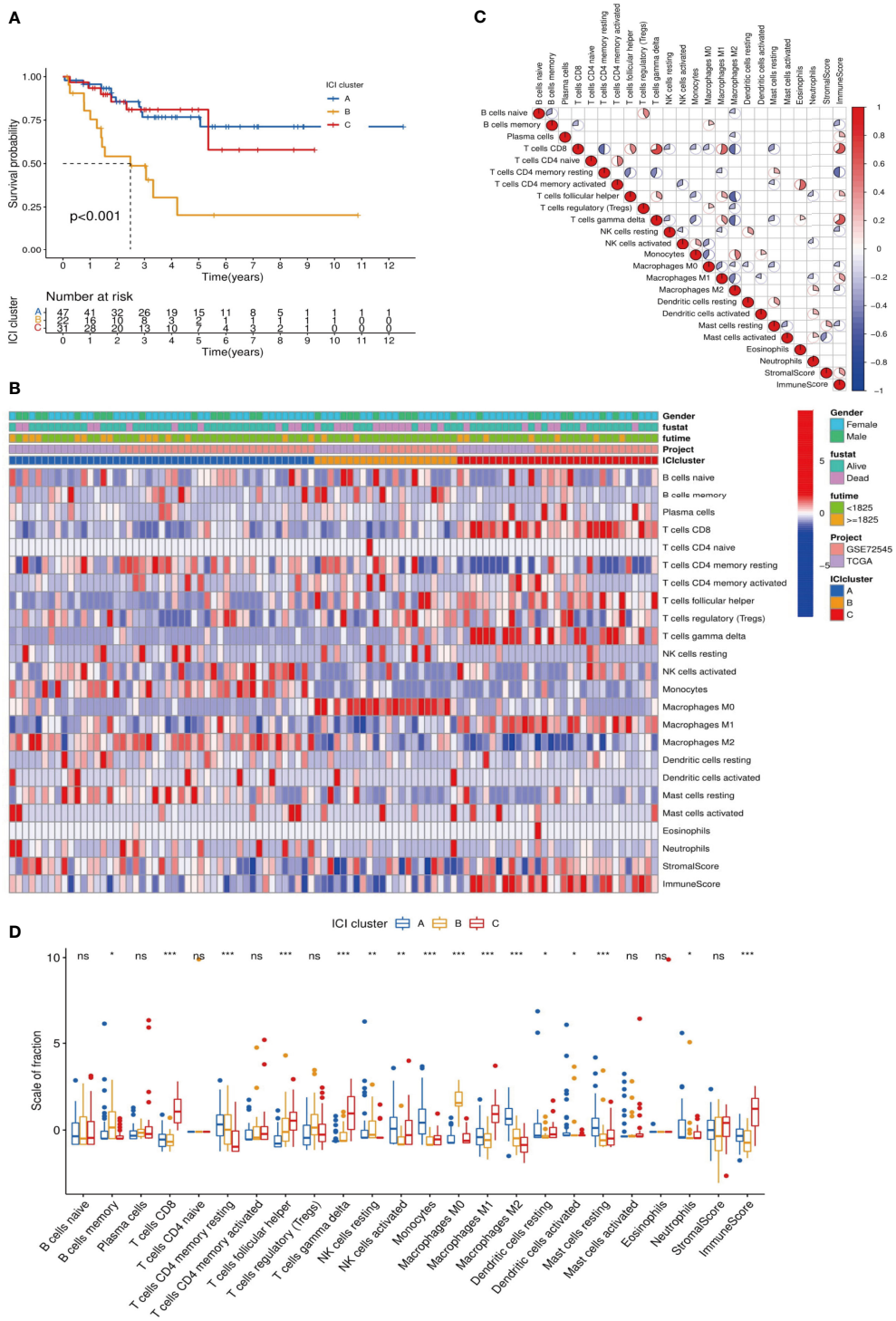

FIGURE 2
Analysis of differences among ICI subtypes and immune infiltration characteristics. **(A)** We analyzed the difference in Overall Survival (OS) among the 3 ICI subtypes and visualized the details *via* a K-M survival curve: compared with ICI cluster A and ICI cluster C, the OS of ICI cluster B was significantly lower, p <0.001; **(B)** Unsupervised cluster analysis was used to analyze the distribution of immune infiltration characteristics in MFS samples. The abscissa represents the immune infiltrating characteristics, and the ordinate represents independent samples; **(C)** We explored the relationships among 24 immune infiltrating characteristics (22 kinds of immune infiltrating cells and Stromal/Immune Score): red indicated a positive correlation, and blue indicated a negative correlation. The higher the correlation, the larger the pie chart area; **(D)** The differences in expression of 24 immune infiltration characteristics in 3 ICI subtypes are visualized in a box plot: ***p <0.001, **p <0.01, and *p <0.05 ns p>0.05,no significance.

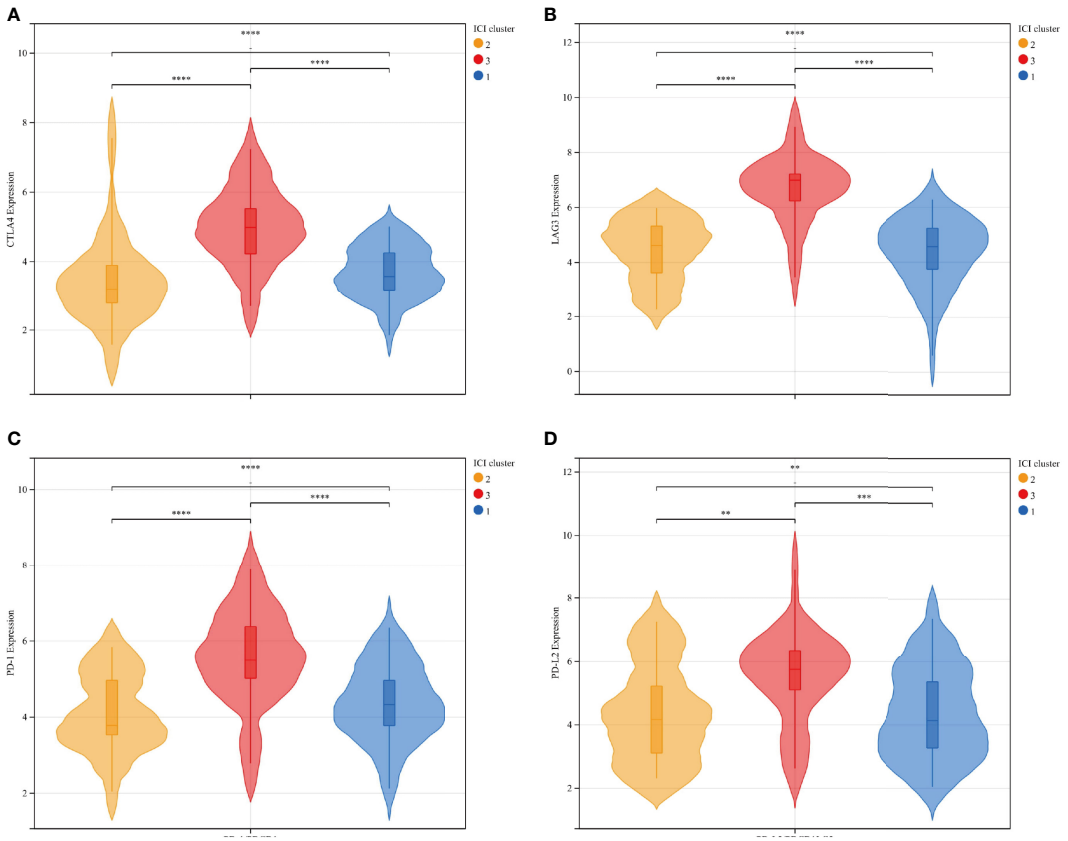

FIGURE 3
The expression differences between immune checkpoint-related genes and ICI subtypes were represented by a violin plot: CTLA4 **(A)**, LAG3 **(B)**, PD-1 **(C)**, and PD-L2 **(D)**: There was a significant statistical difference among the three groups. Among the four independent genes, ICI cluster C exhibited significantly higher expression than ICI clusters A and B, and the average expression of ICI cluster B was relatively lower than ICI cluster **(A)** ICI clusters: 1-blue-A, 2-yellow-B, 3-red-C. ****p<0.0001, ***p <0.001, **p <0.01, and *p <0.05.

obtained under the conditions of |logFC |>1 and corrected p-value <0.05. By clustering the obtained DEGs of the samples with the same arithmetic as the ICI subtypes, the sample sub-types according to genes could also be calculated, which were called gene clusters. Considering the stability within the sub-types, three gene sub-types were divided from the differentiated samples (n = 104): gene cluster A (n = 43), gene cluster B (n = 41), and gene cluster C (n = 20). Gene clusters corresponded to ICI clusters (ICI cluster A–gene cluster A, ICI cluster B–gene cluster B, ICI cluster C–gene cluster C). In the prognostic K–M curve related to genotyping, the OS of gene cluster A was significantly lower than that of the other two clusters (p <0.001) (Figure 4).

KM analysis of three independent gene clusters showed significant differences in OS. The OS of gene cluster A was significantly lower than that of the other two clusters (log-rank test, p <0.001) (Figure 5A). To further clarify the difference in ICI characteristics in the genotyping of MFS, the expression of 24 immune infiltrating characteristics in 101 differentiated MFS samples was analyzed by genotyping. M0 macrophage (p <0.001) exhibited high infiltration levels in gene cluster A; activated NK cells (p <0.001), monocytes (p <0.001), M2 macrophages (p <0.001), activated dendritic cells (p <0.05), and resting mast cells (p <0.001) were highly expressed in gene cluster B. Plasma cells (p <0.05), CD8 T cells (p <0.001), activated CD4 memory T cells (p <0.05), follicular helper T cells (p <0.001), gamma delta T cells (p <0.001), M macrophages (p <0.001), Stromal Score (p <0.05), and Immune Score (p <0.001) were significantly overexpressed in gene cluster C. Additionally, the expression of the resting CD4 memory of T cells in gene cluster C was lower than in gene clusters A and B (Figure 5B).

Subsequently, we sought to stratify according to the relationship between gene expression and ICI characteristics of MFS samples. Positive correlated genes were attributed to class A (n = 70) while negative correlated genes to class B (n = 29), which was displayed in a heatmap (Figure 5C). To describe the relationship between these genes and biological processes (BPs), cellular components (CCs), molecular function (MF),

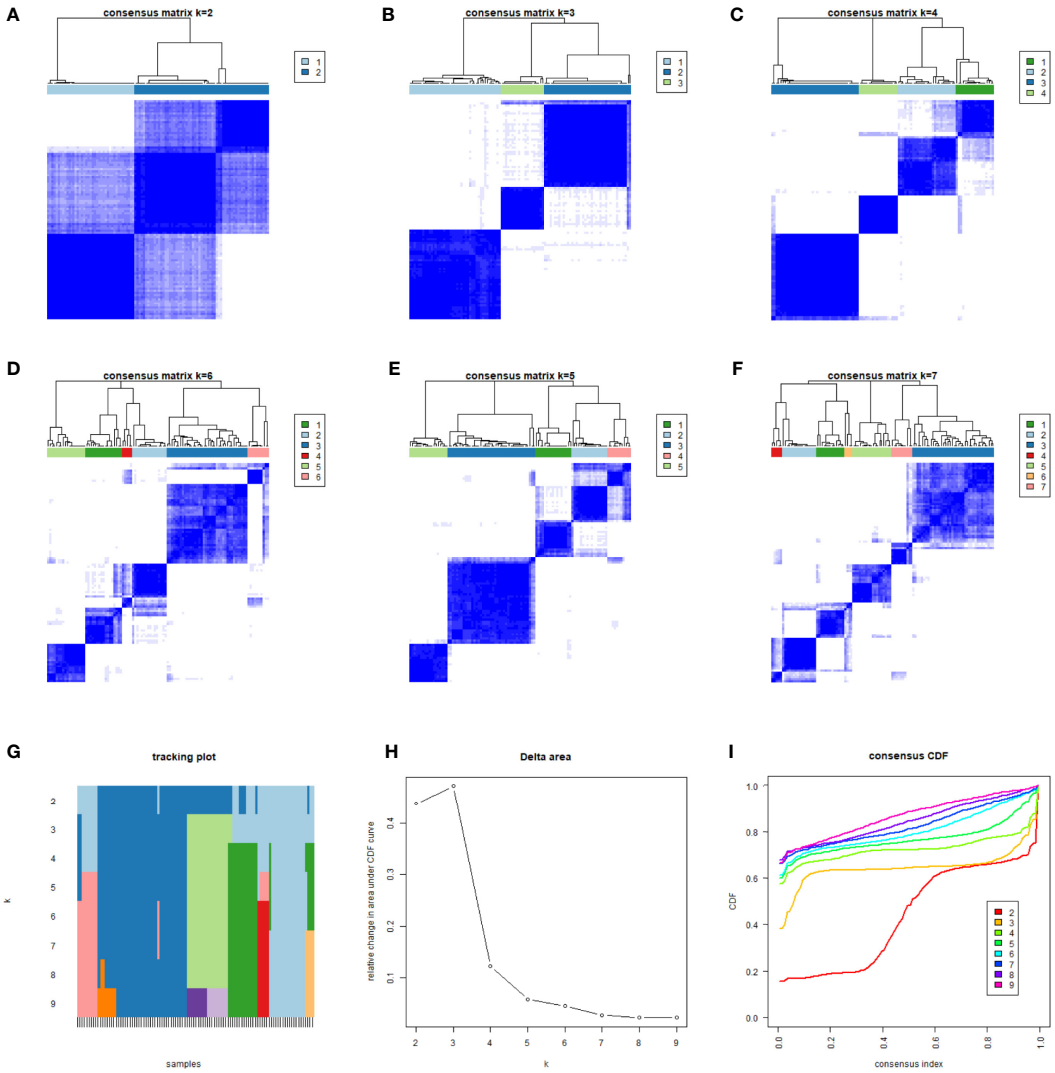

FIGURE 4
We classified 104 different samples through unsupervised clustering. According to the obtained correlation results among types **(A–F)**, the number of gene types was set to 3. The correlation among types was comparable; a low correlation was associated with stable classification results **(G–I)**.

and GO enrichment analysis were conducted. In class A, genes were involved in the proliferation and activation of immune cells, including the activation and degranulation of neutrophils, the proliferation and regulation of leukocytes, positive regulation of cytokine production, the proliferation of lymphocyte and mononuclear cells, which mostly occurred in secretory vesicles, NAD(P)H oxidase complex, and secondary lysosomes in the plasma membrane. Potential molecular functions include the activity of pattern recognition receptors, superoxide-generating NAD(P)H oxidase and oxidoreductase, and the binding of cytokine, peptide, amide and amyloid-beta (Figure 5D). Moreover, we found that class B had a close relationship with the composition of extracellular matrix and was significantly enriched in the biological function of extracellular matrix components of tumor tissue by participating in the composition of extracellular matrix in collagen, collagen trimer, endoplasmic reticulum cavity, integrin complex, and protein complex involved in cell adhesion. (Figure 5E).

To verify the consistency between ICI typing and genotyping, we analyzed the differences in four immune checkpoint-related genes with significant expression differences in ICI subtypes by genotyping. Similar to ICI typing, the four differential genes (CTLA4 (A), Lag3 (B), PD-1 (C), and PD-L2 (D)) in gene cluster C were significantly higher than in the other two clusters. Statistical differences

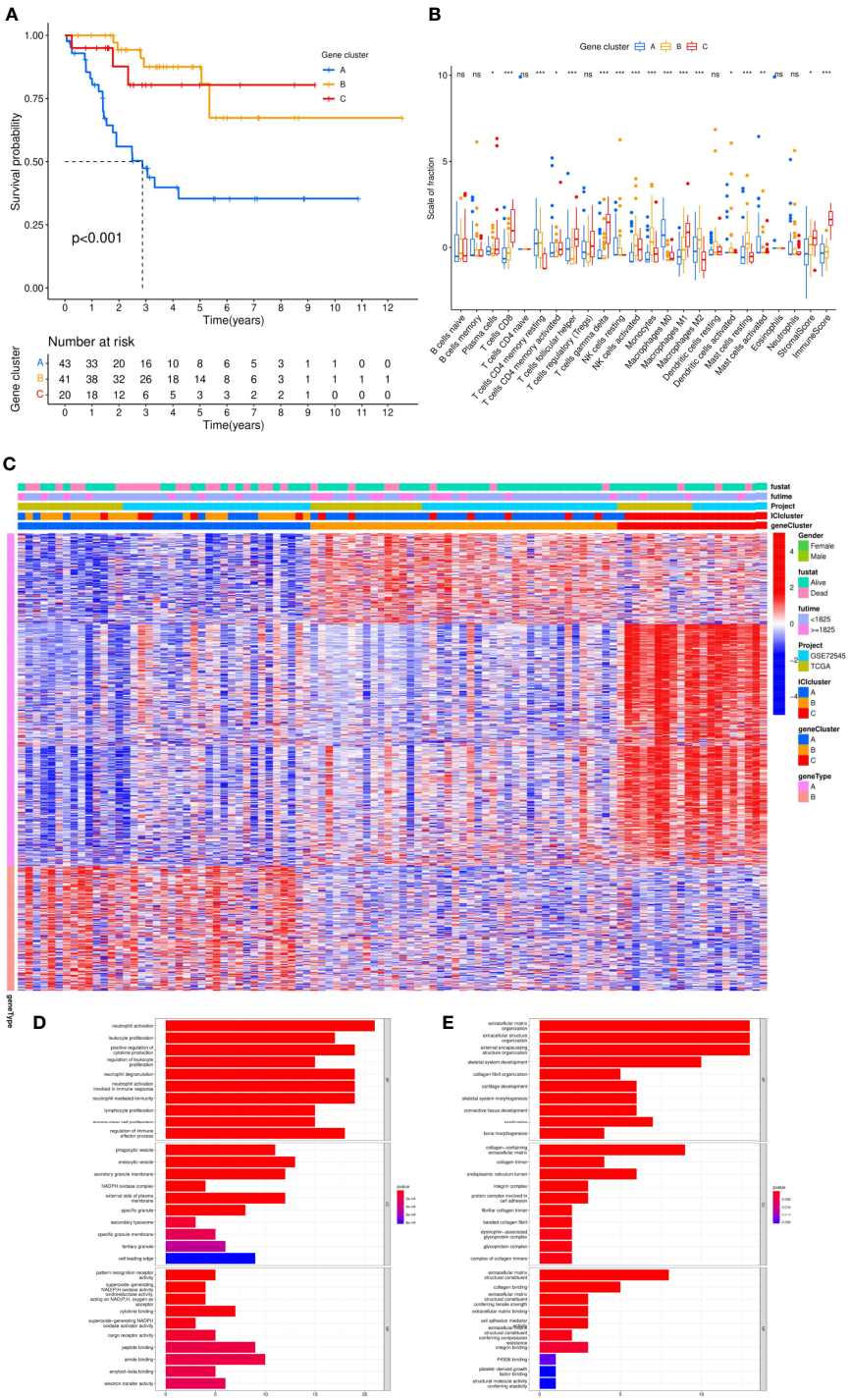

FIGURE 5
Differential analysis of genotyping of immune infiltration. **(A)** After unsupervised cluster analysis of DEGs and samples, we divided the samples into three independent gene clusters, the overall survival (OS) was analyzed by Kaplan–Meier analysis, and the log-rank test showed that P <0.001. **(B)** The differences in expression among 24 kinds of immune infiltrating characteristics in the 3 gene clusters were visualized in a box plot and statistically analyzed by Kruskal–Wallis test. **(C)** The clinical information was divided into two types. The abscissa was the samples, and the ordinate was the genes. **(D, E)** According to gene type A and gene type B, which were positively correlated with the ICI model in DEGs, the ordinate was the name of GO, the abscissa was the number of enriched genes, and the color represented the significance of the correlation (red indicated a positive correlation and blue indicated a negative correlation). ***p <0.001, **p <0.01, *p <0.05 and ns p>0.05,no significance.

among the three subtypes were also significant. The consistency of the expression of immune checkpoint genes in different unsupervised cluster typing confirmed the rationality of ICI typing in MFS (Figure 6).

Acquisition of ICI model score and verification with tumor mutation burden

The rationality and stability of the ICI model were determined in advance. The feature genes and the related sample expression volumes were extracted according to the ICI classification using the "Boruta" algorithm. Then, the "PCA" algorithm was used to obtain the ICI score. High (n = 88) and Low (n = 16) groups were obtained from the samples according to their source, gene clusters, and clinical information. The Sankey diagram provided an objective overview of the relationship among gene clusters, survival outcomes, and ICI scores. All the genes of cluster A and most genes of cluster B belonged to the ICI High group, and the remaining genes of cluster B and some of cluster C belonged to the ICI Low group. Compared with the ICI High group, the ICI Low group reflected a high probability of survival (Figures 7A, C). The immune checkpoint and immune-activating genes (IDO1, CD274 (PD1), HAVCR2, PDCD1 (PD-L1), CTLA4, LAG3, CD8A, CXCL10, CXCL9, GZMA, GZMB, PRF1, IFNG, TBX2, and TNF) were selected as the target genes, and their differential expression in the ICI High and Low Scores groups was observed. Except for TBX2, all related genes exhibited significantly higher expression in the ICI Low Score group than in the High Score group ($p > 0.05$) (Figure 7B). GSEA was conducted to identify the different functional pathways in the ICI High and Low Scores groups; 375 pathways were enriched in the ICI High Scores group and 429 in the ICI Low Scores group. We selected the top 5 related pathways for visualization: Taste Transduction, Calcium Signaling Pathway, Vascular Smooth Muscle Contraction, Neuroactive Ligand Receptor Interaction, and Vasopressin Regulated Water Reabsorption in the ICI High score group and Spliceosome, Proteasome, RNA Degradation, Nucleotide Excision Repair, and DNA Replication in the ICI Low scoring group (Figure 7D).

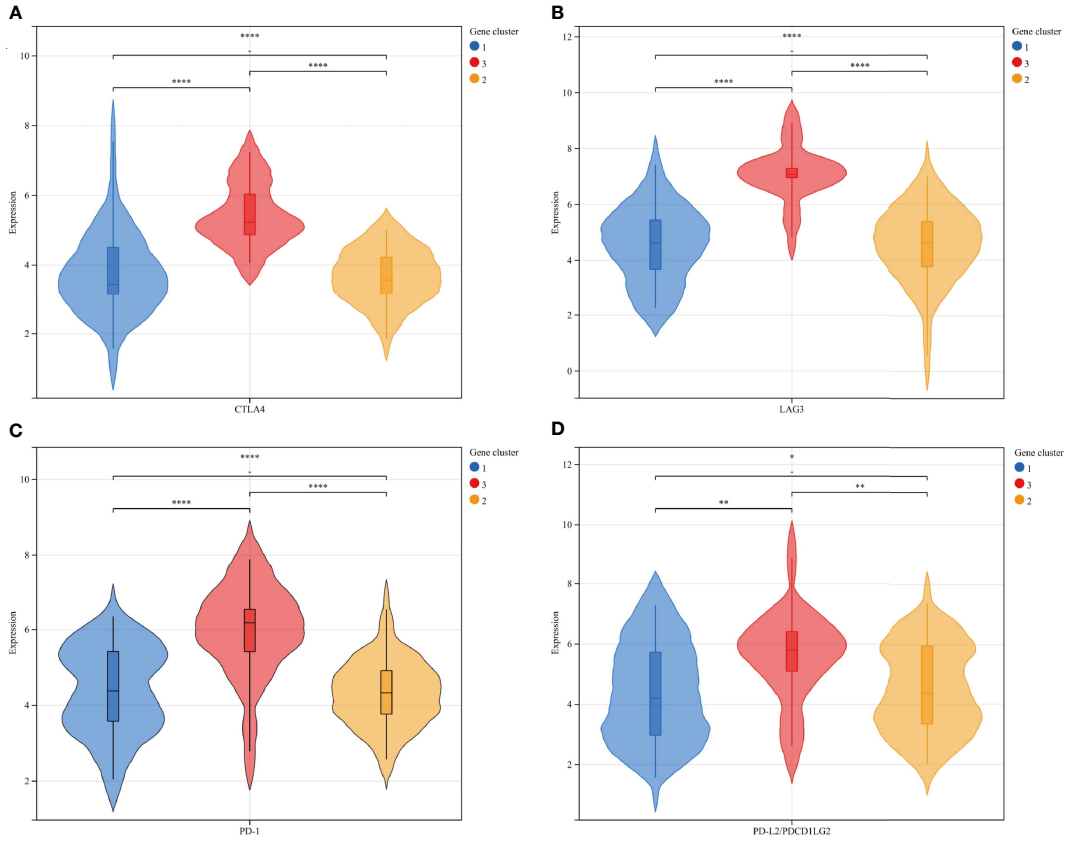

FIGURE 6
The expression differences of 4 immune checkpoint-related genes in gene subtypes were consistent with ICI subtypes: CTLA4 **(A)**, Lag3 **(B)**, PD-1 **(C)**, and PD-L2 **(D)**: Gene clusters: 1-blue-A, 2-yellow-B, 3-red-C. **** p<0.0001 ***P <0.001, **P <0.01, and *P <0.05.

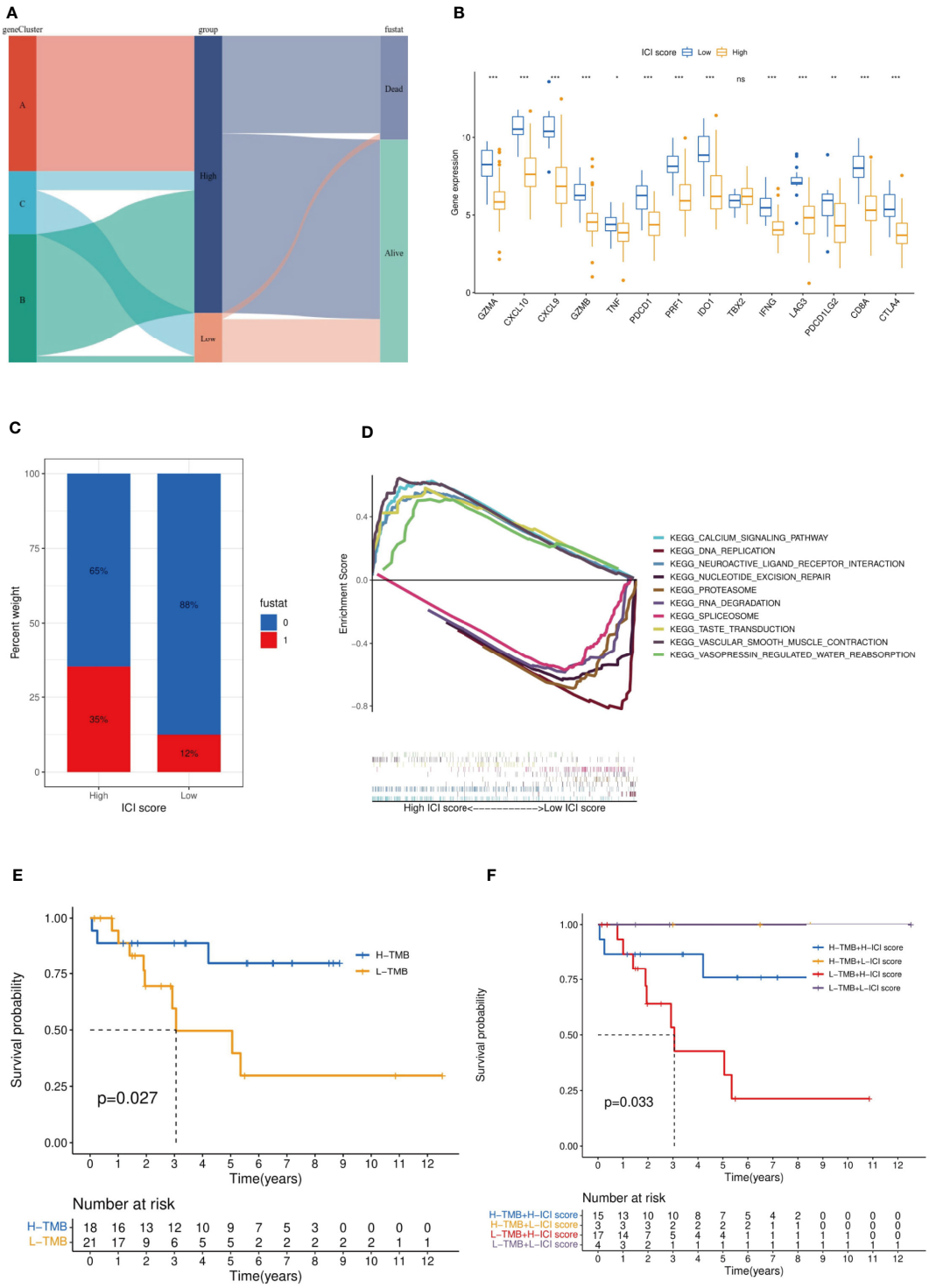

FIGURE 7
Established and verified the ICI score. **(A)** The relationship among gene clusters, ICI high or low groups and survival outcomes is visualized in a Sankey diagram. **(B)** Based on the ICI score, we analyzed the expression difference among the immune checkpoint genes and immune-activating genes. It should be noted that PDCD1LG2 is another name for PD-L2. **(C)** Effect of ICI score on patient survival. **(D)** GSEA indicated significantly enriched signaling pathways corresponding to high and low ICI score groups. **(E)** Survival analysis was performed by TMB score in our selected MFS samples. **(F)** MFS samples were stratified by TMB score and the ICI score established in this study. ***p<0.001,**p<0.01, *p<0.05 and ns p>0.05, no significance.

The current evidence suggests that tumor mutation burden (TMB) is an effective biomarker for immunotherapy of various tumors (24). Previous studies have shown that the TMB High group is more sensitive to ICIs for tumor patients with immunotherapy (25). Stratified analysis is an effective method to explore the relationship between a new model of tumor immunotherapy prognosis and TMB (26). According to the immune characteristics of TMB, we divided the MFS samples into the TMB High and TMB Low groups. The TMB High group had a significantly better OS ($p = 0.027$) (Figure 7E). Then, we began assessing the potential link between TMB and ICI scores. In the stratified analysis, the survival status of ICI Low groups (yellow and purple) was significantly higher than that of ICI High groups (blue and red) ($p = 0.033$), and the survival status of the TMB High groups (yellow and bule) was higher than that of the TMB Low groups (red and purple) (Figure 7F). No relationship was found between the ICI scores and TMB results.

Discussion

Current evidence suggests that tumor immunotherapy is more dependent on the interaction between tumor cells and the tumor microenvironment (TME) than histological findings (27). Overwhelming evidence substantiates that the immune infiltration microenvironment can be harnessed to predict the prognosis of gastric, breast, and lung cancers (28–31). The identification of gene deletions in tumor samples is highly significant for tumor treatment. Interestingly, it has been shown that there are more gene deletions in sarcoma samples with low immune infiltration, while the samples with high immune infiltration exhibit stronger adaptability to the therapeutic effect (32). Similarly, recent studies have proposed that the polygenic immune risk score model based on immune cell infiltration in osteosarcoma is a reliable prognostic tool for osteosarcoma (33, 34). Nonetheless, few studies have hitherto been conducted on MFS. Importantly, our study can improve the current knowledge on the prognosis of MFS from the perspective of autoimmunity.

First, the immune cells infiltrated in 104 MFS samples from different databases were classified by unsupervised cluster analysis. The difference in prognostic information was analyzed based on the obtained ICI classification and the relationships among 24 immune infiltration characteristics (22 immune infiltration cells and immune score, stromal score) were explored. Multiple immune checkpoint-related genes were selected as immune checkpoints, and their differences in expression were analyzed based on immune infiltration typing. Subsequently, after obtaining DEGs related to immune infiltration, genotyping was carried out by unsupervised cluster analysis. Genotyping was used to analyze the differences between clinical prognosis and outcome of MFS samples; the consistency with ICI typing results was verified. Meanwhile, the characteristic genes related to immune infiltration were obtained using "Boruta" and "PCA." Then, the ICI High and Low score groups were obtained by gene analysis of immune infiltration. For this step, GO enrichment analysis was used to explore the genes and protein functions related to the ICI High and Low score groups. At the same time, the differences in immune checkpoint genes were analyzed again by gene typing. The results were compared with the results of the first step to verify the stability and rationality of our ICI typing. Finally, the difference between immune checkpoint and immune activation-related genes was analyzed by the ICI score obtained during the second step, and GSEA enriched the top five signaling pathways between ICI high and low score groups. TMB is often considered as the number of tumor mutations (35). It is well-established that TMB could be used as an independent biomarker related to ICI in various solid tumors. Therefore, the feasibility of our MFS-related ICI prediction model was validated by comparing TMB with our established ICI score (36). Our results showed that the established ICI score had a definite guide value in predicting the prognosis of patients with MFS. However, the results were visualized in a Sankey diagram. It was found that the ICI score could not accurately predict the prognosis, which may be related to the differences in other cytokines, components, and localization points of TME during GO analysis of MFS. These results show that unidentified biological processes may affect the accuracy of our ICI prognosis model.

Interestingly, Chen et al. documented an unprecedented immunophenotypic typing in 2017 (37), including immune-inflamed (characterized by a large number of infiltrated immune cells, B cell activation, T regulatory cell participation, and T cell depletion; checkpoints inhibitors exert an effective antitumor effect), immune-excluded (characterized by a large number of immune cells in the stroma, with high immune and stromal scores, and few immune infiltrating cells overall; checkpoint inhibitors yield poor antitumor efficacy) and immune-desert tumors (characterized by few or no CD8 T cells in the whole sample, exhibiting immune tolerance or immune neglect; checkpoints inhibitors exert no effect). According to the results in Figures 2D, 5B, ICI cluster A and gene cluster A showed the lowest expression of B and T cells, and immune infiltration levels were generally low; cluster C showed higher expression of the immune score and T cells, especially CD8 T cells. The difference in immune infiltration characteristics in our study was consistent with the three immune phenotypes, which further validated the rationality of our typing approach: an immune-inflamed tumor corresponded to

cluster C (red), an immune-excluded tumor to cluster A (blue), and an immune-desert tumor to cluster B (yellow). At the same time, the high expression of immune checkpoint genes in cluster C emphasized the importance of selecting checkpoint inhibitors to achieve an antitumor effect. Our results were consistent with the literature (36, 38, 39), which proved that typing ICI and gene clusters could guide clinical immunotherapy of MFS. Our findings substantiate that the increase of immune infiltrating cells in the TME is a positive factor for the prognosis of the tumor. Therefore, immunotherapies that can improve the degree of immune cell infiltration in the TME are worth advocating. Interestingly, it has been reported that autologous dendritic cell immunotherapy could produce an active immune response in tumors, but reliable biomarkers are warranted to guide the treatment plan (10).

According to the GSEA results, the high-scoring group of tumor samples in ICI was significantly enriched in the activation and proliferation of immune cells. In a study on tumor dichotomy (hot tumor and cold tumor), Li et al. documented that immunotherapy yielded a better effect on hot tumors. In mice experiments, the six-month survival rates of the hot and cold tumor groups were 76.9 and 0.5%, respectively (40). The overlap in characteristics of hot tumors suggested that the prognosis of immunotherapy accounted for the better prognosis in ICI cluster C (41). The difference between the ICI score and the TMB score was significant ($P = 0.033$), which corroborated that the ICI score was a new valuable independent score.

However, we could not further validate the ICI score given the lack of MFS samples, which were from public databases or case collections of our research group. Our ICI score only evaluated the prognosis of MFS from the perspective of immune infiltration without considering other complex mechanisms in TME. At the same time, the difference in some results (especially between immune excluded and immune inflamed) was not significant due to the sample size limitation.

Conclusion

Our study comprehensively analyzed the ICI characteristics of MFS, established the effectiveness of ICI typing and gene typing, predicted the prognosis of MFS samples through ICI scores, and evaluated the therapeutic effect of MFS under ICI typing along with differences in immune checkpoint-related genes, which could assist physicians in developing individualized immunotherapy schemes and prognosis prediction.

Data availability statement

The datasets presented in this study can be found in online repositories. The names of the repository/repositories and accession number(s) can be found in the article/supplementary material.

Author contributions

Z-YZ, Z-YC, HL, and TX designed and implemented the research. Z-YZ, Z-YC, and BY collated and analyzed the data. BX, L-YL, YX, A-YL, P-XW, CX CL, and H-QY provided technical support. Z-YC and HL provided the language polishing for this article. Z-YZ wrote the manuscript. Z-YZ and HL revised the manuscript. All authors listed have made a substantial, direct, and intellectual contribution to the work and approved it for publication.

Funding

The study was supported by the Research Project of Hunan Health Commission (grant number 202204073071).

Acknowledgments

We thank The Cancer Genome Atlas (TCGA) and Gene Expression Omnibus (GEO) for data support, Gene Set Enrichment Analysis (GSEA), and Gene Ontology (GO) for functional enrichment.

Conflict of interest

The authors declare that the research was conducted in the absence of any commercial or financial relationships that could be construed as a potential conflict of interest.

Publisher's note

References

1. Sambri A, Spinnato P, Bazzocchi A, Tuzzato GM, Donati D, Bianchi G, et al. Does pre-operative MRI predict the risk of local recurrence in primary myxofibrosarcoma of the extremities? *Asia Pac J Clin Oncol* (2019) 15:e181–6. doi: 10.1111/ajco.13161

2. Rothenberger C, Jakob L, Betke M, French L, Bartsch H, Knosel T, et al. Myxofibrosarcoma. *Hautarzt* (2020) 71:30–1. doi: 10.1007/s00105-020-04647-7

3. Anderson WJ, Doyle LA. Updates from the 2020 world health organization classification of soft tissue and bone tumours. *Histopathology* (2021) 78:644–57. doi: 10.1111/his.14265

4. Palmerini E, Righi A, Staals EL. Rare primary malignant bone sarcomas. *Cancers (Basel)* (2020) 124. doi: 10.3390/cancers12113092

5. Murphey MD. World health organization classification of bone and soft tissue tumors: modifications and implications for radiologists. *Semin Musculoskelet Radiol* (2007) 11:201–14. doi: 10.1055/s-2008-1038310

6. Widemann BC, Italiano A. Biology and management of undifferentiated pleomorphic sarcoma, myxofibrosarcoma, and malignant peripheral nerve sheath tumors: State of the art and perspectives. *J Clin Oncol* (2018) 36:160–7. doi: 10.1200/JCO.2017.75.3467

7. Zambo I, Veselý K. [WHO classification of tumours of soft tissue and bone 2013: the main changes compared to the 3rd edition]. *Cesk Patol* (2014) 50:64–70.

8. Roland CL, Wang WL, Lazar AJ, Torres KE. Myxofibrosarcoma. *Surg Oncol Clin N Am* (2016) 25:775–88. doi: 10.1016/j.soc.2016.05.008

9. Zhang Y, Zhang Z. The history and advances in cancer immunotherapy: understanding the characteristics of tumor-infiltrating immune cells and their therapeutic implications. *Cell Mol Immunol* (2020) 17:807–21. doi: 10.1038/s41423-020-0488-6

10. Sokratous G, Polyzoidis S, Ashkan K. Immune infiltration of tumor microenvironment following immunotherapy for glioblastoma multiforme. *Hum Vaccin Immunother* (2017) 13:2575–82. doi: 10.1080/21645515.2017.1303582

11. Keenan TE, Tolaney SM. Role of immunotherapy in triple-negative breast cancer. *J Natl Compr Canc Netw* (2020) 18:479–89. doi: 10.6004/jnccn.2020.7554

12. Iams WT, Porter J, Horn L. Immunotherapeutic approaches for small-cell lung cancer. *Nat Rev Clin Oncol* (2020) 17:300–12. doi: 10.1038/s41571-019-0316-z

13. Huang A, Yang XR, Chung WY, Dennison AR, Zhou J. Targeted therapy for hepatocellular carcinoma. *Signal Transduct Target Ther* (2020) 5:146. doi: 10.1038/s41392-020-00264-x

14. Duma N, Santana-Davila R, Molina JR. Non-small cell lung cancer: Epidemiology, screening, diagnosis, and treatment. *Mayo Clin Proc* (2019) 94:1623–40. doi: 10.1016/j.mayocp.2019.01.013

15. Kwapisz D. Pembrolizumab and atezolizumab in triple-negative breast cancer. *Cancer Immunol Immunother* (2021) 70:607–17. doi: 10.1007/s00262-020-02736-z

16. Jia XH, Geng L-Y, Jiang P-P, Xu H, Nan K-J, Yao Y, Jiang L-L, et al. The biomarkers related to immune related adverse events caused by immune checkpoint inhibitors. *J Exp Clin Cancer Res* (2020) 39:284. doi: 10.1186/s13046-020-01749-x

17. Keung EZ, Lazar AJ, Torres KE, Wang W-L, Cormier JN, Guadagnolo BA, et al. Phase II study of neoadjuvant checkpoint blockade in patients with surgically resectable undifferentiated pleomorphic sarcoma and dedifferentiated liposarcoma. *BMC Cancer* (2018) 18:913. doi: 10.1186/s12885-018-4829-0

18. Petitprez F, Reyniès A, Keung EZ, Chen TW-W, Sun C-M, Calderaro J, Jeng Y-M, et al. B cells are associated with survival and immunotherapy response in sarcoma. *Nature* (2020) 577:556–60. doi: 10.1038/s41586-019-1906-8

19. Kim SK, Kim JH, Kim SH, Lee YH, Han JW, Baek W, et al. PD-L1 tumour expression is predictive of pazopanib response in soft tissue sarcoma. *BMC Cancer* (2021) 21:336. doi: 10.1186/s12885-021-08069-z

20. You Y, Guo X, Zhuang R, Zhang C, Wang Z, Shen F, et al. Activity of PD-1 inhibitor combined with anti-angiogenic therapy in advanced sarcoma: A single-center retrospective analysis. *Front Mol Biosci* (2021) 8:747650. doi: 10.3389/fmolb.2021.747650

21. de Miguel M, Calvo E. Clinical challenges of immune checkpoint inhibitors. *Cancer Cell* (2020) 38:326–33. doi: 10.1016/j.ccell.2020.07.004

22. Rizzo A, Mollica V, Santoni M, Ricci AD, Rosellini M, Marchetti A, et al. Impact of clinicopathological features on survival in patients treated with first-line immune checkpoint inhibitors plus tyrosine kinase inhibitors for renal cell carcinoma: A meta-analysis of randomized clinical trials. *Eur Urol Focus* (2021) EUF-1077:17. doi: 10.1016/j.euf.2021.03.001

23. Rizzo A, Ricci AD. PD-L1, TMB, and other potential predictors of response to immunotherapy for hepatocellular carcinoma: how can they assist drug clinical trials? *Expert Opin Investig Drugs* (2022) 31:415–23. doi: 10.1080/13543784.2021.1972969

24. Chan TA, Yarchoan M, Jaffee E, Swanton C, Quezada SA, Stenzinger A, et al. Development of tumor mutation burden as an immunotherapy biomarker: utility for the oncology clinic. *Ann Oncol* (2019) 30:44–56. doi: 10.1093/annonc/mdy495

25. Cristescu R, Mogg R, Ayers M, Albright A, Murphy E, Yearley J, et al. Pan-tumor genomic biomarkers for PD-1 checkpoint blockade-based immunotherapy. *Science* (2018) 3622. doi: 10.1126/science.aar3593

26. Liu L, Bai X, Wang J, Tang X-R, Wu D-H, Du S-S, et al. Combination of TMB and CNA stratifies prognostic and predictive responses to immunotherapy across metastatic cancer. *Clin Cancer Res* (2019) 25:7413–23. doi: 10.1158/1078-0432.CCR-19-0558

27. Mittra A, Takebe N, Florou V, Chen AP, Naqash AR. The emerging landscape of immune checkpoint inhibitor based clinical trials in adults with advanced rare tumors. *Hum Vaccin Immunother* (2021) 17:1935–9. doi: 10.1080/21645515.2020.1854604

28. Li B, Zhang B, Wang X, Zeng Z, Huang Z, Zhang L, et al. Expression signature, prognosis value, and immune characteristics of siglec-15 identified by pan-cancer analysis. *Oncoimmunology* (2020) 9:1807291. doi: 10.1080/2162402X.2020.1807291

29. Zhang B, Wu Q, Li B, Wang D, Wang L, Zhou YL, et al. m(6)A regulator-mediated methylation modification patterns and tumor microenvironment infiltration characterization in gastric cancer. *Mol Cancer* (2020) 19:53. doi: 10.1186/s12943-020-01170-0

30. Wang S, Zhang Q, Yu C, Cao Y, Zuo Y, Yang L, et al. Immune cell infiltration-based signature for prognosis and immunogenomic analysis in breast cancer. *Brief Bioinform* (2021) 22:2020–31. doi: 10.1093/bib/bbaa026

31. Sun J, Zhang Z, Bao S, Yan C, Hou P, Wu N, et al. Identification of tumor immune infiltration-associated lncRNAs for improving prognosis and immunotherapy response of patients with non-small cell lung cancer. *J Immunother Cancer* (2020) 8:1–10. doi: 10.1136/jitc-2019-000110

32. Wu CC, Beird HC, Livingston JA, Advani S, Mitra A, Cao S, et al. Immuno-genomic landscape of osteosarcoma. *Nat Commun* (2020) 11:1008. doi: 10.1038/s41467-020-14646-w

33. Fan L, Ru J, Liu T, Ma C. Identification of a novel prognostic gene signature from the immune cell infiltration landscape of osteosarcoma. *Front Cell Dev Biol* (2021) 9:718624. doi: 10.3389/fcell.2021.718624

34. Chen Y, Zhao B, Wang X. Tumor infiltrating immune cells (TIICs) as a biomarker for prognosis benefits in patients with osteosarcoma. *BMC Cancer* (2020) 20:1022. doi: 10.1186/s12885-020-07536-3

35. Cheng X, Wang X, Nie K, Cheng L, Zhang Z, Hu Y, et al. Systematic pan-cancer analysis identifies TREM2 as an immunological and prognostic biomarker. *Front Immunol* (2021) 12:646523. doi: 10.3389/fimmu.2021.646523

36. Zhang X, Shi M, Chen T, Zhang B. Characterization of the immune cell infiltration landscape in head and neck squamous cell carcinoma to aid immunotherapy. *Mol Ther Nucleic Acids* (2020) 22:298–309. doi: 10.1016/j.omtn.2020.08.030

37. Chen DS, Mellman I. Elements of cancer immunity and the cancer-immune set point. *Nature* (2017) 541:321–30. doi: 10.1038/nature21349

38. Park S, Ock C-Y, Kim H, Pereira S, Park S, Ma M, et al. Artificial intelligence-powered spatial analysis of tumor-infiltrating lymphocytes as complementary biomarker for immune checkpoint inhibition in non-Small-Cell lung cancer. *J Clin Oncol* (2022) 40(17):JCO2102010. doi: 10.1200/JCO.21.02010

39. Xiao Y, Ma D, Zhao S, Suo C, Shi J, Xue M-Z, et al. Multi-omics profiling reveals distinct microenvironment characterization and suggests immune escape mechanisms of triple-negative breast cancer. *Clin Cancer Res* (2019) 25:5002–14. doi: 10.1158/1078-0432.CCR-18-3524

40. Li J, Byrne KT, Yan F, Yamazoe T, Chen Z, Baslan T, et al. Tumor cell-intrinsic factors underlie heterogeneity of immune cell infiltration and response to immunotherapy. *Immunity* (2018) 49:178–193.e177. doi: 10.1016/j.immuni.2018.06.006

41. Galon J, Bruni D. Approaches to treat immune hot, altered and cold tumours with combination immunotherapies. *Nat Rev Drug Discov* (2019) 18:197–218. doi: 10.1038/s41573-018-0007-y

frontiers | Frontiers in Immunology

TYPE Original Research
PUBLISHED 29 July 2022
DOI 10.3389/fimmu.2022.934221

OPEN ACCESS

EDITED BY
Zong Sheng Guo,
University at Buffalo, United States

REVIEWED BY
Jinhui Liu,
Nanjing Medical University, China
Haitao Liu,
Shanghai General Hospital, China
Xuan Gao,
State Key Laboratory of Microbial Resources, Institute of Microbiology, Chinese Academy of Sciences (CAS), China

*CORRESPONDENCE
Hongda Pan
panhongda@shca.org.cn
Jianghong Wu
elite_53@163.com

†These authors have contributed equally to this work

SPECIALTY SECTION
This article was submitted to Cancer Immunity and Immunotherapy, a section of the journal Frontiers in Immunology

RECEIVED 02 May 2022
ACCEPTED 11 July 2022
PUBLISHED 29 July 2022

CITATION
Pan H, Pan J and Wu J (2022) Development and validation of a cancer-associated fibroblast-derived lncRNA signature for predicting clinical outcomes in colorectal cancer. *Front. Immunol.* 13:934221. doi: 10.3389/fimmu.2022.934221

Development and validation of a cancer-associated fibroblast-derived lncRNA signature for predicting clinical outcomes in colorectal cancer

Hongda Pan[1,2*†], Jingxin Pan[3†] and Jianghong Wu[1,2*]

[1]Department of Gastric Surgery, Fudan University Shanghai Cancer Center, Shanghai, China, [2]Department of Oncology, Shanghai Medical College, Fudan University, Shanghai, China, [3]Department of Hematology, The Second Affiliated Hospital of Fujian Medical University, Quanzhou, China

Cancer-associated fibroblasts (CAFs) are actively involved in cancer progression through generating extracellular matrix and orchestrating the crosstalk within the tumor microenvironment (TME). This study aimed to develop and validate a CAF-derived lncRNA (long non-coding RNA) (CAFDL) signature for predicting clinical outcomes in colorectal cancer (CRC). Clinical data and transcriptomic profiles of 2,320 patients with CRC from The Cancer Genome Atlas (TCGA)-COAD and TCGA-READ datasets and 16 Gene Expression Omnibus datasets were included in this study. CAFDLs were identified using weighted gene co-expression network analysis. The CAFDL signature was constructed using the least absolute shrinkage and selection operator analysis in the TCGA-CRC training set. Multiple CRC cohorts and pan-cancer cohorts were used to validated the CAFDL signature. Patients with high CAFDL scores had significantly worse overall survival and disease-free survival than patients with low CAFDL scores in all CRC cohorts. In addition, non-responders to fluorouracil, leucovorin, and oxaliplatin (FOLFOX)/fluorouracil, leucovorin, and irinotecan (FOLFIRI) chemotherapy, chemoradiotherapy, bevacizumab, and immune checkpoint inhibitors had significantly higher CAFDL scores compared with responders. Pan-cancer analysis showed that CAFDL had prognostic predictive power in multiple cancers such as lung adenocarcinoma, breast invasive carcinoma, stomach adenocarcinoma, and thyroid carcinoma. The CAFDL signature was positively correlated with transforming growth factor-beta (TGF-β) signaling, epithelial–mesenchymal transition, and angiogenesis pathways but negatively correlated with the expression of immune checkpoints such as PDCD1, CD274, and CTLA4. The CAFDL signature reflects CAF properties from a lncRNA perspective and effectively predicts clinical outcomes in CRC and across pan-cancer. The CAFDL signature can serve as a useful tool for risk stratification and provide new insights into the underlying mechanisms of CAFs in cancer immunity.

KEYWORDS

cancer-associated fibroblasts, long non-coding RNAs, colorectal cancer, pan-cancer, prognosis, signature

Introduction

Colorectal cancer (CRC) is the third most common cancer and the second leading cause of cancer-related death worldwide. Standard treatments for CRC include surgery, adjuvant or neoadjuvant chemotherapy and radiotherapy, and targeted therapy (1). In recent years, immune checkpoint inhibitors (ICIs) have revolutionized the treatment of patients with CRC, especially those with microsatellite instability-high (MSI-H)/mismatch-repair-deficient (dMMR) status (2). Cancer-associated fibroblasts (CAFs) are the most abundant of all stromal cells that populate the tumor microenvironment (TME). CAFs modulate the biological properties of cancer cells and other stromal cells through orchestrating the crosstalk within TME and releasing a variety of regulatory factors (3). The extracellular matrix remodeled by CAFs acts as a physical barrier supporting tumor cell invasion and inhibiting infiltration of antitumor leukocytes, leading to cancer progression, immune evasion, and immunotherapy resistance (4). In addition, CAFs may confer substantial therapeutic resistance by impairing drug delivery and immune signaling pathways (5). Previous studies have shown that high CAF infiltration indicates poor survival. CAFs are identified by protein biomarkers such as alpha–smooth muscle actin or fibroblast activation protein (6). Herrera et al. recently reported a CAF-derived gene signature for predicting CRC prognosis involving 596 protein-coding genes (7). Accumulating evidence suggests that long non-coding RNAs (lncRNAs), a subset of non-coding RNAs with >200 nucleotides in length, are closely implicated in the biological behaviors of CAFs (8, 9). However, comprehensive analysis of lncRNAs associated with CAFs is still lacking. Therefore, studies revealing the roles of CAF in cancer immunology from a lncRNA perspective are warranted. CAFs have a higher infiltration level in CRC compared with other cancer types, suggesting that CAFs play a more important role in CRC than in other cancers. CRC has a large number of high-quality sequencing datasets containing lncRNA expression profiles.

In this study, we developed and validated a CAF-derived lncRNA (CAFDL) signature based on clinical data and transcriptomic profiles of 2,320 patients with CRC from 18 datasets. The CAFDL signature could serve as a robust predictor of overall survival (OS) and disease-free survival (DFS), as well as response to all mainstay treatments of CRC, including chemotherapy, chemoradiotherapy, targeted therapy, and immunotherapy. Moreover, pan-cancer analysis revealed the predictive power of the CAFDL signature in multiple cancers, and its molecular and immune correlates were explored (Figure 1). Our study opens up new avenues for risk stratification and provides new insights into the underlying mechanisms of CAFs in CRC and across pan-cancer.

Materials and methods

Data acquisition and processing

Transcriptomic RNA sequencing and corresponding clinical data of 10,148 patients across 33 cancer types including colon adenocarcinoma (COAD) and rectal adenocarcinoma (READ) were downloaded from the TCGA database (https://portal.gdc.cancer.gov). The raw read count was converted to transcripts per

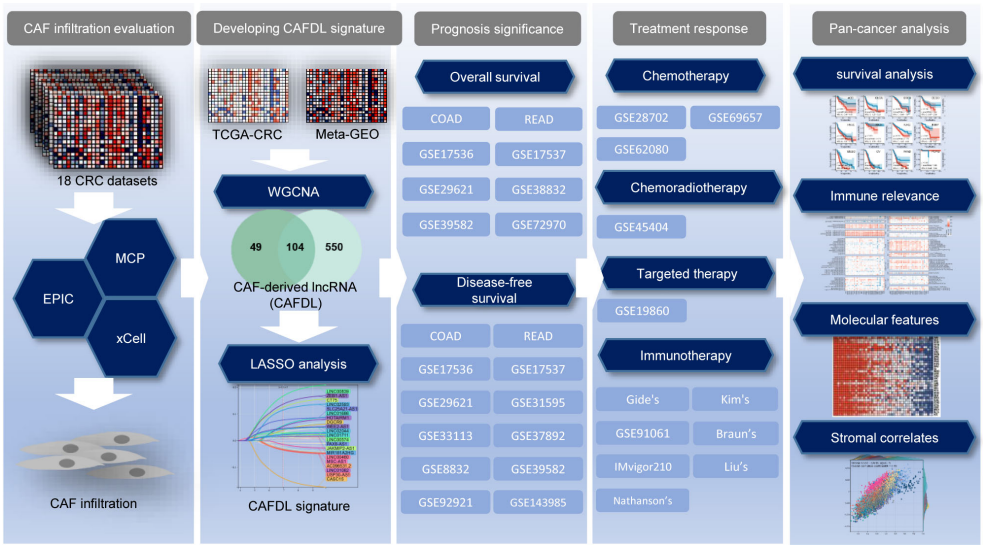

FIGURE 1
Flow chart of this study.

kilobase million (TPM) format and log2(x+1)-transformed. Expression profiles and clinical information obtained from the Gene Expression Omnibus (GEO) for 16 CRC datasets (GSE17536, GSE17537, GSE19860, GSE28702, GSE29621, GSE31595, GSE33113, GSE37892, GSE38832, GSE39582, GSE45404, GSE62080, GSE69657, GSE72970, GSE92921, and GSE143985) using the Affymetrix® GPL570 platform. For immunotherapy cohorts, transcriptome and clinical information of IMvigor210 (10) was downloaded from the online database (http://research-pub.gene.com/IMvigor210CoreBiologies). Gene expression profiles and clinical data of Gide's (11), Nathanson's (12), Kim's (13), Braun's (14), and Liu's (15) cohorts were obtained from their articles. Expression profiling and clinical data of GSE91061 (16) were downloaded from the GEO database. The "ComBat" tool from the "sva" package of the R software was applied to correct for systematic batch effects among the TCGA and GEO datasets. The "ComBat" tool from the "sva" package of the R software was applied to correct for systematic batch effects between the TCGA-COAD and TCGA-READ datasets and among 16 GEO datasets, respectively. Patients with a follow-up or survival duration of less than 30 days were excluded from survival analysis to rule out the bias due to loss to follow-up or perioperative death.

Tumor immune microenvironment analysis

CAF infiltrations were evaluated using three algorithms: EPIC (17), xCELL (18), and MCPcounter (19). Tumor purity and the presence of infiltrating stromal/immune cells in tumor tissues were predicted using ESTIMATE algorithm (20). Immune cell infiltrations in 33 cancer types were calculated using seven algorithms: TIMER (21), EPIC, xCELL, CIBERSORT (22), QUANTISEQ (23), MCPcounter, and TIDE (24).

Weighted gene co-expression network analysis

Weighted gene co-expression network analysis (WGCNA) is a systematic bioinformatics algorithm capable of integrating highly coordinated expressed genes into several gene modules and investigating the relationship of modules to phenotypes of interest. An appropriate soft power threshold (β) was chosen to find the best balance to generate the largest number of modules without loss of gene module membership (MM). WGCNA was conducted using the "WGCNA" package in R.

Construction of the prognostic signature

The TCGA-CRC cohort was randomly divided into a training set and an internal validation set in a 1:1 ratio. All CAFDLs identified from WCGNA were included in the least absolute shrinkage and selection operator (LASSO) Cox regression model to construct the powerful prognostic signature. LASSO analysis was repeated for 1,000 iterations until the area under the curve (AUC) of time-dependent receiver operating characteristic (ROC) analysis reached a maximum value in both the training and internal test cohorts. A multivariate Cox regression model was finally used to determine the coefficient and construct a prognostic signature based on the candidate lncRNAs generated from the LASSO analyses. A risk score for each patient was calculated as the sum of each gene's score, which was obtained by multiplying the expression of each gene and its coefficient. The sensitivity and specificity of the prognostic signature were accessed by ROC curves and area under the ROC curves (AUC values).

Single-sample gene set enrichment analysis

The enrichment scores of cancer hallmark gene sets were calculated by single-sample gene set enrichment analysis (ssGSEA) method with the "ssGSEA" package in R. Cancer hallmark gene sets were downloaded from Molecular Signatures Database.

Quantitative real-time PCR

TRIzol reagent (Thermo Fisher Scientific, Carlsbad, CA, USA) was used to extract the total RNA from CRC and normal tissues according to the manufacturer's protocol. Reverse transcription was performed using a Prime Script RT reagent kit (Takara Biotechnology, China). Applied Biosystems 7900 Real-time PCR System (Thermo Fisher Scientific) was used to perform the quantitative real-time PCR (qRT-PCR) assay. glyceraldehyde 3-phosphate dehydrogenase (GAPDH) was used to normalize lncRNA expression.

Results

Assessing CAF infiltrations in CRC cohorts

First, we established two integrated cohorts, namely, TCGA-CRC and meta-GEO. The TCGA-CRC cohort of 625 patients consisted of TCGA-COAD (N = 458) and TCGA-READ (N = 167) datasets. On the other hand, the meta-GEO cohort of 1,116 patients was pooled from six GEO datasets with OS data: GSE17536 (N = 177), GSE17537 (N = 55), GSE29621 (N = 65), GSE38832 (N = 122), GSE39582 (N = 573), and GSE72970 (N = 124). CAF infiltrations in each CRC sample were evaluated using three algorithms: EPIC, MCPcounter, and xCELL (Table S1).

WGCNA identified CAFDLs

After gene symbol annotation, 12,644 lncRNAs in the TCGA-CRC and 2,023 lncRNAs in the meta-GEO cohort were obtained. A total of 1,993 lncRNAs were shared by both cohorts. We performed WGCNA on the lncRNA expression profiles of TCGA-CRC and meta-GEO cohorts, respectively. The optimal soft threshold used to generate modules was 3 for both cohorts. The numbers of modules identified by WGCNA for TCGA-CRC and meta-GEO cohorts were 14 and 9, respectively (Figure 2A). We analyzed the relationship between modules and CAF infiltrations assessed by EPIC, MCPcounter, and xCell algorithms. CAF infiltration was significantly associated with turquoise module in TCGA-CRC (R_{EPIC} = 0.67, R_{MCP} = 0.74, and R_{xCell} = 0.54, respectively) (Figure 2A). The correlation coefficient between the gene significance (GS) of CAF infiltration and MM in the TCGA-CRC turquoise module reached 0.81 (Figure 2B). In meta-GEO, CAF infiltration was significantly associated with green module (R_{EPIC} = 0.64, R_{MCP} = 0.45, and R_{xCell} = 0.55, respectively) (Figure 2A). The correlation coefficient between GS of CAF infiltration and MM in the meta-GEO green module reached 0.84 (Figure 2C). The turquoise module of TCGA-CRC contains 153 lncRNAs, whereas the green module of meta-GEO contains 654 lncRNAs. We obtained 703 lncRNAs in these two modules, which were defined as CAFDLs (Figure 2D).

Development of the CAFDL signature

The TCGA-CRC cohort was randomly divided into a training set and an internal validation set. LASSO regression analysis was used to select the optimal CAFDLs for building a risk prediction model (Figure 2E). A multivariate Cox regression model was finally used to determine the coefficient and construct a prognostic signature based on the candidate lncRNAs generated from the LASSO analyses (Figure 2F). The CAFDL signature consists of 21 lncRNAs (HOTAIRM1, LINC01082, MSC-AS1, LINC00460, USP30-AS1, AC096531.2, CASC15, DGCR9, CT75, JAKMIP2-AS1, LINC00574, LINC00839, LINC01686, LINC01711, LINC02044, LINC02593, MIR181A2HG, PAX8-AS1, SLC25A21-AS1, WEE2-AS1, and ZEB1-AS1), and its corresponding risk score (CAFDL Score) is the sum of the products of all lncRNA expression values and coefficients. We examined the expression of these 21 lncRNAs in CRC and normal tissues. Among the 21 lncRNAs, 14 lncRNAs (HOTAIRM1, LINC01082, LINC00460, USP30-AS1, AC096531.2, CASC15, CT75, LINC00574, LINC01711, LINC02593, MIR181A2HG, SLC25A21-AS1, WEE2-AS1, and ZEB1-AS1) were significantly differentially expressed between CRC and adjacent normal tissues. LINC00460, CASC15, LINC01711, MIR181A2HG, and ZEB1.AS1 were significantly upregulated in CRC tissues, whereas the remaining lncRNAs were significantly downregulated in CRC compared with normal tissues (Figure 2G). Next, we analyzed the OS and DFS of patients with CRC with high or low expression of the 21 lncRNAs, as suggested by the reviewers. CT75, DGCR9, HOTAIRM1, LINC00460, LINC01082, LINC01711, LINC02044, USP30-AS1, and ZEB1.AS1 were significantly associated with OS (Figure S1A), and AC096531.2, CT75, DGCR9, HOTAIRM1, LINC00839, LINC01082, LINC02044, LINC02593, MIR181A2HG, SLC25A21-AS1, WEE2-AS1, and ZEB1.AS1 were significantly associated with DFS (Figure S1B).

Each cohort was divided into high and low CAFDL groups according to the optimal cutoff value calculated by the "survminer" package in R. Kaplan–Meier survival analysis showed that patients with high CAFDL scores in the TCGA-CRC cohort had significantly worse OS than patients with low CAFDL scores [P < 0.001, hazard ratio (HR) = 2.41, 95% confidence interval (CI) 1.64–3.55] (Figure 3A). We collected 20 pairs of CRC and adjacent normal tissue samples for qRT-PCR analysis. The expression of 11 of 21 lncRNAs (HOTAIRM1, LINC01082, LINC00460, USP30-AS1, CASC15, JAKMIP2-AS1, LINC00574, LINC01711, LINC02593, SLC25A21-AS1, and ZEB1-AS1) was significantly different between CRC and adjacent normal tissues. Among them, LINC00460, CASC15, JAKMIP2-AS1, LINC01711, and ZEB1-AS1 were significantly upregulated in CRC tissues, whereas HOTAIRM1, LINC01082, USP30-AS1, LINC00574, LINC02593, and SLC25A21-AS1 were significantly downregulated in CRC tissues (Figure S2A).

Validation of the predictive value of CAFDL signature for OS in CRC cohorts

We apply the CAFDL signature to eight CRC cohorts to validate its predictive value for OS. In the TCGA-COAD (HR = 2.54, P < 0.001), TCGA-READ (HR = 2.67, P = 0.026), GSE17536 (HR = 2.30, P < 0.001), GSE17537 (HR = 2.91, P = 0.023), GSE29621 (HR = 3.55, P = 0.004), GSE39582 (HR = 2.37, P < 0.001), GSE72970 (HR = 1.90, P = 0.008), and total CRC cohorts (HR = 2.18, P < 0.001), patients with high CAFDL scores had significant worse OS compared with those with low CAFDL scores (Figure 3A, Figure S3), except for GSE38832 (P = 0.172, HR = 1.79), whose OS difference did not reach statistical significance.

Validation of the predictive value of CAFDL signature for DFS in CRC cohorts

Next, we validate predictive value of CAFDL signature for DFS in 12 cohort with DFS data. In the TCGA-COAD (HR =

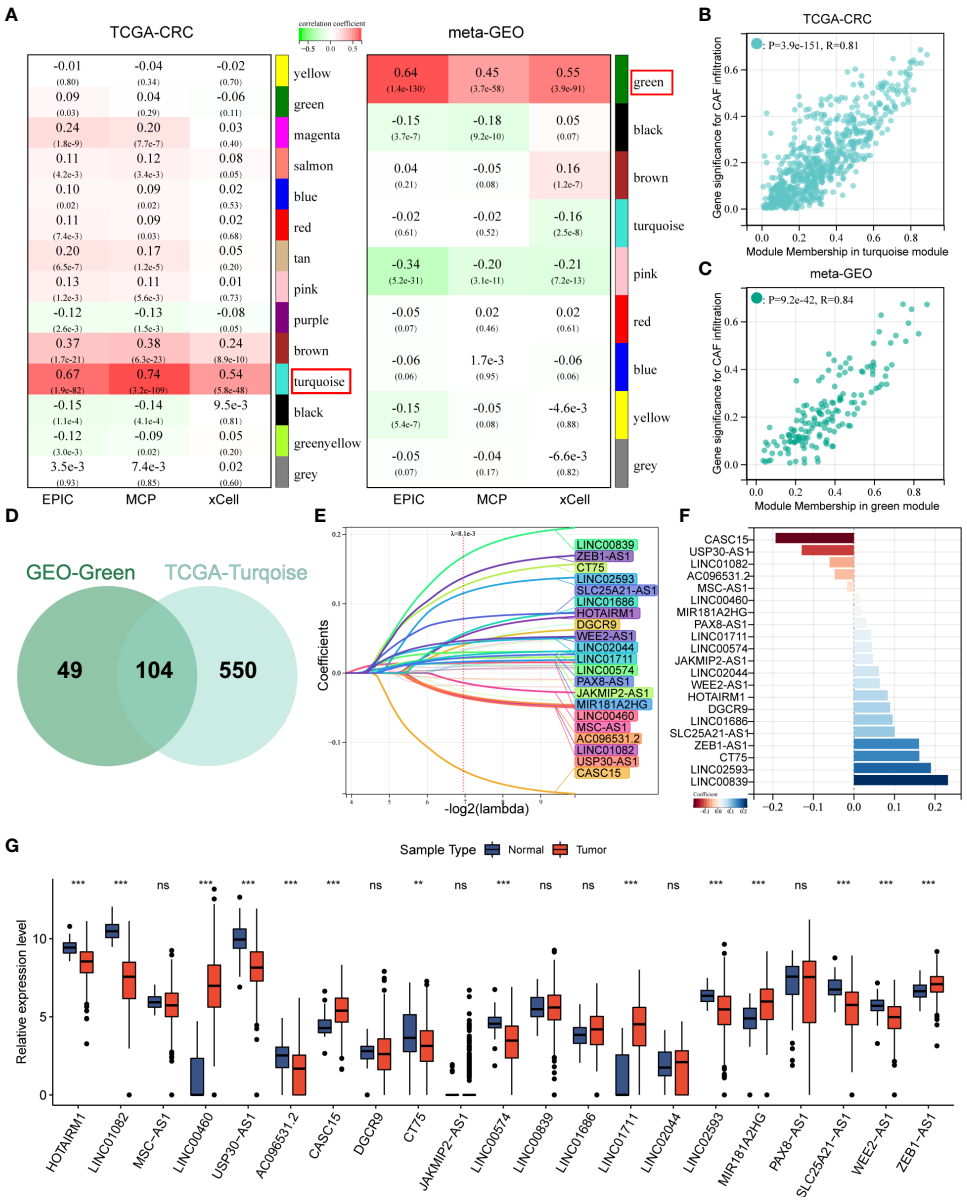

FIGURE 2
WGCNA identified CAFDL and LASSO analysis. **(A)** WGCNA identified modules associated with CAF infiltration calculated by EPIC, MCPcounter, and xCell in TCGA-CRC and meta-GEO cohorts. **(B)** Correlation between gene significance for CAF infiltration and module membership in turquoise module in TCGA-CRC cohort. **(C)** Correlation between gene significance for CAF infiltration and module membership in green module in meta-GEO cohort. **(D)** A Venn diagram showing the number of lncRNAs in the turquoise module in the TCGA-CRC cohort and the green module in the meta-GEO cohort. **(E)** LASSO analysis identifies 21 CAF-derived lncRNAs. **(F)** Multivariate Cox analysis calculated the coefficient for each lncRNA in the CAFDL signature. **(G)** Expression of 21 CAF-derived lncRNAs in CRC and normal tissues. **P < 0.01, ***P < 0.001, NS non-significant.

2.06 P < 0.001), TCGA-READ (HR = 2.05, P = 0.045), GSE17536 (HR = 3.03, P = 0.015), GSE17537 (HR = 2.44, P < 0.029), GSE29621 (HR = 5.29, P = 0.02), GSE31959 (HR = infinity, P = 0.004), GSE33113 (HR = 4.53, P < 0.001), GSE37982 (HR = 2.82, P < 0.001), GSE38832 (HR = 7.26, P = 0.025), GSE39582 (HR = 1.79 P < 0.001), GSE92921 (HR = 8.47 P < 0.019), and GSE143982 (HR = 3.31, P = 0.016) cohorts, all patients with high CAFDL scores had significantly worse DFS compared with those with low CAFDL scores (Figure 3B). We performed ROC analysis of the CAFDL signature in each of the TCGA and GEO datasets for the predictive ability of DFS and OS at 1, 3, and 5 years and calculated its AUC values (Figure S2B).

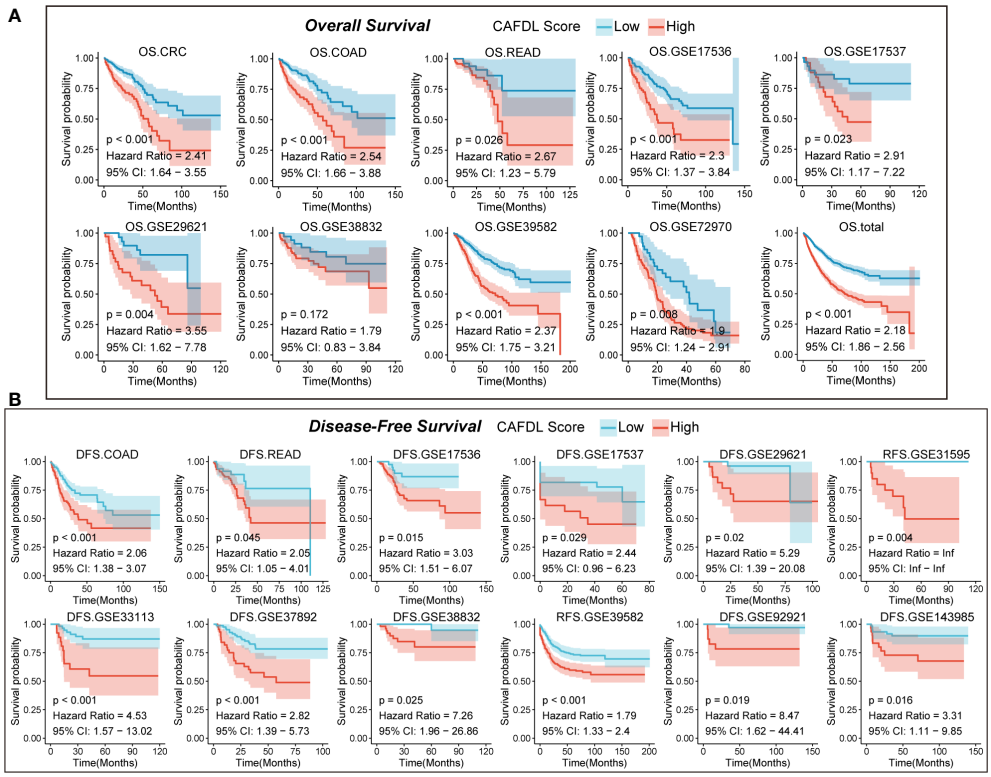

FIGURE 3
CAFDL signature can effectively predict the prognosis of patients with CRC. **(A)** Patients with high CAFDL scores have significantly worse overall survival than those with low CAFDL scores in TCGA-CRC, TCGA-COAD, TCGA-READ, GSE17536, GSE17537, GSE29621, GSE38832, GSE39582, GSE72970, and total CRC cohorts. **(B)** Patients with high CAFDL scores have significantly worse disease-free survival than those with low CAFDL scores in TCGA-COAD, TCGA-READ, GSE17536, GSE17537, GSE29621, GSE31595, GSE33113, GSE37892, GSE38832, GSE39582, GSE92921, and GSE143985 cohorts.

CAFDL signature is an independent prognostic factor for OS and DFS

Univariate (Figures S2C, E) and multivariate Cox analyses (Figures S2D, F) were performed for multiple clinicopathological factors (age, gender, histological differentiation, and American Joint Committee on Cancer (AJCC) TNM stage) together with the CAFDL signature in the TCGA-CRC cohort. The results showed that CAFDL signature, age, and TNM stage were independent prognostic factors for OS, whereas CAFDL signature and TNM stage were independent prognostic factors for DFS.

CAFDL signature predicts response to chemotherapy, radiotherapy, and targeted therapy

Chemotherapy, radiotherapy, and targeted therapy are the mainstay treatments for CRC. Non-responders to FOLFOX (GSE28702 and GSE69657; Figures 4A, B) and FOLFIRI (GSE62080; Figure 4C) chemotherapy had significantly higher CAFDL scores compared with responders. The AUC values of CAFDL signature for predicting response to chemotherapy in GSE28702 (Figure 4A), GSE69657 (Figure 4B), and GSE62080 (Figure 4C) were 0.639, 0.715, and 0.750, respectively. In addition, CAFDL signature can also effectively predict the response to chemoradiotherapy in patients with rectal cancer (GSE45404, AUC = 0.72); non-responders had significantly higher CAFDL score than responders (Figure 4D). Notably, CAFDL signature had excellent predictive power for response to bevacizumab (GSE19860, AUC = 1); all responders belonged to the low CAFDL score group (Figure 4E).

CAFDL signature predicts immunotherapy outcomes

We applied the CAFDL signature to multiple immunotherapy cohorts and found that non-responders to

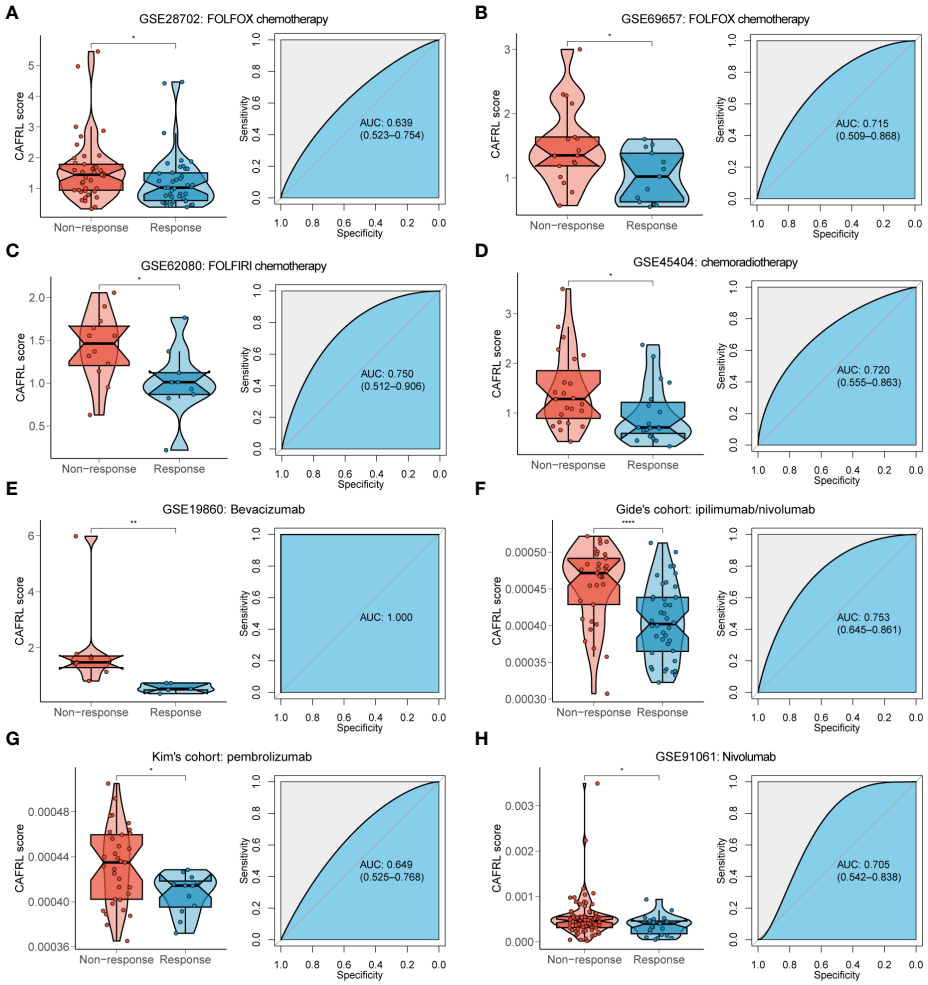

FIGURE 4
CAFDL signature can effectively predict the response to mainstay treatments of CRC. **(A–E)** Non-responders to FOLFOX **(A, B)** and FOLFIRI **(C)** chemotherapy, chemoradiotherapy **(D)**, and bevacizumab targeted therapy **(E)** had significantly higher CAFDL scores compared with responders (left panels). ROC curves demonstrate the predictive power of the CAFDL signature for response to these treatments (right panels). **(F–H)** Non-responders to ipilimumab/nivolumab **(F)**, pembrolizumab **(G)**, and nivolumab **(H)** had significantly higher CAFDL scores compared with responders (left panels). ROC curves demonstrate the predictive power of the CAFDL signature for response to these treatments (right panels). *P < 0.05, **P < 0.01, and ****P < 0.0001.

ICIs had significantly higher CAFDL scores compared with responders in Gide's cohort (melanoma treated with anti–programmed cell death 1 (PD-1)/cytotoxic T-lymphocyte-associated protein 4 (CTLA-4) antibody; Figure 4F), Kim's cohort (gastric cancer treated with anti–PD-1 antibody; Figure 4G), and GSE91061 (melanoma treated with anti–PD-1 antibody; Figure 4H). The AUC values of CAFDL signature for predicting response to immunotherapy in Gide's cohort (Figure 4F), Kim's cohort (Figure 4G), and GSE91061 (Figure 4H) were 0.753, 0.649, and 0.705, respectively. Moreover, patients with high CAFDL scores had a significantly worse prognosis than those with low CAFDL scores in Braun's cohort (clear cell renal cell carcinoma treated with anti–PD-1 antibody), Gide's cohort, IMvigor210 (bladder urothelial carcinoma treated with anti–programmed death ligand 1 (PD-L1) antibody), Liu's cohort (melanoma treated with anti–PD-1 antibody), and Nathanson's cohort (melanoma treated with anti–CTLA-4 antibody) (all P < 0.05; Figure 5A). In the IMvigor210 cohort, patients in the low CAFDL score group had significantly higher PD-L1 protein expression levels in immune cells (Figure 5B) and tumor cells (Figure 5C). The high CAFDL score group had higher proportion of immune desert phenotype, lower proportion of immune-inflamed phenotype (Figure 5D), and lower $CD8^+$ T effector infiltration (Figure 5E).

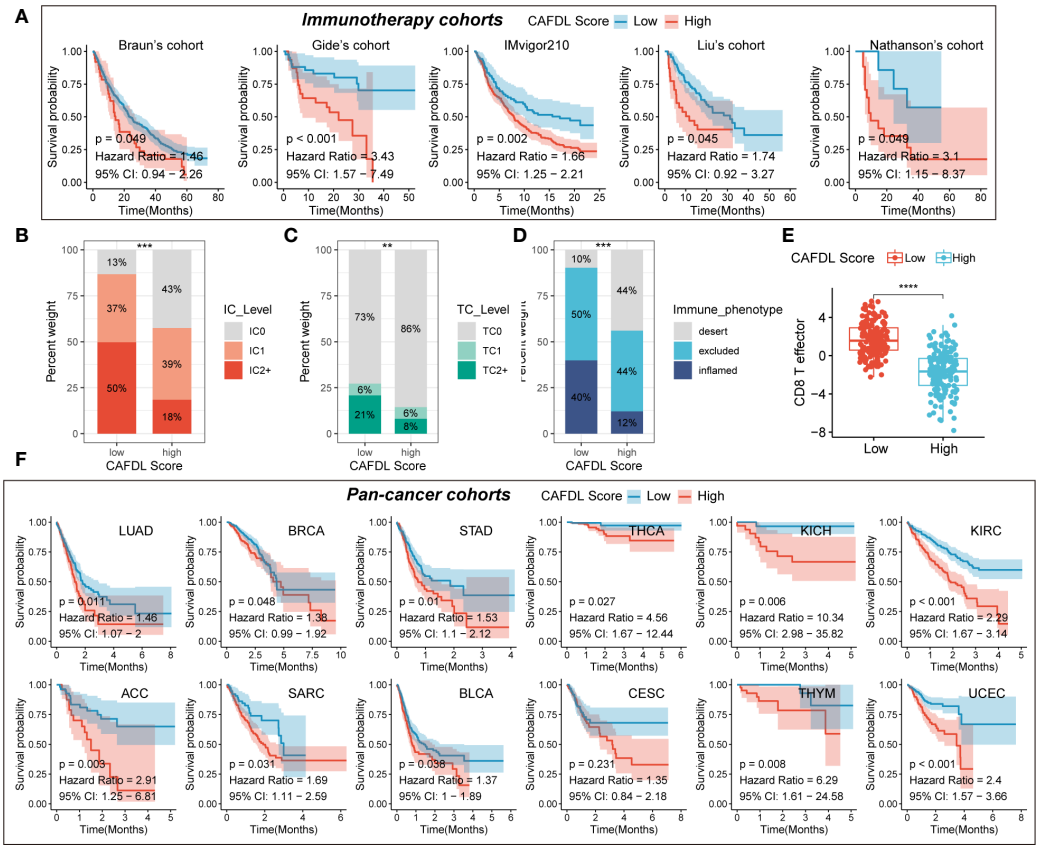

FIGURE 5
CAFDL signature predicts clinical outcomes in immunotherapy cohorts and pan-cancer cohorts. **(A)** Patients with high CAFDL scores have significantly worse overall survival than those with low CAFDL scores in Braun's, Gide's, IMvigor210, Liu's, and Nathanson's cohorts. **(B, C)** In the IMvigor210 cohort, patients in the low CAFDL score group had significantly higher PD-L1 protein expression levels in immune cells **(B)** and tumor cells **(C)**. **(D)**The high CAFDL score group had higher proportion of immune desert phenotype and lower proportion of immune-inflamed phenotype. **(E)** The high CAFDL score group had significantly lower $CD8^+$ T effector infiltration. **(F)** In addition to COAD and READ, patients with high CAFDL scores have significantly worse overall survival than those with low CAFDL scores in 12 TCGA datasets: LUAD, BRCA, STAD, THCA, KICH, KIRC, ACC, SARC, BLCA, CESC, THYM, and UCEC. **P < 0.01, ***P < 0.001, and ****P < 0.0001.

CAFDL signature predicts prognosis across multiple cancers

In addition to COAD and READ, we also attempted to explore the predictive power of the CAFDL signature for clinical outcomes in other cancers. The CAFDL signature is effective in prognostic stratification in the most common cancers, including lung adenocarcinoma (LUAD), breast invasive carcinoma (BRCA), stomach adenocarcinoma (STAD), thyroid carcinoma (THCA), bladder urothelial carcinoma (BLCA), kidney renal clear cell carcinoma (KIRC), adrenocortical carcinoma (ACC), cervical squamous cell carcinoma and endocervical adenocarcinoma (CESC), kidney chromophobe (KICH), sarcoma (SARC), thymoma (THYM), and uterine corpus endometrial carcinoma (UCEC) (all $P < 0.05$; Figure 5F), implying that CAFDL has broad applicability across pan-cancer.

Immune correlates of CAFDL signature across pan-cancer

To fully demonstrate the pan-cancer TME landscape, immune cell infiltrations across pan-cancer were evaluated using seven algorithms: TIMER, EPIC, xCell, CIBERSORT, QUANTISEQ, MCPcounter, and TIDE (Figure 6A). As expected, the CAFDL signature was closely associated with the CAF infiltration (Figure 6A). Epithelial cells, another important member of the stromal component, also had a strong correlation with the CAFDL signature. In addition, the CAFDL signature was also significantly associated with macrophage M2 in COAD and READ. CAFDL signature showed no or negative correlation with major immune cells such as $CD8^+$/$CD4^+$ T cells, B cells, and M1 macrophages.

Next, we used the ESTIMATE algorithm to evaluate the pan-cancer stromal score and immune score. The CAFDL signature

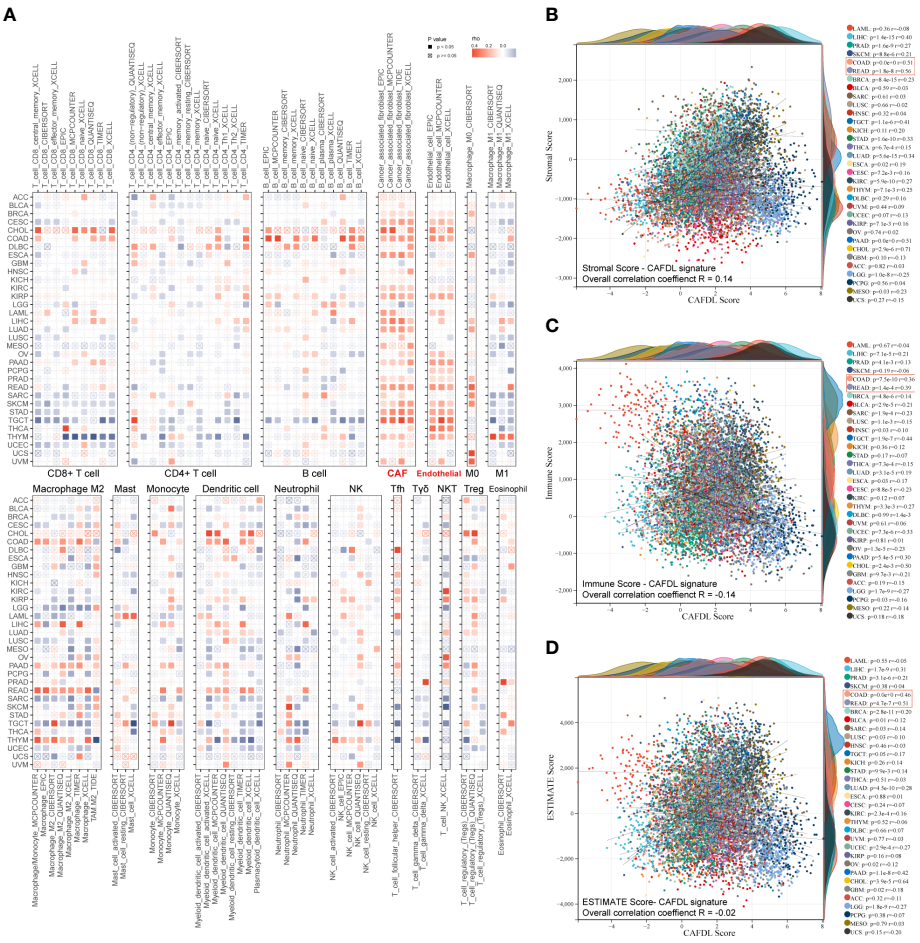

FIGURE 6
Pan-cancer immune correlates of CAFDL signature. **(A)** Correlation of CAFDL signature with immune cell infiltration evaluated using seven algorithms: TIMER, EPIC, xCELL, CIBERSORT, QUANTISEQ, MCPcounter, and TIDE across pan-cancer. **(B–D)** Correlation of CAFDL signature with stromal score **(B)**, immune score **(C)**, and ESTIMATE score **(D)** across pan-cancer.

showed a positive correlation with the stromal score, with an overall correlation of 0.14 for the entire pan-cancer cohort and a median correlation of 0.16 across 33 cancers, ranging from −0.25 to 0.71 (Figure 6B). However, CAFDL exhibited negative correlations with the immune score (R = −0.14; Figure 6C) and the ESTIMATE score (the integration of the stromal score and the immune score, R = −0.02; Figure 6D), respectively. Notably, CAFDL signature showed moderate correlation with stromal score in COAD (R = 0.51) and READ (R = 0.56) and weak correlation with immune score in COAD (R = 0.36) and READ (R = 0.39), respectively. These results indicated that CAFDL could specifically reflect the properties of stromal components in TME but had a weak correlation with immune cell infiltration.

Molecular features of CAFDL signature

We calculated the enrichment scores for cancer hallmark gene sets across 33 cancer types using the ssGSEA method. The CAFDL signature was significantly positively correlated with epithelial–mesenchymal transition (EMT), WNT/β-Catenin signaling, angiogenesis, and TGF-β signaling pathways across pan-cancer, which are important mechanisms that occur in the tumor stroma to promote tumor development and metastasis (Figure 7A). Moreover, we analyzed the correlation of CAFDL signature with expression of immune regulators. TGF-β is well known to be one of the most important regulators of CAF activation (25). The CAFDL signature was significantly positively associated with TGFB1, CD276, CD40, VEGFA, VEGFB, etc., but showed significantly negative correlation with immune checkpoints (such as CD274, PDCD1, CTLA4,

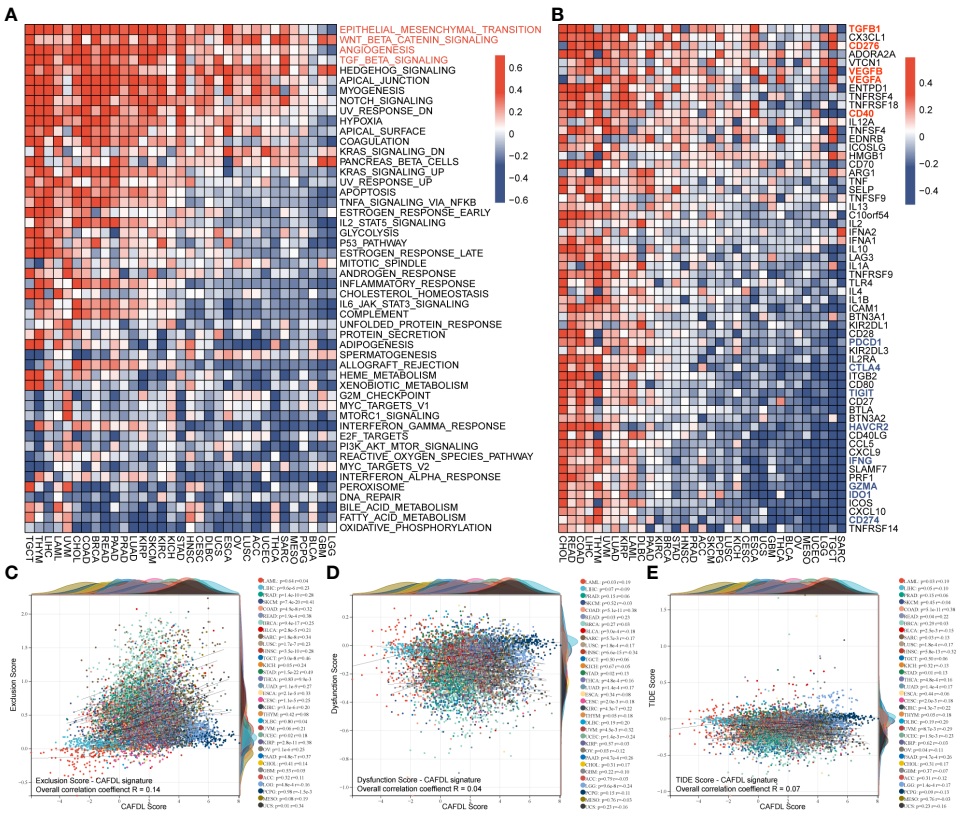

FIGURE 7
Molecular features of CAFDL signature. **(A)** Correlation of CAFDL signature with cancer hallmark gene sets across pan-cancer. **(B)** Correlation of CAFDL signature with common immune regulators across pan-cancer. **(C–E)** Correlation of CAFDL signature with immune exclusion score **(C)**, immune dysfunction score **(D)**, and TIDE score **(E)** across pan-cancer.

TIGHT, and HAVCR2) and anti-cancer immune regulators (IFNG, IDO1, and GZMA) (Figure 7B).

CAFDL signature is associated with immune exclusion

The TIDE online tool was used to assess the potential of immune escape across pan-cancer. The TIDE score consists of two components: immune dysfunction and immune exclusion. CAFDL signature was positively correlated with exclusion score, with an overall correlation of 0.14 for the entire pan-cancer cohort and a median correlation of 0.24 across 33 cancers, ranging from −0.16 to 0.49 (Figure 7C). However, CAFDL signature had little correlation with dysfunction score (R = 0.04; Figure 7D) and TIDE score (R = 0.07; Figure 7E), suggesting that CAF prevents immune cells from killing tumor cells more by generating extracellular matrix (immune exclusion) than by directly causing immune dysfunction.

CAFDL signature is independent of tumor mutation burden and microsatellite instability

Microsatellite instability (MSI) and tumor mutation burden (TMB) are well-established predictors of response to immunotherapy, but they are both intrinsic features of cancer cells and are theoretically unrelated to CAFs. In the GSE39582, GSE92921, and GSE143985 cohorts, there were no significant differences in CAFDL scores between mutant and wild-type tumors of v-raf murine sarcoma viral oncogene homolog B1 (BRAF) (Figures S4A–C), kirsten rat sarcoma viral oncogene (KRAS) (Figures S4D–F), and tumor protein P53 (TP53) (Figures S4G–I). Moreover, we found little correlation between CAFDL signature and TMB across 33 cancers (Figure S5A), including COAD (R = 0.13) and READ (R = 0.02). Likewise, CAFDL scores of MSI-H/dMMR tumors were not significantly different from those of MSS/pMMR tumors in TCGA-COAD, TCGA-READ, GSE39582, GSE92921, and GSE143985 cohorts (Figures S5B–F).

Discussion

CAFs are major components of the TME and interact with cancer cells by secreting extracellular matrix proteins as well as cytokines and growth factors. CAFs block immune cell infiltration and drug delivery, leading to immune escape and resistance to various treatments including chemotherapy, radiotherapy, targeted therapy, and immunotherapy. In recent years, several studies have shown that CAF is closely related to the poor prognosis of patients with cancer (26–28), and the underlying mechanisms have begun to be revealed. Chen et al. reported that CAFs impact the survival outcomes and treatment response in CRC by regulating immune system (27). Li et al. discovered a subgroup of CAFs correlated with poor survival outcomes in patients with gastric cancer using single-cell RNA sequencing (29). Sun et al. demonstrated that prognostic signature based on CAF-secreted cytokines were associated with genetic alterations and clinical outcomes (30). Zheng et al. revealed that CAFs play an important role in TME, and their secreted extracellular protein can serve as a prognostic marker for triple-negative breast cancer (31). However, these studies on CAFs are based on protein-encoding genes, and studies on lncRNAs are still lacking. Herrera et al. (7) reported a CAF-derived gene signature for predicting CRC prognosis involving 596 protein-coding genes rather than lncRNAs, which is different from our study. Zhang et al. (8) found that DNM3OS, a CAF-promoted lncRNA, confers radio-resistance by regulating DNA damage response in esophageal squamous cell carcinoma. This study focused on the biological function of a specific CAF-related lncRNA, whereas our study was a comprehensive analysis of CAF-related lncRNAs. Liu et al. (9) developed an immune-derived lncRNA signature for improving outcomes in CRC using machine learning methods. This study involved immune-derived lncRNAs rather than specifically focusing on CAFDLs. LncRNA signatures have been widely reported in CRC, and these signatures are closely related to specific biological behaviors, including tumor immunity (9), epigenetic modification (32, 33), and cell death (34). To the best of our knowledge, this is the first comprehensive study on CAFDLs in CRC, to establish a CAFDL signature in CRC, which is innovative.

WGCNA has been successfully applied to identify gene modules with various biological functions or cellular characteristics (35, 36). In our study, we used WGCNA to establish a co-expression network of lncRNAs and obtained multiple modules through co-expression relationships. We analyzed the correlation between the expression level of each module and CAF score in CRC tissues, identified CAF-related lncRNA modules, and finally identified CAFDLs.

Many studies have established lncRNA-based prognostic prediction models (37–40). Liu et al. developed a novel immune-related lncRNA signature in endometrial carcinoma (37), patients were randomly divided into training cohort and test cohort, univariate Cox analysis was used to screen lncRNAs associated with prognosis, LASSO regression was used to screen lncRNAs most associated with DFS, and finally multivariate Cox was used to establish a scoring system. In another study developing an EMT-related lncRNA signature (38), patients were also randomly divided into training group and test group, risk prediction model was built, and the weight of each lncRNA was calculated using LASSO regression. Yuan et al. identified m5C-related lncRNAs in pancreatic ductal adenocarcinoma (39), a preliminary screening was performed by univariate Cox, a prediction model was established by LASSO regression, and a risk score was calculated. A recent study constructed a mutation-derived genome instability-related lncRNAs signature in endometrial cancer (40), patients were randomized 1:1 into training or test sets, and risk prediction models were built using univariate and multivariate Cox regression. In our study, we used TCGA-CRC to build a risk prediction model and used the meta-GEO cohort as external validation. The TCGA-CRC cohort is randomly split into a training set and an internal validation set in a 1:1 ratio. The LASSO analysis was repeated for 1,000 iterations until the AUC reached a maximum value in both the training set and the internal test set. Multivariate Cox regression models were finally used to determine coefficients and construct prognostic signatures based on candidate lncRNAs generated by LASSO analysis. In contrast to the previously mentioned literatures, we did not perform a univariate analysis of the initial screening. This is because lncRNAs that constitute prognostic risk models may not reach statistical significance when prognostic analysis is performed on individual genes. Potential prognostic information may be lost if certain important lncRNAs are deleted. Then, because the results of LASSO regression analysis may vary each time, we used multivariate Cox analysis to finally determine the weight coefficient of each lncRNA after LASSO regression established the prognostic model, instead of directly using LASSO regression to calculate the coefficient, which was similar to the analysis method of Liu's study (37).

Our study included 18 datasets of 2,320 patients with CRC, including COAD and READ datasets from the TCGA database, and 16 CRC datasets from the GEO database. We established the CAFDL signature in TCGA-CRC training set and verified its predictive value in all CRC datasets. The CAFDL signature can effectively predict the prognosis of patients with CRC, including OS and DFS. In addition, CAFDL has also demonstrated robust predictive power for response to chemotherapy, radiotherapy, and targeted therapy, which are the mainstays of treatment for CRC. Seven additional immunotherapy datasets were incorporated into our study, and we found that CAFDL can be used as a predictor of response to ICIs. Through comprehensive analysis based on large-scale clinical samples and transcriptomic data, we demonstrate that CAFDL can serve as a robust tool for predicting survival outcomes and treatment response in patients with CRC.

Furthermore, pan-cancer analysis showed that, in addition to COAD and READ, CAFDL had prognostic predictive power in multiple cancers (such LUAD, BRCA, STAD, and THCA). The expression level of CAFDL in pan-cancer is not clear, and the CAFDL signature may not be applicable in all tumors. The purpose of pan-cancer analysis in our study is to try to expand the applicability of CAFDL signature to other cancers. This provides evidence for researchers to conduct further studies in other cancer types in the future.

We further explored the molecular and immune mechanisms and found that CAFDL signature was positively correlated with TGF-β signaling, EMT, and angiogenesis pathways but negatively correlated with the expression of immune checkpoints such as PDCD1, CD274, and CTLA4. Moreover, the CAFDL signature was independent of MSI and TMB, both of which are intrinsic features of cancer cells rather than stromal cells.

Conclusion

In summary, we developed the robust CAFDL signature that can effectively predict the survival outcomes and response to multiple treatments in patients with CRC. Our study provides a roadmap for patient stratification and may help improve strategies for personalized follow-up and individualized decision making for CRC.

Data availability statement

The datasets presented in this study can be found in online repositories. The names of the repository/repositories and accession number(s) can be found in the article/Supplementary Material.

Author contributions

Conception and design: HP and J.W. Acquisition of data: PL. Writing, review, and revision of the manuscript: HP, JP, and PL. Analysis and interpretation of data: HP and JP. Development of methodology: HP and JP. All authors contributed to the article and approved the submitted version.

Funding

This study was funded by the National Natural Science Foundation of China (81902424).

Conflict of interest

The authors declare that the research was conducted in the absence of any commercial or financial relationships that could be construed as a potential conflict of interest.

Publisher's note

Supplementary material

The Supplementary Material for this article can be found online at: https://www.frontiersin.org/articles/10.3389/fimmu.2022.934221/full#supplementary-material

SUPPLEMENTARY FIGURE 1
Survival analysis for the 21 lncRNAs constituting the CAFDL signature. **(A)** Overall survival. **(B)** Disease-free survival.

SUPPLEMENTARY FIGURE 2
Validation of the CAFDL signature. **(A)** qRT-PCR detected the expression levels of 21 lncRNAs constituting the CAFDL signature in paired CRC and adjacent normal tissues. **(B)** ROC analysis of the predictive ability of CAFDL signature on DFS and OS at 1, 3, and 5 years in CRC datasets. **(C, D)** Univariate and multivariate Cox analysis identify independent predictive factors for OS in TCGA-CRC cohort. **(E, F)** Univariate and multivariate Cox analysis identify independent predictive factors for DFS in TCGA-CRC cohort.

SUPPLEMENTARY FIGURE 3
Landmark analysis of GSE17537.

SUPPLEMENTARY FIGURE 4
CAFDL score in patients with wild-type or mutant BRAF, Kras and TP53. **(A-C)** CAFDL score in patients with wild-type or mutant BRAF in GSE39582, GSE92921 and GSE143985 cohorts. **(D-F)** CAFDL score in patients with wild-type or mutant Kras in GSE39582, GSE92921 and GSE143985 cohorts. **(G-I)** CAFDL score in patients with wild-type or mutant TP53 in GSE39582, GSE92921 and GSE143985 cohorts. ns, non-significant.

SUPPLEMENTARY FIGURE 5
Correlation between CAFDL signature and TMB and MSI/MMR status. **(A)** Correlation of CAFDL signature with TMB across pan-cancer. **(B, C)** CAFDL scores of patients with MSI-H, MSI-L and MSS status in COAD **(B)** and READ **(C)**, respectively. **(D)** CAFDL scores of patients with dMMR and pMMR status in GSE39582. **(E, F)** CAFDL scores of patients with MSI-H and MSS status in GSE92921 **(E)** and GSE143985 **(F)**, respectively. ns, non-significant.

References

1. Ciardiello D, Pio Guerrera L, Anna Maiorano B, Parente P, Pia Latiano T, Di Maio M, et al. Immunotherapy in advanced anal cancer: Is the beginning of a new era? *Cancer Treat Rev* (2022) 105:102373. doi: 10.1016/j.ctrv.2022.102373

2. Diaz LAJr., Shiu KK, Kim TW, Jensen BV, Jensen LH, Punt C, et al. Pembrolizumab versus chemotherapy for microsatellite instability-high or mismatch repair-deficient metastatic colorectal cancer (KEYNOTE-177): final analysis of a randomised, open-label, phase 3 study. *Lancet Oncol* (2022) 23 (5):659–70. doi: 10.1016/S1470-2045(22)00197-8

3. Chen Y, McAndrews KM, Kalluri R. Clinical and therapeutic relevance of cancer-associated fibroblasts. *Nat Rev Clin Oncol* (2021) 18(12):792–804. doi: 10.1038/s41571-021-00546-5

4. Kaur A, Ecker BL, Douglass SM, Kugel CH, Webster MR, Almeida FV, et al. Remodeling of the collagen matrix in aging skin promotes melanoma metastasis and affects immune cell motility. *Cancer Discovery* (2019) 9(1):64–81. doi: 10.1158/2159-8290.CD-18-0193

5. Kalluri R. The biology and function of fibroblasts in cancer. *Nat Rev Cancer* (2016) 16(9):582–98. doi: 10.1038/nrc.2016.73

6. Avery D, Govindaraju P, Jacob M, Todd L, Monslow J, Puré E. Extracellular matrix directs phenotypic heterogeneity of activated fibroblasts. *Matrix Biol* (2018) 67:90–106. doi: 10.1016/j.matbio.2017.12.003

7. Herrera M, Berral-González A, López-Cade I, Galindo-Pumariño C, Bueno-Fortes S, Martín-Merino M, et al. Cancer-associated fibroblast-derived gene signatures determine prognosis in colon cancer patients. *Mol Cancer* (2021) 20(1):73. doi: 10.1186/s12943-021-01367-x

8. Zhang H, Hua Y, Jiang Z, Yue J, Shi M, Zhen X, et al. Cancer-associated fibroblast-promoted LncRNA DNM3OS confers radioresistance by regulating DNA damage response in esophageal squamous cell carcinoma. *Clin Cancer Res* (2019) 25(6):1989–2000. doi: 10.1158/1078-0432.CCR-18-0773

9. Liu Z, Liu L, Weng S, Guo C, Dang Q, Xu H, et al. Machine learning-based integration develops an immune-derived lncRNA signature for improving outcomes in colorectal cancer. *Nat Commun* (2022) 13(1):816. doi: 10.1038/s41467-022-28421-6

10. Mariathasan S, Turley SJ, Nickles D, Castiglioni A, Yuen K, Wang Y, et al. TGFβ attenuates tumour response to PD-L1 blockade by contributing to exclusion of T cells. *Nature* (2018) 554(7693):544–8. doi: 10.1038/nature25501

11. Gide TN, Quek C, Menzies AM, Tasker AT, Shang P, Holst J, et al. Distinct immune cell populations define response to anti-PD-1 monotherapy and anti-PD-1/Anti-CTLA-4 combined therapy. *Cancer Cell* (2019) 35(2):238–255.e6. doi: 10.1016/j.ccell.2019.01.003

12. Nathanson T, Ahuja A, Rubinsteyn A, Aksoy BA, Hellmann MD, Miao D, et al. Somatic mutations and neoepitope homology in melanomas treated with CTLA-4 blockade. *Cancer Immunol Res* (2017) 5(1):84–91. doi: 10.1158/2326-6066.CIR-16-0019

13. Kim ST, Cristescu R, Bass AJ, Kim KM, Odegaard JI, Kim K, et al. Comprehensive molecular characterization of clinical responses to PD-1 inhibition in metastatic gastric cancer. *Nat Med* (2018) 24(9):1449–58. doi: 10.1038/s41591-018-0101-z

14. Braun DA, Hou Y, Bakouny Z, Ficial M, Sant' Angelo M, Forman J, et al. Interplay of somatic alterations and immune infiltration modulates response to PD-1 blockade in advanced clear cell renal cell carcinoma. *Nat Med* (2020) 26 (6):909–18. doi: 10.1038/s41591-020-0839-y

15. Wang D, Zheng J, Liu X, Xue Y, Liu L, Ma J, et al. Knockdown of USF1 inhibits the vasculogenic mimicry of glioma cells *via* stimulating SNHG16/miR-212-3p and linc00667/miR-429 axis. *Mol Ther Nucleic Acids* (2019) 14:465–82. doi: 10.1016/j.omtn.2018.12.017

16. Riaz N, Havel JJ, Makarov V, Desrichard A, Urba WJ, Sims JS, et al. Tumor and microenvironment evolution during immunotherapy with nivolumab. *Cell* (2017) 171(4):934–949.e16. doi: 10.1016/j.cell.2017.09.028

17. Racle J, de Jonge K, Baumgaertner P, Speiser DE, Gfeller D. Simultaneous enumeration of cancer and immune cell types from bulk tumor gene expression data. *Elife* (2017) 6:e26476. doi: 10.7554/eLife.26476

18. Aran D, Hu Z, Butte AJ. xCell: digitally portraying the tissue cellular heterogeneity landscape. *Genome Biol* (2017) 18(1):220. doi: 10.1186/s13059-017-1349-1

19. Becht E, Giraldo NA, Lacroix L, Buttard B, Elarouci N, Petitprez F, et al. Estimating the population abundance of tissue-infiltrating immune and stromal cell populations using gene expression. *Genome Biol* (2016) 17(1):218. doi: 10.1186/s13059-016-1070-5

20. Yoshihara K, Shahmoradgoli M, Martínez E, Vegesna R, Kim H, Torres-Garcia W, et al. Inferring tumour purity and stromal and immune cell admixture from expression data. *Nat Commun* (2013) 4:2612. doi: 10.1038/ncomms3612

21. Li T, Fu J, Zeng Z, Cohen D, Li J, Chen Q, et al. TIMER2.0 for analysis of tumor-infiltrating immune cells. *Nucleic Acids Res* (2020) 48(W1):W509–14. doi: 10.1093/nar/gkaa407

22. Newman AM, Liu CL, Green MR, Gentles AJ, Feng W, Xu Y, et al. Robust enumeration of cell subsets from tissue expression profiles. *Nat Methods* (2015) 12 (5):453–7. doi: 10.1038/nmeth.3337

23. Finotello F, Mayer C, Plattner C, Laschober G, Rieder D, Hackl H, et al. Molecular and pharmacological modulators of the tumor immune contexture revealed by deconvolution of RNA-seq data. *Genome Med* (2019) 11(1):34. doi: 10.1186/s13073-019-0638-6

24. Fu J, Li K, Zhang W, Wan C, Zhang J, Jiang P, et al. Large-Scale public data reuse to model immunotherapy response and resistance. *Genome Med* (2020) 12 (1):21. doi: 10.1186/s13073-020-0721-z

25. Tauriello DVF, Palomo-Ponce S, Stork D, Berenguer-Llergo A, Badia-Ramentol J, Iglesias M, et al. TGFβ drives immune evasion in genetically reconstituted colon cancer metastasis. *Nature* (2018) 554(7693):538–43. doi: 10.1038/nature25492

26. Liu X, Yao L, Qu J, Liu L, Lu N, Wang J, et al. Cancer-associated fibroblast infiltration in gastric cancer: the discrepancy in subtypes pathways and immunosuppression. *J Transl Med* (2021) 19(1):325. doi: 10.1186/s12967-021-03012-z

27. Chen YF, Yu ZL, Lv MY, Cai ZR, Zou YF, Lan P, et al. Cancer-associated fibroblasts impact the clinical outcome and treatment response in colorectal cancer *via* immune system modulation: a comprehensive genome-wide analysis. *Mol Med* (2021) 27(1):139. doi: 10.1186/s10020-021-00402-3

28. Zheng H, Liu H, Li H, Dou W, Wang X. Weighted gene Co-expression network analysis identifies a cancer-associated fibroblast signature for predicting prognosis and therapeutic responses in gastric cancer. *Front Mol Biosci* (2021) 8:744677. doi: 10.3389/fmolb.2021.744677

29. Li X, Sun Z, Peng G, Xiao Y, Guo J, Wu B, et al. Single-cell RNA sequencing reveals a pro-invasive cancer-associated fibroblast subgroup associated with poor clinical outcomes in patients with gastric cancer. *Theranostics* (2022) 12(2):620–38. doi: 10.7150/thno.60540

30. Sun C, Wang S, Zhang Y, Yang F, Zeng T, Meng F, et al. Risk signature of cancer-associated fibroblast-secreted cytokines associates with clinical outcomes of breast cancer. *Front Oncol* (2021) 11:628677. doi: 10.3389/fonc.2021.628677

31. Zheng S, Zou Y, Tang Y, Yang A, Liang JY, Wu L, et al. Landscape of cancer-associated fibroblasts identifies the secreted biglycan as a protumor and immunosuppressive factor in triple-negative breast cancer. *Oncoimmunology* (2022) 11(1):2020984. doi: 10.1080/2162402X.2021.2020984

32. Zeng H, Xu Y, Xu S, Jin L, Shen Y, Rajan KC, et al. Construction and analysis of a colorectal cancer prognostic model based on N6-Methyladenosine-Related lncRNAs. *Front Cell Dev Biol* (2021) 9:698388. doi: 10.3389/fcell.2021.698388

33. Song W, Ren J, Xiang R, Yuan W, Fu T. Cross-talk between m(6)A- and m (5)C-related lncRNAs to construct a novel signature and predict the immune landscape of colorectal cancer patients. *Front Immunol* (2022) 13:740960. doi: 10.3389/fimmu.2022.740960

34. Wu Z, Lu Z, Li L, Ma M, Long F, Wu R, et al. Identification and validation of ferroptosis-related LncRNA signatures as a novel prognostic model for colon cancer. *Front Immunol* (2021) 12:783362. doi: 10.3389/fimmu.2021.783362

35. Huang P, Tang L, Zhang L, Ren Y, Peng H, Xiao Y, et al. Identification of biomarkers associated with CD4(+) T-cell infiltration with gene coexpression network in dermatomyositis. *Front Immunol* (2022) 13:854848. doi: 10.3389/fimmu.2022.854848

36. Wang T, Dai L, Shen S, Yang Y, Yang M, Yang X, et al. Comprehensive molecular analyses of a macrophage-related gene signature with regard to prognosis, immune features, and biomarkers for immunotherapy in hepatocellular carcinoma based on WGCNA and the LASSO algorithm. *Front Immunol* (2022) 13:843408. doi: 10.3389/fimmu.2022.843408

37. Liu J, Mei J, Wang Y, Chen X, Pan J, Tong L, et al. Development of a novel immune-related lncRNA signature as a prognostic classifier for endometrial carcinoma. *Int J Biol Sci* (2021) 17(2):448–59. doi: 10.7150/ijbs.51207

38. Gao Y, Liu J, Cai B, Chen Q, Wang G, Lu Z, et al. Development of epithelial-mesenchymal transition-related lncRNA signature for predicting survival and immune microenvironment in pancreatic cancerwithexperiment validation. *Bioengineered* (2021) 12(2):10553–67. doi: 10.1080/21655979.2021.2000197

39. Yuan H, Liu J, Zhao L, Wu P, Chen G, Chen Q, et al. Prognostic risk model and tumor immune environment modulation of m5C-related LncRNAs in pancreatic ductal adenocarcinoma. *Front Immunol* (2021) 12:800268. doi: 10.3389/fimmu.2021.800268

40. Liu J, Cui G, Ye J, Wang Y, Wang C, Bai J. Comprehensive analysis of the prognostic signature of mutation-derived genome instability-related lncRNAs for patients with endometrial cancer. *Front Cell Dev Biol* (2022) 10:753957. doi: 10.3389/fcell.2022.753957

frontiers | Frontiers in Immunology

TYPE Original Research
PUBLISHED 29 July 2022
DOI 10.3389/fimmu.2022.951214

OPEN ACCESS

EDITED BY
Rakesh K Singh,
University of Nebraska Medical Center,
United States

REVIEWED BY
Areeg Elmusrati,
California State University,
Los Angeles, United States
Margareta P. Correia,
Portuguese Oncology Institute,
Portugal

*CORRESPONDENCE
Zhijian Huang
huangzhijian@sysush.com
Yulong He
heyulong@mail.sysu.edu.cn
Changhua Zhang
zhchangh@mail.sysu.edu.cn

†These authors have contributed equally to this work and share first authorship

SPECIALTY SECTION
This article was submitted to Cancer Immunity and Immunotherapy, a section of the journal Frontiers in Immunology

RECEIVED 23 May 2022
ACCEPTED 04 July 2022
PUBLISHED 29 July 2022

CITATION
Mak TK, Li X, Huang H, Wu K, Huang Z, He Y and Zhang C (2022) The cancer-associated fibroblast-related signature predicts prognosis and indicates immune microenvironment infiltration in gastric cancer.
Front. Immunol. 13:951214.
doi: 10.3389/fimmu.2022.951214

The cancer-associated fibroblast-related signature predicts prognosis and indicates immune microenvironment infiltration in gastric cancer

Tsz Kin Mak[1†], Xing Li[1†], Huaping Huang[1†], Kaiming Wu[1], Zhijian Huang[1,2*], Yulong He[1,2*] and Changhua Zhang[1,2*]

[1]Digestive Diseases Center, The Seventh Affiliated Hospital of Sun Yat-sen University, Shenzhen, China, [2]Guangdong Provincial Key Laboratory of Digestive Cancer Research, The Seventh Affiliated Hospital of Sun Yat-sen University, Shenzhen, China

Background: Gastric cancer (GC) is one of the most common cancers, with a wide range of symptoms and outcomes. Cancer-associated fibroblasts (CAFs) are newly identified in the tumor microenvironment (TME) and associated with GC progression, prognosis, and treatment response. A novel CAF-associated prognostic model is urgently needed to improve treatment strategies.

Methods: The detailed data of GC samples were downloaded from The Cancer Genome Atlas (TCGA), GSE62254, GSE26253, and GSE84437 datasets, then obtained 18 unique CAF-related genes from the research papers. Eight hundred eight individuals with GC were classified as TCGA or GSE84437 using consensus clustering by the selected CAF-related genes. The difference between the two subtypes revealed in this study was utilized to create the "CAF-related signature score" (CAFS-score) prognostic model and validated with the Gene Expression Omnibus (GEO) database.

Results: We identified two CAF subtypes characterized by high and low CAFS-score in this study. GC patients in the low CAFS-score group had a better OS than those in the high CAFS-score group, and the cancer-related malignant pathways were more active in the high CAFS-score group, compared to the low CAFS-score group. We found that there was more early TNM stage in the low CAFS-score subgroup, while there was more advanced TNM stage in the high CAFS-score subgroup. The expression of TMB was significantly higher in the low CAFS-score subgroup than in the high CAFS-score subgroup. A low CAFS-score was linked to increased microsatellite instability-high (MSI-H), mutation load, and immunological activation. Furthermore, the CAFS-score was linked to the cancer stem cell (CSC) index as well as chemotherapeutic treatment sensitivity. The patients in the high CAFS-score subgroup had significantly higher proportions of monocytes, M2 macrophages, and resting mast cells, while plasma cells and follicular helper T cells were more abundant in the low-risk subgroup. The CAFS-score was also highly correlated with the

sensitivity of chemotherapeutic drugs. The low CAFS-score group was more likely to have an immune response and respond to immunotherapy. We developed a nomogram to improve the CAFS-clinical score's usefulness.

Conclusion: The CAFS-score may have a significant role in the TME, clinicopathological characteristics, prognosis, CSC, MSI, and drug sensitivity, according to our investigation of CAFs in GC. We also analyzed the value of the CAFS-score in immune response and immunotherapy. This work provides a foundation for improving prognosis and responding to immunotherapy in patients with GC.

KEYWORDS

CAFS-score, CAFs gene, Gastric cancer, immune therapy, immune microenvironment infiltration

Introduction

Cancer is the leading cause of premature death, which causes a huge public health and economic burden (1). According to the global cancer statistics, there were 19.3 million new cancer cases and nearly 10 million cancer-associated deaths worldwide in 2020. Among them, gastric cancer (GC) represents more than 1 million new cases and 769,000 deaths, ranking fifth in incidence (5.6%) and fourth in mortality (7.7%) (2). Cases of GC were frequently diagnosed in the advanced stage (3). Meanwhile, a trend of augmented younger GC cases (aged<50 years) also brings a severe test in therapy (2). GC is a highly molecular and phenotypic heterogeneity with a complex tumor microenvironment (TME). Research on the TME may help to explore the underlining mechanisms of tumorigenesis and development.

The TME is a heterogeneous collection of various immune cells, stromal cells, vessels, and extracellular matrix (ECM). Tumor cells and the TME act as seed and soil; the TME fosters tumor progression and mediates relapse (4). Cancer-associated fibroblasts (CAFs) are one of the most abundant cells and act as critical components among them. Activated CAFs create a conducive environment for tumorigenesis and progression. According to the research papers from PubMed, 18 CAF-related genes that were confirmed by fundamental experiments in GC were chosen for modeling purposes. Activated CAFs create a conducive environment for cancer proliferation and maintaining CSC by secreting a plethora of cytokines and chemokines, such as CXC-chemokine ligand 12 (CXCL12), interleukin-6 (IL-6), and IL-33 (5–8). Secretion of IL-6 can promote the epithelial–mesenchymal transition (EMT) and metastasis of GC *via* the JAK2/STAT3 signaling pathway. Simultaneously, IL-6 also prompts cancer immune escape by recruiting immunosuppressive cells into the TME (8, 9). Secretion of ECM-degrading proteases matrix metalloproteinases (MMPs), such as MMP11 and MMP14, directly confers a migration track by remodeling the ECM and physically pulling, promoting cancer invasion and metastasis (10–12). Besides that, CXCL12 and fibroblast growth factor 9 (FGF9) produced by CAFs facilitate tumor neovascularization to overcome a hypoxic and acidic TME (5, 7, 13). The CAF-derived hyaluronan and proteoglycan link protein 1 (HAPLN1) promotes ECM remodeling by decreasing the density and size of fibers, as well as increasing the fiber alignment, resulting in tumor invasion and aggression in GC (14, 15). Meanwhile, GC cells also release the transforming growth factor-β+ (TGFβ+) exosomes to convert mesenchymal stem cells (MSCs) into activated CAFs. The crosstalk biological aspects between CAFs and GC create a positive feedback loop to stimulate GC progression and metastasis (5). Other CAF-related genes, such as mucin 1 (MUC1), Krüppel-like Zinc-Finger Transcription Factor 5 (KLF5), tumor endothelial marker 1 (TEM1), vascular adhesion molecule 1 (VCAM1), periostin (POSTN), lysyl oxidase like 2 (LOXL2), neuropilin-2 (NRP2), rhomboid 5 homolog 2 (RHBDF2), and serum amyloid A1 (SAA1), are characterized by high expression of genes associated with a poor prognosis in patients with GC (12, 16–22). In contrast, CAF-related genes such as Sorbin and SH3 domain-containing protein 1 (SORBS1), and secreted protein acidic and rich in cysteine (SPARC) have a significantly low expression in CAF and are closely related to poor prognosis in GC (23, 24). Carcinogenesis and development are characteristic of the interaction between multiple genes and signal pathways. It is not sufficient to focus on one or two genetic biomarkers to correlate with the GC prognosis. Hence, we put up an 18-CAF-related gene subgroup classification and CAFS-score model that may provide important insights into predicting prognosis and guiding clinical practice.

In this present study, we constructed a GC scoring model (CAFS-score) based on 808 GC patients with transcriptome data and clinical information and 14 identified GC-related CAF genes, and validated its reliability with multiple datasets. We clustered those patients into two CAF subtypes according to the CAF genes' expression levels and identified the differentially expressed genes (DEGs). Then, patients were classified into three DEG-related gene subtypes and established the CAFS-score system. The clinical practice of this scoring model was validated in GC patients, including prognosis, immune microenvironment, and drug sensitivity.

Methods

Dataset collection and sample information

The flowchart is described in Supplementary Figure S1 and the samples were analyzed with staging statistics. The data of gene expression, somatic mutation, and corresponding clinical information of GC samples from The Cancer Genome Atlas (TCGA) database (https://tcga-data.nci.nih.gov/tcga/) were collected, which include tumor samples and para-cancer samples with detailed information for further analysis. In addition, 433 GC samples in South Korea (GSE84437) and 300 GC samples in the ACRG (Asian Cancer Research Group) study (GSE62254) with detailed characteristic information and survival duration were obtained from the GEO database (https://www.ncbi.nlm.nih.gov/geo/). Moreover, GSE26253 was obtained from the GEO database.

Defining the CAF-related regulators

In the previous research study, Zang et al. (11) found that matrix metalloproteinase 11 (MMP11) secreted by CAFs is not only overexpressed in exosomes purified from plasma and GC samples, but also associated with the overall survival (OS) of GC patients. Shen et al. (15) showed that HAPLN1 is a significantly upregulated gene in CAFs of GC, and higher expression is associated with shorter OS in GC patients. CAF-derived IL-33 is upregulated in the human GC and served as a poorly prognostic marker in GC patients proved by Su et al. (6). In the research study of CAFs, Wand et al. (12) demonstrated that MMP14, LOXL2, and POSTN are characterized by high expression of genes associated with gastric tumor invasion. The previous research studies found that SORBS1, IL-6, MUC1, FGF9, KLF5, SPARC, TEM1, NRP2, CXCL12, RHBDF2, SAA1, and VCAM are significant expressions in CAF and have an association with GC (7, 8, 13, 16–24). According to our search in research papers from PubMed, we chose the 18 genes (MMP11, HAPLN1, IL-33, IL-6, SORBS1, MUC1, FGF9, KLF5, SPARC, TEM1, VCAM1, POSTN, MMP14, LOXL2, NRP2, CXCL12, RHBDF2, and SAA1) that related to CAFs in GC.

Consensus clustering and gene clustering

According to the selected CAF-related genes, consensus clustering was utilized to identify and classify the patient into molecular subtypes by the k-means method. The "ConsensuClusterPlus" package was applied to determine the number of clusters and their stability. In addition, 1,000 repetitions were performed to ensure the stability of classification (25).

Setting the criteria of $|\log2(\text{Fold Change})| > 1$ and false discovery rate (FDR)< 0.05, a list of DEGs from consensus clustering was identified by utilizing the R package limma. Secondly, according to the expression of prognostic DEGs, an unsupervised clustering method was used to classify the patient into different subtype groups (Gene subtype A, Gene subtype B, and Gene subtype C) for further analysis.

To further examine the clinical value of the consensus clustering and gene clustering, we evaluated the correlations among the molecular subtypes, clinicopathological characteristics, and prognosis. The clinical characteristics included age, gender, TNM stage, and grade. Furthermore, we perform the Kaplan–Meier survival analysis in different clusters using the survival package of the R software.

Gene set variation analysis

Gene set variation analysis is typically used to estimate variation in pathway and biological process activity in expression dataset samples (26). This method was performed to explain the differences in biological processes between two CAFs-score subtypes by using "GSVA" R packages. The gene sets of "c2.cp.kegg.v7.4.symbols.gmt" were downloaded from the MSigDB database for further GSVA. DEGs were analyzed using the R package clusterProfiler in Gene Ontology (GO) and Kyoto Encyclopedia of Genes and Genomes (KEGG),with a cutoff value of FDR< 0.05.

Construction and validation of the prognostic model

LASSO-Cox analysis was utilized to minimize the risk of over-fitting using the "glmnet" R package. Multivariate Cox analysis was used to select the candidate genes for establishing a prognostic model (CAFS-score) in the training cohort. The CAFS-score was calculated as follows:

$$\text{CAFS} - \text{score} = \sum (\text{Expi} \times \text{coefi})$$

where Coefi and Expi denote the risk coefficient and expression of each gene, respectively. The cutoff point was determined using the "survminer" package. According to the CAFS-score, we revealed that the survival curve was used for visualization with both training and testing cohorts in the high- or low-risk group by Kaplan–Meier analysis. p-values< 0.05 were considered to be statistically significant.

Clinical correlation and stratification analyses of the CAFS-score

Between the risk score and clinicopathological variables, univariate and multivariate Cox regression analysis was done to validate whether the CAFS-score is an independent prognostic predictor. The results were revealed in the forest map. Thorsson et al. (27) found that all tumors could be divided into six immune subtypes, namely, wound healing (C1), IFN-γ dominant (C2), inflammatory (C3), lymphocyte depleted (C4), immunologically quiet (C5), and TGF-β dominant (C6). Therefore, we performed the factor of immune sub-type (https://tcga-pancan-atlas-hub.s3.us-east-1.amazonaws.com/download/Subtype_Immune_Model_Based.txt.gz) between different risk groups, using the R software of "RColorBrewer".

For the gene mutation analysis, information on genetic alteration was downloaded from the TCGA and GEO databases. The R package "Maftools" was utilized for analyzing the gene mutation in different risk subgroups. Moreover, the correlation between the CAFS-score and total mutation burden (TMB) was analyzed and performed in our study. Further analysis, we revealed the relationship between the CAFS-score and CSC index. The CSC index was calculated by using innovative one-class logistic regression (OCLR) machine-learning algorithm (28). In addition, we explored the relationship between the different risk groups and MSI.

Identification of immune characteristics for the CAFS-score

CIBERSORT (https://cibersort.stanford.edu/) is a common algorithm to obtain cell composition from solid tumors or gene expression profiles, which was used to analyze the enrichment of immune cells in the CAFS-score for our study. The different content of immune infiltrating cells between the high- and low-risk groups was analyzed by Wilcoxon signed rank test and performed on the box chart for the TCGA cohort. In further analysis, we showed the correlations between the abundance of immune cells and four genes in the prognostic model according to the training cohort.

Assessment of immunotherapy

For the predicted assessment of the patient with immunotherapy in the prognostic value of the CAFS-score, the time-dependent receiver operating characteristic (ROC) curve analysis was performed for obtaining the area under the curve (AUC). In addition, we not only downloaded the tumor immune dysfunction and exclusion (TIDE) score online (http://tide.dfci.harvard.edu/) but obtained the T-cell-inflamed signature (TIS) score calculating the average value of a log2-scale normalized expression in the 18 signature genes (29). Thereafter, we revealed the results after comparing the prognostic values of the CAFS-score, TIDE, and TIS by using the R package "timeROC" and performed time-dependent ROC curve analyses to obtain the AUC.

Besides comparing the prognostic values of the CAFS-score, TIDE, and TIS, we also utilized the immunophenoscore (IPS) to predict the response of immune checkpoint inhibitors (ICIs) based on the expression of the main component in tumor immunity. According to a scale with a range of 0–10 based on representative cell-type gene expression z-scores, IPS was calculated where the immunogenicity was positively correlated with the score of IPS (30). The IPSs of patients with GC were derived from The Cancer Immunome Atlas (TCIA) (http://tcia.at/home). The result was performed using the R package "ggpubr".

Assessment of drug sensitivity

The sensitivity of various drugs was predicted in patients between two CAFS-score subgroups. The pRRophetic R package was utilized for drug prediction (31). Wilcoxon signed-rank test was utilized to explore the difference in IC_{50} between different risk groups. The results were performed by using the R package "ggplot2".

Establishment and validation of a nomogram scoring system

According to the independent prognosis outcome, a predictive nomogram was produced by the clinical characteristics and the CAFS-score using the "rms" package of R. In the nomogram scoring system, each variable has a corresponding score, and the total score is obtained by adding up the scores of all variables for each sample (32). The nomogram was evaluated using ROC curves for the 1-, 3-, and 5-year survival rates. The nomogram calibration plots were used to describe the predictive value of the anticipated 1-, 3,- and 5-year survival events in relation to the actual observed outcomes.

Statistical analysis

R software and R Bioconductor packages were used for the data analysis.(version 4.1.2; https://www.R-project.org).

Comparison of non-parametric or parametric method differences was carried out using Wilcoxon test, Kruskal–Wallis test, and *t*-test or one-way ANOVA. Spearman's and distance correlation analyses were used to calculate the correlation coefficients. The validity of the model was verified by the receiver operating characteristic (ROC) curve. Based on the correlation between the CAFS-score and patient survival, the best cutoff point of survival information for each cohort was determined by the Survminer package. Kaplan–Meier test and Log-rank test were used to analyze the prognosis of survival curve, which were used to assess differences between groups. The hazard ratio (HR) of CAF regulators and CAF-related genes was computed by using the univariate Cox regression model. To verify whether the CAFS-score was an independent prognostic predictor, we incorporated the CAFS-score and CAF-related clinical parameters into a multivariate Cox regression model analysis. All statistical analyses were bilateral, and statistical significance was set at $p< 0.05$.

Result

Overview of genetic changes and expression variations of CAF-related regulators in GC

First, we analyzed the gene mutations to understand the mutation types of the selected CAF-related genes in GC samples (Figure 1A). At the genetic level, CAF-related regulator mutations were found in 82 of the 433 samples (approximately 18.94%). The study revealed that POSTN had the highest frequency of mutations. In contrast, we observed that IL-33, IL-6, CXCL12, and SAA1 do not have any mutations in any GC samples. We determined the frequency of copy number variants (CNVs) in selected CAF-related genes and discovered changes in selected CAF-related genes with CNVs on the chromosome (Figures 1B, C). For example, KLF5 was shown to be a frequent modification, with the majority of the changes focusing on copy number amplification on the 13 chromosomes. In terms of expression levels, 14 of 18 selected genes in tumor samples showed a significant difference as compared with normal samples (Figure 1D). A network was created to show the whole landscape of the selected genes' interconnections, regulator linkages, and prognostic significance in patients with GC (Figure 1E).

Identification of CAF subtypes in GC

First, we analyzed and revealed the selected CAF genes of prognostic value in the 808 GC patients using the univariate Cox regression and Kaplan–Meier analysis (Figure S2). We used the unsupervised clustering technique to identify different regulatory patterns based on the expression levels of 18 CAF-related regulators. For classifying the entire cohort into subtypes A ($n = 444$) and B ($n = 364$), the result revealed that k = 2 seems to be the perfect choice (Figure 2A and Table S1). For the survival analysis, the results showed that cluster B had a better survival probability than cluster A (Figure 2B). Moreover, the variations in biological behavior between these two patterns were investigated using gene set variation analysis (GSVA) enrichment analysis (Figure 2C and Table S2). It showed that cluster A was enriched in terms of pathways associated with ECM and tumor invasion, including the ECM–receptor interaction and Focal adhesion. Figure 2D illustrates that the CAF gene subtype B patterns were also linked to advanced TNM stages, particularly the T stage. We explored the 22 infiltrating immune cell types in the two GC subtypes (Figure 2E). The result showed that most of the infiltrating immune cells were significantly different between the two GC subtypes, except CD56 bright natural killer cells, CD56 dim natural killer cells, monocytes, and Type 2 T helper cells. In addition, infiltrating immune cells were abundant in cluster A, except activated CD4 T cells, neutrophils, and Type 17 T helper cells. Following this, we confirmed that the 18 CAF-related regulators could be used to discriminate the two regulatory patterns (Figure S3A).

Setting the criteria of $|\log2(\text{Fold Change})| > 1$ and FDR< 0.05, 342 DEGs from consensus clustering were identified. Under the functional enrichment analysis, GO analysis and KEGG pathway analysis were performed, significantly related to the DEGs. For Figure S3B, a total of 342 DEGs were significantly associated with 789 GO terms (details in Table S3), such as ECM organization for Biological Process (BP), collagen-containing ECM for Cellular Component (CC), and ECM structural constituent for Molecular Function (MF). In addition, the result of the top 18 KEGG pathways associated with candidate genes is illustrated in Figure S3C, such as PI3K-Akt signaling pathway, Focal adhesion, and Protein digestion and absorption. The results of GO term and KEGG suggested that the CAFs play a dynamic role in the ECM and tumor invasion.

Identification of gene subtypes based on DEGs

After further analysis of univariate Cox regression in DEGs, we identified 316 genes related to survival time ($p< 0.05$), which were used in further analysis. A consensus clustering technique was utilized to classify patients into three genomic subgroups based on prognostic genes, termed gene subtypes A to C, to further validate this regulatory mechanism. According to Kaplan–Meier curves, patients in subtype A had the worst survival, whereas patients in cluster C had a favorable survival time (Figure 3A). Furthermore, the gene subtype A pattern was linked to an advanced TNM stage (Figure 3B). Expression of 14 of the previous18 selected CAF-related genes had a significant

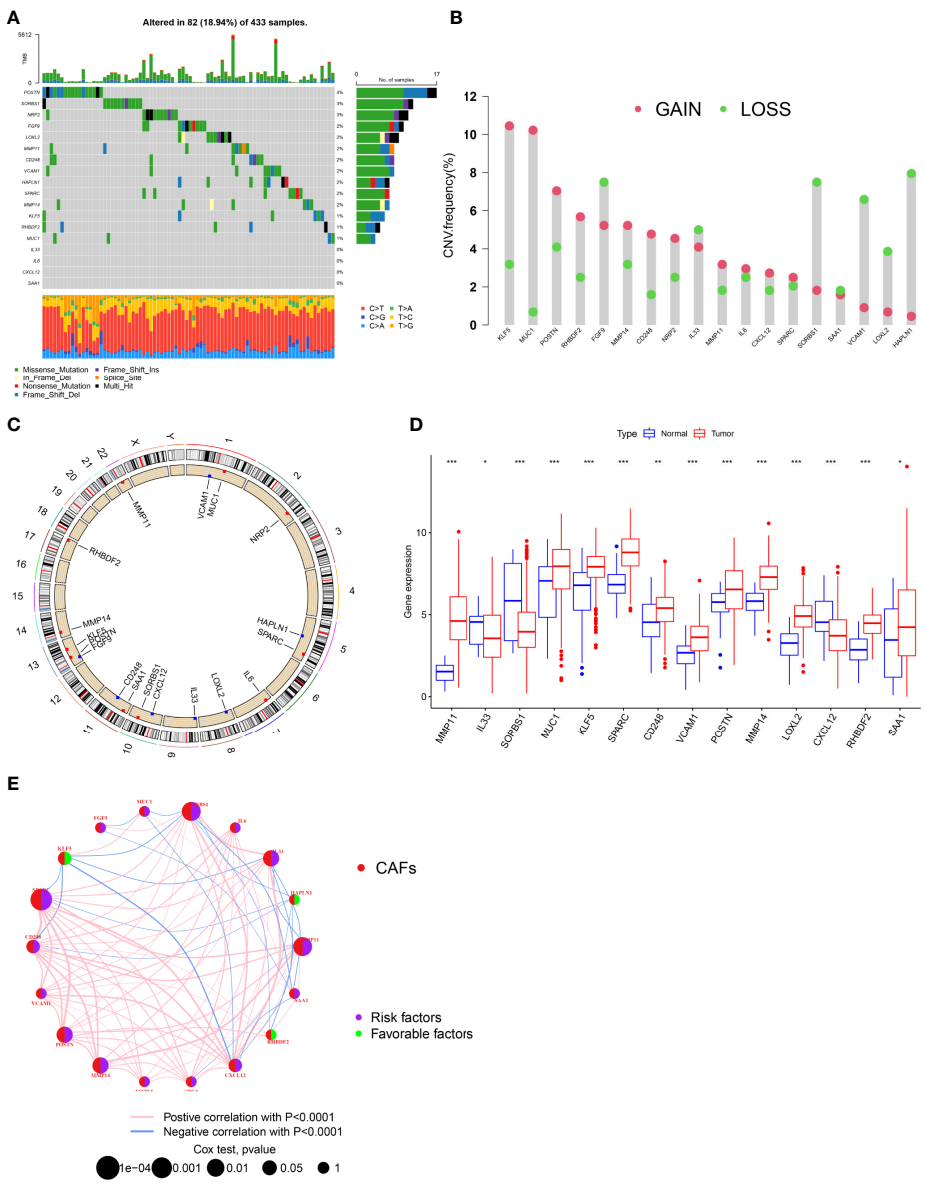

FIGURE 1
Genetic and transcriptional alterations of CAFs-related genes in GC. **(A)** Mutation frequencies of 18 CAFs-related genes in 433 patients with STAD from the TCGA cohort. **(B)** Frequencies of CNV gain, loss, and non-CNV among CAFs-related genes. **(C)** Locations of CNV alterations in CAFs-related genes on 23 chromosomes. **(D)** Expression distributions of 1 8 CAFs-related genes in normal and GC tissues. **(E)** Interactions among CAFs-related genes in GC. The connecting line among CAFs-related genes indicates their interaction, and the thickness of lines represents the strength of the association between CAFs-related genes. Blue and pink represent negative and positive correlations, respectively. *P<0.05, **P<0.01, ***P<0.001.

difference among the three gene subtypes, as expected based on the patterns (Figure 3C).

Establishment risk assessment model and survival outcomes in GC

The CAFS-score was constructed using DEGs connected to subtypes. The distribution of patients in the two CAFs subtypes, three gene subtypes, and two CAFS-score groups is revealed in Figure 4A. According to the least partial likelihood deviance, 10 OS-associated genes remained after LASSO regression analysis (Figures S4A, B). This was followed by multivariate Cox regression analysis, wherein four genes (MMP11, HEYL, NNMT, and PDK) were eventually obtained to construct the prognostic model, named the "CAFS-score". Based on the results of the multivariate Cox regression analysis, the CAFS-score was constructed as follows:

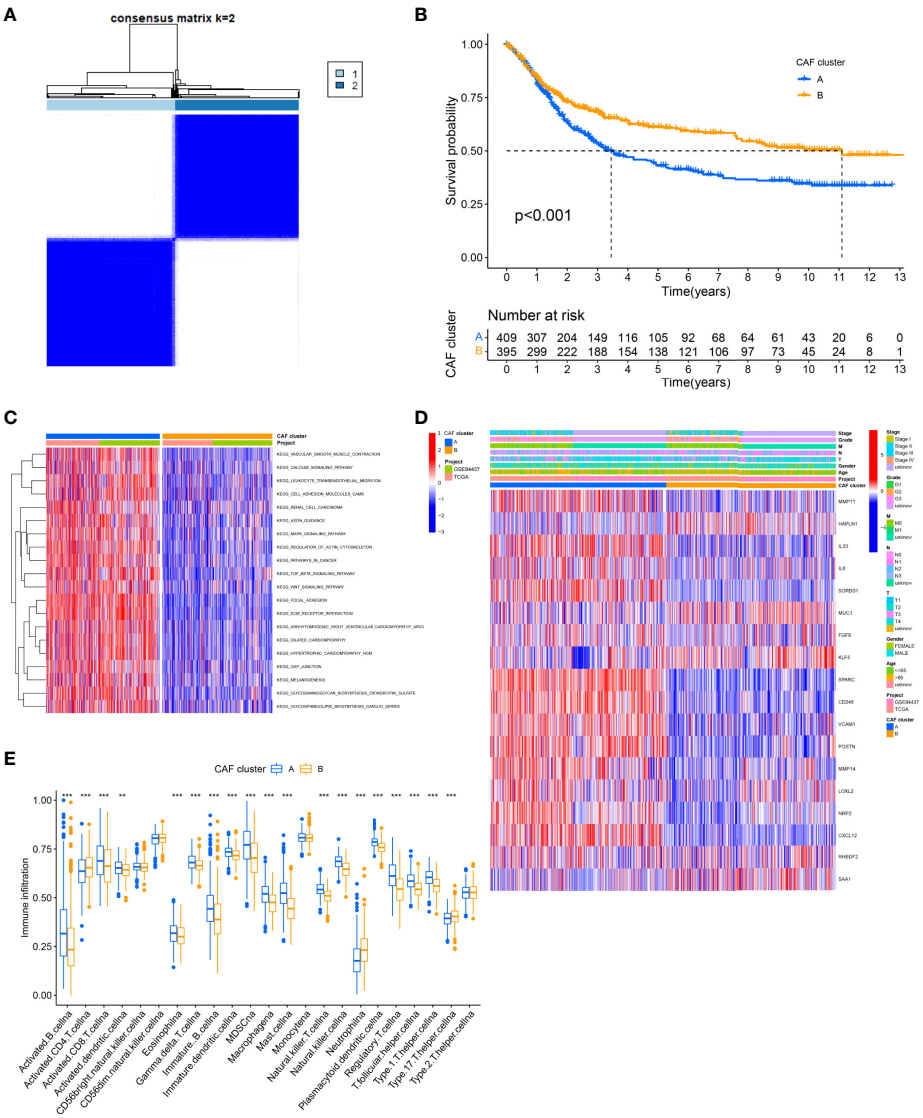

FIGURE 2
Identification of CAFs subtypes in GC. **(A)** Consensus matrix heatmap defining two clusters (k = 2) and their correlation area. **(B)** Univariate analysis indicating 18 CAFs-related genes corelated with the OS time. **(C)** GSVA of biological pathways between two distinct subtypes. (Red and blue represent activated and inhibited pathways, respectively). **(D)** Differences in clinicopathologic features and expression levels of CAFs-related genes between the two distinct subtypes. **(E)** The 22 infiltrating immune cell types in the two GC subtypes. **P<0.01, ***P<0.001.

$$\text{Risk score} = \text{expression level of MMP11} * (0.13641) + \text{expression level of HEYL} * (0.13075) + \text{expression level of NNMT} * (0.11341) + \text{expression level of PDK4} * (0.12228)$$

After further analysis of applying risk score, there was a significant difference in the CAFS-score between CAF subtypes and gene subtypes (Figures 4B, C). The distribution plot of the CAFS-score demonstrated that the survival times were reduced while the CAFS-score increased (Figures 4D, E). Finally, we used the risk score to re-distinguish high- and low-risk groups in the training cohort and testing cohort. As illustrated in Figures 4F, G, low-risk patients had a better OS than high-risk patients ($p< 0.05$, log-rank test) whether in the training cohort or the GSE62254 cohort. Consistent with the results of the training cohort, patients from the low-risk group had a better OS than high-risk patients ($p< 0.05$, log-rank test) in the GSE26253 cohort (Figure 4H).

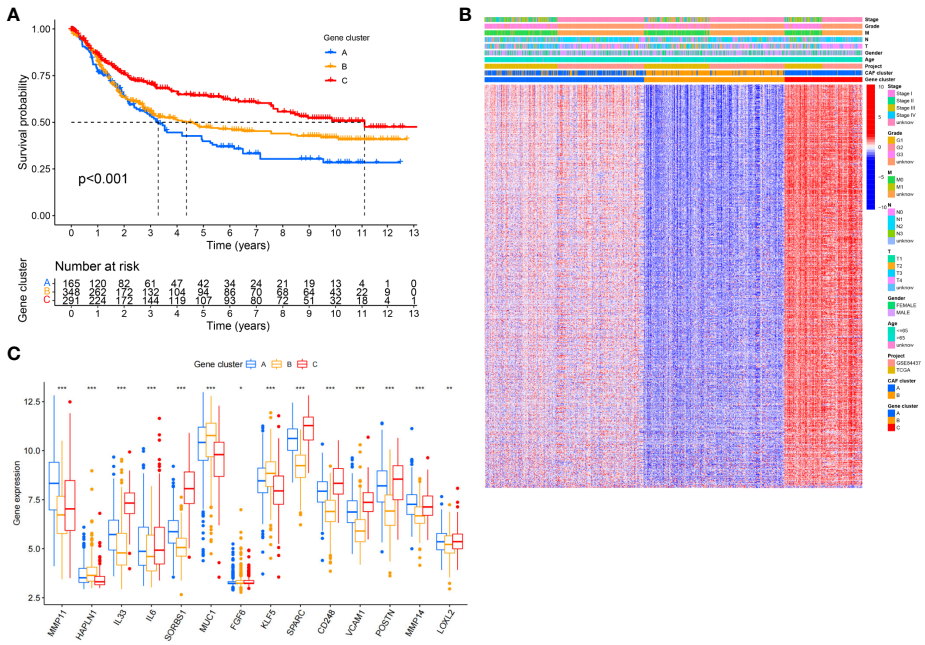

FIGURE 3
Identification of gene subtypes based on DEGs. **(A)** Kaplan-Meier curves for RFS of the three gene subtypes (log-rank tests, p < 0.001). **(B)** Relationships between clinicopathologic features and the three gene subtypes. **(C)** Differences in the expression of 18 CAFs-related genes among the three gene subtypes. *P<0.05, **P<0.01, ***P<0.001.

Clinicopathologic characteristics of TCGA in the CAFS-score

Based on univariate Cox regression analysis, Figure 5A illustrates that age, CAFS-score, and stage were significantly associated with the prognosis of GC. After further multivariate Cox regression analysis, Figure 5B shows that the CAFS-score presented as an independent prognostic factor after adjusting for other clinicopathologic factors. The clinicopathologic characteristics of GC patients in the TCGA cohort are shown in Figure 5C, which revealed a significant difference in grade and TNM stage, especially for T stage. Furthermore, we found that there was more early TNM stage in the low-risk subgroup, while there was more advanced TNM stage in the high-risk subgroup (Figure 5D, $p< 0.05$). In addition, we found that the immune sub-types were significantly related to the risk between the two risk subgroups (Figure 5E, $p< 0.05$). Meanwhile, GSVA enrichment analysis was used to explore the differences in biological behavior between the two risk subgroups (Figure S5). It illustrated that the high-risk groups were associated with ECM and tumor invasion, including the ECM–receptor interaction and Focal adhesion.

Relationship of the CAFS-score with TMB, MSI, and CSC index

We analyzed the gene mutations to further understand the immunological nature in different risk subgroups. We identified the top 20 genes with the highest mutation rates in the high-risk subgroup (Figure 6A) and low-risk subgroup (Figure 6B). The results illustrated that missense mutation was the most common mutation type. The mutation rates of TTN, MUC16, and TP53 were not only higher than 25% in both groups, but the most common in both groups. Moreover, we analyzed the relationship between the risk score and TMB. The expression of TMB was significantly higher in the low-risk subgroup than in the high-risk subgroup (Figure 6C). In addition, the risk score was correlated with TMB in gene subtypes ($r = -0.26$, $p< 0.05$), as revealed in Figure 6D.

Moreover, we observed that the risk score was correlated with the CSC index ($r = -0.66$, $p< 0.05$), as shown in Figure 6E. Finally, we revealed that a low CAFS-score was linked to MSI-H status, whereas a high CAFS-score was linked to microsatellite stable (MSS) status (Figures 6F, G).

Immune infiltration in CAFS-score subgroup

The gene expression matrix of the TCGA database in GC was uploaded into CIBERSORT web to estimate the fractions of 22 immune cells. Next, we explored the composition of immune cells in different risk subgroups (Figure 7A) in the TCGA database of GC samples. The result illustrated that the patients in the high-risk subgroup had significantly higher proportions of monocytes, M2

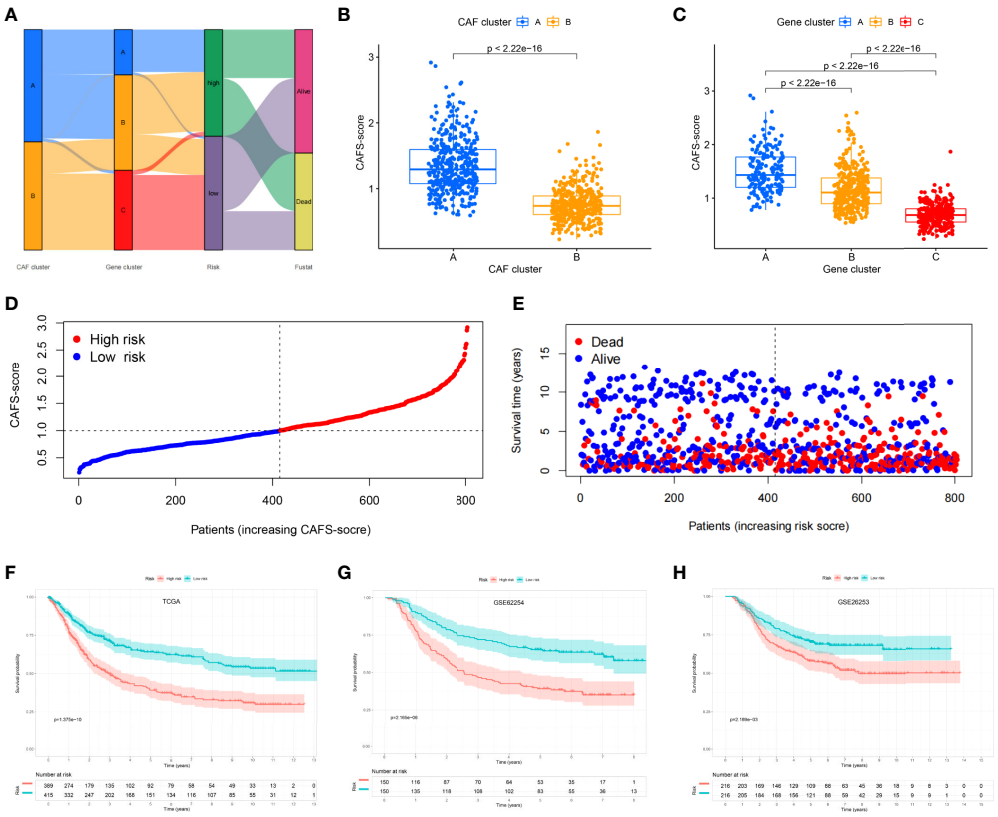

FIGURE 4
Establishment risk assessment model and survival outcomes in GC. **(A)** Alluvial diagram of the subtype distributions in groups with different CAFS-score and survival outcomes. **(B)** Differences in CAFS-score between two CAF subtypes. **(C)** Differences in CAFS-score between three gene subtypes. **(D, E)** Ranked dot and scatter plots representing the CAFS-score distribution and patient survival status. **(F-H)** Kaplan-Meier analysis of the RFS between the two risk groups in the TCGA, GSE62254, and GSE26253 cohort.

macrophages, and resting mast cells, while plasma cells and follicular helper T cells were more abundant in the low-risk subgroup ($p< 0.05$) (Figure 7B). We also found that the infiltrating abundance of M0 macrophages, resting mast cells, resting dendritic cells, M2 macrophages, resting NK cells, and CD8 T cells was significantly related to OS ($p< 0.05$) (Figure S6). The higher infiltrating abundance of macrophages M2 was associated with poorer OS.

Based on the training set, we explored that the CAFS-score was positively correlated to naïve B cells, M2 macrophages, resting mast cells, monocytes, and CD4 memory resting T cells (Figure 7C). The four genes were also shown to be highly linked to the majority of immune cells (Figure 7D). Therefore, the CAFS-score is statistically correlated with the infiltration of most kinds of immune cells. This means that the CAFS-score has the potential to indicate poor prognosis under different immune infiltrations.

Immunotherapy prediction

This study aims to assess the potential efficacy of immunotherapy in a clinical setting in different risk subgroups. To illustrate, a higher TIDE prediction score corresponded with a higher potential for immune evasion, which proved that the patients were unlikely to benefit from the treatment of immunotherapy. The subgroup with low risk had lower TIDE scores than the subgroup with high risk, which means that patients with low risk were more likely to benefit from ICI treatment than those with high risk (Figure 8A), whereas higher TIDE prediction scores are associated with poorer benefits from ICI treatment. For a lower TIDE score, the patients with low risk might have a better prognosis than those with high risk. Moreover, we found that the T-cell exclusion score (Figure 8C) and T-cell dysfunction (Figure 8D) were significantly different between the two risk subgroups, except the MSI score (Figure 8B). Under the AUC, the result illustrated that our risk model was the best compared with TIS and TIDE (Figure 8E). Therefore, we suggested that the predictive value of risk was comparable with 18-gene TIS and TIDE.

Besides utilizing the TIDE score, we also analyzed the correlation between the risk and IPS in GC patients to predict the response of ICIs. For the IPS, cytotoxic T lymphocyte

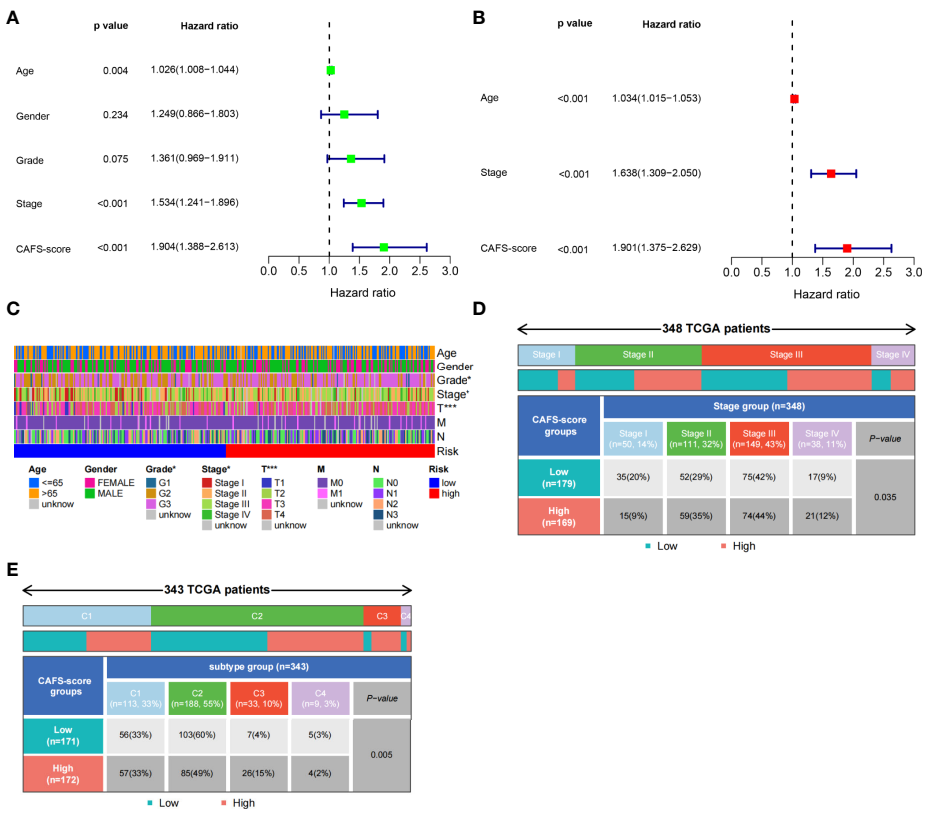

FIGURE 5
Clinicopathologic characteristics of TCGA in CAFS-score. **(A)** The Univariate Cox regression analysis in CAFS-score subgroups. **(B)** The multiple Cox regression analysis in CAFS-score subgroups. **(C)** The clinicopathologic characteristics of GC patients in the TCGA cohort. **(D, E)** The staging and the immune subtypes was significantly related to the risk between the two CAFS-score subgroups, respectively. *P<0.05, ***P<0.001.

antigen-4 (CTLA-4), programmed cell death protein 1 (PD-1), and programmed death ligand-1 (PD-L1) were the immune checkpoints. Therefore, their immune checkpoints were utilized to evaluate the potential ICI treatment (Figure 9). As a result, we found that they were significantly elevated in the low-risk group, which was categorized by the risk, which means more immunogenicity on ICIs in the low-risk group. Collectively, these results suggested that the low-risk group was more likely to have an immune response and respond to immunotherapy.

Drug sensitivity

Except for assessment of ICI treatment, we tried to find the links between different risk groupings and the effectiveness of chemotherapy for treating GC in the training cohort. We illustrated that the low risk was associated with a lower half inhibitory concentration (IC_{50}) of chemo-therapeutics such as Mitomycin C, Paclitaxel, and Sorafenib ($p< 0.05$), whereas the high risk was associated with a low IC_{50} such as Pazopanib, Imatinib, and Bryostatin ($p< 0.05$). Therefore, Figure 10 illustrates that the CAFS-score acted as a potential predictor for chemo-sensitivity, and details are shown in Table S4.

Establishment of a nomogram to predict survival

Given the inconvenient clinical value of the CAFS-score in predicting OS in patients with GC, a nomogram incorporating the CAFS-score and clinicopathological characteristics was developed to predict 1-, 3-, and 5-year OS rates in patients with GC (Figure 11A). For the TCGA, GSE62254, and GSE26253 cohorts, our AUC studies on the nomogram model revealed a good accuracy for OS at 1, 3, and 5 years (Figures 11B–D). In the TCGA, GSE62254, and GSE26253 cohorts, the proposed nomogram performed similarly to an ideal model according to the calibration plots (Figures 11E–G). Finally, we compared the nomogram's prediction accuracy to that of the TNM stage in the TCGA, GSE62254, and GSE26253

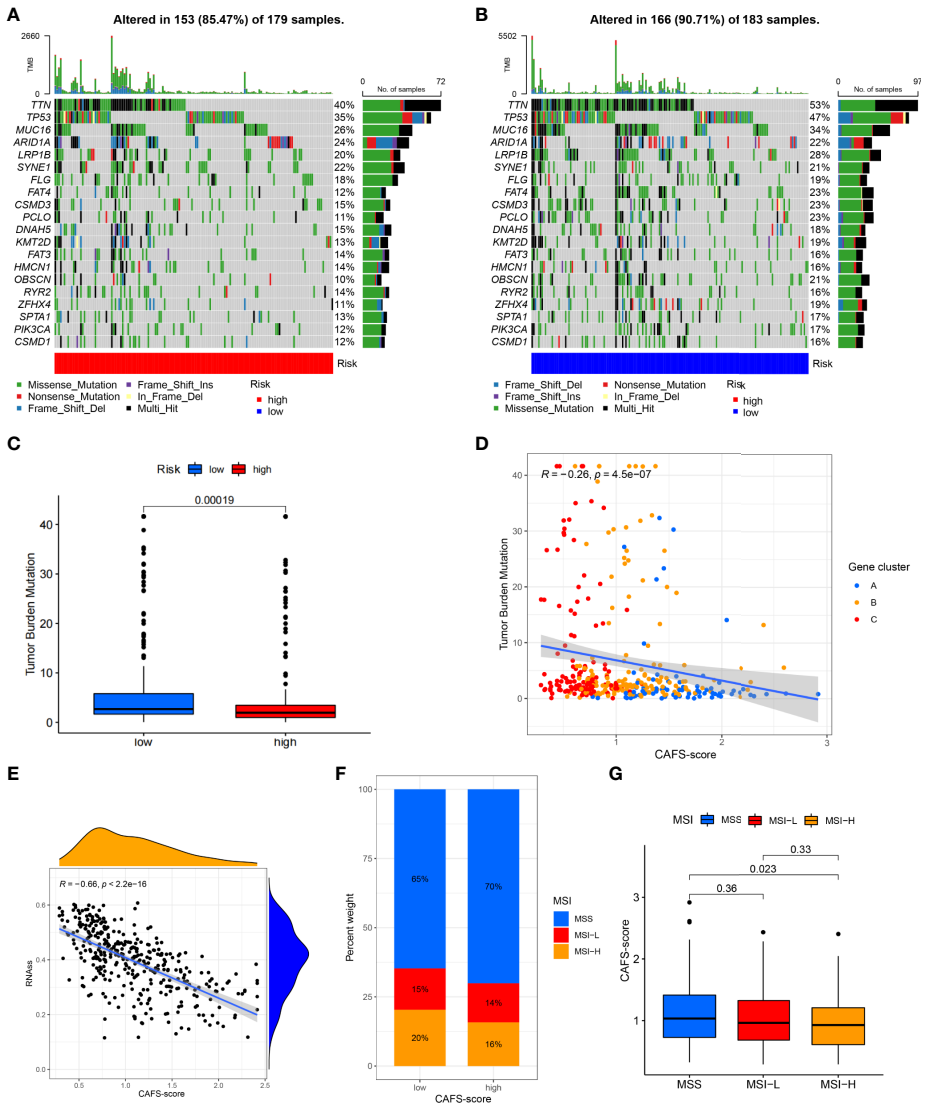

FIGURE 6
Characteristic in gene mutation and relationship of CAFS-score with MSI and CSC index. **(A, B)** Significantly mutated genes in the mutated GC samples of the high and the low risk groups, respectively. Mutated genes (rows, top 20) are ordered by mutation rate; samples (columns) are arranged to emphasize mutual exclusivity among mutations. The right shows mutation percentage, and the top shows the overall number of mutations. The color-coding indicates the mutation type. **(C)** The TMB of two differen risk subgroups. **(D)** Relationships between CAFS-score and TMR in three gene subtypes. **(E)** Relationships between CAFS-score and CSC index. **(F, G)** Relationships between CAFS-score and MSI.

cohorts (Figure S7). The results illustrated that the nomogram's AUC values were greater than the TNM stage in three cohorts.

Discussion

Globally, GC is one of the leading causes of preventable death and ranks fifth in incidence (5.6%) and fourth in mortality (7.7%) among malignant tumors (2, 33). The etiology of this tumor remains poorly understood. Despite the rapid development of biological agents, the choices of treatment in GC are limited until now. Meanwhile, the prognosis of advanced GC under the primary treatment remains disappointing (34). CAFs are the most abundant cell in the TME of GC. By exerting ECM deposition and remodeling, the activated CAFs exhibit extensive reciprocal signaling interaction, crosstalk with immune cells, and mediate oncogenesis and progression of GC (5, 9, 35). However, it is not precise to focus on a single gene or an entire CAF-related gene set to correlate with GC prognosis. Hence, the results of the present study are based on an 18-identified GC-related CAF gene set and constructed a CAFS-risk score to predict

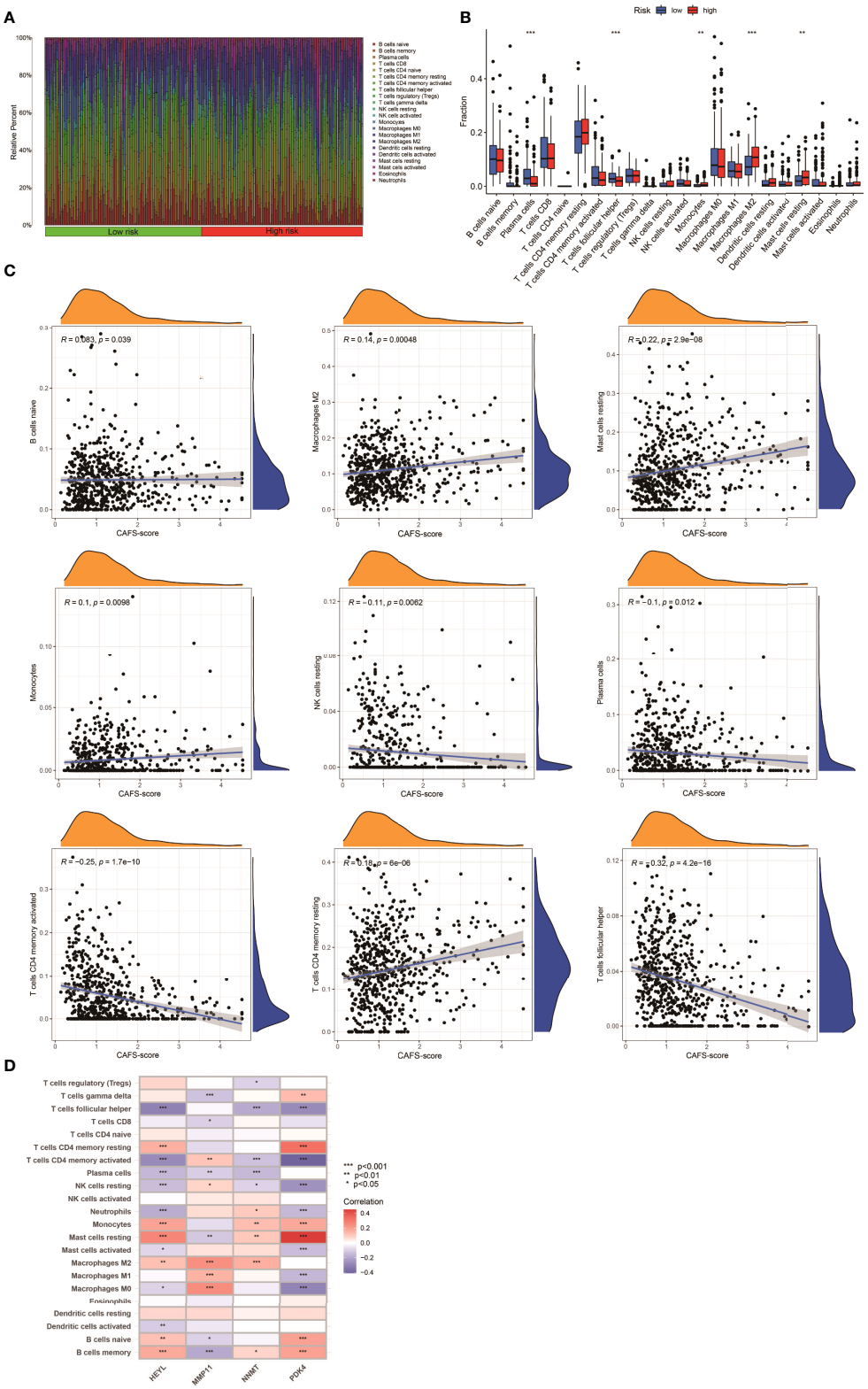

FIGURE 7
Immune Infiltration in two CAFS-score subgroup (TCGA). **(A)** Composition of immune cells in two CAFS-score subgroup. **(B)** The Relative immune infiltration score of 22 immune cells between low- and high-risk groups. **(C)** Relationships between CAFS-score and different immune cells. **(D)** Correlations between the abundance of immune cells and four genes in the proposed model. *P<0.05, **P<0.01, ***P<0.001

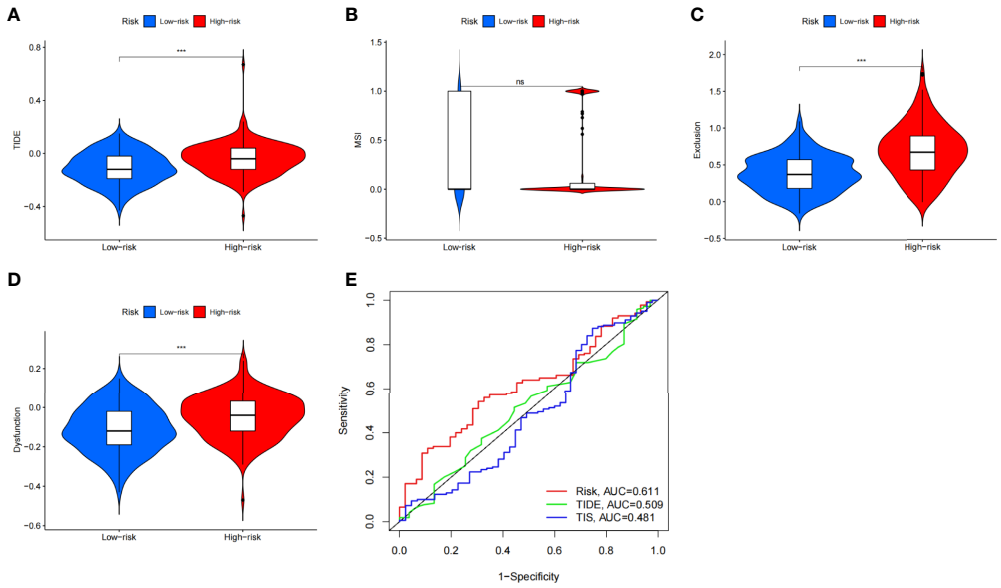

FIGURE 8
The prognostic value of CAFS-score in immunotherapy from TCGA cohort. **(A–D)** TIDE, MSI, T cell exclusion, and T cell dysfunction score in two CAFS-score subgroup, respectively. **(E)** ROC analysis of CAFS-score, TIDE, and TIS on OS in GC cohort. ***P<0.001, ns, P>0.05.

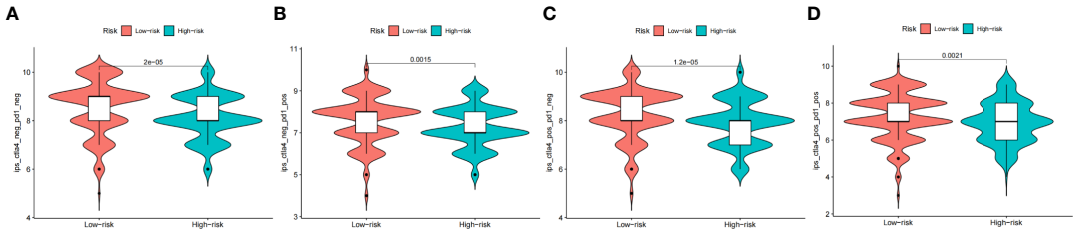

FIGURE 9
The prognostic value of CAFS-score in immunotherapy from TCGA cohort. **(A–D)** The vioplot of the difference expression of CTLA4 and PD-1 between high- and low-risk groups.

prognosis and guidelines for the individualized clinical strategies of GC.

Consensus clustering algorithms offer the ability to efficiently analyze and identify clusters of patients with different characteristics in a large amount of data (36). Therefore, we used this unsupervised algorithm to identify two distinct molecular subtypes based on the expression levels of 18 CAF-related regulators. We found that patients with subtype B had a better survival probability than subtype A patients. We also used GSVA enrichment analysis to investigate the variations in biological behavior between these two subtypes. Subtype A was enriched in terms of pathways associated with ECM and tumor invasion, especially ECM–receptor interaction and Focal adhesion. Some literature proved that the ECM receptor contributes to GC progression and poor survival (37). Focal adhesion-related proteins independently predicted the poor clinical prognosis of GC (38). Moreover, this consensus clustering algorithm was also used to classify the patient into three different subtype groups for deeper analysis according to the expression of prognostic DEGs.

In this study, we constructed the powerfully effective prognostic model and demonstrated its predictive ability. The expression levels of four genes (MMP11, PDK4, HEYL, and NNMT), including the CAF-related gene, MMP11, were also explored in GC. MMP11, one kind of ECM-degrading protease, in exosomes was secreted from CAFs and promoted GC cell migration and invasion by regulating and shaping the TME. Normally, MMP11 is absent in human organs, and the

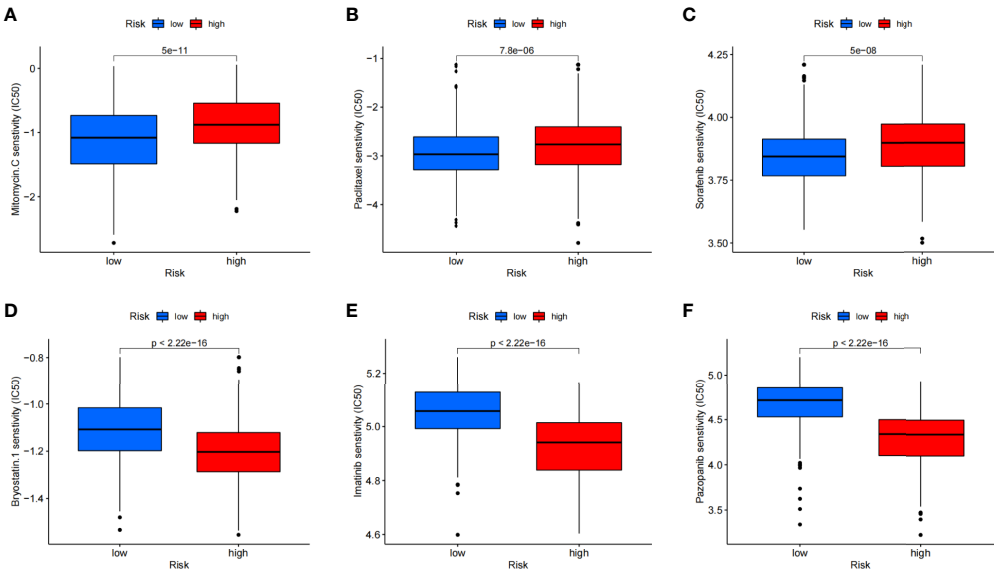

FIGURE 10
Relationships between CAFS-score and medicine sensitivity. Lower IC50 of indicated chemo-therapeutics drugs in low **(A–C)** and high **(D–F)** CAFS-score group, respectively.

expression level of MMP11 correlates to the OS of gastric patients (10, 11). HEYL and NNMT are usually upregulated in GC. Both act as an oncogenic factor to promote the carcinogenic and progressive process of GC *via* activating CDH11 and transforming growth factor-β (TGF-β) expression, respectively (39, 40). PDK4 promotes the Warburg effect in GC and the overexpression of PDK4 also leads to drug resistance and GC metastasis (41).

To further improve the accuracy of prognostic prediction, we constructed and validated a nomogram by screening various indexes, CAFS-score, age, gender, and pathological stage. The result illustrated that age, CAFS-score, and pathological stage were significantly associated with the prognosis of GC. Under the newest edition of AJCC, In et al. found that the pathological stage was closely associated with the prognosis of GC (42, 43). Moreover, we developed a quantitative nomogram that increased performance and made it easier to use the CAFS-score. GC is considered as an age-related disease, because older cancer patients have been shown to have poorer OS outcomes (44). According to the result, we found that the CAFS-score presented as an independent prognostic factor. Thorsson et al. (27) found that all tumors could be divided into six immune subtypes that are intended to serve as a resource for future targeted studies to further advance the field. Therefore, we found that the factor of immune subtypes was closely correlated with the risk score. These immune subtypes represent features of the TME that largely cut across traditional cancer classifications to create subgroups and suggest that certain treatments may be independent of histological type (27).

Numerous studies on various tumors have shown that patients with high TMB tend to favor good survival rates (45). Similarly, we illustrated that higher TMB was seen in the low risk of the CAFS-score. It means that high TMB has significantly better OS than the patients with a low TMB. In some literature, MUC16 mutations are associated with better prognosis and higher TMB in GC, while TTN mutations are associated with better response to immune checkpoint blockade in solid tumors (43, 46, 47). Even though TP53 is one of the most frequently mutated genes, it is insufficient to properly predict patient outcomes (48, 49). Patients with a high level of MSI respond better to immunotherapy and may benefit from it (50). Therefore, GC patients with a low-risk score had a better benefit from immunotherapy. In addition, GC cells with a lower CAFS-score exhibited more pronounced stem cell characteristics and a lower degree of cell differentiation.

To explore the importance of immune cell infiltration in GC with different risk groups for our study, CIBERSORT was utilized for analyzing the relative proportion of 22 immune cells in each GC specimen. As we know, circulating monocytes in peripheral blood migrate to tissue where they differentiate to macrophages or dendritic cells. Macrophages can be differentiated into two main types (M1 macrophages and M2 macrophages) depending on mode of activation and function. Meanwhile, some literature indicated that M2 macrophages can promote tumor growth in GC (51, 52). Consistent with these studies, we illustrated that less infiltration of M2 had a better prognosis. Wang et al. analyzed that the greater risk score resulted in a considerably shorter total survival time, and there was a positive association between risk

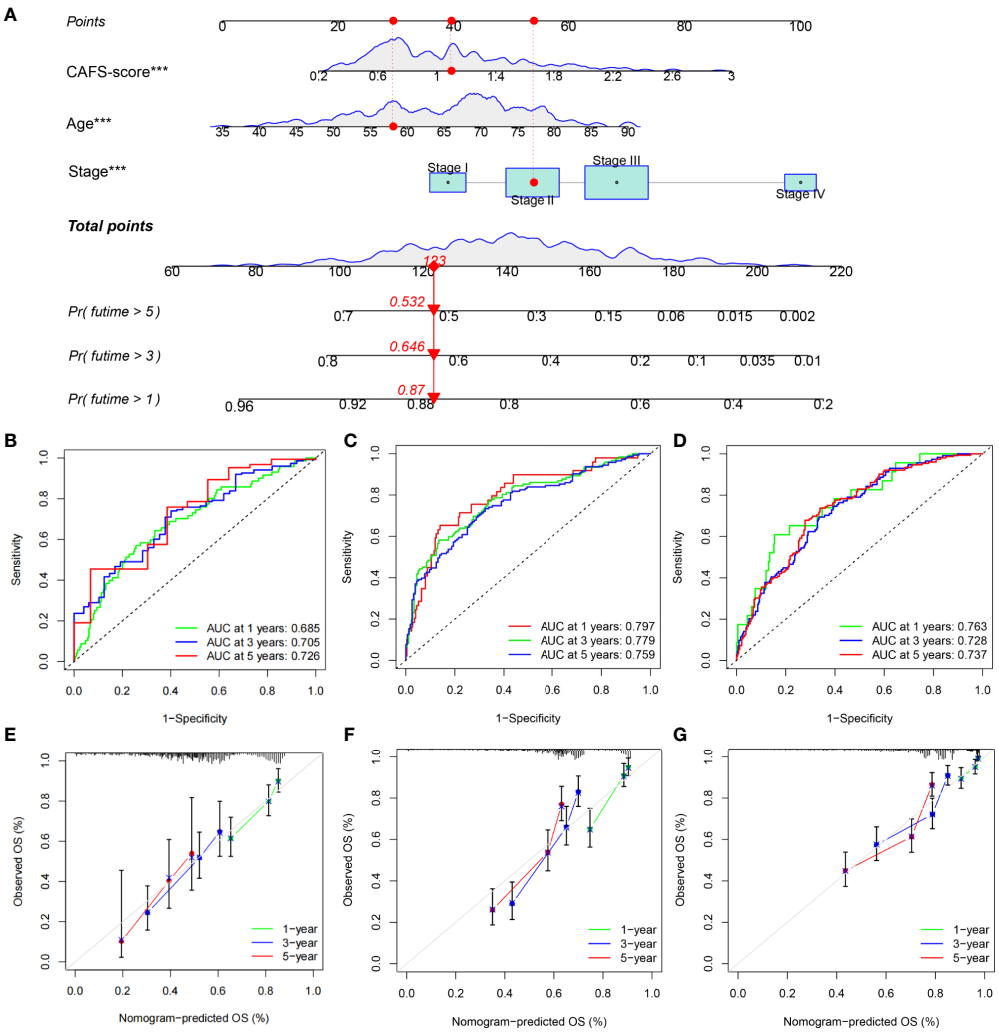

FIGURE 11
Construction and validation of a nomogram. **(A)** Nomogram for predicting the 1-, 3-, and 5-year OS of GC patients in TCGA cohort. **(B-D)** ROC curves for predicting the 1-, 3-, and 5-year ROC curves in TCGA, GSE62254, and GSE26253 cohorts. **(E-G)** Calibration curves of the nomogram for predicting of 1-, 3-, and 5-year OS in the TCGA, GSE62254, and GSE26253 cohorts. ***P<0.001.

score and dendritic cell infiltration in GC (53). Our result showed that the CAFs gene is associated with ECM-associated pathways. Therefore, less infiltration of dendritic cells had a better prognosis according to our result. The literature revealed that infiltrating mast cells are seen in large numbers in GC, which is linked to tumor growth and predicts poorer OS (54). Consistent with this study, we illustrated that more infiltration of mast cells had a poorer prognosis. According to the evidence, we believed that the CAFS-score had the potential to reflect immune cell infiltration as well as the prognostic significance of various immune cell types.

In our study, we explored the CAFS-based differences in the TME that might reflect different immune benefits from ICI therapy by utilizing TIDE and IPS. Firstly, the TIDE score is associated with the two different mechanisms of immune escape, namely, dysfunction of tumor-infiltrating cytotoxic T lymphocytes (CTLs) and exclusion of CTL. For the evidence, TIDE scores correlate to the potential of anti-tumor immune escape and thus show the response rate to ICI treatment (55). According to our analysis, we found that the lower CAFS-score corresponds to a lower score of the TIDE than high CAFS-score patients, and thus higher ICI response might predictably occur. Secondly, the IPS is mainly associated with a couple of immune checkpoints, including CTLA-4, PD-1, and PD-L1. For the clinical trial with immunotherapy, literature demonstrated that avelumab (anti-PD-1) has anti-tumor activity and is safe for patients with GC, which is administered as maintenance therapy (after the disease is under control with standard chemotherapy) (56). Consistent with our results, it was significantly higher in

the low-risk group, which was categorized by the CAFS-score. Based on the results identified with TIDE and IPS, we discovered that the CAFS-score may distinguish between various outcomes in individuals receiving immunotherapy. The CAFS-predictive score's value has the potential to offer a theoretical foundation for ICI treatment selection in clinical trials. This predictive model could assist to speed up the development of personalized cancer therapies.

According to the clinical trial, the literature showed that immune therapy in patients with GC had a great outcome before the disease was under control by standard chemotherapy (56). We wanted to figure out if the combination treatment with chemotherapy and immune therapy in GC had a better efficacy for further study. Therefore, we explored the sensitivity of various drugs in patients between two risk subgroups. Our study demonstrated that the low-risk group had a high potential for ICI response; meanwhile, we found out that the low risk was highly associated with sensitive drugs, including Mitomycin C, Paclitaxel, and Sorafenib. It means that further studies can focus on the combined treatment for GC patients. These drugs were found by the predictive model of the CAFS-score and had potential to treat GC under specific conditions (57–59).

Our comprehensive analysis demonstrated that the CAFS-score grouping might help to differentiate the clinicopathological features, immune infiltration, and clinical prognosis of GC patients. Furthermore, this study sheds light on the role of the CAFS-score in prognosis predictive value, and provides insights into individualized strategies, guiding immunotherapy, and chemotherapy. However, further studies on interactions among these model genes and their biological mechanisms are needed.

Data availability statement

The datasets presented in this study can be found in online repositories. The names of the repository/repositories and accession number(s) can be found in the article/**supplementary material**.

Author contributions

Conceptualization: TM, XL, HH, and ZH. Data curation: TM, XL, HH, and KW. Formal analysis: TM, XL, HH, and KW. Data analysis: TM and XL. Investigation: TM, XL, and HH. Methodology: TM, XL, and HH. Project administration: CZ, YH, and ZH. Resources: TM, XL, and HH. Original draft: TM, XL, and HH. Writing, review, and editing: TM, XL, HH, and ZH. All authors contributed to the article and approved the submitted manuscript.

Funding

This study was supported by the Guangdong Provincial Key Laboratory of Digestive Cancer Research (No. 2021B1212040006), the Shenzhen Sustainable Project (KCXFZ202002011010593), the National Natural Science Foundation of China (82073148), the National Natural Science Foundation of China (81772579), the Sanming Project of Medicine in Shenzhen (No. SZSM201911010), the Shenzhen Key Medical Discipline Construction Fund (No.SZXK016), and the Guangdong–Hong Kong–Macau University Joint Laboratory of Digestive Cancer Research (2021LSYS003).

Conflict of Interest

The authors declare that the research was conducted in the absence of any commercial or financial relationships that could be construed as a potential conflict of interest.

Publisher's note

Supplementary material

The Supplementary Material for this article can be found online at: https://www.frontiersin.org/articles/10.3389/fimmu.2022.951214/full#supplementary-material.

References

1. Bray F, Laversanne M, Weiderpass E, Soerjomataram I. The ever-increasing importance of cancer as a leading cause of premature death worldwide. *Cancer* (2021) 127(16):3029–30. doi: 10.1002/cncr.33587

2. Sung H, Ferlay J, Siegel RL, Laversanne M, Soerjomataram I, Jemal A, et al. Global cancer statistics 2020: GLOBOCAN estimates of incidence and mortality worldwide for 36 cancers in 185 countries. *CA Cancer J Clin* (2021) 71(3):209–49. doi: 10.3322/caac.21660

3. Smyth EC, Nilsson M, Grabsch HI, van Grieken NC, Lordick F. Gastric cancer. *Lancet* (2020) 396(10251):635–48. doi: 10.1016/S0140-6736(20)31288-5

4. Quail DF, Joyce JA. Microenvironmental regulation of tumor progression and metastasis. *Nat Med* (2013) 19(11):1423–37. doi: 10.1038/nm.3394

5. Kobayashi H, Enomoto A, Woods SL, Burt AD, Takahashi M, Worthley DL. Cancer-associated fibroblasts in gastrointestinal cancer. *Nat Rev Gastroenterol Hepatol* (2019) 16(5):282–95. doi: 10.1038/s41575-019-0115-0

6. Zhou Q, Wu X, Wang X, Yu Z, Pan T, Li Z, et al. The reciprocal interaction between tumor cells and activated fibroblasts mediated by TNF-alpha/IL-33/ST2L signaling promotes gastric cancer metastasis. *Oncogene* (2020) 39(7):1414–28. doi: 10.1038/s41388-019-1078-x

7. Qin Y, Wang F, Ni H, Liu Y, Yin Y, Zhou X, et al. Cancer-associated fibroblasts in gastric cancer affect malignant progression *via* the CXCL12-CXCR4 axis. *J Cancer* (2021) 12(10):3011–23. doi: 10.7150/jca.49707

8. Wu X, Tao P, Zhou Q, Li J, Yu Z, Wang X, et al. IL-6 secreted by cancer-associated fibroblasts promotes epithelial-mesenchymal transition and metastasis of gastric cancer *via* JAK2/STAT3 signaling pathway. *Oncotarget* (2017) 8 (13):20741–50. doi: 10.18632/oncotarget.15119

9. Chen X, Song E. Turning foes to friends: targeting cancer-associated fibroblasts. *Nat Rev Drug Discov* (2019) 18(2):99–115. doi: 10.1038/s41573-018-0004-1

10. Kessenbrock K, Plaks V, Werb Z. Matrix metalloproteinases: regulators of the tumor microenvironment. *Cell* (2010) 141(1):52–67. doi: 10.1016/j.cell.2010.03.015

11. Xu G, Zhang B, Ye J, Cao S, Shi J, Zhao Y, et al. Exosomal miRNA-139 in cancer-associated fibroblasts inhibits gastric cancer progression by repressing MMP11 expression. *Int J Biol Sci* (2019) 15(11):2320–9. doi: 10.7150/ijbs.33750

12. Li X, Sun Z, Peng G, Xiao Y, Guo J, Wu B, et al. Single-cell RNA sequencing reveals a pro-invasive cancer-associated fibroblast subgroup associated with poor clinical outcomes in patients with gastric cancer. *Theranostics* (2022) 12(2):620–38. doi: 10.7150/thno.60540

13. Wang R, Sun Y, Yu W, Yan Y, Qiao M, Jiang R, et al. Downregulation of miRNA-214 in cancer-associated fibroblasts contributes to migration and invasion of gastric cancer cells through targeting FGF9 and inducing EMT. *J Exp Clin Cancer Res* (2019) 38(1):20. doi: 10.1186/s13046-018-0995-9

14. Piersma B, Hayward MK, Weaver VM. Fibrosis and cancer: A strained relationship. *Biochim Biophys Acta Rev Cancer* (2020) 1873(2):188356. doi: 10.1016/j.bbcan.2020.188356

15. Zhang T, Li X, He Y, Wang Y, Shen J, Wang S, et al. Cancer-associated fibroblasts-derived HAPLN1 promotes tumour invasion through extracellular matrix remodeling in gastric cancer. *Gastric Cancer* (2022) 25(2):346–59. doi: 10.1007/s10120-021-01259-5

16. Fujii S, Fujihara A, Natori K, Abe A, Kuboki Y, Higuchi Y, et al. TEM1 expression in cancer-associated fibroblasts is correlated with a poor prognosis in patients with gastric cancer. *Cancer Med* (2015) 4(11):1667–78. doi: 10.1002/cam4.515

17. Ishimoto T, Miyake K, Nandi T, Yashiro M, Onishi N, Huang KK, et al. Activation of transforming growth factor beta 1 signaling in gastric cancer-associated fibroblasts increases their motility, *via* expression of rhomboid 5 homolog 2, and ability to induce invasiveness of gastric cancer cells. *Gastroenterology* (2017) 153(1):191–204 e16. doi: 10.1053/j.gastro.2017.03.046

18. Shen J, Zhai J, You Q, Zhang G, He M, Yao X, et al. Cancer-associated fibroblasts-derived VCAM1 induced by h. pylori infection facilitates tumor invasion in gastric cancer. *Oncogene* (2020) 39(14):2961–74. doi: 10.1038/s41388-020-1197-4

19. Wang X, Che X, Liu C, Fan Y, Bai M, Hou K, et al. Cancer-associated fibroblasts-stimulated interleukin-11 promotes metastasis of gastric cancer cells mediated by upregulation of MUC1. *Exp Cell Res* (2018) 368(2):184–93. doi: 10.1016/j.yexcr.2018.04.028

20. Yang T, Chen M, Yang X, Zhang X, Zhang Z, Sun Y, et al. Down-regulation of KLF5 in cancer-associated fibroblasts inhibit gastric cancer cells progression by CCL5/CCR5 axis. *Cancer Biol Ther* (2017) 18(10):806–15. doi: 10.1080/15384047.2017.1373219

21. Yang Y, Ma Y, Yan S, Wang P, Hu J, Chen S, et al. CAF promotes chemoresistance through NRP2 in gastric cancer. *Gastric Cancer* (2022) 25 (3):503–14. doi: 10.1007/s10120-021-01270-w

22. Yasukawa Y, Hattori N, Iida N, Takeshima H, Maeda M, Kiyono T, et al. SAA1 is upregulated in gastric cancer-associated fibroblasts possibly by its enhancer activation. *Carcinogenesis* (2021) 42(2):180–9. doi: 10.1093/carcin/bgaa131

23. Jin X, Qiu X, Huang Y, Zhang H, Chen K. miR-223-3p carried by cancer-associated fibroblast microvesicles targets SORBS1 to modulate the progression of gastric cancer. *Cancer Cell Int* (2022) 22(1):96. doi: 10.1186/s12935-022-02513-1

24. Ma Y, Zhu J, Chen S, Ma J, Zhang X, Huang S, et al. Low expression of SPARC in gastric cancer-associated fibroblasts leads to stemness transformation and 5-fluorouracil resistance in gastric cancer. *Cancer Cell Int* (2019) 19:137. doi: 10.1186/s12935-019-0844-8

25. Wilkerson MD, Hayes DN. ConsensusClusterPlus: a class discovery tool with confidence assessments and item tracking. *Bioinformatics* (2010) 26 (12):1572–3. doi: 10.1093/bioinformatics/btq170

26. Hänzelmann S, Castelo R, Guinney J. GSVA: gene set variation analysis for microarray and RNA-seq data. *BMC Bioinf* (2013) 14:7. doi: 10.1186/1471-2105-14-7

27. Thorsson V, Gibbs DL, Brown SD, Wolf D, Bortone DS, Ou Yang TH, et al. The immune landscape of cancer. *Immunity* (2018) 48(4):812–830 e14. doi: 10.1016/j.immuni.2018.03.023

28. Malta TM, Sokolov A, Gentles AJ, Burzykowski T, Poisson L, Weinstein JN, et al. Machine learning identifies stemness features associated with oncogenic dedifferentiation. *Cell* (2018) 173(2):338–354 e15. doi: 10.1016/j.cell.2018.03.034

29. Ayers M, Lunceford J, Nebozhyn M, Murphy E, Loboda A, Kaufman DR, et al. IFN-gamma-related mRNA profile predicts clinical response to PD-1 blockade. *J Clin Invest* (2017) 127(8):2930–40. doi: 10.1172/JCI91190

30. Charoentong P, Finotello F, Angelova M, Mayer C, Efremova M, Rieder D, et al. Pan-cancer immunogenomic analyses reveal genotype-immunophenotype relationships and predictors of response to checkpoint blockade. *Cell Rep* (2017) 18 (1):248–62. doi: 10.1016/j.celrep.2016.12.019

31. Geeleher P, Cox N, Huang RS. pRRophetic: an r package for prediction of clinical chemotherapeutic response from tumor gene expression levels. *PloS One* (2014) 9(9):e107468. doi: 10.1371/journal.pone.0107468

32. Iasonos A, Schrag D, Raj GV, Panageas KS. How to build and interpret a nomogram for cancer prognosis. *J Clin Oncol* (2008) 26(8):1364–70. doi: 10.1200/JCO.2007.12.9791

33. Bray F, Ferlay J, Soerjomataram I, Siegel RL, Torre LA, Jemal A. Global cancer statistics 2018: GLOBOCAN estimates of incidence and mortality worldwide for 36 cancers in 185 countries. *CA Cancer J Clin* (2018) 68(6):394–424. doi: 10.3322/caac.21492

34. Ajani JA, D'Amico TA, Almhanna K, Bentrem DJ, Chao J, Das P, et al. Gastric cancer, version 3.2016, NCCN clinical practice guidelines in oncology. *J Natl Compr Canc Netw* (2016) 14(10):1286–312. doi: 10.6004/jnccn.2016.0137

35. Biffi G, Tuveson DA. Diversity and biology of cancer-associated fibroblasts. *Physiol Rev* (2021) 101(1):147–76. doi: 10.1152/physrev.00048.2019

36. Alyousef AA, Nihtyanova S, Denton C, Bosoni P, Bellazzi R, Tucker A. Nearest consensus clustering classification to identify subclasses and predict disease. *J Healthc Inform Res* (2018) 2(4):402–22. doi: 10.1007/s41666-018-0029-6

37. Yang X, Chen L, Mao Y, Hu Z, He M. Progressive and prognostic performance of an extracellular matrix-receptor interaction signature in gastric cancer. *Dis Markers* (2020) 2020:8816070. doi: 10.1155/2020/8816070

38. Park JH, Lee BL, Yoon J, Kim J, Kim MA, Yang HK, et al. Focal adhesion kinase (FAK) gene amplification and its clinical implications in gastric cancer. *Hum Pathol* (2010) 41(12):1664–73. doi: 10.1016/j.humpath.2010.06.004

39. Liu H, Ni S, Wang H, Zhang Q, Weng W. Charactering tumor microenvironment reveals stromal-related transcription factors promote tumor carcinogenesis in gastric cancer. *Cancer Med* (2020) 9(14):5247–57. doi: 10.1002/cam4.3133

40. Zhu AK, Shan YQ, Zhang J, Liu XC, Ying RC, Kong WC. Exosomal NNMT from peritoneum lavage fluid promotes peritoneal metastasis in gastric cancer. *Kaohsiung J Med Sci* (2021) 37(4):305–13. doi: 10.1002/kjm2.12334

41. Miao Y, Li Q, Sun G, Wang L, Zhang D, Xu H, et al. MiR-5683 suppresses glycolysis and proliferation through targeting pyruvate dehydrogenase kinase 4 in gastric cancer. *Cancer Med* (2020) 9(19):7231–43. doi: 10.1002/cam4.3344

42. Amin MBAmerican Joint Committee on Cancer and American Cancer Society. AJCC cancer staging manual. eight edition. In: MB Amin, SB Edge, DM Gress and LR Meyer, editors. *Chicago IL: American Joint committee on cancer*, vol. xvii. New York: Springer (2017). p. 1024.

43. In H, Solsky I, Palis B, Langdon-Embry M, Ajani J, Sano T. Validation of the 8th edition of the AJCC TNM staging system for gastric cancer using the national cancer database. *Ann Surg Oncol* (2017) 24(12):3683–91. doi: 10.1245/s10434-017-6078-x

44. Coleman MP, Forman D, Bryant H, Butler J, Rachet B, Maringe C, et al. Cancer survival in Australia, Canada, Denmark, Norway, Sweden, and the UK, 1995-2007 (the international cancer benchmarking partnership): an analysis of population-based cancer registry data. *Lancet* (2011) 377(9760):127–38. doi: 10.1016/S0140-6736(10)62231-3

45. Marabelle A, Fakih M, Lopez J, Shah M, Shapira-Frommer R, Nakagawa K, et al. Association of tumour mutational burden with outcomes in patients with advanced solid tumours treated with pembrolizumab: prospective biomarker analysis of the multicohort, open-label, phase 2 KEYNOTE-158 study. *Lancet Oncol* (2020) 21(10):1353–65. doi: 10.1016/S1470-2045(20)30445-9

46. Li X, Pasche B, Zhang W, Chen K. Association of MUC16 mutation with tumor mutation load and outcomes in patients with gastric cancer. *JAMA Oncol* (2018) 4(12):1691–8. doi: 10.1001/jamaoncol.2018.2805

47. Yang Y, Zhang J, Chen Y, Xu R, Zhao Q, Guo W. MUC4, MUC16, and TTN genes mutation correlated with prognosis, and predicted tumor mutation burden and immunotherapy efficacy in gastric cancer and pan-cancer. *Clin Transl Med* (2020) 10(4):e155. doi: 10.1002/ctm2.155

48. Park S, Lee J, Kim YH, Park J, Shin JW, Nam S. Clinical relevance and molecular phenotypes in gastric cancer, of TP53 mutations and gene expressions, in combination with other gene mutations. *Sci Rep* (2016) 6:34822. doi: 10.1038/srep34822

49. Robles AI, Harris CC. Clinical outcomes and correlates of TP53 mutations and cancer. *Cold Spring Harb Perspect Biol* (2010) 2(3):a001016. doi: 10.1101/cshperspect.a001016

50. Ganesh K, Stadler ZK, Cercek A, Mendelsohn RB, Shia J, Segal NH, et al. Immunotherapy in colorectal cancer: rationale, challenges and potential. *Nat Rev Gastroenterol Hepatol* (2019) 16(6):361–75. doi: 10.1038/s41575-019-0126-x

51. Li W, Zhang X, Wu F, Zhou Y, Bao Z, Li H, et al. Gastric cancer-derived mesenchymal stromal cells trigger M2 macrophage polarization that promotes metastasis and EMT in gastric cancer. *Cell Death Dis* (2019) 10(12):918. doi: 10.1038/s41419-019-2131-y

52. Yamaguchi T, Fushida S, Yamamoto Y, Tsukada T, Kinoshita J, Oyama K, et al. Tumor-associated macrophages of the M2 phenotype contribute to progression in gastric cancer with peritoneal dissemination. *Gastric Cancer* (2016) 19(4):1052–65. doi: 10.1007/s10120-015-0579-8

53. Wang Z, Wang Z, Hu X, Han Q, Chen K, Pang G. Extracellular matrix-associated pathways promote the progression of gastric cancer by impacting the dendritic cell axis. *Int J Gen Med* (2021) 14:6725–39. doi: 10.2147/IJGM.S334245

54. Lv Y, Zhao Y, Wang X, Chen N, Mao F, Teng Y, et al. Increased intratumoral mast cells foster immune suppression and gastric cancer progression through TNF-alpha-PD-L1 pathway. *J Immunother Cancer* (2019) 7(1):54. doi: 10.1186/s40425-019-0530-3

55. Jiang P, Gu S, Pan D, Fu J, Sahu A, Hu X, et al. Signatures of T cell dysfunction and exclusion predict cancer immunotherapy response. *Nat Med* (2018) 24(10):1550–8. doi: 10.1038/s41591-018-0136-1

56. Chung HC, Arkenau HT, Lee J, Rha SY, Oh DY, Wyrwicz L, et al. Avelumab (anti-PD-L1) as first-line switch-maintenance or second-line therapy in patients with advanced gastric or gastroesophageal junction cancer: phase 1b results from the JAVELIN solid tumor trial. *J Immunother Cancer* (2019) 7(1):30. doi: 10.1186/s40425-019-0508-1

57. Blum Murphy M, Ikoma N, Wang X, Estrella J, Roy-Chowdhuri S, Das P, et al. Phase I trial of hyperthermic intraperitoneal chemoperfusion (HIPEC) with cisplatin, mitomycin, and paclitaxel in patients with gastric adenocarcinoma and associated carcinomatosis or positive cytology. *Ann Surg Oncol* (2020) 27(8):2806–11. doi: 10.1245/s10434-020-08226-x

58. Shitara K, Ozguroglu M, Bang YJ, Di Bartolomeo M, Mandala M, Ryu MH, et al. Pembrolizumab versus paclitaxel for previously treated, advanced gastric or gastro-oesophageal junction cancer (KEYNOTE-061): a randomised, open-label, controlled, phase 3 trial. *Lancet* (2018) 392(10142):123–33. doi: 10.1016/S0140-6736(18)31257-1

59. Xu X, Tang X, Wu X, Feng X. Biosynthesis of sorafenib coated graphene nanosheets for the treatment of gastric cancer in patients in nursing care. *J Photochem Photobiol B* (2019) 191:1–5. doi: 10.1016/j.jphotobiol.2018.11.013

frontiers | Frontiers in Immunology

TYPE Original Research
PUBLISHED 02 September 2022
DOI 10.3389/fimmu.2022.940801

OPEN ACCESS

EDITED BY
Uday Kishore,
Brunel University London,
United Kingdom

REVIEWED BY
Amr Amin,
The University of Chicago,
United States
Alice Masserdotti,
Catholic University of the Sacred Heart, Italy

*CORRESPONDENCE
Xiaodan Fu
jessicafu0225@163.com;
fuxiaodan@csu.edu.cn
Qihui Wu
146511038@csu.edu.cn
Hong Tan
tanhong@csu.edu.cn

†These authors have contributed equally to this work and share first authorship

SPECIALTY SECTION
This article was submitted to Cancer Immunity and Immunotherapy, a section of the journal Frontiers in Immunology

RECEIVED 10 May 2022
ACCEPTED 15 August 2022
PUBLISHED 02 September 2022

CITATION
Li Y, Tian R, Liu J, Li J, Tan H, Wu Q and Fu X (2022) Deciphering the immune landscape dominated by cancer-associated fibroblasts to investigate their potential in indicating prognosis and guiding therapeutic regimens in high grade serous ovarian carcinoma. *Front. Immunol.* 13:940801. doi: 10.3389/fimmu.2022.940801

Deciphering the immune landscape dominated by cancer-associated fibroblasts to investigate their potential in indicating prognosis and guiding therapeutic regimens in high grade serous ovarian carcinoma

Yimin Li[1,2,3†], Ruotong Tian[4†], Jiaxin Liu[5], Juanni Li[1,6], Hong Tan[7*], Qihui Wu[6,8*] and Xiaodan Fu[1,6*]

[1]Department of Pathology, Xiangya Hospital, Central South University, Changsha, China, [2]Department of Pathology, Fudan University Shanghai Cancer Center, Shanghai, China, [3]Department of Oncology, Shanghai Medical College, Fudan University, Shanghai, China, [4]Department of Pharmacology, School of Basic Medical Sciences, Shanghai Medical College, Fudan University, Shanghai, China, [5]Department of Pathology, School of Basic Medical Sciences, Central South University, Changsha, China, [6]National Clinical Research Center for Geriatric Disorders, Xiangya Hospital, Changsha, China, [7]Department of Pathology, The Second Xiangya Hospital, Central South University, Changsha, China, [8]Department of Obstetrics and Gynecology, Xiangya Hospital, Central South University, Changsha, China

Limited immunotherapeutic effect in high-grade serous ovarian carcinoma (HGSOC) propels exploration of the mechanics behind this resistance, which may be partly elucidated by investigating characters of cancer-associated fibroblasts (CAFs), a significant population in HGSOC involved in shaping tumor immune microenvironment. Herein, leveraging gene expression data of HGSOC samples from The Cancer Genome Atlas and Gene Expression Omnibus datasets, we suggested that CAFs detrimentally affected the outcomes of HGSOC patients. Subsequently, we performed weighted gene co-expression network analysis (WGCNA) to identify a CAFs-related module and screened out seven hub genes from this module, all of which were positively correlated with the infiltration of immunosuppressive macrophages. As one of the hub genes, the expression of fibrillin 1 (FBN1) and its relevance to CD206 were further verified by immunohistochemistry staining in HGSOC samples. Meanwhile, we extracted genes that correlated well with CAF signatures to construct a CAFscore. The capacity of the CAFscore as an independent prognostic factor was validated by Cox regression analyses, and its relevance to components as well as signals in the tumor immune microenvironment was also investigated. Under the evaluation by the CAFscore, HGSOC patients with relatively high CAFscore had worse outcomes, activated mesenchymal signaling pathways, and immune checkpoint blockade (ICB) resistance signatures, which was consistent with the fact that non-responders in anti-PD-1 treatment cohorts tended to have

higher CAFscore. Besides, the possibility of CAFscore to guide the selection of sensitive chemotherapeutic agents was explored. In conclusion, individualized assessment of the CAFscore could uncover the extent of stroma activation and immunosuppression and inform therapeutic strategies to improve the benefit of therapies.

KEYWORDS

high grade serous ovarian carcinoma, cancer-associated fibroblast, tumor immune microenvironment, prognosis, therapy prediction

Highlights

From the view of the intricate interplay between CAFs and the immune microenvironment of HGSOC, we identify a gene module associated with CAF traits and generate a CAFscore evaluation system. As an independent prognostic factor, the CAFscore extensively contacts with components and signals in the HGSOC microenvironment. Evaluating the CAFscore of individual may contribute to gaining a greater understanding of stroma and the immune status of each patient, enhancing the accuracy of prognostic prediction, and suggesting effective treatment options.

Introduction

Ovarian carcinoma is the most fatal of all gynecologic cancers, of which high-grade serous ovarian carcinoma is characterized by a high recurrence rate with poor long-term survival and results in the highest death tolls (1–3). Its malignant biological properties are reflected in its early and widespread dissemination to peritoneal surfaces, which largely relies on communication between tumor cells and their adjacent stromal microenvironment. Previous studies including The Cancer Genome Atlas (TCGA) have identified various subtypes of HGSOC, among which the mesenchymal subtype was linked to conspicuously poorer survival when compared with other subtypes, with increased stromal components such as myofibroblasts and microvascular pericytes (4, 5), highlighting the importance of the tumor stroma for the survival of HGSOC patients.

Cancer-associated fibroblasts (CAFs), originating from diverse groups of mesenchymal cells, are a prominent stromal population in almost all tumors (6). Multiple mechanisms, such as inflammatory signals, DNA damage, and physiological stress, can lead to CAFs activation (7). Through secreting growth factors, inflammatory ligands, and extracellular matrix (ECM) proteins, activated CAFs extensively interact with cancer cells and exert protumorigenic and antitumorigenic effects. In the past decade, the adverse effects of CAFs on ovarian cancer have mostly been illustrated. Functionally, ovarian tumor cells activate fibroblasts or induce cancer-associated fibroblasts-phenotype to promote ovarian cancer progression and reduce overall survival by secreting lysophosphatidic acid, interleukin-1β (IL-1β), and C-C motif chemokine ligand 5 (CCL5) (8–10). Reciprocally, activated ovarian CAFs contribute to epithelial ovarian cancer metastasis by promoting angiogenesis and tumor cell invasion, and even the resistance to platinum-based chemotherapy, through releasing growth factors and metabolites (11–13). Prior studies have shown a predominance of the fibroblast in the HGSOC patient samples, based on the analysis of single-cell separation and sequence (14, 15). Remarkably, myofibroblasts and cancer-associated fibroblasts driven by transforming growth factor-β (TGF-β) predicted the poor outcome of HGSOC patients (16). As such a major component of the stroma, CAFs affect each cancer developmental stage, from initiation to invasion and metastasis, leading to an unfavorable prognosis of ovarian cancer, which inspired us to develop a prognostic model of ovarian cancer based on the status and content of CAFs.

In addition to considering the interactions between CAFs and tumor cells, CAFs' engagement in crosstalk with other cells within the tumor microenvironment (TME) also deserves attention. The contribution of CAFs to establishing an immunosuppressive TME has been supported by several lines of evidence. In detail, CAFs not only impaired the functionality of dendritic cells (DCs) and the infiltration of natural killer (NK) cells but also facilitated the immunoinhibitory phenotype of macrophages and the differentiation of naïve T cells into regulator T cells (Tregs) (17–20). The potential intervention of fibroblasts in TME is not limited to expressing ligands of immune checkpoint molecules (ICMs), including programmed death ligand 1 (PD-L1), PD-L2, and B7-H3/H4 on their own surface (21). Also, CAFs upregulates the expression of ICMs on other cells in the TME, thereby contributing to the impaired function of tumor-infiltrating T lymphocytes. In the past decade, immune checkpoint blockade, which has revolutionized the treatment of several cancer types shows only modest results in

HGSOC (22–25). Nevertheless, little is known about the molecular mechanisms that dictate response or resistance to these modalities. Considering the above backgrounds, investigating interactions between CAFs and the immune microenvironment helps elucidate the mechanism beneath the limited effectiveness of immunotherapies in HGSOC and develop CAFs-targeting immunotherapies.

Herein, prognosis-oriented clustering analysis distinguishing two groups of HGSOC patients with a significant difference in CAFs infiltration suggested that CAFs were significantly involved in the outcomes of HGSOC. Leveraging global gene expression data from several independent sets of clinical HGSOC tumor samples, we identified a gene co-expression module that presents high correlations with signatures of CAFs and significantly overlaps with participators of ECM. Subsequently, we screened out seven hub genes from this CAF-related module, among which FBN1 was further verified by immunohistochemistry (IHC) staining of HGSOC samples. To a large extent, these hub genes might be interpreted as fibroblast markers and correlated well with macrophage infiltration. Meanwhile, we extracted genes that correlated well with CAF signatures to construct a CAFscore. Under the evaluation by the CAFscore, HGSOC patients with relatively high CAFscore had worse outcomes, activated mesenchymal signaling pathways, and ICB resistance signatures, which was consistent with the fact that non-responders in anti-PD-1 treatment cohorts tended to have higher CAFscore. Besides, the possibility of CAFscore to guide chemotherapeutic drug selection was explored.

Materials and methods

Dataset acquisition and preprocessing

The R package "TCGAbiolinks" was used to download TCGA RNA-seq data (FPKM normalized), and clinical data were obtained from the cBioPortal website (http://www.cbioportal.org/). Then, the FPKM values were transformed into transcripts per kilobase million (TPM) values. The RNA sequencing data and clinicopathological characteristics of TCGA pan-cancer were obtained from UCSC Xena (https://xenabrowser.net/datapage/). For the HGSOC cohort, the expression data and detailed clinical information of GSE140082, GSE17260, GSE18520, GSE26193, GSE30161, and GSE32063 were downloaded from the Gene Expression Omnibus (GEO) (http://www.ncbi.nlm.nih.gov/geo/). Our study included two immune checkpoint blockade treatment cohorts with available expression and clinical information: the IMvigor210 cohort (obtained from http://research-pub.Gene.com/imvigor210corebiologies) and the GSE78220 cohort (downloaded from GEO). The data preprocessing methods were previously reported (26). Only patients with complete related information were included in each cohort above in this study. Batch effects from non-biological technical biases were corrected using the "ComBat" algorithm of the "sva" package.

To further verify the expression of relevant key genes, 41 HGSOC samples were collected from Xiangya Hospital of Central South University and written informed consent was obtained from the Xiangya Hospital Ethics Committee. The patients were informed and signed informed consent forms.

Estimation of TME cell infiltration

The immune score, stromal score, ESTIMATE score, and tumor purity for tumor samples were estimated using the R package "ESTIMATE" (27). Meanwhile, the levels of infiltrating CAFs that was calculated by EPIC, MCPcounter and tumor immune dysfunction and exclusion (TIDE), and other immune cells that were calculated by CIBERSORT, EPIC, TIMER, and MCPcounter algorithms in the TME of ovarian cancer (27–31).

Weighted gene co-expression network analysis

In this study, we conducted weighted gene co-expression analysis (WGCNA) using the R package "WGCNA" to cluster gene modules most correlated with CAFs based on EPIC, MCPcounter, and TIDE (32). We selected a soft threshold power β=3 and then constructed the adjacency matrix by raising the intergenic Pearson correlation matrix to the soft threshold power. The correlation between each module and the different CAFs groups was further selected by selecting the modules with the highest module-CAFs associations to further select candidate modules related to CAFs infiltration. Module membership (MM) represented the correlation between module eigengenes and gene expression profiles, while gene significance (GS) was defined as the absolute value of the correlation between the gene and the clinical trait.

Generation of the CAFscore

The WGCNA was used to recognize co-expressed gene modules closely related to the CAFs, and a total of 145 genes were determined in the brown gene module with GS>0.3 and MM>0.6. Then, we used the ssGSEA (Single-sample Gene Set Enrichment Analysis) algorithm to construct a CAF-relevant gene signature to quantify the content of the CAFs of individual patients.

Functional and pathway enrichment analysis

Gene ontology (GO) and Kyoto Encyclopedia of Genes and Genomes (KEGG) pathway analyses *via* the R package

"clusterprofiler" with a strict cutoff value of false discovery rate (FDR)<0.05 (33). We performed gene set variation analysis (GSVA) enrichment analysis as in our previous study (34). The R package "IOBR" constructed a gene set that stored genes associated with some biological processes (35). The stroma pathways, DNA damage repair pathways, and immune-related pathways were downloaded, and the ssGSEA method was chosen in the process of pathway score evaluation (36).

Immunohistochemistry (IHC) staining

IHC was performed as described previously (37). Primary antibodies against CK (Ready to use, Maxim, MAB-0828), CD206 (1:10000, Proteintech, Cat No.60143-1-Ig), FBN1 (1:500, Proteintech,Cat No.26935-1-AP) were used for IHC staining.

Association analysis of the CAFscore and Immuno-/Chemotherapeutic Response prediction

We investigated the predictive capacity of CAFscore in responding to immunotherapy and chemotherapies/targeted therapies. First, the TIDE algorithm and the Immune Cell Abundance Identifier (ImmuCellAI) algorithm were used to predict the response to ICB therapy as previously described (38). The drugs' 50% inhibiting concentration (IC_{50}) value was predicted using the "pRRophetic" algorithm, and the correlation between CAFscore and the IC_{50} value of the drugs was determined using Spearman correlation analysis.

Statistical analysis

The statistical difference in the distribution in the two groups was examined by unpaired Student's t-tests (normally distributed) and the Wilcoxon rank-sum test (nonnormally distributed). Pearson's or Spearman's correlation analysis was used to examine the relationships between two continuous variables. The chi-square and Fisher's exact tests were adopted to analyze the difference between categorical variables. We used the R package "Survminer" to determine the optimal cutoffs, and samples were classified into high and low score groups based on the cutoff. Then, survival analysis was carried out using the Kaplan-Meier method, and the log-rank test was utilized to calculate the statistical significance. A univariate Cox regression model was adopted to calculate the hazard ratios (HR) for CAFs, and a multivariable Cox regression model was used to ascertain the independent prognostic factors. All statistical analyses were conducted using R software (version 4.0.5). The p values were two-sided, and p values < 0.05 was considered statistically significant.

Results

Validation of consistency of CAF algorithms and identification of CAF as an adverse prognostic factor in HGSOC

To examine whether CAF signatures calculated by three recently established algorithms (MCP-CAFs, EPIC-CAFs, and TIDE-CAFs) are generally consistent and stable, we evaluated the correlation between any two signatures from the three algorithms in each HGSOC patient from the integrated cohort (Figure 1A). The strong positive correlation between each signature is reflected by R=0.914, 0.868, and 0.866, respectively. In order to characterize CAFs comprehensively and convincingly, all three algorithms would be applied simultaneously during the subsequent analysis. HGSOC patients were grouped according to the content of CAFs, and significant prognostic differences were observed between groups (Figure 1B). Further, univariate Cox regression analysis determined CAF signatures as indexes suggesting adverse prognosis (Figure 1C).

Investigating the relevance between CAF signatures and components as well as signals in HGSOC immune microenvironment

Given the impressive ability of CAF signatures to distinguish between patients with widely varying outcomes, the role of CAFs in the prognosis of HGSOC patients deserves further exploration. The relevance of CAFs to prognosis should be demonstrated by more proof. Specifically, CAF algorithms and acknowledged sub-CAF signatures (myofibroblastic CAFs, myCAFs; inflammatory CAFs, iCAFs), as well as markers, are supposed to measure the content of CAFs. Prognostic-oriented clustering in the HGSOC integrated cohort exhibited distinct CAF signatures as well as markers between the two groups (Figure 2A). As a prominent population in the TME of HGSOC, CAFs undeniably engage in shaping the immune microenvironment. Thus, we demonstrated correlations between CAF signatures with cytokines including interleukins and chemokines, in which CCL11, CXCL12, and CXCL14 were remarkable because of their apparent positive correlations with CAFs (Figure 2B). Based on the CAF signature displayed by the MCP algorithm, the ESTIMATE algorithm showed that CAFs were inversely correlated with Tumor Purity but positively correlated with the ImmuneScore, StromalScore, and

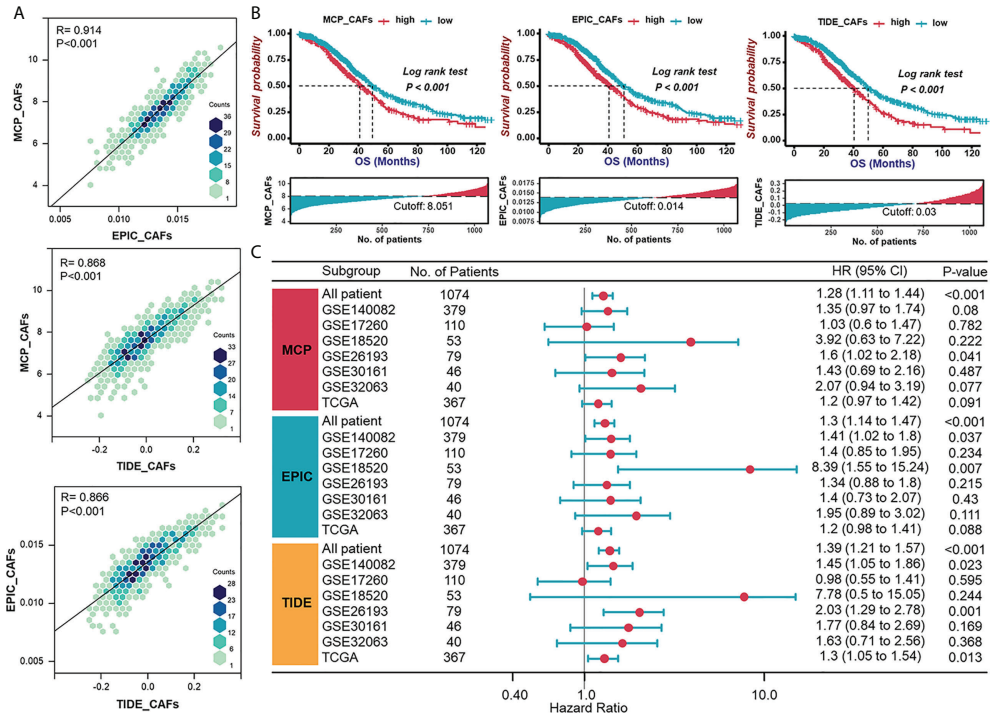

FIGURE 1
Validation of consistency of CAF algorithms and identification of CAF as an adverse prognostic factor in HGSOC. **(A)** The correlation between any two signatures obtained by three CAF algorithms (MCP, EPIC, and TIDE) in each patient in the integrated cohort (TCGA-OV and GEO datasets). **(B)** Survival analyses for patient with relatively high or low CAF signatures in the integrated cohort using Kaplan–Meier curves. **(C)** Forest plot of univariate Cox analysis of CAF signatures in TCGA and GEO datasets.

ESTIMATEScore (Figure 2C). Additionally, CAF signatures positively correlated with macrophage abundance (Figure 2D), enhanced immunotherapy resistance, and mesenchymal activation, including epithelial-mesenchymal transition (EMT), TGF-β signals, and pan-fibroblast TGF-β response (Pan-F-TBRS) in the high CAFs group (Figure 2E). Heretofore, the adverse role of CAFs in HGSOC was reflected by not only the overall survival of patients but also possible participation in mesenchyme activation, immunosuppression, and resistance to immunotherapy.

Detection and functional interpretations of a gene co-expression module shared CAF characteristics in HGSOC

Identification of genes that show similar expression patterns across samples might help shed light on shared biological processes, for example, the mechanism for activation of CAFs in TME. Thus, we investigated this by applying WGCNA to an integrated HGSOC cohort generated from TCGA and GEO datasets. β=3 was selected to construct a standard scale-free network with the pick soft threshold function (Figure S1A), where genes were assigned to eight different modules using a cluster dendrogram (Figure 3A). To identify the module regulating CAFs, we correlated each module eigengene with different CAF traits, suggesting the brown module's potential. The full module-trait correlation table is presented in Figure 3B. The brown module members present good correlations with CAF signatures (Figure 3C). Furthermore, GO analysis revealed that brown module genes were mainly enriched in functions such as extracellular matrix organization, collagen-containing extracellular matrix, and extracellular matrix structural constituents (Figure 3D). KEGG analysis of brown module genes emphasized the PI3K-Akt signaling pathway, focal adhesion, and ECM-receptor interaction (Figure S1B). The above results raise the possibility that the brown module is a specific gene network regulating the ECM and sharing similarities with the CAF traits of HGSOC.

The hub genes extracted from CAFs-related module as potential CAF markers participating in the shaping of TME

Highly connected "hub" genes are thought to be paramount in managing the behavior of biological modules (39). Therefore,

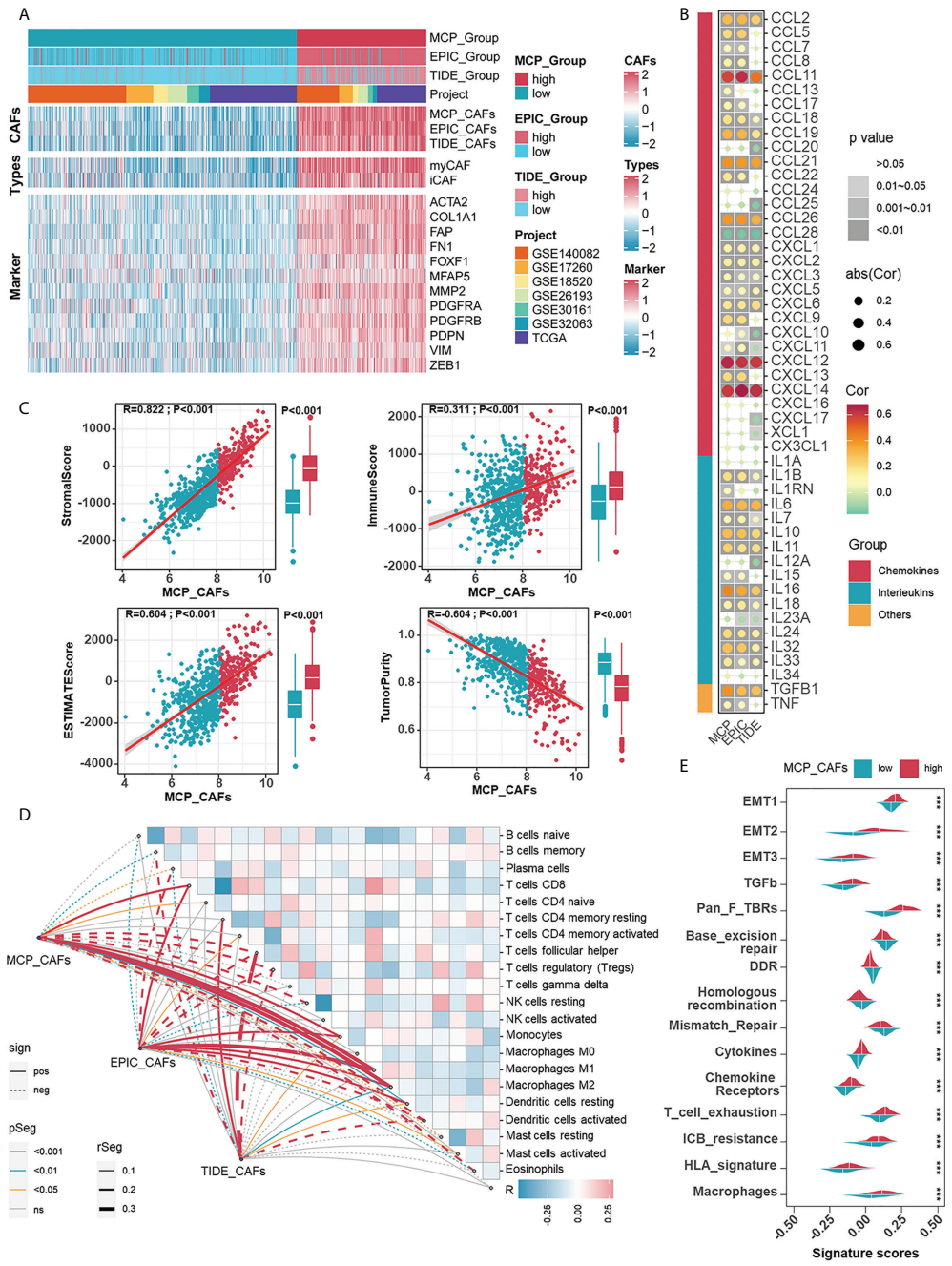

FIGURE 2
Investigating the relevance between CAF signatures and components as well as signals in HGSOC immune microenvironment. **(A)** The heatmap shows the correlations between CAF signatures and acknowledged makers of CAFs in 1074 HGSOC patients in meta cohort. Pink represented the relatively high score or expression and blue represented the relatively low score or expression. **(B)** Correlations between CAF signatures with cytokines including chemokines, interleukins, and other cytokines. **(C)** Correlations between CAF signatures (MCP) and ImmuneScore, StromalScore, ESTIMATEScore as well as Tumor Purity. **(D)** Correlations between CAF signatures (MCP) and immune cells (cibersort). **(E)** Differences in ICB response-related signatures between low- and high-CAF (MCP) groups. ***, P < 0.001.

we set out to identify the hub genes in the brown module and hypothesized that those hub genes might be associated with CAFs in HGSOC. The relationships between genes in the brown module and CAFs signatures were evaluated with GS and MM. In the end, seven hub genes, including anthrax toxin receptor 1 (ANTXR1), pericytes derived growth factor receptor beta (PDGFRB), adipocyte enhancer-binding protein 1 (AEBP1), collagen type V alpha 2 chain (COL5A2), collagen type V

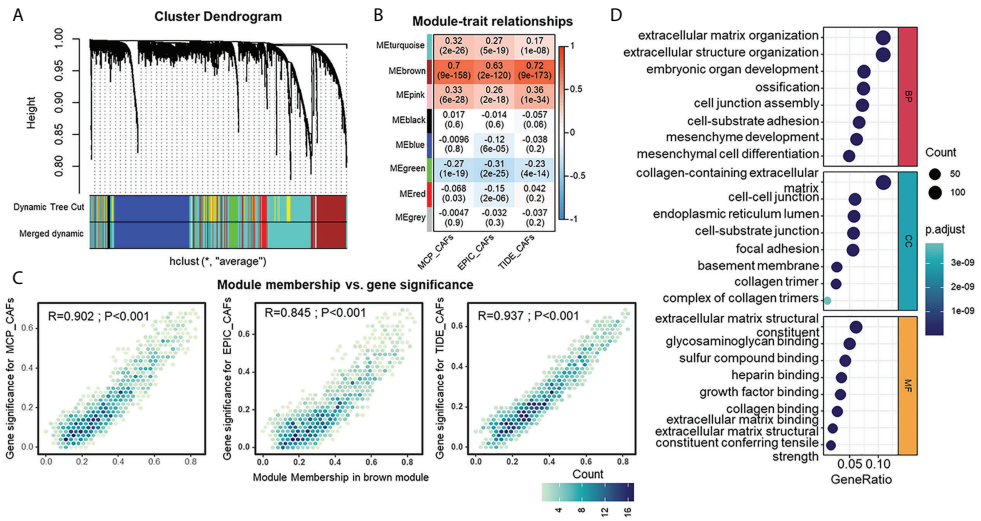

FIGURE 3
Detection and functional interpretations of a gene co-expression module shared CAFs characteristics in HGSOC. **(A)** Network analysis of gene expression in HGSOC cohort. Dendrograms obtained by average linkage hierarchical clustering of genes on the basis of topological overlap. Modules of co-expressed genes were assigned colors. The color row underneath the dendrogram shows the modules assigned by the Dynamic Tree Cut and merged to produce eight distinct modules. **(B)** Module-trait relationships: Each column corresponds to a trait, and each row corresponds to a module eigengene. The number in the rectangle indicates the correlation coefficients (P-values in the brackets). The table is color-coded by correlation based on the color legend: red to blue indicates a positive to negative correlation of module eigengenes with traits. **(C)** Scatter plot of module eigengenes in brown module. **(D)** Gene Ontology analysis of genes in the brown module. CC, cellular component (upper); MF, molecular function (middle); BP, biological process (bottom).

alpha 1 chain (COL5A1), FBN1, and secreted protein acidic and cysteine rich (SPARC), were screened out with GS >0.3 and MM >0.8 (Figure 4A). Among them, PDGFRB is an acknowledged marker of CAFs (40), which supports the accuracy of our results and suggests the potential of other genes to characterize the abundance or properties of CAFs. Univariate regression analysis confirmed the adverse role of hub genes in the prognosis of HGSOC (Figure 4B). Significant functions of these hub genes in modulating biological processes relating to CAFs were validated by fair positive correlations between hub genes and signatures as well as markers of CAFs (Figure 4C). To extend other biological features from hub genes themselves, we performed GSVA enrichment analysis and revealed strong positive correlations between hub genes with mesenchymal activation and classic cancer-promoting pathways such as TGF-β signaling pathway, EMT, apical junction, and angiogenesis (Figure 4D).

In the further investigation of relationships between hub genes and the immune microenvironment of HGSOC, we focused on FBN1, an ECM glycoprotein that has been reported to promote the structure formation of calcium-binding microfibrils (41). The ESTIMATE algorithm was performed to assess components in the TME of patient samples ranked by the mRNA level of FBN1. Those patients with relatively high FBN1 expression also owned higher StromalScore and ImmuneScore (Figure 4E). As for specific immune components, FBN1 was positively correlated with the infiltration of subpopulations of T cells and myeloid cells, especially macrophages, which was further verified by the EPIC and TIMER methods (Figures 4F, G). Also, there were positive correlations between FBN1 and biomarkers of immunosuppressive macrophages as well as some immune checkpoints (Figures 4H, S2A). The preference of the FBN1 expression in fibroblasts was confirm in a single cell RNA set (GSE118828) downloaded from the Tumor Immune Single-cell Hub (TISCH) (Figures S2B-D). Immunohistochemical staining further verified that FBN1 was mainly expressed in mesenchymal cells, and patients with relatively high FBN1 expression also had a higher positive rate of CD206 (a marker of immunosuppressive macrophages) (Figure 4I). From the above results, we could speculate that CAFs expressing FBN1 may be involved in the formation and maintenance of the immunosuppressive microenvironment of HGSOC. The morphological distribution and approximate protein levels of other hub genes that existed in The Human Protein Atlas and TISCH are visualized in Figures S3A-C. Besides, each hub gene was also assessed on its correlations with scores calculated by the ESTIMATE algorithm and the enrichment scores of various types of immune cells (Figure S4A).

10.3389/fimmu.2022.940801

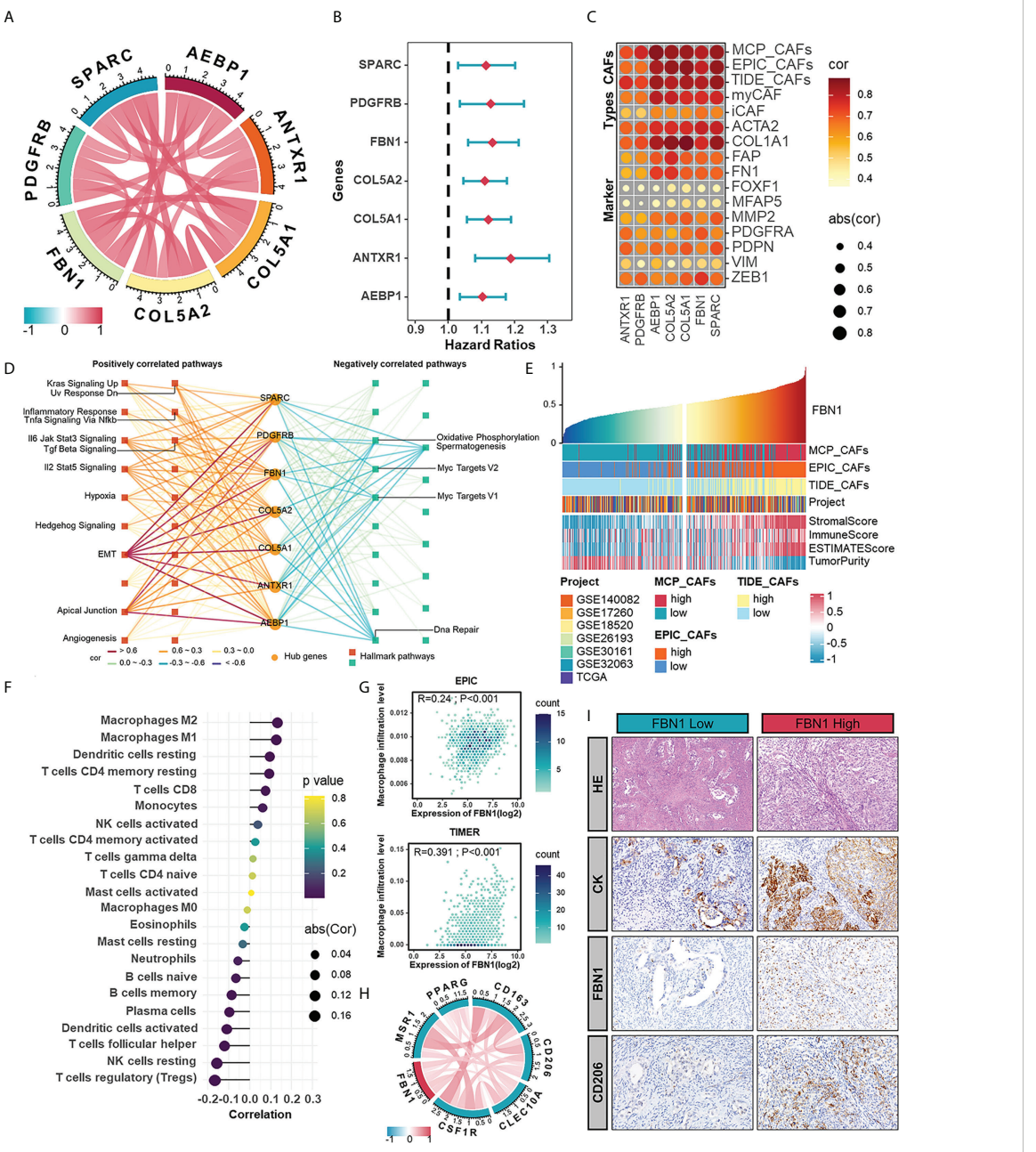

FIGURE 4
The hub genes extracted from CAFs-related module as potential CAF markers participating in the shaping of tumor microenvironment. **(A)** The correlations between any two hub genes. **(B)** Forest plot of univariate Cox analysis of hub genes in meta-cohort. **(C)** The correlations between hub genes and CAF signatures (MCP, EPIC, and TIDE) and CAF markers. **(D)** Hallmark pathways in which hub genes were involved. **(E)** The TME scores in HGSOC samples ranked by the mRNA level of FBN1. **(F)** The correlation between the mRNA expression of FBN1 and the level of immune cell infiltration calculated by CIBERSORT. **(G)** The positive correlations between the mRNA expression of FBN1 and the level of macrophage infiltration calculated by EPIC and TIMER. **(H)** The correlations between the expression of FBN1 and M2 macrophage markers in mRNA levels. **(I)** HE staining and IHC staining of CK, FBN1 and CD206 in one sample with relatively low protein expression of FBN1 and the other with high protein expression of FBN1.

Establishment of the CAFscore evaluation system as a prognostic indicator in HGSOC and its involvement in TME

Considering the significant impact of CAF traits on prognosis, we picked out 145 genes in the brown module when setting GS >0.3 and MM >0.6 to construct a scoring system which was termed CAFscore, using ssGSEA for measuring the prognosis of HGSOC patients. These 145 genes were enriched in extracellular matrix organization and mesenchymal activation, as revealed by GO and KEGG analyses, similar to the enriched pathways of the entire brown module (Figures S5A, B). Besides, the CAFscore correlated well with hub genes and CAF signatures (Figure 5A). Meanwhile, HGSOC patients were divided into a high CAFscore group (n=330) and a low CAFscore group (n=744) based on an optimal cutoff value for the CAFscore. Kaplan-Meier analyses and univariate regression analysis suggested the CAFscore was a prominently adverse prognostic factor in the integrated cohort and most HGSOC patient datasets with sufficient samples (Figures 5B, S6A, B). Particularly, in the TCGA-OV cohort, multivariate Cox regression analysis revealed that the CAFscore was an independent prognostic factor (Figure S6C). In the pan-cancer univariate regression analysis, the CAFscore as a risk factor was also applicable to most cancer types (Figure S6D). The heatmap in Figure 5C demonstrated the enhanced EMT and inflammatory signaling pathways ("IL6-JAK-STAT3 signaling", "TNFα signaling *via* NF-κb", "inflammatory response", and "IL2-STAT5 signaling"), the release of cytokines ("TGF-β signaling pathway" and "cytokine-cytokine receptor interaction"), activated immunoreaction ("Fc Gamma R mediated phagocytosis" and "leukocyte transendothelial migration"), and impaired "apoptosis" in the high CAFscore group. The CAFscore evaluation system was used to create a landscape of TME characteristics and immune cell infiltration, which revealed that the CAFscore was positively correlated with not only the StromalScore and ImmuneScore (Figure 5D) but also the infiltration of endothelial cells, myeloid cells, and CD4+ T cells (Figure 5E), particularly immunosuppressed macrophages (Figure S7A). Also, the CAFscore, it should be noted, is well related to the expression of immune checkpoints, especially PD-L2 and TIM-3 (Figures 5F, G). Paramount biological pathways engaging in the tumor immune microenvironment were evaluated in high- and low-CAFscore groups. Among them, signatures related to immunotherapy resistance and mesenchymal activation were enriched, but the DNA damage repair pathway was impaired in the high CAFscore group (Figure 5H). The above results suggest the capacity of the CAFscore for indicating individual prognosis and the ability of CAFs to form the immunosuppressive and stroma-activated TME of HGSOC.

The role of the CAFscore in the prediction of immunotherapy benefits and the selection of sensitive chemotherapeutic agents

To further elucidate the effects of CAFscore in the context of immunotherapy (represented by ICBs), we first extended our analysis to associations between CAFscore and tumor mutation burden (TMB), which may influence cancer immunogenicity. In the TCGA-OV cohort, there were limited correlations between CAFscore and mutation counts and a less significant difference in TMB across CAF groups (Figure S8A). To predict ICB response, newly identified predictors, such as TIDE scores and ImmuCellA (Figures 6A, B, S8B), are widely used to evaluate the immune response (30, 38). The CAFscore was positively correlated with TIDE, dysfunction, and exclusion and negatively correlated with MSI Expr sig, and the CAFscore of HGSOC patients who responded to immunotherapy was lower than those who did not. Next, assessing the ability of the CAFscore to predict patients' responses to ICB in both immunotherapy cohorts: GSE78220 (Figures 6C–E) and IMvigor210 (Figures 6F–H) revealed that survival benefits and response to ICB treatment were observed in patients with a low CAFscore (Figures 6C–H, S8C, D). In the IMvigor210 cohort, patients were divided into deserted, excluded, and inflamed subgroups based on the infiltration status of CD8+ T cells (42). In different immune phenotype subgroups, the overall survival of patients and responses to ICB treatment varied based on the CAFscore system. For example, a high CAFscore represents poor prognosis and resistance to ICB in the excluded subgroups (Figure 6G, S8E) but not in the deserted subgroup (Figure S8C). This suggests that different levels of activation or infiltration of CAFs result in different degrees of immunosuppression if there are immune components, thus leading to variations in resistance to immunotherapy and the outcome of patients.

To understand the effect of CAFscore on the clinical efficacy of HGSOC treatments, we analyzed correlations between CAFscore and IC_{50} of drug candidates in the Genomics of Drug Sensitivity in Cancer (GDSC) database (Figure 6I). A total of 31 drug candidates with $|Rs|$ >0.5 were screened out, the IC_{50} of the most of which (30 candidates) inversely correlated with CAFscore, targeting PI3K-mTOR signaling, RTK signaling, and other kinases (Figure 6J). Remarkably, the estimated IC_{50} of imatinib exerted a pretty negative correlation with the CAFscore, which means this agent might benefit patients with a high CAFscore (Figure 6K). Together, these results implied that CAFs played crucial roles in mediating the immune response and correlated with drug sensitivity. Thus, the CAFscore might be a potential biomarker for establishing appropriate treatment strategies.

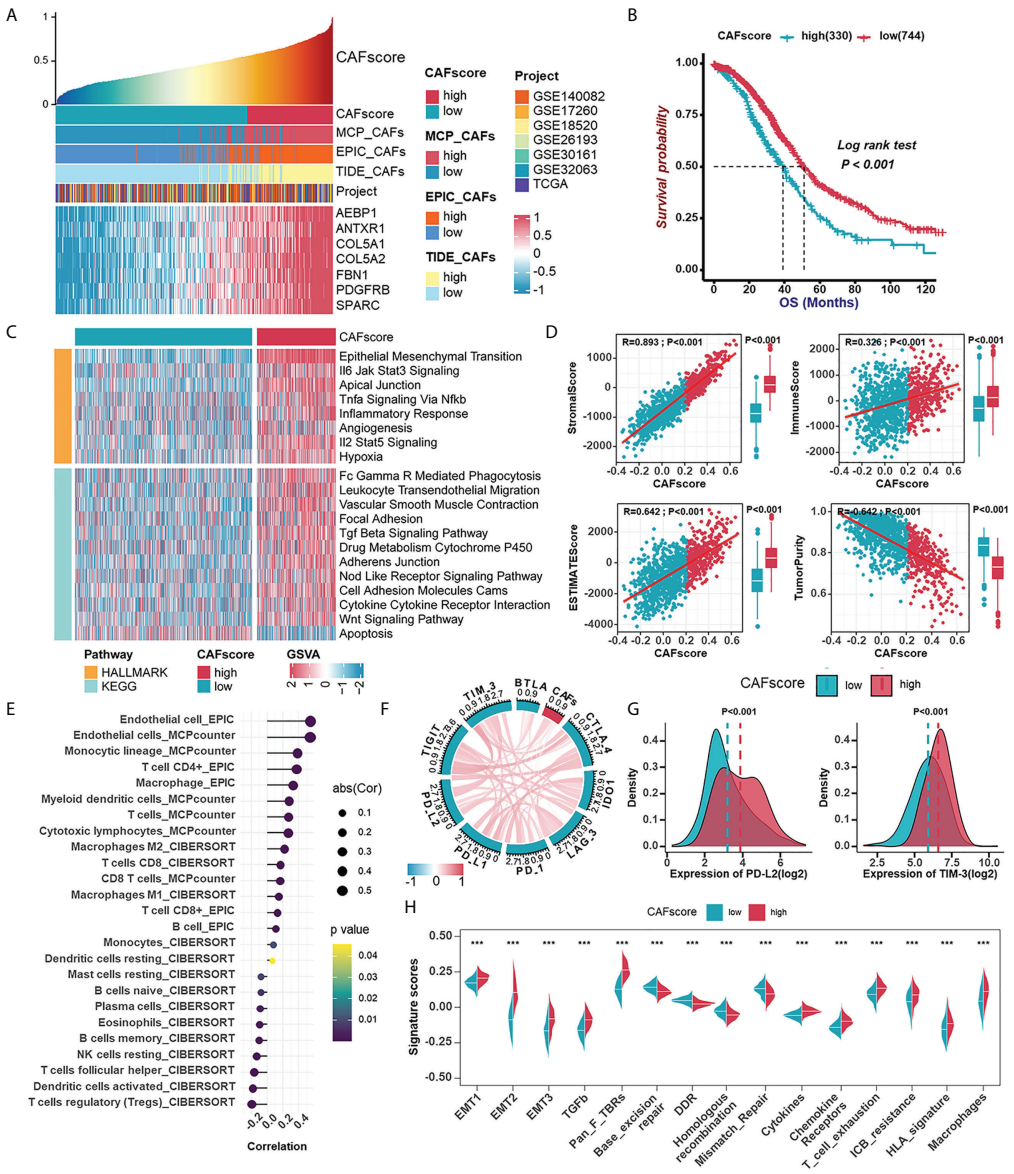

FIGURE 5
Establishment of the CAFscore evaluation system as a prognostic indicator in HGSOC and its involvement with immune microenvironment. **(A)** The correlations between the mRNA expression of hub genes and CAFscore. **(B)** Survival analyses for patient with relatively high- or low-CAFscore in the integrated cohort using Kaplan–Meier curves. **(C)** GSVA enrichment analysis showing the activation states of biological pathways in high- and low-CAFscore group. The heatmap was used to visualize these biological processes, and yellow represented HALLMARK database and blue represented KEGG database. **(D)** The correlations between CAFscore and TME scores. **(E)** The correlations between the CAFscore and the level of immune cell infiltration. **(F)** The correlations between the CAFscore and the expression of ICMs (CTLA4, IDO-1, LAG-3, PD-1, PD-L1, PD-L2, TIGIT, TIM-3, BYLA). **(G)** Comparisons of PD-L2 (left) and TIM-3 (right) expression levels between high- and low-CAFscore groups. **(H)** The differences in the enrichment scores of stroma-activated pathways, DNA damage repair pathways and ICB response-related signatures between high- and low-CAFscore groups. ***, P < 0.001.

Discussion

Tumor stroma and the immune microenvironment have received an extensive concern for nearly a decade. The effector cells that can kill tumor cells always garner much attention in the development of immunotherapy. Nevertheless, the limited benefit to HGSOC patients from ICB drives researchers to investigate the mechanisms of this resistance and other novel targets. As early as 2010, TCGA termed four HGSOC subtypes based on gene content, of which the mesenchymal subtype was characterized by high expression of HOX genes and increased stromal components such as for myofibroblasts and

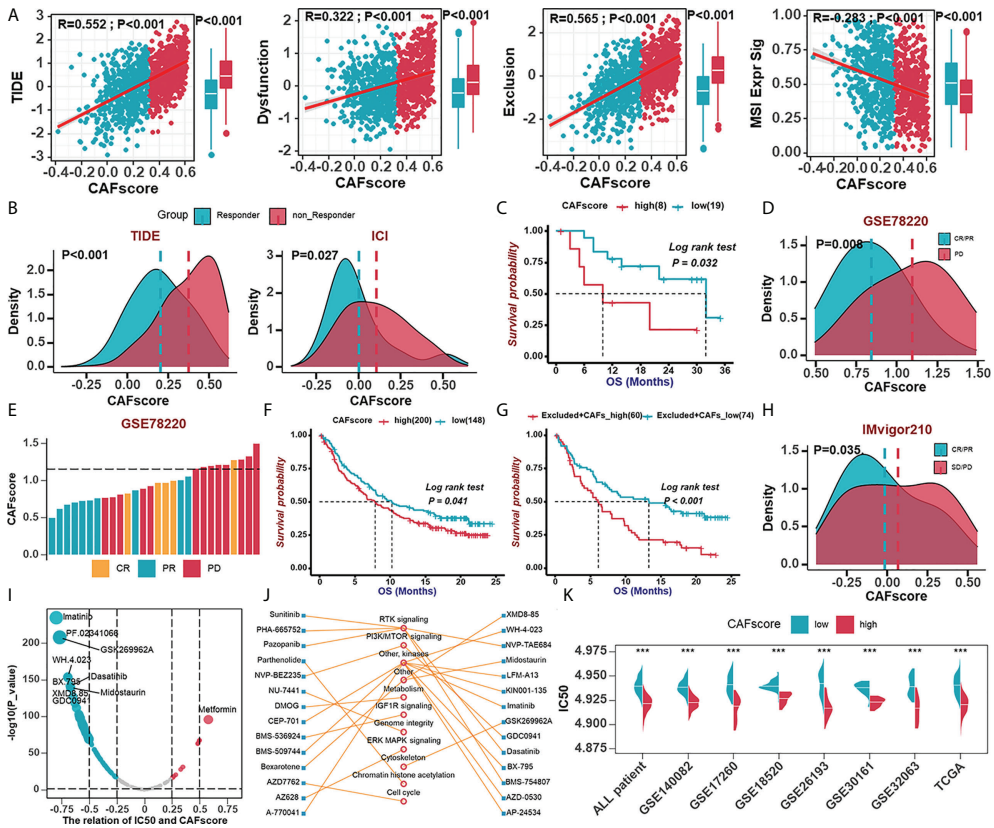

FIGURE 6
The role of the CAFscore in the prediction of immunotherapy benefits and the selection of sensitive chemotherapeutic agents. **(A)** The correlations between CAFscore and TIDE, Dysfunction, Exclusion, and MSI expression signature. **(B)** The comparison of CAFscores between responder and non-responder groups, according to TIDE (left) and ImmuCellAI (right) algorithms. **(C)** Survival analyses for low (19 cases) and high (8 cases) CAFscore patient groups in the GSE78220 cohort using Kaplan–Meier curves. **(D)** The CAFscore in the group with complete response (CR) or partial response (PR) versus the group with progressive disease (PD) in GSE78220. **(E)** The association of the CAFscore with clinical response to anti-PD-1 immunotherapy per patient in GSE78220 cohort. **(F)** Survival analyses for low (148 cases) and high (200 cases) CAFscore patient groups in IMvigor210 cohort using Kaplan–Meier curves. **(G)** Survival analyses for low (74 cases) and high (60 cases) CAFscore patient groups in the excluded immune subgroup. **(H)** The CAFscore in the group with CR/PR versus the group with PD/stable disease (SD) in IMvigor210 cohort. **(I)** The correlations between CAFscore and the estimated IC_{50} for drugs evaluated by the Spearman analysis. Each point represents a drug. **(J)** The lines represent the relationship between candidate drugs and pathways. **(K)** The differences in the estimated IC_{50} for Imatinib between high- and low-CAFscore groups in TCGA and GEO datasets, respectively. ***, P < 0.001.

microvascular pericytes (4). Also, the mesenchymal subtype was identified by several independent studies. Thus, targeting CAFs, a major component of the stroma, by altering their numbers, subtypes, or functionality, is being explored as an avenue to improve cancer therapies. In this study, we aim to evaluate the effect of CAFs on the prognosis and response to immunotherapy of HGSOC patients.

Several independent CAF signatures, as well as some well-known fibroblast markers, including fibroblast activation protein alpha (FAP), collagen 1A1 (COL1A1), and platelet-derived growth factor receptor alpha (PDGFRA), were employed to evaluate the content of CAFs. Kaplan-Meier survival estimation and univariate Cox regression analysis confirmed that CAF could be a risk factor for HGSOC patients, further verified by prognostic-oriented clustering of HGSOC samples.

As a substantial source of growth factors and cytokines, CAFs certainly orchestrate the composition and content of soluble substances in TME and thus contribute to tumor progression. The correlations between CAF signatures and components of the immune microenvironment as well as ICB-related signatures implied that elevated expression of cytokines (e.g., CCL11, CCL21, CXCL12, CXCL14, IL-6, IL-16, and TGF-β), the enrichment of immunosuppressive macrophages, mesenchymal activation, and enhanced immunotherapy resistance were all linked to CAFs-enriched microenvironment. There have been specific studies about CXCL12 and CXCL14 in CAFs in tumor progression. Fibroblast-derived CXCL12 facilitated tumor cell intravasation and limited T cell-mediated tumor control (42–44). Also, CAFs expressed CXCL14 for their tumor-supporting properties (45,

46). Besides, it is not known whether CCL11 (a chemokine for eosinophils, engaging in ovarian cancer progression) (10, 47), CCL21 (a chemokine for thymocytes and activated T cells, mediating homing of lymphocytes) and IL-16 (a modulator of T cell activation) participate in the functionality of CAFs and the remodeling of the tumor immune microenvironment, which might deserve further exploration. What is noteworthy is that enhanced expressions of IL-6 and TGF-β are linked. Experiments and observations show that iCAFs express less ACTA2 (actin alpha2 smooth muscle, also abbreviated as -SMA) and secrete more IL-6 and other inflammatory factors (e.g., IL-8, IL-11, CXCL1, and CXCL2), thereby participating in immune suppression, whereas myCAFs are responsible for ECM remodeling, with high TGF-β and ECM proteins such as fibronectin 1, and COL1A1 (48, 49). Given the relatively weaker expression of iCAF markers than ECM components and myCAF markers in CAFs-enriched samples, we suppose that myofibroblasts are predominant CAF population in HGSOC. As regards macrophages, CAFs-enriched environments also exhibited high expression of CCL2 (also named monocyte chemoattractant protein-1, MCP-1), which might partly explain the abundance of macrophages.

For a deeper understanding of the potential molecular mechanisms of the link between CAFs and prognosis in HGSOC patients, we performed WGCNA to find modules of highly correlated genes and correlated modules to CAF traits, and focused on the brown module that was characterized by enrichment pathways and GO groups defining ECM production and remodeling, cell adhesion, and angiogenesis. Afterward, we extracted intramodular hub genes from the brown module that exhibit excellently positive correlations with CAF traits. These hub genes, conceivably, contain markers of collagen (COL5A2 and COL5A1) and PDGFRB. To identify a potential novel gene target, we looked for highly connected genes that have not been extensively studied as cancer targets and then focused on FBN1, a structural component of calcium-binding microfibrils. A few studies reveal that FBN1 is a risk factor for hematogenous and lymphatic metastasis in serous ovarian cancer and promotes chemoresistance in ovarian cancer organoids (50, 51). The predominance of FBN1 in fibroblasts were confirmed in a single cell RNA set (GSE118828) downloaded from the TISCH database (52). Based on the contribution of CAFs, we hypothesize that FBN1 plays an adverse role in HGSOC prognosis.

In addition to the contribution to tumor growth, CAFs also influence the infiltration and properties of other tumor microenvironment components, which greatly accounts for resistance to ICB. All signatures, from CAF algorithms to hub genes in CAF-related modules to the CAFscore, indicate the importance of macrophages and T leukocytes in the immune microenvironment remolded by CAFs. In detail, CAFs advanced the recruitment of monocytes (macrophage precursors) and their differentiation into immunosuppressive macrophages (usually referred to as M2 macrophages) *via* multiple regulatory molecules, including macrophage colony-stimulating factor 1 (M-CSF1), IL-6, CCL2, and TGF-β, thereby impairing responses from effector T cells and inducing immune suppression in the TME (53–57). In turn, M2 macrophages were also able to enhance EMT to stimulate activation of CAFs and influence the trans-differentiation and activity of mesenchymal stem cells (one of the cellular precursors of CAFs) (58). Besides, the relevance between immunosuppressive macrophages and CAFs was confirmed by IHC staining of CD206 and FBN1 in our study, further supporting the adverse role of FBN1 in HGSOC. Numerous studies have illustrated the role of CAFs in modulating T cell activities and functions. CAFs can recruit CD8+ cytotoxic T cells. A study based on the single-cell dissection of cellular components in ovarian cancer revealed that CAFs-T cells cross-talk relies on the CXCL12/14-CXCR4 axis (59). However, immunosuppression is a general feature of the TME of HGSOC, which is consistent with the result that CAF signatures and the CAFscore are positively correlated with T cell exhaustion as well as dysfunction and resistance to ICB. Also, CAFs stimulate the migratory activity of Treg cells and markedly increase their frequency in colorectal tumor sites, and promote Th2 polarization in pancreatic cancer (60, 61). Furthermore, CAFs exerted immunosuppressive effects from the following several aspects: modulating the degree of tumor-associated neutrophils (TANs) activation (62); cooperating with mast cells to induce the early malignant morphological transition of benign epithelial cells (63); impairing the functionality of infiltrating NK cells (64, 65); blocking DC maturation and antigen presentation (18); increasing attraction and differentiation of Tregs (66).

The CAFscore was contracted to indicate the relative content of CAFs in individuals, which was further suggested as an independent prognostic factor by univariate Cox regression analysis, not only in HGSOC samples but also in pan-cancer. HGSOC samples with high CAFscore exhibited poor overall survival and enrichment of immune and inflammatory pathways, cell connection and adhesion, and angiogenesis, which inspired us to explore the potential of the CAFscore in predicting the response to immunotherapy in HGSOC. Prior studies indicate that cancers with high TMB are more likely to benefit from ICBs (67). However, there were limited correlations between CAFscore and mutation counts and less significant differences in TMB across CAF groups, which could be explained as extensive cross-talk between CAFs and other ICB response determinants, such as mesenchymal activation and immunosuppressive TME. HGSOC samples with high CAFscore had significant stroma activation status (including the highly expressed EMT and TGF-β pathways, as well as Pan-F-TBRS), as well as increased infiltration of immunosuppressive cells and ICM expression. HGSOC patients with higher CAFscore not only tended not to respond to ICBs but also

were more prone to immune escape when using TIDE and ImmuCellA to evaluate the immune response. Further, survival benefits and response to ICB treatment were observed in a patient with a low CAFscore from two anti-PD-1 immunotherapy cohorts. In the IMvigor210 cohort, when patients were divided into deserted, excluded, and inflamed subgroups based on the infiltration status of CD8+ T cells (42), high CAFscore represented poor prognosis and resistance to ICB in the excluded subgroup, but not in the deserted subgroup. Tumors with immune excluded phenotypes have an abundance of immune cells retained in the stroma rather than penetrating the tumor mass. The activation of stroma in TME was thought to suppress T cells (68). The existence of CD8+ T cells enables CAFs to exert their influence on shaping the immune microenvironment. Different levels of activation and infiltration of CAFs result in different degrees of immunosuppression if there are immune components, thus leading to variations in resistance to immunotherapy and the outcome for patients. Besides, more potential drug treatments were adapted in the high CAFscore group in the drug sensitivity analysis, suggesting another treatment strategy.

There are still many deficiencies in this study that should be paid attention to and further explored. Firstly, we retrospectively construct the CAFscore based on public datasets and patient samples of our own, but complete clinical parameters alone are not sufficient to support our prognosis model. Secondly, HGSOC patients are divided into two groups just based on the content rather than the different properties of CAFs. Finally, prospective cohorts of HGSOC patients receiving immunotherapy are needed to validate our findings further.

In conclusion, this study provides a valuable tool to evaluate the content of CAFs from gene expression data, which is represented as the CAFscore, with the properties of predicting HGSOC patient prognosis and revealing the degree of immunosuppression. Individualized assessment of CAFscore informs therapeutic strategies to improve clinical benefit from cancer therapies.

Data availability statement

The original contributions presented in the study are included in the article/Supplementary Material. Further inquiries can be directed to the corresponding authors.

Ethics statement

The study was reviewed and approved by Ethics Committee of Xiangya Hospital Central South University, approval number 202204081. The ethics committee waived the requirement of written informed consent for participation.

Author contributions

Conceptualization, YL and RT; formal analysis, YL; funding acquisition, JLi; investigation, RT; methodology, RT and YL; project administration, QW; supervision, XF; visualization, HT; writing—original draft, RT; writing—review and editing, JLiu and YL. All authors have read and agreed to the published version of the manuscript.

Funding

This work was supported by National Natural Science Foundation of China (Grant No.82103300); Natural Science Foundation of Hunan Province of China (Project No. 2019JJ50857).

Conflict of interest

The authors declare that the research was conducted in the absence of any commercial or financial relationships that could be construed as a potential conflict of interest.

Publisher's note

Supplementary material

The Supplementary Material for this article can be found online at: https://www.frontiersin.org/articles/10.3389/fimmu.2022.940801/full#supplementary-material

SUPPLEMENTARY FIGURE 1
Detection and functional interpretations of a gene co-expression module shared CAFs characteristics in HGSOC. **(A)** Left: An examination of the scale-free fit index for a variety of soft-threshold values (β); Right: An analysis of the mean connectedness for different soft-threshold values. **(B)** KEGG pathway analysis of genes in the brown module.

SUPPLEMENTARY FIGURE 2
The correlations between the expression of FBN1 and immune microenvironment **(A)** The correlations between the expression of FBN1 and ICMs in mRNA levels. **(B)** Scatter plot showing the cell clusters in GSE118828. **(C-D)** Scatter plot **(C)** and violin plot **(D)** showing the distribution of cells expressing a high level of FBN1 in GSE118828.

SUPPLEMENTARY FIGURE 3
The hub genes extracted from CAFs-related module as potential CAFs markers participating in the shaping of immune microenvironment. **(A, B)** Scatter plot **(A)** and violin plot **(B)** showing the expression of other hub genes for all cell types in GSE118828. **(C)** The morphological distribution and approximate protein levels of other hub genes.

SUPPLEMENTARY FIGURE 4
The correlations between hub genes and immune cells.

SUPPLEMENTARY FIGURE 5
Enrichment analyses of CAFs-related genes. **(A, B)** GO pathways **(A)** and KEGG pathways **(B)** in which genes constructing CAFscore were enriched.

SUPPLEMENTARY FIGURE 6
The CAFscore is a prognostic indicator in HGSOC. **(A)** Survival analyses for patient with relatively high- or low-CAFscore in GEO database (GSE140082, GSE18520, GSE26193) and TCGA-OV database using Kaplan–Meier curves. **(B)** Univariate Cox regression analyses estimating prognostic value of the CAFscore in different HGSOC cohorts. **(C)** Univariate and multivariate Cox regression analyses of the CAFscore with age, tumor grade and stage in the TCGA-OV cohort. HR and p-values were displayed. **(D)** Univariate Cox regression analyses estimating prognostic value of the CAFscore in different cancer types from TCGA dataset.

SUPPLEMENTARY FIGURE 7
The correlations between the CAFscore with the expression of immunosuppressive macrophage markers in mRNA levels.

SUPPLEMENTARY FIGURE 8
The role of the CAFscore in the prediction of immunotherapy benefits **(A)** The correlations between the CAFscore and synonymous mutation counts, non-synonymous mutation counts, and all mutation counts in TCGA-OV cohort. **(B)** The comparison of CAFscores between Responder and non-Responder groups in TCGA and GEO datasets, respectively, according to TIDE algorithms. *, $P < 0.05$; **, $P < 0.01$; ***, $P < 0.001$. **(C, D)** Survival analyses for low and high CAFscore patient groups in the desert **(C)** and inflamed **(D)** immune subgroups. **(E)** The CAFscore in the group with CR/PR versus the group with PD/(SD) in the desert (left), excluded (middle) and inflamed (right) immune subgroups.

References

1. Siegel RL, Miller KD, Fuchs HE, Jemal A. Cancer statistics, 2022. *CA Cancer J Clin* (2022) 72(1):7–33. doi: 10.3322/caac.21708

2. Koonings PP, Campbell K, Mishell DRJr., Grimes DA. Relative frequency of primary ovarian neoplasms: A 10-year review. *Obstet Gynecol* (1989) 74(6):921–6.

3. Bowtell DD, Bohm S, Ahmed AA, Aspuria PJ, Bast RCJr., Beral V, et al. Rethinking ovarian cancer ii: Reducing mortality from high-grade serous ovarian cancer. *Nat Rev Cancer* (2015) 15(11):668–79. doi: 10.1038/nrc4019

4. Bell D, Berchuck A, Birrer M, Chien J, Cramer DW, Dao F, et al Integrated genomic analyses of ovarian carcinoma. *Nature* (2011) 474(7353):609–15. doi: 10.1038/nature10166

5. Tothill RW, Tinker AV, George J, Brown R, Fox SB, Lade S, et al. Novel molecular subtypes of serous and endometrioid ovarian cancer linked to clinical outcome. *Clin Cancer Res* (2008) 14(16):5198–208. doi: 10.1158/1078-0432.CCR-08-0196

6. Rimal R, Desai P, Daware R, Hosseinnejad A, Prakash J, Lammers T, et al. Cancer-associated fibroblasts: Origin, function, imaging, and therapeutic targeting. *Adv Drug Deliv Rev* (2022) 110504. doi: 10.1016/j.addr.2022.114504

7. Sahai E, Astsaturov I, Cukierman E, DeNardo DG, Egeblad M, Evans RM, et al. A framework for advancing our understanding of cancer-associated fibroblasts. *Nat Rev Cancer* (2020) 20(3):174–86. doi: 10.1038/s41568-019-0238-1

8. Radhakrishnan R, Ha JH, Jayaraman M, Liu J, Moxley KM, Isidoro C, et al. Ovarian cancer cell-derived lysophosphatidic acid induces glycolytic shift and cancer-associated fibroblast-phenotype in normal and peritumoral fibroblasts. *Cancer Lett* (2019) 442:464–74. doi: 10.1016/j.canlet.2018.11.023

9. Schauer IG, Zhang J, Xing Z, Guo X, Mercado-Uribe I, Sood AK, et al. Interleukin-1beta promotes ovarian tumorigenesis through a P53/Nf-Kappab-Mediated inflammatory response in stromal fibroblasts. *Neoplasia* (2013) 15 (4):409–20. doi: 10.1593/neo.121228

10. Li X, Fang T, Xu S, Jin P, Zhou D, Wang Z, et al. Parp inhibitors promote stromal fibroblast activation by enhancing Ccl5 autocrine signaling in ovarian cancer. *NPJ Precis Oncol* (2021) 5(1):49. doi: 10.1038/s41698-021-00189-w

11. Zhang Y, Tang H, Cai J, Zhang T, Guo J, Feng D, et al. Ovarian cancer-associated fibroblasts contribute to epithelial ovarian carcinoma metastasis by promoting angiogenesis, lymphangiogenesis and tumor cell invasion. *Cancer Lett* (2011) 303(1):47–55. doi: 10.1016/j.canlet.2011.01.011

12. Wang W, Kryczek I, Dostal L, Lin H, Tan L, Zhao L, et al. Effector T cells abrogate stroma-mediated chemoresistance in ovarian cancer. *Cell* (2016) 165 (5):1092–105. doi: 10.1016/j.cell.2016.04.009

13. Kwon Y, Smith BD, Zhou Y, Kaufman MD, Godwin AK. Effective inhibition of c-Met-Mediated signaling, growth and migration of ovarian cancer cells is influenced by the ovarian tissue microenvironment. *Oncogene* (2015) 34(2):144–53. doi: 10.1038/onc.2013.539

14. Izar B, Tirosh I, Stover EH, Wakiro I, Cuoco MS, Alter I, et al. A single-cell landscape of high-grade serous ovarian cancer. *Nat Med* (2020) 26(8):1271–9. doi: 10.1038/s41591-020-0926-0

15. Hao Q, Li J, Zhang Q, Xu F, Xie B, Lu H, et al. Single-cell transcriptomes reveal heterogeneity of high-grade serous ovarian carcinoma. *Clin Transl Med* (2021) 11(8):e500. doi: 10.1002/ctm2.500

16. Olbrecht S, Busschaert P, Qian J, Vanderstichele A, Loverix L, Van Gorp T, et al. High-grade serous tubo-ovarian cancer refined with single-cell rna sequencing: Specific cell subtypes influence survival and determine molecular subtype classification. *Genome Med* (2021) 13(1):111. doi: 10.1186/s13073-021-00922-x

17. Cohen N, Shani O, Raz Y, Sharon Y, Hoffman D, Abramovitz L, et al. Fibroblasts drive an immunosuppressive and growth-promoting microenvironment in breast cancer *via* secretion of chitinase 3-like 1. *Oncogene* (2017) 36(31):4457–68. doi: 10.1038/onc.2017.65

18. Cheng JT, Deng YN, Yi HM, Wang GY, Fu BS, Chen WJ, et al. Hepatic carcinoma-associated fibroblasts induce ido-producing regulatory dendritic cells through il-6-Mediated Stat3 activation. *Oncogenesis* (2016) 5:e198. doi: 10.1038/oncsis.2016.7

19. Li T, Yang Y, Hua X, Wang G, Liu W, Jia C, et al. Hepatocellular carcinoma-associated fibroblasts trigger nk cell dysfunction *via* Pge2 and ido. *Cancer Lett* (2012) 318(2):154–61. doi: 10.1016/j.canlet.2011.12.020

20. Chen W, Jin W, Hardegen N, Lei KJ, Li L, Marinos N, et al. Conversion of peripheral Cd4+Cd25- naive T cells to Cd4+Cd25+ regulatory T cells by tgf-beta induction of transcription factor Foxp3. *J Exp Med* (2003) 198(12):1875–86. doi: 10.1084/jem.20030152

21. Lakins MA, Ghorani E, Munir H, Martins CP, Shields JD. Cancer-associated fibroblasts induce antigen-specific deletion of Cd8 (+) T cells to protect tumour cells. *Nat Commun* (2018) 9(1):948. doi: 10.1038/s41467-018-03347-0

22. Brahmer J, Reckamp KL, Baas P, Crino L, Eberhardt WE, Poddubskaya E, et al. Nivolumab versus docetaxel in advanced squamous-cell non-Small-Cell lung cancer. *N Engl J Med* (2015) 373(2):123–35. doi: 10.1056/NEJMoa1504627

23. Wolchok JD, Chiarion-Sileni V, Gonzalez R, Rutkowski P, Grob JJ, Cowey CL, et al. Overall survival with combined nivolumab and ipilimumab in advanced melanoma. *N Engl J Med* (2017) 377(14):1345–56. doi: 10.1056/NEJMoa1709684

24. Liu YL, Zamarin D. Combination immune checkpoint blockade strategies to maximize immune response in gynecological cancers. *Curr Oncol Rep* (2018) 20 (12):94. doi: 10.1007/s11912-018-0740-8

25. Matulonis UA, Shapira-Frommer R, Santin AD, Lisyanskaya AS, Pignata S, Vergote I, et al. Antitumor activity and safety of pembrolizumab in patients with advanced recurrent ovarian cancer: Results from the phase ii keynote-100 study. *Ann Oncol* (2019) 30(7):1080–7. doi: 10.1093/annonc/mdz135

26. Li Y, Tian R, Liu J, Ou C, Wu Q, Fu X. A 13-gene signature based on estrogen response pathway for predicting survival and immune responses of patients with ucec. *Front Mol Biosci* (2022) 9:833910. doi: 10.3389/fmolb.2022.833910

27. Newman AM, Liu CL, Green MR, Gentles AJ, Feng W, Xu Y, et al. Robust enumeration of cell subsets from tissue expression profiles. *Nat Methods* (2015) 12 (5):453–7. doi: 10.1038/nmeth.3337

28. Racle J, de Jonge K, Baumgaertner P, Speiser DE, Gfeller D. Simultaneous enumeration of cancer and immune cell types from bulk tumor gene expression data. *Elife* (2017) 6. doi: 10.7554/eLife.26476

29. Becht E, Giraldo NA, Lacroix L, Buttard B, Elarouci N, Petitprez F, et al. Estimating the population abundance of tissue-infiltrating immune and stromal cell populations using gene expression. *Genome Biol* (2016) 17(1):218. doi: 10.1186/s13059-016-1070-5

30. Jiang P, Gu S, Pan D, Fu J, Sahu A, Hu X, et al. Signatures of T cell dysfunction and exclusion predict cancer immunotherapy response. *Nat Med* (2018) 24(10):1550–8. doi: 10.1038/s41591-018-0136-1

31. Li T, Fan J, Wang B, Traugh N, Chen Q, Liu JS, et al. Timer: A web server for comprehensive analysis of tumor-infiltrating immune cells. *Cancer Res* (2017) 77 (21):e108–e10. doi: 10.1158/0008-5472.CAN-17-0307

32. Langfelder P, Horvath S. Wgcna: An r package for weighted correlation network analysis. *BMC Bioinf* (2008) 9:559. doi: 10.1186/1471-2105-9-559

33. Yu G, Wang LG, Han Y, He QY. Clusterprofiler: An r package for comparing biological themes among gene clusters. *OMICS* (2012) 16(5):284–7. doi: 10.1089/omi.2011.0118

34. Tian R, Li Y, Shu M. Circadian regulation patterns with distinct immune landscapes in gliomas aid in the development of a risk model to predict prognosis and therapeutic response. *Front Immunol* (2021) 12:797450. doi: 10.3389/fimmu.2021.797450

35. Zeng D, Ye Z, Shen R, Yu G, Wu J, Xiong Y, et al. Iobr: Multi-omics immuno-oncology biological research to decode tumor microenvironment and signatures. *Front Immunol* (2021) 12:687975. doi: 10.3389/fimmu.2021.687975

36. Gu W, Kim M, Wang L, Yang Z, Nakajima T, Tsushima Y, et al. Multi-omics analysis of ferroptosis regulation patterns and characterization of tumor microenvironment in patients with oral squamous cell carcinoma. *Int J Biol Sci* (2021) 17(13):3476–92. doi: 10.7150/ijbs.61441

37. Li Y, Gan Y, Liu J, Li J, Zhou Z, Tian R, et al. Downregulation of Meis1 mediated by Elfn1-As1/Ezh2/Dnmt3a axis promotes tumorigenesis and oxaliplatin resistance in colorectal cancer. *Signal Transduct Target Ther* (2022) 7(1):87. doi: 10.1038/s41392-022-00902-6

38. Miao YR, Zhang Q, Lei Q, Luo M, Xie GY, Wang H, et al. Immucellai: A unique method for comprehensive T-cell subsets abundance prediction and its application in cancer immunotherapy. *Adv Sci (Weinh)* (2020) 7(7):1902880. doi: 10.1002/advs.201902880

39. Han JD, Bertin N, Hao T, Goldberg DS, Berriz GF, Zhang LV, et al. Evidence for dynamically organized modularity in the yeast protein-protein interaction network. *Nature* (2004) 430(6995):88–93. doi: 10.1038/nature02555

40. Li W, Ding Z, Zhang H, Shi Q, Wang D, Zhang S, et al. The roles of blood lipid-metabolism genes in immune infiltration could promote the development of idd. *Front Cell Dev Biol* (2022) 10:844395. doi: 10.3389/fcell.2022.844395

41. Chen J, Cai Y, Xu R, Pan J, Zhou J, Mei J. Identification of four hub genes as promising biomarkers to evaluate the prognosis of ovarian cancer *in silico*. *Cancer Cell Int* (2020) 20:270. doi: 10.1186/s12935-020-01361-1

42. Mariathasan S, Turley SJ, Nickles D, Castiglioni A, Yuen K, Wang Y, et al. Tgfbeta attenuates tumour response to pd-L1 blockade by contributing to exclusion of T cells. *Nature* (2018) 554(7693):544–8. doi: 10.1038/nature25501

43. Ahirwar DK, Nasser MW, Ouseph MM, Elbaz M, Cuitino MC, Kladney RD, et al. Fibroblast-derived Cxcl12 promotes breast cancer metastasis by facilitating tumor cell intravasation. *Oncogene* (2018) 37(32):4428–42. doi: 10.1038/s41388-018-0263-7

44. Feig C, Jones JO, Kraman M, Wells RJ, Deonarine A, Chan DS, et al. Targeting Cxcl12 from fap-expressing carcinoma-associated fibroblasts synergizes with anti-Pd-L1 immunotherapy in pancreatic cancer. *Proc Natl Acad Sci USA* (2013) 110(50):20212–7. doi: 10.1073/pnas.1320318110

45. Augsten M, Sjoberg E, Frings O, Vorrink SU, Frijhoff J, Olsson E, et al. Cancer-associated fibroblasts expressing Cxcl14 rely upon Nos1-derived nitric oxide signaling for their tumor-supporting properties. *Cancer Res* (2014) 74 (11):2999–3010. doi: 10.1158/0008-5472.CAN-13-2740

46. Augsten M, Hagglof C, Olsson E, Stolz C, Tsagozis P, Levchenko T, et al. Cxcl14 is an autocrine growth factor for fibroblasts and acts as a multi-modal stimulator of prostate tumor growth. *Proc Natl Acad Sci USA* (2009) 106(9):3414–9. doi: 10.1073/pnas.0813144106

47. Nolen BM, Lokshin AE. Targeting Ccl11 in the treatment of ovarian cancer. *Expert Opin Ther Targets* (2010) 14(2):157–67. doi: 10.1517/14728220903512983

48. Ohlund D, Handly-Santana A, Biffi G, Elyada E, Almeida AS, Ponz-Sarvise M, et al. Distinct populations of inflammatory fibroblasts and myofibroblasts in pancreatic cancer. *J Exp Med* (2017) 214(3):579–96. doi: 10.1084/jem.20162024

49. Dubey S, Dubey PK, Umeshappa CS, Ghebre YT, Krishnamurthy P. Inhibition of Runx1 blocks the differentiation of lung fibroblasts to myofibroblasts. *J Cell Physiol* (2022) 237(4):2169–82. doi: 10.1002/jcp.30684

50. Yue H, Wang J, Chen R, Hou X, Li J, Lu X. Gene signature characteristic of elevated stromal infiltration and activation is associated with increased risk of hematogenous and lymphatic metastasis in serous ovarian cancer. *BMC Cancer* (2019) 19(1):1266. doi: 10.1186/s12885-019-6470-y

51. Wang Z, Chen W, Zuo L, Xu M, Wu Y, Huang J, et al. The fibrillin-1/Vegfr2/Stat2 signaling axis promotes chemoresistance *Via* modulating glycolysis and angiogenesis in ovarian cancer organoids and cells. *Cancer Commun (Lond)* (2022) 42(3):245–65. doi: 10.1002/cac2.12274

52. Sun D, Wang J, Han Y, Dong X, Ge J, Zheng R, et al. Tisch: A comprehensive web resource enabling interactive single-cell transcriptome visualization of tumor microenvironment. *Nucleic Acids Res* (2021) 49(D1): D1420–D30. doi: 10.1093/nar/gkaa1020.7

53. Tan B, Shi X, Zhang J, Qin J, Zhang N, Ren H, et al. Inhibition of rspo-Lgr4 facilitates checkpoint blockade therapy by switching macrophage polarization. *Cancer Res* (2018) 78(17):4929–42. doi: 10.1158/0008-5472.CAN-18-0152

54. Mace TA, Ameen Z, Collins A, Wojcik S, Mair M, Young GS, et al. Pancreatic cancer-associated stellate cells promote differentiation of myeloid-derived suppressor cells in a Stat3-dependent manner. *Cancer Res* (2013) 73 (10):3007–18. doi: 10.1158/0008-5472.CAN-12-4601

55. Nagarsheth N, Wicha MS, Zou W. Chemokines in the cancer microenvironment and their relevance in cancer immunotherapy. *Nat Rev Immunol* (2017) 17(9):559–72. doi: 10.1038/nri.2017.49

56. Zhang R, Qi F, Zhao F, Li G, Shao S, Zhang X, et al. Cancer-associated fibroblasts enhance tumor-associated macrophages enrichment and suppress nk cells function in colorectal cancer. *Cell Death Dis* (2019) 10(4):273. doi: 10.1038/s41419-019-1435-2

57. Zhang J, Chen L, Xiao M, Wang C, Qin Z. Fsp1+ fibroblasts promote skin carcinogenesis by maintaining mcp-1-Mediated macrophage infiltration and chronic inflammation. *Am J Pathol* (2011) 178(1):382–90. doi: 10.1016/j.ajpath.2010.11.017

58. Hashimoto O, Yoshida M, Koma Y, Yanai T, Hasegawa D, Kosaka Y, et al. Collaboration of cancer-associated fibroblasts and tumour-associated macrophages for neuroblastoma development. *J Pathol* (2016) 240(2):211–23. doi: 10.1002/path.4769

59. Hornburg M, Desbois M, Lu S, Guan Y, Lo AA, Kaufman S, et al. Single-cell dissection of cellular components and interactions shaping the tumor immune phenotypes in ovarian cancer. *Cancer Cell* (2021) 39(7):928–44 e6. doi: 10.1016/j.ccell.2021.04.004

60. Jacobs J, Deschoolmeester V, Zwaenepoel K, Flieswasser T, Deben C, Van den Bossche J, et al. Unveiling a Cd70-positive subset of cancer-associated fibroblasts marked by pro-migratory activity and thriving regulatory T cell accumulation. *Oncoimmunology* (2018) 7(7):e1440167. doi: 10.1080/2162402X.2018.1440167

61. De Monte L, Reni M, Tassi E, Clavenna D, Papa I, Recalde H, et al. Intratumor T helper type 2 cell infiltrate correlates with cancer-associated fibroblast thymic stromal lymphopoietin production and reduced survival in pancreatic cancer. *J Exp Med* (2011) 208(3):469–78. doi: 10.1084/jem.20101876

62. Song M, He J, Pan QZ, Yang J, Zhao J, Zhang YJ, et al. Cancer-associated fibroblast-mediated cellular crosstalk supports hepatocellular carcinoma progression. *Hepatology* (2021) 73(5):1717–35. doi: 10.1002/hep.31792

63. Pereira BA, Lister NL, Hashimoto K, Teng L, Flandes-Iparraguirre M, Eder A, et al. Tissue engineered human prostate microtissues reveal key role of mast cell-derived tryptase in potentiating cancer-associated fibroblast (Caf)-induced morphometric transition *in vitro*. *Biomaterials* (2019) 197:72–85. doi: 10.1016/j.biomaterials.2018.12.030

64. Habif G, Crinier A, Andre P, Vivier E, Narni-Mancinelli E. Targeting natural killer cells in solid tumors. *Cell Mol Immunol* (2019) 16(5):415–22. doi: 10.1038/s41423-019-0224-2

65. Balsamo M, Scordamaglia F, Pietra G, Manzini C, Cantoni C, Boitano M, et al. Melanoma-associated fibroblasts modulate nk cell phenotype and antitumor cytotoxicity. *Proc Natl Acad Sci USA* (2009) 106(49):20847–52. doi: 10.1073/pnas.0906481106

66. Givel AM, Kieffer Y, Scholer-Dahirel A, Sirven P, Cardon M, Pelon F, et al. Mir200-regulated Cxcl12beta promotes fibroblast heterogeneity and immunosuppression in ovarian cancers. *Nat Commun* (2018) 9(1):1056. doi: 10.1038/s41467-018-03348-z

67. Chabanon RM, Pedrero M, Lefebvre C, Marabelle A, Soria JC, Postel-Vinay S. Mutational landscape and sensitivity to immune checkpoint blockers. *Clin Cancer Res* (2016) 22(17):4309–21. doi: 10.1158/1078-0432.CCR-16-0903

68. Chen DS, Mellman I. Elements of cancer immunity and the cancer-immune set point. *Nature* (2017) 541(7637):321–30. doi: 10.1038/nature21349

frontiers | Frontiers in Immunology

TYPE Original Research
PUBLISHED 08 November 2022
DOI 10.3389/fimmu.2022.1030969

OPEN ACCESS

EDITED BY
Yun Chen,
Nanjing Medical University, China

REVIEWED BY
Katie June Lee,
Dermatology Research Centre, The University of Queensland, Australia
Xingxing Zhu,
Mayo Clinic, United States

*CORRESPONDENCE
Xiuwen Wang
xiuwenwang12@sdu.edu.cn
Yanguo Liu
liuyanguo@sdu.edu.cn

SPECIALTY SECTION
This article was submitted to Cancer Immunity and Immunotherapy, a section of the journal Frontiers in Immunology

RECEIVED 29 August 2022
ACCEPTED 25 October 2022
PUBLISHED 08 November 2022

CITATION
Zhang W, Xia H, Yang R, Zhang Y, Zheng Q, Shang X, Liu N, Ma X, Wei C, Chen H, Mu X, Wang X and Liu Y (2022) Fibroblast growth factor receptor family mutations as a predictive biomarker for immune checkpoint inhibitors and its correlation with tumor immune microenvironment in melanoma. *Front. Immunol.* 13:1030969. doi: 10.3389/fimmu.2022.1030969

Fibroblast growth factor receptor family mutations as a predictive biomarker for immune checkpoint inhibitors and its correlation with tumor immune microenvironment in melanoma

Wengang Zhang[1], Handai Xia[1], Rui Yang[1], Yuqing Zhang[1], Qi Zheng[1], Xiaoling Shang[1], Ni Liu[1], Xinchun Ma[1], Chenxi Wei[1], Hang Chen[2], Xin Mu[3], Xiuwen Wang[1]* and Yanguo Liu[1]*

[1]Department of Medical Oncology, Qilu Hospital of Shandong University, Jinan, Shandong, China, [2]School of Basic Medical Sciences, Shandong First Medical University, Jinan, China, [3]Department of Medical Imaging Center, Third People's Hospital of Jinan, Jinan, China

Background: The emergence of immune checkpoint inhibitors (ICIs) has significantly improved the clinical outcomes of patients with metastatic melanoma. However, survival benefits are only observed in a subset of patients. The fibroblast growth factor receptor (FGFR) family genes are frequently mutated in melanoma, yet their impacts on the efficacy of ICIs remain unclear. Our study aimed to explore the association of FGFR mutations with ICIs efficacy in metastatic melanoma.

Methods: The Cancer Genome Atlas (TCGA) data (PanCancer Atlas, skin cutaneous melanoma (SKCM), n = 448) in cBioPortal were collected as a TCGA cohort to investigate the association between FGFR mutations and prognosis of melanoma patients. To explore the impact of FGFR mutations on the efficacy of ICIs in melanoma, clinical and tumor whole-exome sequencing (WES) data of four ICI-treated studies from cBioPortal were consolidated as an ICIs-treated cohort. Moreover, the relationship between FGFR mutations and immunogenicity (tumor mutation burden (TMB), neo-antigen load (NAL), mismatch repair (MMR)-related genes and DNA damage repair (DDR)-related genes) of melanoma was evaluated utilizing data from the ICIs-treated cohort. The influence of FGFR mutations on the tumor immune microenvironment (TIME) of melanoma was also analyzed using the TCGA cohort.

Results: In the TCGA cohort, survival in melanoma patients with or without FGFR mutations was nearly equivalent. In the ICIs-treated cohort, patients with FGFR mutations had better survival than those without (median overall survival: 60.00 vs. 31.00 months; hazard ratio: 0.58, 95% CI: 0.42-0.80; P = 0.0051).

10.3389/fimmu.2022.1030969

Besides, the objective response rate was higher for patients harboring FGFR mutations (55.56%) compared to wild-type patients (22.40%) (P = 0.0076). Mechanistically, it was revealed that FGFR mutations correlated with increased immunogenicity (e.g., TMB, NAL, MMR-related gene mutations and DDR-related gene mutations). Meanwhile, FGFR mutant melanoma tended to exhibit an enhanced antitumor TIME compared with its wild-type counterparts.

Conclusions: Our study demonstrated that FGFR mutations is a promising biomarker in stratifying patients with advanced melanoma who might benefit from ICIs therapy.

KEYWORDS

FGFR mutations, immune checkpoint inhibitors, melanoma, biomarker, tumor immune microenvironment

Introduction

Melanoma is one of the most common malignancies in skin cancer and its incidence is escalating annually (1). It is characterized by being the leading cause of skin cancer-related mortalities. Notably, the introduction of immune checkpoint inhibitors (ICIs) and targeted agents have significantly improved the survival of patients with advanced melanoma, boosting the five-year survival rate from less than 10% historically to approximately 40% currently (2–4). ICIs, especially agents targeting the cytotoxic T-lymphocyte antigen 4 (CTLA-4) and programmed death-1 (PD-1)/programmed death-ligand 1 (PD-L1), provide robust benefits for patients with advanced melanoma (5). The data from Checkmate 067 showed that the five-year survival rates for advanced melanoma patients receiving nivolumab plus ipilimumab and nivolumab were 52% and 44%, respectively (2). However, only a minority of patients respond to ICIs and benefit from them in terms of survival (6, 7). Moreover, some patients may experience substantial toxicity from ICIs in both clinical trials and real-world clinical practice (8). Therefore, identifying predictive biomarkers for ICI efficacy and elucidating the potential mechanisms modulating sensitivity to ICIs are of crucial importance.

Multiple factors have been identified to be critical in predicting or influencing the success of ICIs in the treatment of melanoma. It is acknowledged that tumor mutational burden (TMB) can predict response to ICIs across a variety of cancers, including melanoma, with higher TMB indicating a greater probability of response (9). However, some patients with low TMB respond to ICIs as well. Additionally, the optimal cutoff value of TMB has not been determined, resulting in differing perspectives on TMB among clinicians (10). It has been determined that IFN-γ (11), tumor T-cell infiltration (12) and lactate dehydrogenase (13) are associated with the efficacy of ICIs. Notwithstanding, none of them are sensitive and precise enough to identify patients who would benefit most from ICIs. Recently, it was found that gene mutations play important roles in modulating the efficacy of ICIs (14). For example, PTPRT mutant melanoma was more responsive to ICIs (15). In addition, mutations in IGF1R (16), MAP2K1/2 (17), ARID1A (18) and NOTCH4 (19) were associated with more benefit from ICIs in melanoma, with the tumor immune microenvironment (TIME) modulation and immunogenicity alteration as their potential mechanisms. Hence, it is worthwhile to identify novel key genetic mutations affecting the efficacy of ICIs and explore their potential mechanisms, thereby maximizing the therapeutic benefit of ICIs and reducing immune-related toxicities for patients with melanoma.

Abbreviations: CR, Complete response; CTLA-4, cytotoxic T-lymphocyte antigen 4; DSS, disease-free survival; DDR, DNA damage repair; FGFR Mut, FGFR mutations; FGFR Wt, FGFR wild-type; FGFR, fibroblast growth factor receptor; FDA, Food and Drug Administration; GSEA, Gene Set Enrichment Analysis; HR, hazard ratio; ICIs, immune checkpoint inhibitors; MHC, major histocompatibility complex; MMR, mismatch repair; NAL, neo-antigen load; NA, not attached; ORR, objective response rate; OS, overall survival; PR, partial response; PD-1, programmed death-1; PD-L1, programmed death-ligand 1; PFS, progression-free survival; PD, progressive disease; RTKs, receptor tyrosine kinases; ssGSEA, single-sample gene set enrichment analysis; SKCM, skin cutaneous melanoma; SD, stable disease; TCR, T cell receptor; TCGA, The Cancer Genome Atlas; TIME, tumor immune microenvironment; TMB, tumor mutation burden; WES, whole-exome sequencing.

The fibroblast growth factor receptor (FGFR) family consist of four highly conserved transmembrane receptors, FGFR1-4, which play key roles in embryonic development, proliferation, angiogenesis, and tumor metastasis (20). There is compelling evidence that FGFR is mutated across numerous cancers and its mutation triggers the FGFR signaling pathway, hence promoting tumor progression (21). Therefore, numerous studies have been devoted to the development of agents targeting FGFR alternations to suppress cancer progression. Currently, several FGFR inhibitors, such as erdafitinib and pemigatinib, have been approved by Food and Drug Administration (FDA) for the treatment of cholangiocarcinoma with FGFR fusion or rearrangement (22, 23). In terms of metastatic urothelial carcinoma, erdafitinib, a tyrosine kinase inhibitor of FGFR1–4, showed great antitumor activity in patients with FGFR alterations (mutations or fusions) (24). RAGNAR study in 2022 ASCO showed that multiple FGFR-altered (mutations or fusions) solid tumors responded to erdafitinib. However, there are no effective targeted drugs for metastatic melanoma with FGFR mutations. Therefore, ICIs are important candidates for FGFR-mutated melanoma. What is to be noted is that studies have proved that genetic mutations can affect the efficacy of ICIs, with some mutations (IGF1R, NOTCH4 and ARID1A) favoring ICIs (16, 18, 19) whereas others (EGFR and ALK) (25, 26) weakening their efficacy. In terms of FGFR mutations, a recent study found that FGFR-altered and wild-type bladder cancers had equivalent response rates to ICIs (27). However, there is no relevant study on whether FGFR mutations influence the effectiveness of ICIs in melanoma.

In this study, survival analysis was performed using the ICI-treated melanoma cohort from cBioPortal to explore the impact of FGFR mutations on the efficacy of ICIs in melanoma. Furthermore, the immunogenicity and TIME of melanoma with and without FGFR mutations were compared to investigate the mechanisms underlying FGFR mutations in predicting the efficacy and benefit of ICIs.

Materials and methods

Data collection and processing

The flowchart of this study was depicted in Figure 1. FGFR mutation frequency in pan-cancer was calculated using all TCGA PanCancer Atlas studies in cBioPortal (https://www.cbioportal.org/) (28). The TCGA data (PanCancer Atlas, SKCM, n = 448) in cBioPortal was rigorously consolidated as TCGA cohort. In addition, clinical and tumor whole-exome sequencing (WES) data concerning melanoma patients from four studies, consisting of 110 (DFCI, Science 2015) (29), 64 (MSKCC, NEJM 2014) (30), 38 (UCLA, Cell 2016) (31), and 320 (MSKCC, Nat Genet 2019) (32) samples, respectively, were downloaded to consolidated as ICIs-treated cohort. Among patients in ICIs-treated cohort, three samples with overall survival of 0 were excluded. A total of 529 samples were finally enrolled in ICIs-treated cohort. All patients in ICIs-treated cohort have been treated with ICIs, including antibodies targeting PD-(L)1 and CTLA-4. The majority of patients in the ICIs cohort were treated with ICIs in second-line or more advanced line settings. All data in TCGA cohort and ICIs-treated cohort were downloaded in the cBioPortal database (https://www.cbioportal.org/) (28). In our study, FGFR mutations (FGFR Mut) meant that melanoma patients harbor any FGFR mutations, including FGFR1, FGFR2, FGFR3 or FGFR4 mutations. In contrast, when a patient did not harbor any FGFR mutations, it

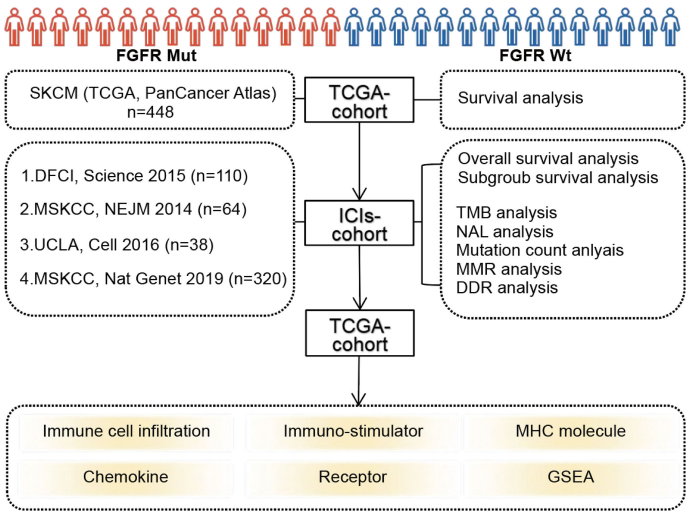

FIGURE 1
Flow diagram of the study.

was considered FGFR wild-type (FGFR Wt). All nonsynonymous mutation types, including missense, translation start site, nonstop, splice site, frameshift, and nonsense mutations, were included in this study.

Analysis of the relationship between FGFR mutations and clinical outcomes

Firstly, survival analyses were performed based on FGFR mutation status using TCGA cohort and ICIs-treated cohort, respectively. Then, subgroup survival analyses using ICIs-treated cohort were performed based on FGFR mutation subtypes and TMB level, respectively. In the subgroup analysis based on TMB level, high TMB and low TMB were determined by the median TMB of all samples in ICIs-treated cohort. When a patient's TMB was ≥ median TMB, it was classified as high TMB subgroup, otherwise it was considered low TMB. Response Evaluation Criteria in Solid Tumors (RECIST) version 1.1 was employed to evaluate response to ICIs. Objective response rate (ORR) reflects the percentage of patients with complete response (CR) and partial response (PR). In addition, we have constructed the nomogram for predicting survival of ICIs-treated melanoma patients by integrating clinicopathological variables including age, sex, ICIs categories, TMB, and FGFR1/2/3/4 status utilizing Sangerbox.

Analysis of indicators relating cancer immunogenicity

Multiple parameters involving immunogenicity, including TMB, mutation count, neo-antigen load (NAL), mismatch repair (MMR)-associated gene mutations and DNA damage repair (DDR)-associated gene mutations, were compared between FGFR Mut and FGFR Wt melanoma in ICIs-treated cohort. Besides, 13 melanoma studies (DFCI, Nature Medicine 2019; UCLA, Cell 2016; Broad/Dana Farber, Nature 2012; MSKCC, Clin Cancer Res 2021; MSKCC, NEJM 2014; TCGA, Cell 2015; DFCI, Science 2015; MSKCC, JCO Precis Oncol 2017; Broad, Cell 2012; TCGA, PanCancer Atlas; Yale, Nat Genet 2012; Broad, Cancer Discov 2014; Broad Institute, Nat Genet 2015) from cBioPortal (https://www.cbioportal.org/) were used to analyze the correlation of FGFR mutation frequency with TMB (median TMB and average TMB).

Analysis of TIME in FGFR mutant melanoma

TCGA data (PanCancer Atlas, SKCM, n = 448) from cBioPortal and RNA-seq data of corresponding samples retrieved from UCSC Xena data portal (https://xenabrowser.net) (33) were utilized to analyze the association of FGFR mutations with TIME in melanoma. CIBERSORT algorithm was used to calculate the proportion of 22 immune cells in each patient with melanoma (34). Single-sample gene set enrichment analysis (ssGSEA) method from R package GSVA was applied to calculate the infiltration level of 28 immune cell types according to the 28 published gene sets for immune cells (35, 36). ESTIMATE, a method of evaluating the fractions of stromal and immune cells, was applied to calculate stromal score (stromal content), immune score (extent of immune cell infiltration), ESTIMATE score (synthetic mark of stroma and immune) and tumor purity of each patient with melanoma (37). Four types of immune-related genes modulating TIME, including immune-stimulator related genes, major histocompatibility complex (MHC) molecule-related genes, chemokines and their receptors, were obtained from previous studies (38) and then compared between melanoma with FGFR Mut and FGFR Wt. Gene Set Enrichment Analysis (GSEA) was performed using the GSEA software (version 4.1.0) (http://www.broadinstitute.org/gsea/index.jsp) with 1000 gene-set permutations.

Statistical analysis

The Kaplan-Meier method and the log-rank test were used to construct survival curves (overall survival (OS), disease-free survival (DSS), and progression-free survival (PFS)) and evaluate the survival analysis, respectively. Clinical parameters of continuous variables (such as TMB, mutation count and NAL) between FGFR Mut and FGFR Wt melanoma were analyzed using Mann–Whitney U test. Categorical variables (such as CR, PR, stable disease (SD), progressive disease (PD) and ORR) were compared by χ 2 test or Fisher's exact test. Spearman correlation coefficient was calculated to evaluate the correlation of FGFR mutation frequency with median TMB or average TMB in melanoma patients. When a P value was < 0.05, it was considered statistically significant. All statistical analysis was conducted by R software (version 4.1.3), GraphPad Prism (version 9.0) or GSEA software (version 4.1.0).

Results

The features of FGFR mutations in melanoma

Through TCGA PanCancer Atlas studies, the frequency of FGFR mutations across various cancers was evaluated. Melanoma ranked 1st with a mutation frequency of 22.05% among all 27 cancers, as depicted in Figure 2A, followed by endometrial carcinoma and bladder urothelial carcinoma, respectively. Subgroup analyses showed that the mutation frequencies of

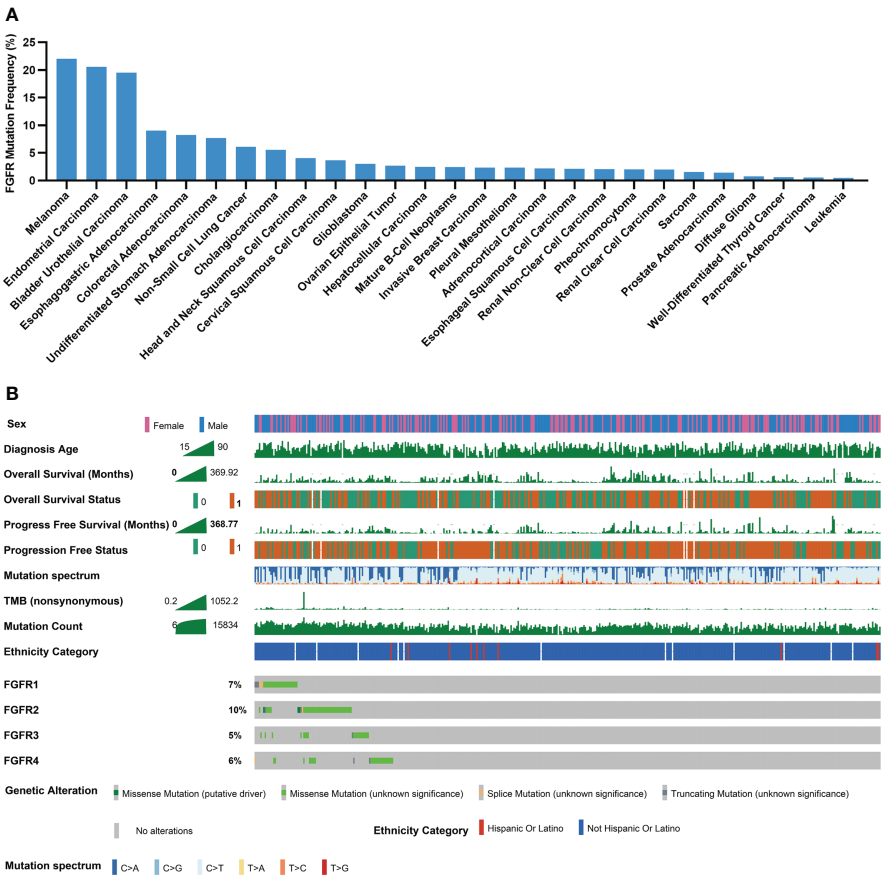

FIGURE 2
Mutational landscape of FGFR in melanoma cohorts. **(A)** The prevalence of FGFR mutations across 27 cancers. **(B)** Association of FGFR mutations and clinical characteristics in TCGA cohort (0 means no ending event occurred, 1 means ending event occurred).

melanoma regarding FGFR1, FGFR2, FGFR3 and FGFR4 ranked 1st, 2nd, 2nd, and 2nd across all cancers, respectively (Figures S1A-D). Multiple clinical characteristics of patients in TCGA cohort, including age, gender and survival, were calculated, as shown in Figure 2B. In addition, FGFR mutation subtypes were counted, with P486/F/L/S, E731K, S787F and S342F being the most prevalent mutation subtypes in FGFR1, FGFR2, FGFR3, and FGFR4, respectively (Figures S2A-D).

Association of FGFR mutations with survival in TCGA cohort

Patients with melanoma in TCGA cohort were mainly treated with chemotherapy and surgery. Survival analysis showed patients with FGFR Mut and FGFR Wt had comparable OS (median OS (mOS): 98.40 vs. 78.97 months, hazard ratio (HR) 0.93, 95% CI 0.67-1.30, P = 0.6520) (Figure S3A). Similarly, there was no significant difference in PFS (mPFS: 42.77 vs. 33.80 months, HR 0.91, 95% CI 0.69-1.19, P = 0.4938) and DSS (mDSS: 102.11 vs. 93.01 months, HR 0.84, 95% CI 0.59-1.20, P = 0.3560) between FGFR Mut and FGFR Wt patients (Figures S3B-C).

Association of FGFR mutations with clinical outcomes in ICIs-treated cohort

Patients in the ICIs-treated cohort were all subjected to ICIs treatment, including anti-PD-(L)1 or anti-CTLA-4. Patient characteristics in the ICIs-treated cohort were shown in Table 1. Notably, patients harboring FGFR Mut had substantially longer survival with a mOS of 60.00 months compared to the FGFR Wt patients with a mOS of 31.00 months (HR 0.58, 95%CI 0.42-0.80; P = 0.0051) (Figure 3A). Then, ICIs-treated cohort was divided into four subgroups based on FGFR mutation status and TMB levels. The results revealed that the mOS of patients in the $FGFR^{Mut}TMB^{high}$ (HR 0.52, 95% CI 0.34-0.79, P = 0.0085), $FGFR^{Mut}TMB^{low}$ (HR 0.57, 95% CI 0.37-0.88, P = 0.0148) and $FGFR^{Wt}TMB^{high}$ (HR 0.64, 95% CI 0.50-0.84, P = 0.0057) subgroups were significantly longer than that of patients in the

10.3389/fimmu.2022.1030969

FGFR^{Wt}TMB^{low} subgroup, respectively (Figure 3B). In addition, patients in the FGFR^{Mut}TMB^{high} subgroup survived the longest with mOS of not reached (NR), followed by FGFR^{Mut}TMB^{low} and FGFR^{Wt}TMB^{high} subgroups with mOS of 44.00 months and 41.00 months, respectively, although no statistical differences were observed between them (all P > 0.05) (Figure 3B). FGFR mutations were correlated with responsiveness to ICIs, with higher response rate in patients with FGFR Mut (47.37%) than that in patients with FGFR Wt (35.14%) (Figure 3C), but the difference was not statistically significant (P = 0.4268). Meanwhile, CR rate (16.67% vs. 5.60%, P = 0.1143), PR rate (38.89% vs. 16.80%, P = 0.0502), SD rate (16.67% vs. 7.20%, P = 0.1774), and ORR (55.56% vs. 22.40%, P = 0.0076) were found to be higher in FGFR Mut group, whereas PD rate (70.40% vs. 27.78%, P = 0.0009) was higher in FGFR Wt group (Figure 3D).

TABLE 1 Patient characteristics in the ICIs-treated cohort.

Characteristics	No. (%)
No. of patients	529
Gender	
Male	344 (65.0)
Female	185 (35.0)
Age	
< 65	276 (52.2)
≥65	253 (47.8)
Treatment	
Anti-CTLA4	245 (46.3)
Anti-PD-(L)1	284 (53.7)
FGFR status	
FGFR Wt	77 (14.6)
FGFR Mut	452 (85.4)

Analyses of FGFR mutation subtypes with survival in ICIs-treated cohort

Subgroup survival analyses based on FGFR mutation subtypes were performed. FGFR1 Mut patients had significantly longer survival compared to patients with FGFR1 Wt (mOS: NR vs. 31.20 months; HR 0.19, 95%CI 0.10-0.35; P = 0.0076) (Figure 4A). Similarly, melanoma patients harboring FGFR2 Mut had a pronounced survival advantage over those with FGFR2 Wt (mOS: 60.00 months vs. 31.20 months; HR 0.60, 95%CI 0.37-0.88; P = 0.0366) (Figure 4B). Regarding FGFR3, a

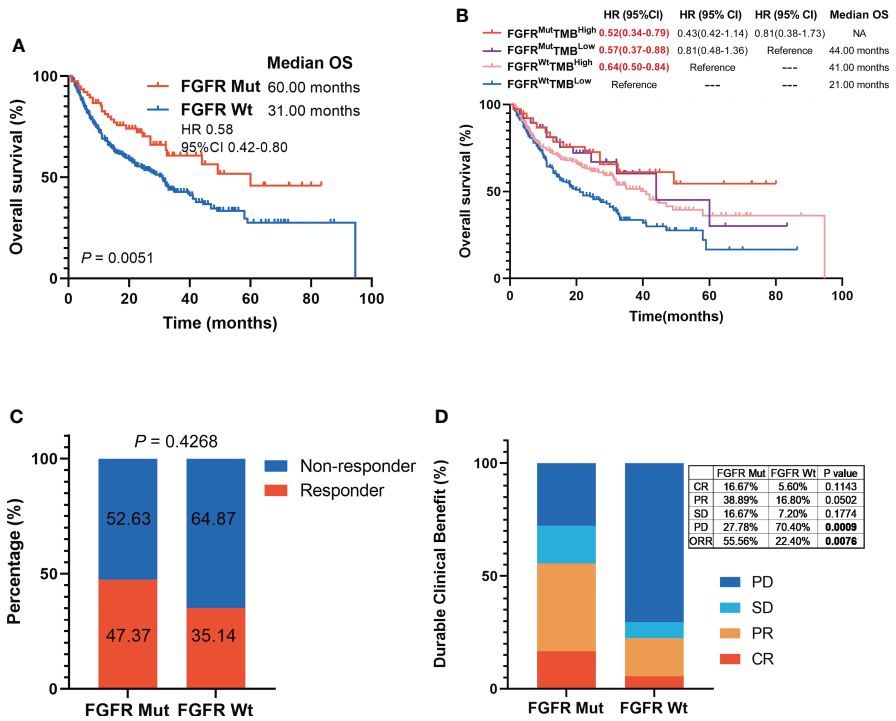

FIGURE 3
Association of FGFR mutations with melanoma clinical outcomes in ICIs-cohort. **(A)** The Kaplan-Meier survival analysis comparing OS between FGFR Mut and FGFR Wt patients in ICIs-cohort. **(B)** The Kaplan-Meier survival analyses comparing OS among FGFRMutTMBhigh, FGFRMutTMBlow, FGFRWtTMBhigh and FGFRWtTMBlow subgroups in ICIs-cohort. **(C)** Proportion of responders to ICIs in melanoma patients with FGFR mutations versus FGFR wild-type. **(D)** Comparison of the proportion of patients with complete response (CR), partial response (PR), stable disease (SD) and progression disease (PD) between FGFR Mut and FGFR Wt melanoma in ICIs-cohort.

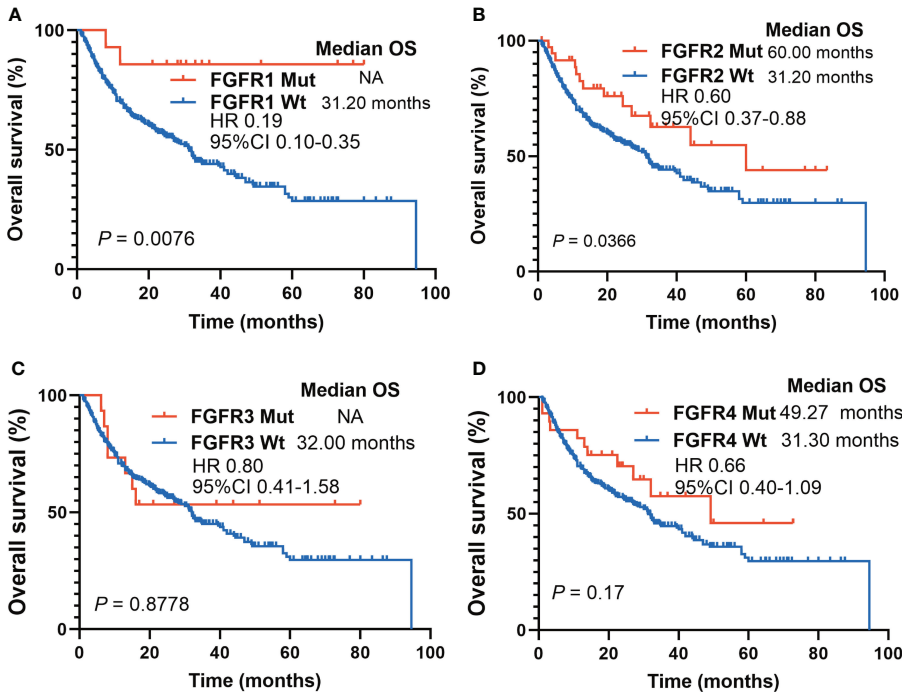

FIGURE 4
Survival analyses based on FGFR mutations subtypes in ICIs-cohort. **(A)** The Kaplan-Meier survival analysis comparing OS between FGFR1 Mut and FGFR1 Wt patients in ICIs-cohort. **(B)** The Kaplan-Meier survival analysis comparing OS between FGFR2 Mut and FGFR2 Wt patients in ICIs-cohort. **(C)** The Kaplan-Meier survival analysis comparing OS between FGFR3 Mut and FGFR3 Wt patients in ICIs-cohort. **(D)** The Kaplan-Meier survival analysis comparing OS between FGFR4 Mut and FGFR4 Wt patients in ICIs-cohort.

slight tendency was observed that patients harboring FGFR3 Mut benefited more from ICIs (mOS: NR vs. 32.00 months; HR 0.80, 95%CI 0.41-1.58; P = 0.8778), but no statistical difference was obtained (Figure 4C). Melanoma patients harboring FGFR4 Mut showed a similar tendency, whose survival was longer than those with FGFR4 Wt, though the difference was not statistically significant (mOS: 49.27 months vs. 31.30 months; HR 0.66, 95% CI 0.40-1.09; P = 0.17) (Figure 4D).

Construction of the nomogram to predict survival of melanoma patients

A nomogram, integrating clinicopathological variables including age, sex, ICIs categories, TMB, and FGFR1/2/3/4 status, was formulated to predict the 1-year OS, 3-year OS and 5-year OS of those ICIs-treated melanoma patients based on multivariable analysis (Figure 5A). As shown in Figure 5B, the receiver operating characteristic (ROC) curve showed that nomogram had relatively stronger predictability for 1-year OS, 3-year OS, and 5-year OS, with area under curves (AUC) of 0.65 (95% CI 0.59-0.70), 0.55 (95% CI 0.47-0.62) and 0.60 (95% CI 0.46-0.74), respectively. (Figure 5B). Besides, we have calculated the risk score of each patient based on multivariable analysis. Consequently, patients in the low-risk score group had significantly longer survival than those in the high-risk score group (mOS: 44.0 months vs. 20.9 months; HR 0.58, 95%CI 0.45-0.75; P < 0.001) (Figure 5C). The risk map exhibited that patients in in the low-risk score group had lower incidence of dead events and higher incidence of FGFR mutation (Figure 5D).

Association of FGFR mutations with parameters involving immunogenicity

To explore the underlying mechanisms of FGFR mutation affecting ICIs efficacy, various immunogenicity-related parameters were analyzed. FGFR mutation was associated with higher TMB (P < 0.0001), as shown in Figure 6A. Furthermore, 13 melanoma cohorts were employed to analyze the correlation between FGFR mutation frequency and TMB. A strongly positive correlation was found between FGFR mutation frequency and median TMB (r = 0.874, P < 0.001) (Figure 6B) or average TMB (P < 0.001) (Figure S4). Besides, we observed higher mutation count in FGFR Mut melanoma compared to its Wt counterparts (P < 0.0001) (Figure 6C). Likewise, compared with wild-type melanoma, FGFR Mut melanoma exhibited higher NAL (P < 0.0001) (Figure 6D). Given the close association of DDR or MMR process with tumor

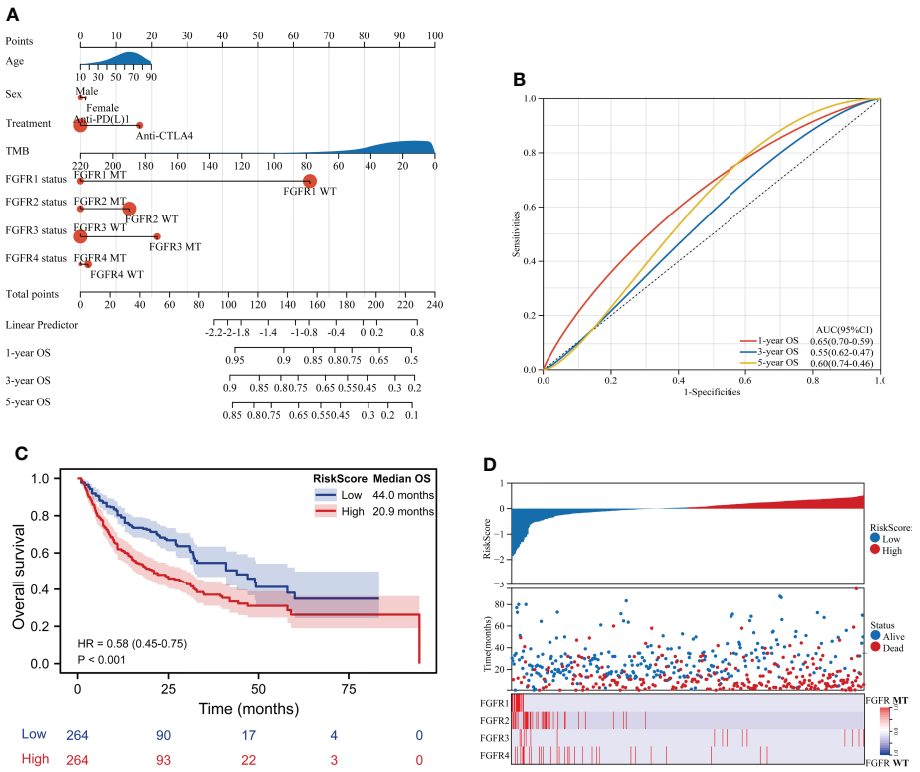

FIGURE 5
Construction of the nomogram to predict survival of melanoma patients. **(A)** A nomogram integrating clinicopathological variables including age, sex, ICIs categories, TMB, and FGFR1/2/3/4 status to predict the 1-year OS, 3-year OS and 5-year OS of patients in ICIs-treated cohort. **(B)** The ROC curve showed the predictive performance of the nomogram. **(C)** Survival curve of OS for patients from the ICIs-treated cohort based on risk score. **(D)** The risk score map exhibited the risk score level, survival status and FGFR status for each patient from the ICIs-treated cohort.

immunogenicity, the mutation frequencies of nine DDR genes and four MMR genes were examined. Higher mutation frequencies of DDR genes (ATM, ATR, BARD1, BRCA1, BRCA2, CDK12, ERCC2, FANCA and PALB2) were detected in FGFR Mut melanoma (all $P < 0.05$) (Figure 6E). Consistently, four MMR genes, including MLH1, MSH2, MSH6 and PMS2, mutated more frequently in FGFR Mut melanoma (all $P < 0.05$) (Figure 6F). In terms of PD-L1, there was a tendency that FGFR Mut melanoma expressed higher levels of PD-L1 than Wt melanoma ($P > 0.05$) (Figure 6G).

Association of FGFR mutations with immune cell infiltration in the TIME

CIBERSORT, ssGSEA and ESTIMATE were utilized to assess the impact of FGFR mutations on the TIME of melanoma. As shown in Figure 7A, the FGFR Mut melanomas exhibited a mild tendency of higher proportion of anti-tumor immune cells, such as CD8+ T cells, activated CD4+ memory T cells, activated DC, activated NK and M1 macrophages, but the difference was not statistically significant (all $P > 0.05$). In contrast, lower proportion of M2 macrophages was observed in FGFR Mut melanoma ($P > 0.05$) (Figure 7A). Notably, ssGSEA exhibited that activated CD4+ T cells, activated DC and memory B cells were significantly abundant in FGFR Mut melanoma (all $P < 0.05$) (Figure 7B). Furthermore, immune cell infiltration levels were evaluated based on FGFR mutant subtypes and similar results were obtained (Figures S5, S6). Immune score and ESTIMATE score, calculated by ESTIMATE, were higher in FGFR Mut melanoma (Figure 7C), but not statistically significant, which were in line with results from CIBERSORT. According to these findings, we tentatively concluded that FGFR Mut melanomas were associated with increased infiltration of immune cells, which are essential mediators of ICIs to kill tumor cells.

Association of FGFR mutations with the TIME signatures

To further elucidate the impact of FGFR mutations on the TIME of melanoma, four types of pivotal signatures modulating TIME were analyzed. Firstly, we compared the expression levels

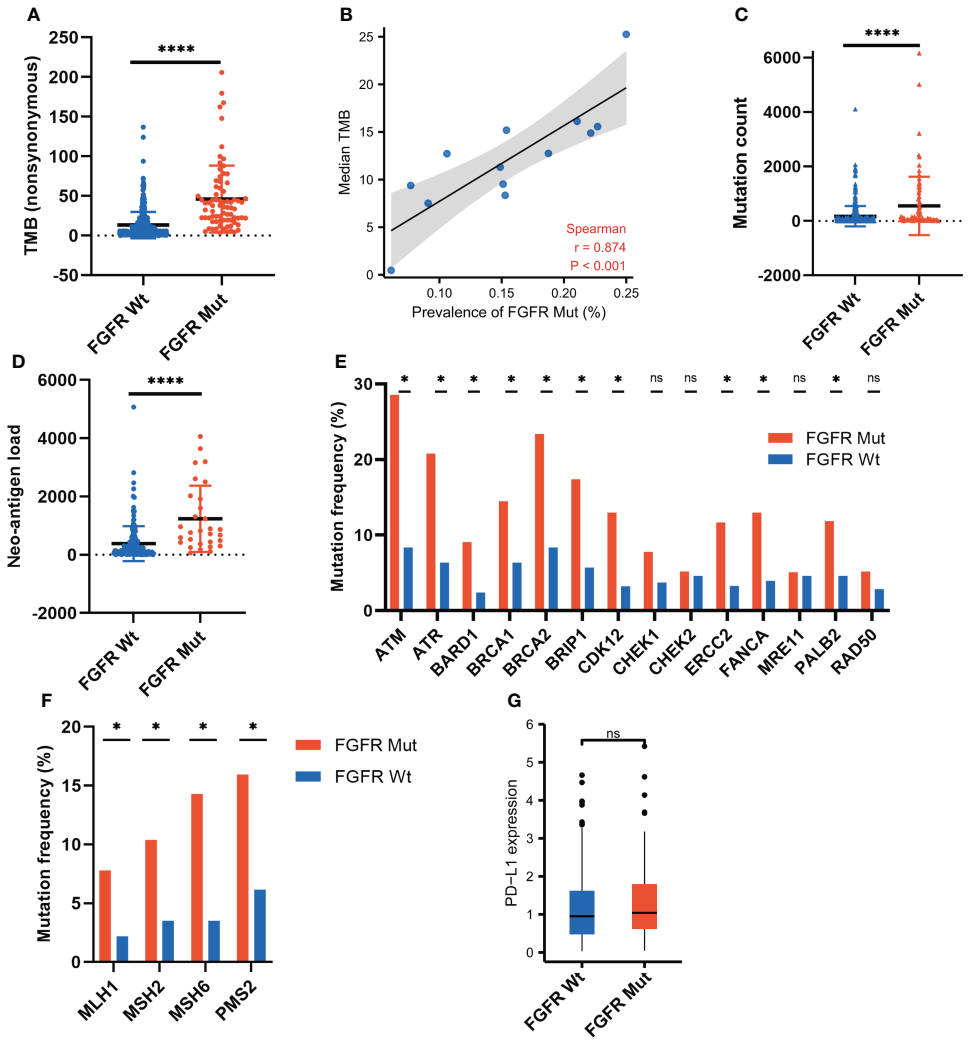

FIGURE 6
Association of FGFR mutations with parameters involving immunogenicity. **(A)** Comparison of TMB between FGFR Mut and FGFR Wt melanoma in ICIs-cohort. **(B)** Correlation of FGFR mutation frequency with median TMB in 13 melanoma studies. **(C)** Comparison of mutation count between FGFR Mut and FGFR Wt melanoma in ICIs-cohort. **(D)** Comparison of neo-antigen burden between FGFR Mut and FGFR Wt melanoma in ICIs-cohort. **(E)** Comparison of DDR-related gene mutations between FGFR Mut and FGFR Wt melanoma in ICIs-cohort. **(F)** Comparison of MMR-related gene mutations between FGFR Mut and FGFR Wt melanoma in ICIs-cohort. **(G)** Comparison of PD-L1 expression between FGFR Mut and FGFR Wt melanoma using TCGA data (ns = not significant, *P < 0.05, ****P < 0.0001).

of 43 immune-stimulator genes between FGFR Mut and FGFR Wt melanoma, with the majority of genes expressing higher in FGFR Mut melanoma, especially ICOSLG and TNFSF13 ($P < 0.05$) (Figure 8A). Secondly, diverse MHC molecules were evaluated and it was discovered that they were expressed slightly higher in FGFR Mut melanoma, though the difference was not statistically significant (all $P > 0.05$) (Figure 8B). Thirdly, chemokines and their receptors were explored. Regarding chemokines, CCL1, CCL17, CCL22 and CCL23, were significantly increased in FGFR Mut melanoma (all $P < 0.05$). For other chemokines, most of them tended to express higher in FGFR Mut melanoma, such as CCL5, CCL19, CXCL9, CXCL10, CXCL11, CXCL13 and CXCL14 (all $P > 0.05$) (Figure 8C). Regarding chemokine receptors, FGFR Mut melanoma expressed higher levels of CCR5, CCR7, CXCR3, CXCR4 and CXCR6 than their wild-type counterparts, but no statistical difference was observed (all $P > 0.05$) (Figure 8D). Furthermore, subgroup analyses were performed based on FGFR mutation subtypes, and the results showed that the expression levels of immune-stimulators, MHC, chemokines and their receptors in melanoma with FGFR mutation subtypes were mostly similar with the results above (Figures S7-S10). Meanwhile, immune-related signatures (including immune cell infiltration levels, immuno-stimulators, MHC and

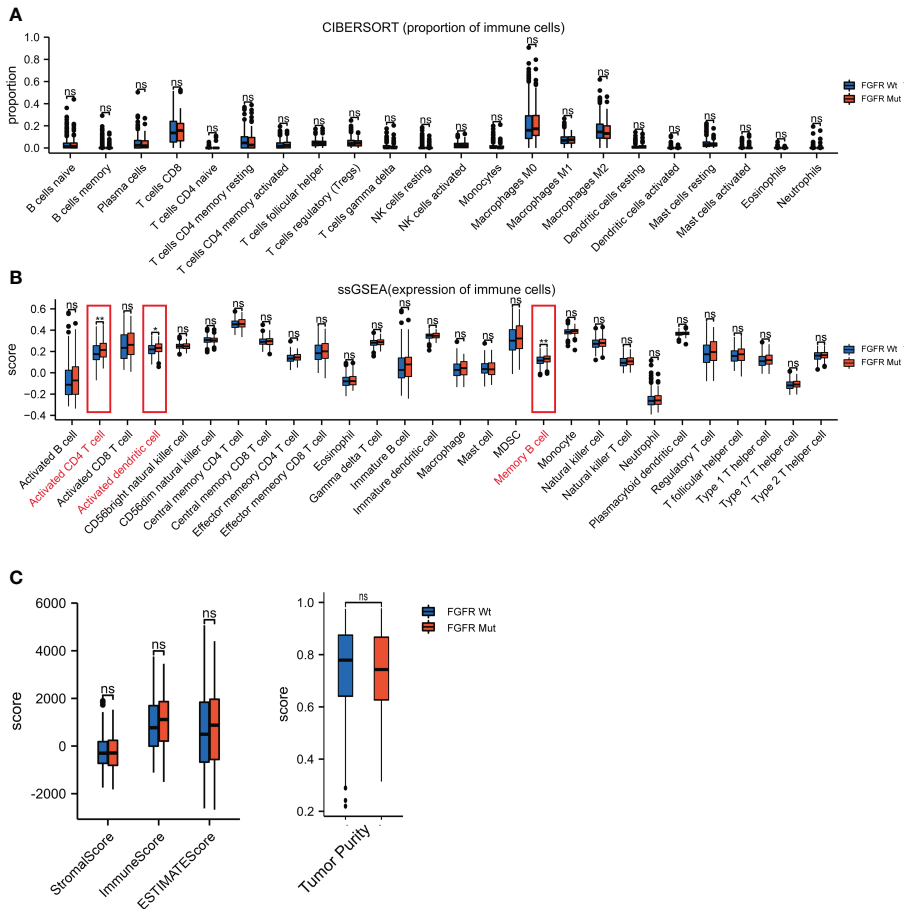

FIGURE 7
Difference of immune cell infiltration between FGFR Mut and FGFR Wt melanoma. **(A)** Comparison of proportion of immune cells between FGFR Mut and FGFR Wt melanoma. **(B)** Comparison of expression of immune cells between FGFR Mut and FGFR Wt melanoma. **(C)** Comparison of immune-related score between FGFR Mut and FGFR Wt melanoma (ns = not significant, *P < 0.05, **P < 0.01).

chemokines) were compared between patients with $FGFR^{Mut}TMB^{high}$ and those with $FGFR^{Wt}TMB^{low}$. Consequently, there was a mild tendency for most immune-related signatures were more highly expressed in melanomas with $FGFR^{Mut}TMB^{high}$, but most did not show a statistically significant difference (Figure S11).

GSEA analysis

GSEA analyses were performed to further explore the potential pathways by which FGFR mutations modulated the efficacy of ICIs. KEGG_T_CELL_RECEPTOR and KEGG_B_CELL_RECEPTOR signaling pathways were enriched in FGFR Mut melanoma, both of which played vital roles in modulating immune surveillance of B cells and T cells (Figures 9A, B). Besides, evident enrichment of anti-tumor immunity-related signatures in FGFR Mut melanoma was observed (such as KEGG_CHEMOKINE, INTERFERON_GAMMA_RESPONSE, TNFA_SIGNALING, INFLAMMATORY_ RESPONSE) (Figures 9C-H). IL6_JAK_STAT3_SIGNALING, a typical pathway related to TIME regulation, was found to be abundant in FGFR Mut melanoma (Figure 9I).

Discussion

ICIs have significantly prolonged the survival of patients with metastatic melanoma (2). Nevertheless, only a subset of patients could benefit from ICIs (6). Indeed, the factors that influence ICI efficacy are extremely diverse and complex. Besides the widely recognized TMB, an increasing number of studies have demonstrated that gene mutations exert considerable impacts on the efficacy of ICIs, with some mutations favoring ICIs and some attenuating ICIs (14, 16, 25, 26). Notably, FGFR family driver genes are frequently mutated in melanoma,

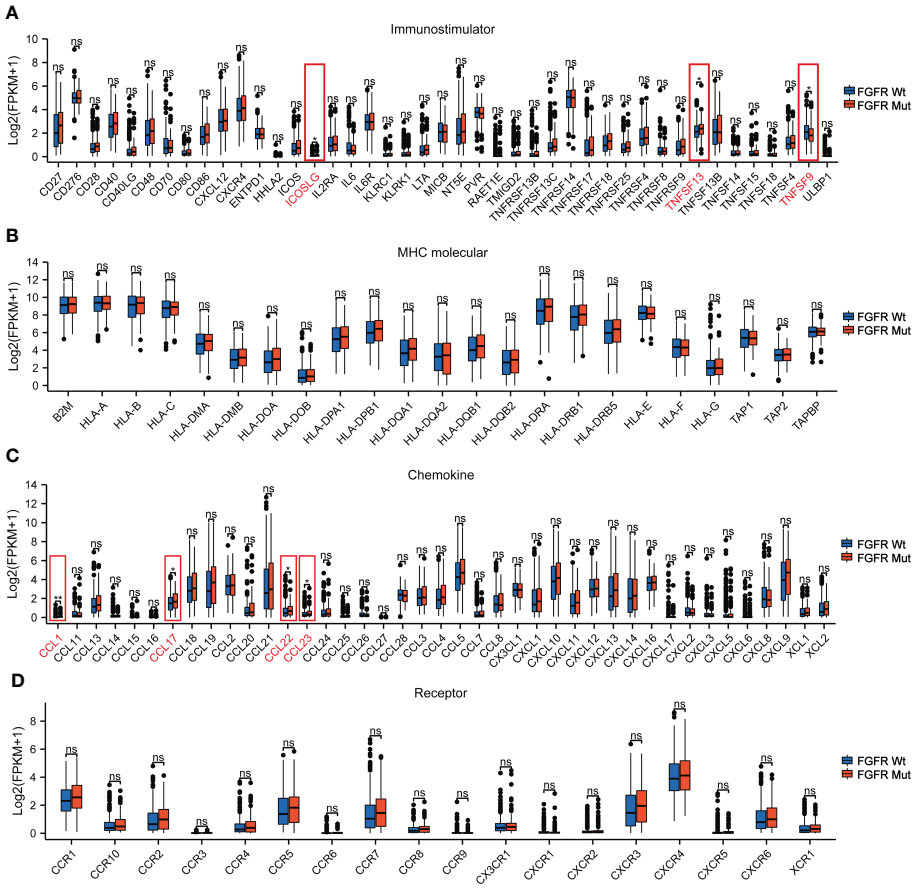

FIGURE 8
The association of FGFR Mut with anti-tumor immunity signatures in melanoma. **(A)** The expression levels of immuno-stimulator related genes in FGFR Mut versus FGFR Wt melanoma. **(B)** The expression levels of MHC molecule related genes in FGFR Mut versus FGFR Wt melanoma. **(C, D)** Comparison of chemokines and their receptors between FGFR Mut and FGFR Wt melanoma (ns = not significant, *P < 0.05, **P < 0.01).

whereas its influence on ICIs efficacy in melanoma remains unknown. In this study, we found that melanoma patients with FGFR mutations who were treated with ICIs apparently survived longer than those with FGFR wild-type. Besides, increased immunogenicity and enhanced anti-tumor immunity in FGFR mutant melanoma could be the potential mechanisms that contribute to melanoma with FGFR mutations being more responsive to ICIs.

FGFR, a subfamily of receptor tyrosine kinases, comprises four members of FGFR1-4 (20). Similar to EGFR, FGFR is driver gene playing key roles the development of cancer (21). Aberrant FGFR could induce proliferation and migration of cancer cells (21). However, the survival of FGFR mutant melanoma was equivalent to that of the wild-type in our study. Substantial studies have proven that some driver gene mutations play crucial roles in modulating the efficacy of ICIs. Representatively, lung cancer harboring EGFR mutations is generally not considered for treatment with ICIs given that multiple clinical trials have found that ICIs provide limited survival benefit for this particular population (26), whereas KRAS mutation is a favorable biomarker for ICIs benefit (39). In terms of FGFR, it was found that ICIs provided comparable survival benefit for metastatic urothelial cancer with and without FGFR3 mutation (27). Strikingly, we found that melanoma with FGFR mutations benefited more from ICIs than their wild-type counterparts. Subgroup analysis based on FGFR mutation subtypes discovered similar results, especially for FGFR1 and FGFR2. Therefore, not only should melanoma patients with FGFR mutations be considered for treatment with ICIs, but they should also be given priority access. With the distinct survival benefit from ICIs in patients with FGFR mutations compared to these wild-type, FGFR mutations could be a novel biomarker for stratifying a dominant subgroup of patients with advanced melanoma for ICIs therapy.

It is well-accepted that immunogenicity plays a critical role in the activation of anti-tumor immune cells to enhance ICIs efficacy (40). Increased TMB is associated with the generation of neoantigens, representing enhanced immunogenicity (41). In

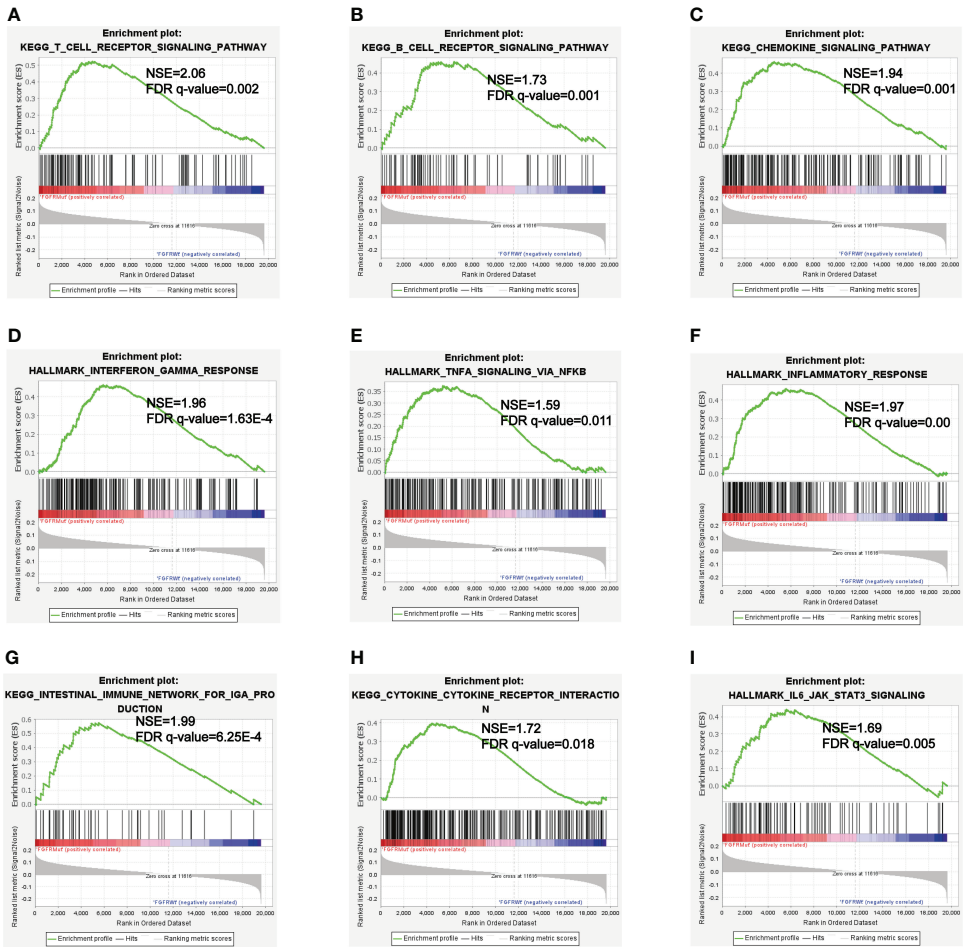

FIGURE 9
(A-I) Enriched Gene Sets in FGFR Mut and FGFR Wt melanoma.

the study, we found that FGFR mutant melanoma exhibiting increased TMB, which could be an important factor behind their more survival benefit from ICIs. Likewise, higher NAL was identified in FGFR mutant melanoma, providing greater evidence for prolonged survival and high response rate of FGFR mutant melanoma patients who received ICIs. Besides, the mutation frequencies of MMR-related genes and DDR-related genes were higher in FGFR mutant melanoma, correlating with genomic instability (42, 43), thereby promoting the effectiveness of ICIs in killing cancer cells. Collectively, we speculated that FGFR mutations would enhance the immunogenicity of melanoma, thereby favoring ICIs efficacy.

It is well acknowledged that the cancer-immunity cycle plays key roles in recognizing and eliminating cancer cells, which is an indispensable process in ICIs promoting anti-tumor immune response (44). Of note, multiple factors are involved in modulating the process of the cancer-immunity cycle. The presentation of cancer antigens by antigen presenting cells is the crucial first step (45). Dendritic cell, the most potent antigen-presenting cells (46), infiltrated more pronounced in FGFR mutant melanoma, which could intensify antigen presentation and T cell activation. Next, trafficking of the activated effector T cells into tumors guarantees its function (44). Higher expression of chemokines (e.g., CCL17 and CCL22) that attract anti-tumor immune cells (47–49) was found in FGFR mutant melanoma. Consistently, immune cells, such as activated CD4+ T cell and memory B cell, were more abundant in FGFR mutant melanoma. Then, specific recognition *via* the interaction between T cell receptor (TCR) on T cell and MHC on tumor cell is the important final step ensuring the cancer-immunity cycle (44). Thus, the mild tendency of increased MHC expression in FGFR mutant melanoma (all P values > 0.05) could improve the efficacy of ICIs. Meanwhile, significant enrichment of B_CELL_RECEPTOR and T_CELL_RECEPTOR pathways in FGFR mutant melanoma may further

reinforce this crucial last step. Collectively, FGFR mutations predominantly boost essential processes of the cancer-immunity cycle in melanoma, which partially explains why patients with FGFR mutations benefited more from ICIs.

Inflammatory TIME is universally acknowledged to be associated with high response to ICIs (50, 51). GSEA showed that patients with FGFR mutations were more abundant in immunoinflammatory-related hallmark, such as INTERFERON_GAMMA_RESPONSE, INFLAMMATORY_RESPONSE and KEGG_CHEMOKINE (52). Therefore, it is speculated that FGFR mutations can facilitate the formation of an inflammatory TIME, which synergistically promotes ICIs to activate immune cells to kill cancer cells.

In this study, we comprehensively investigated the influence of FGFR mutations on the efficacy of ICIs in melanoma. Meanwhile, a nomogram for predicting survival of melanoma patients treated with ICIs was constructed. Furthermore, the association of FGFR mutations with immunogenicity, factors modulating the cancer-immunity cycle, and pathway enrichment were investigated to unravel the potential mechanisms of FGFR mutations affecting ICIs efficacy. Notwithstanding, there are certain limitations for this study. Firstly, the sample size of ICIs-treated cohort from public database was relatively small, especially in terms of the number of FGFR mutant patients. Therefore, prospective research with larger sample size is required for further verification. Secondly, the potential associations of FGFR mutations with immunogenicity and the cancer-immunity cycle were explored exclusively based on the analysis of public databases, which could influence the reliability of the findings. Therefore, biological validation by *in vitro* and *in vivo* experimentation is necessary. Thirdly, a certain degree of study heterogeneity existed. Patients in the ICIs-treated cohort were treated with different ICIs, including anti-PD-(L)1 and anti-CTLA-4. FGFR mutations may affect the efficacy of different ICIs differently. Fourthly, the data in this study were extracted from public database and some specific information is not available, which can impair the reliability of our results. Therefore, the predictive value of FGFR mutations in specific ICIs warrants further investigation.

Conclusions

In the study, we first demonstrated that melanoma patients with FGFR mutations benefited more from ICIs compared with their wild-type counterparts. FGFR mutation subtypes (FGFR1, FGFR2, FGFR3 and FGFR4) showed similar results. In conclusion, it was revealed that FGFR mutations could be a favorable biomarker in predicting the efficiency of ICIs for melanoma. Mechanistically, FGFR mutations were strongly associated with strengthened tumor immunogenicity and inflamed antitumor immunity, which could be the underlying mechanisms for FGFR-mutated melanomas benefit more from ICIs.

Data availability statement

The original contributions presented in the study are included in the article/Supplementary Material. Further inquiries can be directed to the corresponding authors.

Author contributions

Conceptualization: YL and XW; methodology: WZ and RY; software: WZ, XS, and YZ; validation: QZ and HX; formal analysis: NL; XCM and XM; resources: CW; data curation: HC; writing—original draft preparation: WZ; writing—review and editing: YL; visualization: WZ; supervision: XW; project administration: XW; funding acquisition: XW and YL. All authors contributed to the article and approved the submitted version.

Funding

This study was funded by grants from the National Natural Science Foundation of China (No. 81874044) and the Shandong Provincial Natural Science Foundation (No. ZR2020MH236 and No. ZR2019MH050).

Conflict of interest

The authors declare that the research was conducted in the absence of any commercial or financial relationships that could be construed as a potential conflict of interest.

Publisher's note

Supplementary material

The Supplementary Material for this article can be found online at: https://www.frontiersin.org/articles/10.3389/fimmu.2022.1030969/full#supplementary-material

References

1. Sung H, Ferlay J, Siegel RL, Laversanne M, Soerjomataram I, Jemal A, et al. Global cancer statistics 2020: GLOBOCAN estimates of incidence and mortality worldwide for 36 cancers in 185 countries. *CA Cancer J Clin* (2021) 3:209–49. doi: 10.3322/caac.21660

2. Larkin J, Chiarion-Sileni V, Gonzalez R, Grob JJ, Rutkowski P, Lao CD, et al. Five-year survival with combined nivolumab and ipilimumab in advanced melanoma. *N Engl J Med* (2019) 16:1535–46. doi: 10.1056/NEJMoa1910836

3. Wolchok JD, Chiarion-Sileni V, Gonzalez R, Grob J-J, Rutkowski P, Lao CD, et al. CheckMate 067: 6.5-year outcomes in patients (pts) with advanced melanoma. *J Clin Oncol* (2021) 15_suppl:9506–6. doi: 10.1200/JCO.2021.39.15_suppl.9506

4. Tsao H, Atkins MB, Sober AJ. Management of cutaneous melanoma. *N Engl J Med* (2004) 10:998–1012. doi: 10.1056/NEJMra041245

5. Carlino MS, Larkin J, Long GV. Immune checkpoint inhibitors in melanoma. *Lancet* (2021) 10304:1002–14. doi: 10.1016/S0140-6736(21)01206-X

6. Wolchok JD, Chiarion-Sileni V, Gonzalez R, Grob JJ, Rutkowski P, Lao CD, et al. Long-term outcomes with nivolumab plus ipilimumab or nivolumab alone versus ipilimumab in patients with advanced melanoma. *J Clin Oncol* (2022) 2:127–37. doi: 10.1200/JCO.21.02229

7. Larkin J, Hodi FS, Wolchok JD. Combined nivolumab and ipilimumab or monotherapy in untreated melanoma. *N Engl J Med* (2015) 13:1270–1. doi: 10.1056/NEJMc1509660

8. Bowyer S, Prithviraj P, Lorigan P, Larkin J, McArthur G, Atkinson V, et al. Efficacy and toxicity of treatment with the anti-CTLA-4 antibody ipilimumab in patients with metastatic melanoma after prior anti-PD-1 therapy. *Br J Cancer* (2016) 10:1084–9. doi: 10.1038/bjc.2016.107

9. Forschner A, Battke F, Hadaschik D, Schulze M, Weissgraeber S, Han CT, et al. Tumor mutation burden and circulating tumor DNA in combined CTLA-4 and PD-1 antibody therapy in metastatic melanoma - results of a prospective biomarker study. *J Immunother Cancer* (2019) 1:180. doi: 10.1186/s40425-019-0659-0

10. Baltussen JC, Welters MJP, Verdegaal EME, Kapiteijn E, Schrader AMR, Slingerland M, et al. Predictive biomarkers for outcomes of immune checkpoint inhibitors (ICIs) in melanoma: A systematic review. *Cancers (Basel)* (2021) 24:6366. doi: 10.3390/cancers13246366

11. Cui C, Xu C, Yang W, Chi Z, Sheng X, Si L, et al. Ratio of the interferon-gamma signature to the immunosuppression signature predicts anti-PD-1 therapy response in melanoma. *NPJ Genom Med* (2021) 1:7. doi: 10.1038/s41525-021-00169-w

12. Gide TN, Quek C, Menzies AM, Tasker AT, Shang P, Holst J, et al. Distinct immune cell populations define response to anti-PD-1 monotherapy and anti-PD-1/Anti-CTLA-4 combined therapy. *Cancer Cell* (2019) 2:238–255.e236. doi: 10.1016/j.ccell.2019.01.003

13. Diem S, Kasenda B, Spain L, Martin-Liberal J, Marconcini R, Gore M, et al. Serum lactate dehydrogenase as an early marker for outcome in patients treated with anti-PD-1 therapy in metastatic melanoma. *Br J Cancer* (2016) 3:256–61. doi: 10.1038/bjc.2015.467

14. Hilke FJ, Sinnberg T, Gschwind A, Niessner H, Demidov G, Amaral T, et al. Distinct mutation patterns reveal melanoma subtypes and influence immunotherapy response in advanced melanoma patients. *Cancers (Basel)* (2020) 9:2359. doi: 10.3390/cancers12092359

15. Zhang W, Shi F, Kong Y, Li Y, Sheng C, Wang S, et al. Association of PTPRT mutations with immune checkpoint inhibitors response and outcome in melanoma and non-small cell lung cancer. *Cancer Med* (2022) 3:676–91. doi: 10.1002/cam4.4472

16. Ma D, Zhang Q, Duan Q, Tan Y, Sun T, Qi C, et al. Identification of IGF1R mutation as a novel predictor of efficacious immunotherapy in melanoma. *J Transl Med* (2022) 1:172. doi: 10.1186/s12967-022-03324-8

17. Ye T, Zhang JY, Liu XY, Zhou YH, Yuan SY , Yang MM, et al. The predictive value of MAP2K1/2 mutations on efficiency of immunotherapy in melanoma. *Front Immunol* (2021) 17:785526. doi: 10.3389/fimmu.2021.785526

18. Thielmann CM, Matull J, Roth S, Placke JM, Chorti E, Zaremba A, et al. Genetic and clinical characteristics of ARID1A mutated melanoma reveal high tumor mutational load without implications on patient survival. *Cancers (Basel)* (2022) 9:2090. doi: 10.3390/cancers14092090

19. Long J, Wang D, Yang X, Wang A, Lin Y, Zheng M, et al. Identification of NOTCH4 mutation as a response biomarker for immune checkpoint inhibitor therapy. *BMC Med* (2021) 1:154. doi: 10.1186/s12916-021-02031-3

20. Turner N, Grose R. Fibroblast growth factor signalling: from development to cancer. *Nat Rev Cancer* (2010) 2:116–29. doi: 10.1038/nrc2780

21. Chioni AM, Grose RP. Biological significance and targeting of the FGFR axis in cancer. *Cancers (Basel)* (2021) 22:5681. doi: 10.3390/cancers13225681

22. Hoy SM. Pemigatinib: First approval. *Drugs* (2020) 9:923–9. doi: 10.1007/s40265-020-01330-y

23. Al-Obaidy KI, Cheng L. Fibroblast growth factor receptor (FGFR) gene: pathogenesis and treatment implications in urothelial carcinoma of the bladder. *J Clin Pathol* (2021) 8:491–5. doi: 10.1136/jclinpath-2020-207115

24. Loriot Y, Necchi A, Park SH, Garcia-Donas J, Huddart R, Burgess E, et al. Erdafitinib in locally advanced or metastatic urothelial carcinoma. *N Engl J Med* (2019) 4:338–48. doi: 10.1056/NEJMoa1817323

25. Seegobin K, Majeed U, Wiest N, Manochakian R, Lou Y , Zhao Y. Immunotherapy in non-small cell lung cancer with actionable mutations other than EGFR. *Front Oncol* (2021) 11:750657. doi: 10.3389/fonc.2021.750657

26. Lee CK, Man J, Lord S, Links M, Gebski V, Mok T, et al. Checkpoint inhibitors in metastatic EGFR-mutated non-small cell lung cancer-a meta-analysis. *J Thorac Oncol* (2017) 2:403–7. doi: 10.1016/j.jtho.2016.10.007

27. Rose TL, Weir WH, Mayhew GM, Shibata Y, Eulitt P, Uronis JM, et al. Fibroblast growth factor receptor 3 alterations and response to immune checkpoint inhibition in metastatic urothelial cancer: a real world experience. *Br J Cancer* (2021) 9:1251–60. doi: 10.1038/s41416-021-01488-6

28. Cerami E, Gao J, Dogrusoz U, Gross BE, Sumer SO, Aksoy BA, et al. The cBio cancer genomics portal: an open platform for exploring multidimensional cancer genomics data. *Cancer Discovery* (2012) 5:401–4. doi: 10.1158/2159-8290.CD-12-0095

29. Van Allen EM, Miao D, Schilling B, Shukla SA, Blank C, Zimmer L, et al. Genomic correlates of response to CTLA-4 blockade in metastatic melanoma. *Science* (2015) 6257:207–11. doi: 10.1126/science.aad0095

30. Snyder A, Makarov V, Merghoub T, Yuan J, Zaretsky JM, Desrichard A, et al. Genetic basis for clinical response to CTLA-4 blockade in melanoma. *N Engl J Med* (2014) 23:2189–99. doi: 10.1056/NEJMoa1406498

31. Hugo W, Zaretsky JM, Sun L, Song C, Moreno BH, Hu-Lieskovan S, et al. Genomic and transcriptomic features of response to anti-PD-1 therapy in metastatic melanoma. *Cell* (2016) 1:35–44. doi: 10.1016/j.cell.2016.02.065

32. Samstein RM, Lee CH, Shoushtari AN, Hellmann MD, Shen R, Janjigian YY, et al. Tumor mutational load predicts survival after immunotherapy across multiple cancer types. *Nat Genet* (2019) 2:202–6. doi: 10.1038/s41588-018-0312-8

33. Goldman MJ, Craft B, Hastie M, Repecka K, McDade F, Kamath A, et al. Visualizing and interpreting cancer genomics data *via* the xena platform. *Nat Biotechnol* (2020) 6:675–8. doi: 10.1038/s41587-020-0546-8

34. Newman AM, Liu CL, Green MR, Gentles AJ, Feng W, Xu Y, et al. Robust enumeration of cell subsets from tissue expression profiles. *Nat Methods* (2015) 5:453–7. doi: 10.1038/nmeth.3337

35. Bindea G, Mlecnik B, Tosolini M, Kirilovsky A, Waldner M, Obenauf AC, et al. Spatiotemporal dynamics of intratumoral immune cells reveal the immune landscape in human cancer. *Immunity* (2013) 4:782–95. doi: 10.1016/j.immuni.2013.10.003

36. Hanzelmann S, Castelo R, Guinney J. GSVA: gene set variation analysis for microarray and RNA-seq data. *BMC Bioinf* (2013) 14:7. doi: 10.1186/1471-2105-14-7

37. Yoshihara K, Shahmoradgoli M, Martinez E, Vegesna R, Kim H, Torres-Garcia W, et al. Inferring tumour purity and stromal and immune cell admixture from expression data. *Nat Commun* (2013) 4:2612. doi: 10.1038/ncomms3612

38. Thorsson V, Gibbs DL, Brown SD, Wolf D, Bortone DS, Ou Yang TH, et al. The immune landscape of cancer. *Immunity* (2018) 4:812–830.e814. doi: 10.1016/j.immuni.2018.03.023

39. Dong ZY, Zhong WZ, Zhang XC, Su J, Xie Z, Liu SY, et al. Potential predictive value of TP53 and KRAS mutation status for response to PD-1 blockade immunotherapy in lung adenocarcinoma. *Clin Cancer Res* (2017) 12:3012–24. doi: 10.1158/1078-0432.CCR-16-2554

40. Rizvi NA, Hellmann MD, Snyder A, Kvistborg P, Makarov V, Havel JJ, et al. Cancer immunology. mutational landscape determines sensitivity to PD-1 blockade in non-small cell lung cancer. *Science* (2015) 6230:124–8. doi: 10.1126/science.aaa1348

41. Schumacher TN, Schreiber RD. Neoantigens in cancer immunotherapy. *Science* (2015) 6230:69–74. doi: 10.1126/science.aaa4971

42. Le DT, Durham JN, Smith KN, Wang H, Bartlett BR, Aulakh LK, et al. Mismatch repair deficiency predicts response of solid tumors to PD-1 blockade. *Science* (2017) 6349:409–13. doi: 10.1126/science.aan6733

43. Ye Z, Shi Y, Lees-Miller SP , Tainer JA. Function and molecular mechanism of the DNA damage response in immunity and cancer immunotherapy. *Front Immunol* (2021) 12:797880. doi: 10.3389/fimmu.2021.797880

44. Chen DS, Mellman I. Oncology meets immunology: the cancer-immunity cycle. *Immunity* (2013) 1:1–10. doi: 10.1016/j.immuni.2013.07.012

45. Jhunjhunwala S, Hammer C, Delamarre L. Antigen presentation in cancer: insights into tumour immunogenicity and immune evasion. *Nat Rev Cancer* (2021) 5:298–312. doi: 10.1038/s41568-021-00339-z

46. Wculek SK, Cueto FJ, Mujal AM, Melero I, Krummel MF, Sancho D. Dendritic cells in cancer immunology and immunotherapy. *Nat Rev Immunol* (2020) 1:7–24. doi: 10.1038/s41577-019-0210-z

47. Matsuo K, Yoshie O, Nakayama T. Multifaceted roles of chemokines and chemokine receptors in tumor immunity. *Cancers (Basel)* (2021) 23:6132. doi: 10.3390/cancers13236132

48. Kazanietz MG, Durando M , Cooke M. CXCL13 and its receptor CXCR5 in cancer: Inflammation, immune response, and beyond. *Front Endocrinol (Lausanne)* (2019) 10:471. doi: 10.3389/fendo.2019.00471

49. Lu J, Chatterjee M, Schmid H, Beck S, Gawaz M. CXCL14 as an emerging immune and inflammatory modulator. *J Inflammation (Lond)* (2016) 13:1. doi: 10.1186/s12950-015-0109-9

50. Chen DS, Mellman I. Elements of cancer immunity and the cancer-immune set point. *Nature* (2017) 7637:321–30. doi: 10.1038/nature21349

51. Binnewies M, Roberts EW, Kersten K, Chan V, Fearon DF, Merad M, et al. Understanding the tumor immune microenvironment (TIME) for effective therapy. *Nat Med* (2018) 5:541–50. doi: 10.1038/s41591-018-0014-x

52. Grasso CS, Tsoi J, Onyshchenko M, Abril-Rodriguez G, Ross-Macdonald P, Wind-Rotolo M, et al. Conserved interferon-gamma signaling drives clinical response to immune checkpoint blockade therapy in melanoma. *Cancer Cell* (2020) 4:500–515.e503. doi: 10.1016/j.ccell.2020.08.005

frontiers | Frontiers in Immunology

TYPE Review
PUBLISHED 22 March 2023
DOI 10.3389/fimmu.2023.1152312

OPEN ACCESS

EDITED BY
Denisa Baci,
University of Insubria, Italy

REVIEWED BY
Luo Yuhao,
Southwest Medical University, China
Christian Stockmann,
University of Zurich, Switzerland
Wan Zhuo,
Air Force Medical University, China

*CORRESPONDENCE
Fu Peng
pengf@scu.edu.cn

SPECIALTY SECTION
This article was submitted to Cancer Immunity and Immunotherapy, a section of the journal Frontiers in Immunology

RECEIVED 27 January 2023
ACCEPTED 09 March 2023
PUBLISHED 22 March 2023

CITATION
Li X, Zhou J, Wang X, Li C, Ma Z, Wan Q and Peng F (2023) Pancreatic cancer and fibrosis: Targeting metabolic reprogramming and crosstalk of cancer-associated fibroblasts in the tumor microenvironment. *Front. Immunol.* 14:1152312. doi: 10.3389/fimmu.2023.1152312

Pancreatic cancer and fibrosis: Targeting metabolic reprogramming and crosstalk of cancer-associated fibroblasts in the tumor microenvironment

Xin Li, Jianbo Zhou, Xue Wang, Chunxi Li, Zifan Ma, Qiaoling Wan and Fu Peng*

Department of Pharmacology, Key Laboratory of Drug-Targeting and Drug Delivery System of the Education Ministry, Sichuan Engineering Laboratory for Plant-Sourced Drug and Sichuan Research Center for Drug Precision Industrial Technology, West China School of Pharmacy, Sichuan University, Chengdu, China

Pancreatic cancer is one of the most dangerous types of cancer today, notable for its low survival rate and fibrosis. Deciphering the cellular composition and intercellular interactions in the tumor microenvironment (TME) is a necessary prerequisite to combat pancreatic cancer with precision. Cancer-associated fibroblasts (CAFs), as major producers of extracellular matrix (ECM), play a key role in tumor progression. CAFs display significant heterogeneity and perform different roles in tumor progression. Tumor cells turn CAFs into their slaves by inducing their metabolic dysregulation, exacerbating fibrosis to acquire drug resistance and immune evasion. This article reviews the impact of metabolic reprogramming, effect of obesity and cellular crosstalk of CAFs and tumor cells on fibrosis and describes relevant therapies targeting the metabolic reprogramming.

KEYWORDS

pancreatic cancer, cancer-associated fibroblasts, fibrosis, metabolic reprogramming, crosstalk, heterogeneity

Abbreviations: TME, tumor microenvironment; ECM, extracellular matrix; CAF, cancer-associated fibroblast; PDAC, pancreatic ductal adenocarcinoma; PSC, pancreatic stellate cell; myCAF, myofibroblastic CAF; iCAF, inflammatory CAF; α-SMA, α-smooth muscle actin; IL, interleukin; apCAF, antigen-presenting CAF; meCAF, CAF with a highly activated metabolic state; csCAF, complement-secreting CAF; LIF, leukemia inhibitory factor; TGF-β, transforming growth factor-β; Tregs, regulatory T cells; PDGF, platelet derived growth factor; JNK, c-Jun N-terminal kinase; ERK, extracellular signal-regulated kinase; TCA, tricarboxylic acid; HIF, hypoxia-inducible factor; MCT, monocarboxylate transporter; NetG1, Netrin G1; BCAA, branched-chain amino acid; BCAT, branched-chain amino acid transaminase; BCKA, branched-chain α-keto acid; PAI-1, plasminogen activator inhibitor-1; VEGF, vascular endothelial growth factor; TIMP-1, tissue inhibitor of metalloproteinase-1; MMP, matrix metallopeptidase; CECR4, C-X-C motif chemokine receptor 4; SATB-1, special AT-rich sequence-binding protein 1; NF-κB, nuclear factor KB; ESE3, epithelium-specific E-twenty six factor 3; IRAK4, IL-1 receptor-associated kinase 4; NUFIP1, nuclear fragile X mental retardation-interacting protein 1; SHH, sonic hedgehog; LOXL2, lysyl oxidase-like protein 2; MSC, mesenchymal stem cell; YAP1, Yes-associated protein 1.

Introduction

Pancreatic cancer is one of the most aggressive types of cancer, being more common in developed countries and by low survival rates (1). As the main form of pancreatic cancer, pancreatic ductal adenocarcinoma (PDAC) has a discouraging prognosis, with a very low five-year survival rate (2). There is a correlation between lifestyle habits including smoking, alcohol consumption, and genetic and environmental factors and the onset of pancreatic cancer (1). Notably, the hormones, pro-angiogenic factors and pro-inflammatory cytokines secreted by obese tissues make obesity a risk factor for the occurrence of pancreatic cancer (3, 4). Diabetes associated with obesity and chronic pancreatitis also show a relevance to pancreatic cancer (5). Surgery is the treatment that has the potential to cure pancreatic cancer now, whilst chemotherapy, immunotherapy and targeted therapies have been demonstrated to help enhance the overall survival rate of patients (6–8).

Fibrosis driven by chronic inflammation occurs commonly in a variety of cancers, such as liver, pancreatic, and lung cancers (9–11). This formation of excessive intratumoral connective tissue is also referred to as desmoplasia by pathologists (12). Desmoplasia is one of the major pathological features and is intimately connected with its occurrence, progression and prognosis of pancreatic cancer. The desmoplastic reaction caused by inflammation gives pancreatic cancer an extraordinarily rich ECM (13). The fibrotic response in tumors is by the same mechanism as wound healing, being an excessive accumulation of ECM components and involving multiple cytokines and growth factors (14). ECM proteins are rich in composition, including fiber-forming proteins, glycoproteins, proteoglycans and matricellular proteins (15). The dense stroma leads to hypoxia in the tumor microenvironment and makes it difficult for chemotherapeutic agents to penetrate, thus imparting chemoresistance to pancreatic cancer (16).

TME of pancreatic cancer contains abundant stroma, blood vessels, and soluble proteins (17). Apart from cancer cells, three types of normal cells are found in the TME, namely stromal cells, fibroblasts, and immune cells (18). TME as a dynamic system has a changing composition and influences the progression of fibrosis in pancreatic cancer. Cancer-associated fibroblasts are extraordinarily abundant and secrete a range of extracellular matrix proteins, growth factors, and cytokines (19). CAFs crosstalk with tumor cells and immune cells and perform metabolic reprogramming to promote tumor development and fibrosis. In this review, we give a summary of current information about the heterogeneity of CAFs in pancreatic cancer cells, as well as updates on the metabolic reprogramming, crosstalk and therapies in the TME.

Heterogeneity of CAFs

CAFs were initially thought to be homogeneous, but subsequent studies proved that CAFs varied in origin, expression, and function (20). Their typing remains incompletely elucidated, but existing work demonstrates that functionally distinct or even completely opposite subtypes exist. Öhlund et al. found pancreatic stellate cells (PSCs) were able to differentiate into two CAF subtypes, myofibroblastic CAFs (myCAFs) and inflammatory CAFs (iCAFs) in mouse PDAC (21). They differed significantly in spatial distribution and cytokine expression. myCAFs were distributed in the periglandular region at a closer distance from tumor cells, with high expression of α-smooth muscle actin (α-SMA) and low expression of interleukin (IL)-6, whereas iCAFs were distributed more distantly throughout the tumor, with low expression of α-SMA but high expression of cytokines such as IL-6, IL-11, and leukemia inhibitory factor (LIF) (21). This classification still has not reached the end point, as three subgroups of iCAFs were identified (22). Antigen-presenting CAFs (apCAFs) was identified in PDAC, named for its ability to express MHC class II molecules (23). A new CAF subtype with a highly activated metabolic state (meCAFs) was found in loose-type PDAC (24). Complement-secreting CAFs (csCAFs) were found in PDAC featuring a specific expression of complement components such as C3, C7, C1R/S, CFD, CFH, CFI (25). In the same study, Chen et al. defined PSCs as a subtype of CAF and found that PSCs dominated in PDAC stages I, II and III (25). The state of differentiation is reversible as iCAFs and myCAFs are able to convert into each other and apCAFs can also differentiate into myCAFs (21, 23). Modulation of transforming growth factor-β (TGF-β), IL-1/JAK/STAT signaling and hedgehog signaling impact on the differentiation of myCAFs and iCAFs (26, 27). Hypoxia within the TME probably converted fibroblasts to iCAFs (28). Neuzillet et al. proved the presence of at least four CAF subtypes in PDAC, which were featured by distinct mRNA expression profiles, with POSTN, MYH11, and PDPN as markers for three of the subtypes (29). PDPN-positive CAFs are molecularly similar to an iCAF subset, while POSTN-positive CAFs are not associated with the classical myCAF/iCAF classification (30). And these two subsets cooperate in the TME to induce the recruitment of monocytes/macrophages (30). It is worth mentioning that the identified subtypes of CAFs are not only present in pancreatic cancer, but also can be found in breast, ovarian and lung cancer models (31).

The major CAF subtypes show significant heterogeneity not only in phenotypes but also in function (Figure 1). The pathways enriched by myCAFs included ECM organization, and collagen formation were significantly upregulated, and its high α-SMA expression indicated its possible involvement in ECM formation and fibrosis (23). iCAFs highly expressed inflammatory cytokines, and up-regulated IFN-γ response, TNF/NF-κB, IL-2/STAT5, IL-6/JAK/STAT3, and the complement pathway (23). PDAC iCAFs were classified into different subsets, and OGN was a unique marker for one of those linked to a good prognosis (22). are correlated with a poorer prognosis, whereas another study linked higher abundance of iCAFs to a better prognosis (28, 30). This may result from the presence of different subgroups in iCAFs, but it also demonstrates that iCAFs simultaneously have tumor-promoting and inhibiting properties. circCUL2 regulated miR-203a-5p/MyD88/NF-κB/IL-6 axis to induce the production of iCAFs, which increased the secretion of IL-6, thereby promoting PDAC progression and immunosuppression (32). Huang et al. found that mesothelial cells were induced to differentiate into apCAFs by IL-1/NF-κB

10.3389/fimmu.2023.1152312

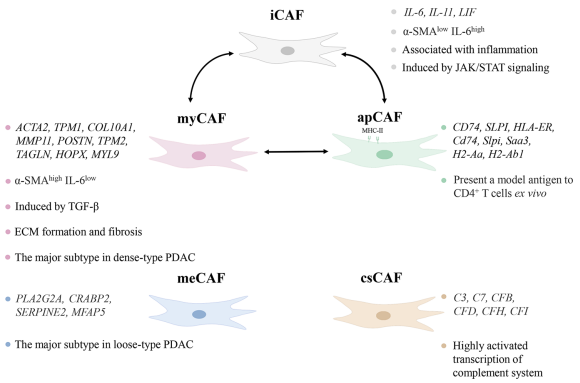

FIGURE 1
Characteristics of subtypes of cancer-associated fibroblasts (CAFs). The different subtypes of CAFs show heterogeneity in distribution, marker genes, and pathways in the tumor microenvironment. iCAF, inflammatory CAF; α-SMA, α-smooth muscle actin; IL-6, interleukin-6; myCAF, myofibroblastic CAF; TGF-β, transforming growth factor-β; ECM, extracellular matrix; PDAC, pancreatic ductal adenocarcinoma; apCAF, antigen-presenting CAF; meCAF, CAF with a highly activated metabolic state; csCAF complement-secreting CAF.

and TGF-β signaling (33). apCAFs promoted the transition of naive $CD4^+$ T cells into regulatory T cells (Tregs), which means that it may be related to immunosuppression (33).

Although PSCs are generally considered to be the major precursor cells for CAFs within pancreatic cancer, a recent study indicated that PSCs produced only a small fraction of CAFs in PDAC (34). However, the promotion of fibrosis by PSCs remains an important component of pancreatic cancer progression. While activated PSCs are considered to be CAFs, for a clearer representation of the source, PSCs are described separately from CAFs in this review. PSCs were first identified in the intralobular and interlobular connective tissues of normal pancreas with lipid droplets containing vitamin A in 1982 (35). A study showed that vitamin A deficiency contributed to the transition of PSCs from a quiescent to the activated state (36). When injury or inflammation activates the quiescent PSCs, this vitamin A droplet disappears while the expression of collagen, fibronectin, laminin and α-SMA increases, and EMT production rises. The activation of PSCs is influenced by a variety of factors, including alcohol, diabetes, oxidative stress, cytokines, growth factors, etc. TGF-β1 is considered to be the main regulator, while platelet derived growth factor (PDGF), IL-6, IL-11, c-Jun N-terminal kinase (JNK) and extracellular signal-regulated kinase (ERK) are also implicated (37–40).

Metabolic reprogramming in CAFs

Tumor cells still produce energy through less efficient aerobic glycolysis even under adequate oxygen, enhancing glucose transformation to pyruvate, termed the Warburg effect (41). However, this is not due to mitochondrial damage as originally envisioned by Warburg, but rather spontaneous metabolic reprogramming of tumor cells, where activation of a series of signaling factors and pathways leads to a switch from oxidative phosphorylation to glycolysis (42). Similar metabolic reprogramming exists in CAFs, and the Warburg effect is more obvious (43). Pancreatic cancer is one of the most severely hypoxic tumors as known, and hypoxia-inducible factors (HIFs) are the main regulators of hypoxia adaptation (44). Since the identification of HIF-1α in 1995, a wide range of roles of HIF-1 is continuously revealed in angiogenesis, cell metabolism, cell survival, and so forth (45, 46). In breast cancer, ROS production by cancer cells induces loss of Cav-1 in stromal cells, allowing CAFs to accumulate ROS and activate HIF-1α, consequently reprogramming CAFs and inducing autophagy (47, 48). The same alterations are shown in the PDAC model, where Cav-1 is lost in response to PSCs activation, correlating with stromal and cancer cells metabolic coupling (49). To conclude, HIF-1α connects oxidative stress and metabolic reprogramming of CAFs. Under such harsh conditions with hypoxia and low nutrition, there is metabolic crosstalk between CAFs with tumor cells and immune cells, all of which interact with each other to make TME a more habitable system (Figure 2).

Glucose metabolism

Pavlides et al. proposed the reverse Warburg effect, elucidating that CAFs were able to perform glycolysis, producing pyruvate and

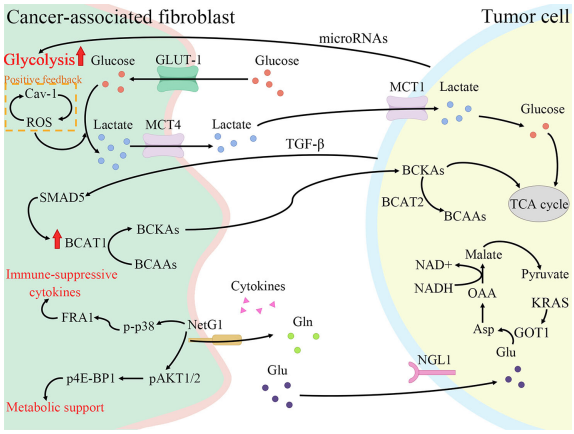

FIGURE 2
Cancer-associated fibroblasts (CAFs) promote fibrosis and tumor growth through metabolic reprogramming. CAFs increase glycolysis and glutamine secretion to supply lactate, branched-chain α-keto acids (BCKAs), glutamine, and cytokines to tumor cells. Meanwhile, tumor cells also secrete cytokines and microRNAs to regulate the metabolic reprogramming of CAFs to enable themselves to survive in a low-nutrient environment. Cav-1, Caveolin-1; ROS, reactive oxygen species; GLUT-1, glucose transporter-1; MCT4, monocarboxylate transporters 4; BCAT1, branched-chain amino acid transaminase 1; BCAAs, branched-chain amino acids; NetG1, Netrin G1; p-p38, phosphorylation of p38; FRA1, FOS-related antigen 1; pAKT1/2, phospho-AKT1/2; p4E-BP1, p4E-BP1; Gln, glutamine; Glu, glutamate; NGL1, Netrin-G ligand-1; TGF-β, transforming growth factor-β; MCT1, monocarboxylate transporters 1; BCAT2, branched-chain amino acid transaminase 2; TCA cycle, tricarboxylic acid cycle; GOT1, aspartate transaminase; Asp, aspartate; OAA, oxaloacetate.

lactate and making them available to cancer cells for use in the mitochondrial tricarboxylic acid (TCA) cycle (50). In other words, CAFs are captured by engaging with cancer cells and reprogrammed to a glycolytic phenotype. thereby supplying metabolic intermediates that enable cancer cells to compensatively generate energy *via* mitochondrial OXPHOS (51, 52). Glycolysis is the main metabolic mode of CAFs due to the increased expression of HIF-1α and monocarboxylate transporter (MCT) 4 (53). HIF-1α is a key cytokine that enables cells to adjust to hypoxic environments and undergo metabolic changes by promoting glycolysis through genes which encode glucose transporter proteins and enzymes of the glycolytic pathway (54). MCTs are passive transporter proteins that transport monocarboxylic acid ions and are highly expressed in tumors (55). MCT1 and MCT4 exhibit proton-coupled symport, with MCT4 generally involved in the export of lactate and MCT1 generally involved in the import of lactate (56). The expression of two glycolytic enzymes, lactate dehydrogenase A and pyruvate kinase M2, was found to be increased in CAFs (57). Furthermore, when pancreatic cancer cells were co-cultured with CAFs, MCT1 protein, succinate dehydrogenase and fumarate hydratase expression increased, demonstrating the metabolic coupling existing between CAFs and cancer cells (57). Positive feedback of Caveolin-1-ROS signaling prompted activation of PSCs and upregulated the expression of glycolytic enzymes, and the transporter protein MCT4, and downregulated the expression of OXPHOS enzymes and the transporter protein MCT1, while the protein expression in cancer cells was completely opposite (49). Moreover, MiR-21 promotes glucose uptake and lactate secretion by CAFs, indirectly enhancing pancreatic cancer cell invasion (58). Interestingly, CAFs also show heterogeneity in metabolic pathways, for iCAF had the highest metabolic activity and was more biased to glycolysis, whereas myCAF scored higher in OXPHOS than iCAF and apCAF (28).

Amino acid metabolism

Glutamine, an amide of glutamate, is an essential origin of carbon and nitrogen in pancreatic cancer (59). Son et al. found that PDAC cells metabolized glutamine using a specific aspartate transaminase (glutamic-oxoacetic transaminase 1)-mediated pathway to produce biomass precursors and redox power (60). Glutamine also serves as an important energy source for CAFs and is metabolized and secreted into metabolites such as glutamate, α-ketoglutarate, aspartate and malate (53). Both Netrin G1 (NetG1) on NetG1$^+$ CAFs and NetG1 ligand on tumor cells were highly expressed, resulting in the provision of glutamate/glutamine to tumor cells (61). NetG1 acts as a key regulator involved in ECM deposition, survival under low nutrient conditions and immunosuppression through the regulation of downstream pathways p38/FRA1 and AKT/4E-BP1 (61). PSCs increase glutamine synthetase expression by regulating the Wnt/β-catenin/TCF7 axis, thus promoting glutamine synthesis (62).

In addition to glutamine, alanine also acts as an important carbon source in the TCA of tumor cells. Tumor cells stimulate CAFs to catabolize metabolized proteins through autophagy to produce alanine and transaminate it to pyruvate (63). When glutamine is depleted, CAFs take up extracellular proteins through CaMKK2-AMPK-RAC1 signaling-dependent macropinocytosis and supply the produced amino acids to tumor cells (64). The macropinocytosis recovers CAFs to restore the production of collagen VI and fibronectin which is inhibited during glutamine depletion (64). In addition, the study also showed that protein-derived alanine was a secreted amino acid when serum albumin was cultured as a nutritional source for PSCs (64). It was demonstrated that pancreatic cancer cells and PSCs express SLC38A2 and SLC1A4 respectively to perform alanine exchange so as to meet the high alanine requirement of pancreatic cancer cells (65).

Furthermore, branched-chain amino acids (BCAAs), also known as leucine, isoleucine and valine, participate in metabolic reprogramming and crosstalk in CAFs and pancreatic cancer cells (66). Branched-chain amino acid transaminases (BCATs) can reversibly catalyze the transamination reaction of BCAAs to branched-chain α-keto acids (BCKAs) (67). TGF-β secreted by cancer cells upregulates BCAT1 activity by activating SMAD5 in CAFs, thereby increasing the secretion of BCKAs, which are supplied to cancer cells for BCAA synthesis (68).

Lipid metabolism

Lipids form an important part of cellular biological membranes and building blocks, and are also involved in signaling and supplying energy (69). Multiple studies have demonstrated the existence of lipid metabolic reprogramming of CAFs in different cancer types, but regrettably there are not enough research in pancreatic cancer (70–72). PSCs undergo lipidomic remodeling upon activation, releasing lysophosphatidylcholine in large quantities to promote migration and proliferation of PDAC cells *via* the lysophosphatidylcholine-autotaxin-lysophosphatidic acid axis (73). Recently, a study found that activation of one PSC subpopulation is associated with elevated expression of lipoprotein-uptake very low-density lipoprotein receptor, which drives the expression of IL-33 (74). ROS-induced, endoplasmic reticulum stress-dependent increase in IL-33 expression mediates innate lymphoid type-2 cells activation, which induces proliferation and activation of PSCs, thereby stimulating pancreas fibrosis (74).

Crosstalk: Complex communication between CAFs and tumor cells

CAFs take part in multiple stages of tumor progression, enabling bidirectional communication with other cells in the TME through intercellular contacts, secreted proteins and extracellular vesicles (75). Tumor cells signal CAFs to activate or secrete cytokines and matrix proteins, while CAFs promote drug resistance, proliferation, and migration of tumor cells. Here, we

mainly summarize the signals from tumor cells that are significant for fibrosis.

Extracellular vesicles

Extracellular vesicles are a form of intercellular communication that is currently of great interest. They are classified as prostasomes, apoptotic bodies, microvesicles and exosomes due to their size and origin (76). Exosomes contain a variety of nucleic acids(DNA, microRNA, lncRNA, circRNA), proteins, lipids and cytokines (77). We mention the ability of cancer cells to initiate metabolic reprogramming of CAFs, allowing them to provide nutrients to cancer cells. CD9, a specific exosome marker present on the surface of extracellular vesicles rich in annexin A6, enhances p38 mitogen-activated protein kinase signaling to induce PDAC cell migration (78, 79). Exosomes derived from PDAC cells expressing oncogenic KRAS mutants contain Survivin, imparting cell survival benefits to nearby CAFs (80). MiR-1246 and miR-1290 contained in pancreatic cancer cell-derived exosomes promote the expression of profibrogenic genes in PSCs (81).

Secreted proteins

Mutated *KRAS* induces upregulation of plasminogen activator inhibitor-1 (PAI-1) in pancreatic cancer cells which induces PSCs activation *via* LRP-1/ERK/c-JUN pathway to promote immunosuppression and fibrosis (82). Meanwhile, PAI-1 expression was regulated by acyl-CoA synthetase long-chain 3, which may be associated with the regulation of TGF-β (83). High expression of PAI-1 not only promoted PSCs activation but also was associated with a high tumor infiltration of M2 macrophages (83). TGF-β1 represents a critical factor in the activation of PSCs. The secretion of TGF-β1 in pancreatic cancer cells is modulated by proteasome activator subunit 3-mediated activation protein-1, thus regulating the proliferation of PSCs (84). The induction of CAFs by TGF-β1 can be indirect, mediated through extracellular matrix proteins and growth factors such as PDGF, vascular endothelial growth factor (VEGF) and IL-6 (85). PDGF activates the hippo pathway and adds phosphorylation of yes-associated protein 1 in PSCs, and yes-associated protein 1 regulates the transcription of genes triggered by the TGF-β1/SMAD pathway, such as connective tissue growth factor and IL-6 (86). It has been shown that overexpression of galectin-1 stimulates the TGF-β1/Smad signaling pathway, with tissue inhibitor of metalloproteinase-1 (TIMP-1) expression increasing more than matrix metallopeptidase (MMP) 2, resulting in inhibition of ECM degradation and increased expression of fibronectin, collagen I and α-SMA (87). In addition, the paracrine of galectin-1 enhances the tumorigenic capacity of pancreatic epithelial cells (88). CXCL12/CXCR4 participates in the fibrotic process and the conversion of fibroblasts to myofibroblasts in multiple organs (89). Tumor-produced lactate causes epigenomic reprogramming when mesenchymal stem cells differentiate into CAFs (90). The increase of α-ketoglutarate causes C-X-C motif chemokine receptor 4 (CXCR4) promoter demethylation, leading to CXCR4 upregulation (90). Increase of special AT-rich sequence-binding protein 1 (SATB-1) expression in pancreatic cancer cells by CAFs through the SDF-1/CXCR4 axis further promotes CAFs activation (91). Furthermore, it has been established that tumor cells and CAFs crosstalk through nuclear factor KB (NF-κB) activated by paracrine-IL-1β. NF-κB activation by tumor-secreted IL-1β induces the expression of ESE3 in PSCs, then epithelium-specific E-twenty six factor 3 (ESE3) binds to the promoters of α-SMA, collagen-I and IL-1β, activating PSCs and promoting PDAC fibrosis (92). PDAC cells secrete IL-1β to activate IL-1 receptor-associated kinase 4 (IRAK4) in CAFs, forming an IL1β-IRAK4 feedforward circuitry that initiates fibrotic function in CAFs (93).

Autophagy

Autophagy refers to a catabolic process to maintain intracellular homeostasis (94). But there is growing proof that autophagy takes part in the process of cellular secretion (95). Meanwhile, tumor cells are capable of secreting cytokines to induce autophagy in PSCs (63, 96). TGF-β1/Smad signaling-mediated autophagy promotes the conversion of fibroblasts to CAFs and facilitates their glycolysis (97). Activation of PSCs depends on autophagy, which is associated with the production of ECM and the secretion of IL-6 (96). CAFs conduct ribosomal RNA autophagy in a nuclear fragile X mental retardation-interacting protein 1 (NUFIP1)-dependent way, producing nucleosides available for PDAC cells under low nutrient conditions and initiating metabolic reprogramming (98). Collagen secretion can be facilitated by the mitophagy-regulated synthesis of proline in CAFs (99). In addition, a recent study found that PDAC cells generate lnc-FSD2-31:1 to promote the autophagy of CAFs *via* miR-4736, thereby inhibiting the activation of CAFs (100).

Impact of crosstalk between CAFs and cancer cells on fibrosis

In TME, CAFs secrete large amounts of ECM proteins and remodeling enzymes to reorganize and stiffen the matrix (101). The main contribution of tumor cells to ECM deposition is the recruitment and activation of stromal cells. Multiple pathways of intercellular communication including protein secretion and extracellular vesicles enable pancreatic cancer cells to regulate the cellular activities of CAFs. Cancer cells are involved in the cross-linked sclerosis and degradation of ECM, aiding their invasion and migration from different aspects. Pancreatic cancer cells rely on multiple cytokines such as TGF-β, IL-1, sonic hedgehog (SHH), and microRNAs to activate CAFs and thus promote ECM stiffness (102). Meanwhile, pancreatic cancer cells also produce enzymes to promote matrix protein cross-linking in ECM such as lysyl oxidase-like protein 2 (LOXL2) (103). We summarize the cytokines and modes of action associated with fibrosis during the crosstalk between pancreatic cancer cells and CAFs (Table 1).

TABLE 1 Overview of the impact of crosstalk between CAFs and tumor cells on fibrosis.

Factor	Source	Mode of Action	Recipient cells	Functional Relevance	Reference
PAI-1	Pancreatic cancer cells	Paracrine	PSCs	Activates PSCs and promotes fibrosis	(82)
TGF-β1	Pancreatic cancer cells	Paracrine	PSCs	Promotes proliferation of PSCs	(84)
IL-1α	PDAC cells	Paracrine	PSCs	Promote ECM remodeling	(104)
IL-1β	PDAC cells	Paracrine	PSCs	promotes PSCs activation and expression of α-SMA, collagen I and IL-1β and activates CAFs to promote fibrosis	(92, 93)
PDGF	Pancreatic cancer cells	Paracrine	PSCs	Induces PSCs activation and promotes desmoplasia formation	(105)
SHH	Pancreatic cancer cells	Paracrine	PSCs	induces the expression of Gremlin 1 in PSCs	(106)
SATB-1	Pancreatic cancer cells	Paracrine	CAFs	Maintains CAFs identity and promotes the activation of CAFs	(91)
CXCL8	Pancreatic tumor cells	Paracrine	CAFs	maintains the survival of CAFs and further promotes FGF-2 production.	(107)
Oncogenic Kras-induced factors	PDAC cells	Paracrine	CAFs	Up-regulates the expression of CXCR2 and CXCR2 ligands in CAFs and induces the conversion of CAFs into iCAFs	(108)
miR-4736	PDAC cells	Extracellular vesicles	CAFs	Activates autophagy in CAFs, inhibits CAF activation and reduces fibrosis.	(100)
miR-155	Pancreatic cancer cells	Microvesicles	CAFs	Reprograms neighboring normal fibroblasts into CAFs	(109)
miR-1246, miR-1290 and miR-21-5p	Pancreatic cancer cells	Exosomes	PSCs	Promote the activation of PSCs and the production of collagen	(81)
Lin28B	Pancreatic cancer cells	Exosomes	Pancreatic cancer cells	Recruits PSCs	(110)
CCN2 or miR-21	PSCs	Exosomes	PSCs	Promotes collagen expression	(111)

PAI-1, plasminogen activator inhibitor-1; PSC, pancreatic stellate cells; TGF-β1, transforming growth factor-β1; IL, interleukin; ECM, extracellular matrix; α-SMA, α-smooth muscle actin; CAF, cancer-associated fibroblast; PDGF, platelet derived growth factor; SHH, sonic hedgehog; SATB-1, special AT-rich sequence-binding protein 1; FGF-2, fibroblast growth factor 2; PDAC, pancreatic ductal adenocarcinoma; iCAF, inflammatory CAF; Lin28B, lin-28 homolog B; CCN2, connective tissue growth factor.

Obesity: An accomplice to pancreatic cancer fibrosis

Obesity is a critical independent risk factor for pancreatic cancer and is consistently associated with the development of pancreatic cancer. Obesity leads to hypertrophy and hyperplasia of adipocytes and causes chronic inflammation of the adipose tissue around or within the pancreas, which promotes tumor progression (112). And along with the advancement of pancreatic cancer stages, patients with pancreatic cancer experience adipose tissue loss as one of the manifestations of cachexia (113). Adipose tissue is divided into white, brown, and beige adipose tissue, while white adipose tissue is further classified into subcutaneous white adipose tissue and visceral white adipose tissue, with the latter playing a more pivotal role in the progression of pancreatic cancer (114). The cellular composition of white adipose tissue includes adipocytes, preadipocytes, immune cells, pericytes, endothelial cells, and multipotent stem cells (115). Some researches demonstrated the correlation of adipose tissue with fibroblast transformation and the formation and remodeling of ECM.

On the one hand, cells in adipose tissue have the ability to be reprogrammed into CAFs by pancreatic cancer cells. Adrenomedullin in the exosomes of pancreatic cancer cells promotes lipolysis in adipocytes (116). The lipolysis may explain the weight loss of the patients and represents a phenomenon of adipocytes dedifferentiation. Consequently, the dedifferentiation possibly connects the cachexia with fibroplasia in pancreatic cancer. When co-cultured with pancreatic cancer cells, 3T3-L1 adipocytes dedifferentiated to fibroblast-like cells, losing lipid droplets and expressing S100A4, MMP11, collagen I and α-SMA (117, 118). The reprogramming is closely correlated with WNT5a signaling (119). Adipose tissue-derived stromal cells can also be recruited to extrapancreatic invasive lesions and differentiate into CAFs, producing a more rigid ECM (120). Mucin 5AC secreted by pancreatic cancer cells recruits mesenchymal stem cells (MSCs) to a-SMA$^+$ CAFs (121). Activin A produced by PDAC cells was found to be associated with the loss of adipose tissue and the promotion of fibrosis, with an induction of trans-differentiation of white adipocytes into fibrotic cells (122). On the other hand, adipocytes mediate fibrosis by crosstalk with neighboring cells *via* paracrine secretion. Adipocytes secrete IL-1β to recruit neutrophils, thereby enhancing the activation of PSCs (123).

10.3389/fimmu.2023.1152312

The therapy progress of reprogramming

Ideas for targeting CAFs as therapeutic targets in pancreatic cancer for clinical benefit are diverse including depletion of CAFs, reprogramming CAFs to make them normal, and blocking signals from CAFs (Figure 3) (124). However, studies concerning the depletion of CAFs demonstrated that this treatment could lead to the exact opposite of what was expected, a facilitation of tumor progression (125, 126). Reprogramming CAFs to the stationary case is currently considered a feasible approach. It has been preliminarily demonstrated to be viable to normalize CAFs through endogenous substances, gene regulation, agents and intercellular interactions. Lipoxin A4 reversed the activation of PSCs to CAFs for matrix reprogramming, with decreased expression of α-SMA and collagen I (127). The increase of retinoic acid was able to inhibit CAFs and reduce the expression of α-SMA and FAP (128). Zhao et al. constructed a targeted drug delivery system based on red blood cells vesicles partial protection to deliver retinoic acid to CAFs to disrupt the Golgi apparatus and thereby inhibit the secretion of proteins such as MMP2, MMP9 and CCL2 (129). In addition, all-transretinoic acid inactivated PSCs by inhibiting Yes-associated protein 1 (YAP1) (130). Vitamin D and its receptor were involved in stromal reprogramming as well by inactivating CAF/PSC (131, 132). The activation of p53 could directly induce the accumulation of cytoplasmic lipid droplets in PSCs, thus effectively reprogramming PSCs to a quiescent state (133). Integrin subtype α 11 was also considered as a viable target for controlling the phenotype and activation of PSCs (134). Several studies have shown that metformin can reprogram PSCs to improve desmoplasia (135–137). Metformin inhibited TGF-β1 secretion by activating AMPK in pancreatic cancer cells, leading to blocking the activation of PSCs (136). In addition, eribulin also showed potential for normalizing CAFs due to its simulation of TGF-β downregulation (138). Mechanical regulation of intercellular interactions such as N-cadherin and N-cadherin ligand linkages could reprogram PSCs to a stationary state, however not in all cases, as this reprogramming was associated with mechanical dosing (139). Unfortunately, studies on the regulation of the metabolism of CAFs are scarce, because the mechanism of metabolic reprogramming of CAFs is still not entirely clarified. Chen et al. designed a liposome carrying hydroxychloroquine and paclitaxel to target autophagy in CAFs, with advantages for crosstalk and fibrosis inhibition (140). A biomimetic nanocarrier was devised to disrupt metabolic crosstalk by blocking lactate production in both CAFs and cancer cells (141).

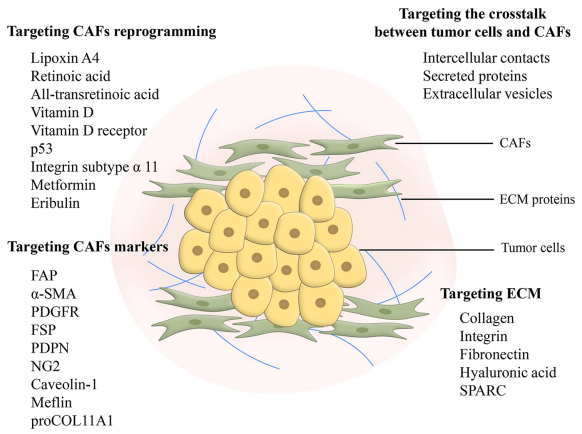

FIGURE 3
Feasible design ideas for targeting fibrosis. Targeting CAFs in metabolic reprogramming and signaling communication with cancer cells is considered as a promising therapeutic modality. Targeting markers of CAFs can inhibit CAFs, but there is a problem of non-specificity and further search and research is still needed. Targeting ECM elimination requires limitations, as sustained defibrosis implies enhanced invasion. In addition, ECM protein interactions may become an emerging therapeutic target. CAF, cancer-associated fibroblast; FAP, fibroblast activation protein; α-SMA, α-smooth muscle actin; PDGFR, platelet-derived growth factor receptor; FSP, fibroblast-specific protein; PDPN, podoplanin; NG2, nerve/glial antigen 2; ECM, extracellular matrix; SPARC, secreted protein acidic and rich in cysteine.

Discussion

CAF synthesizes, remodels and crosslinks ECM to increase stiffness leading to the generation of a dense fibrotic tumor stroma (101). CAFs act in pancreatic cancer progression as an essential component of the stroma. Five subtypes of CAFs have been identified so far, namely myCAFs, iCAFs, apCAFs, meCAFs and csCAFs, showing differences in expression and function in pancreatic cancer. This is still not the endpoint of the classification of CAFs, and the subtypes may contain subpopulations. As we mentioned before, different subpopulations of iCAFs may have opposite effects on tumor development. It implies that therapies targeting CAFs need more specific biomarkers. Different subtypes of CAFs relate to the discrepant prognosis of pancreatic cancer patients (24, 28).

Cells in the TME interact with each other to co-construct a microenvironment suitable for tumor survival. CAFs conduct metabolic reprogramming to provide available metabolites to tumor cells (Table 2). Oxidative stressed-driven metabolic changes in CAFs are known as the reverse Warburg effect, manifested by glycolysis as the main mode of metabolism and increased utilization of glutamine. Multiple forms of crosstalk including direct contact, extracellular vesicles, paracrine and autophagy-dependent secretion between tumor cells and CAFs activate CAFs for fibrosis on the one hand and enhance tumor cells proliferation and migration on the other. Cellular communication also exists between adipocytes and other cells in the TME. Lipolysis occurs when adipocytes dedifferentiate into CAFs, which perhaps partially explains both the cachexia and desmoplasia.

Experimentally, depletion of CAFs proved to be an infeasible treatment. Reprogramming CAFs to a normal state or blocking signaling may be promising ways to target pancreatic cancer

TABLE 2 Summary of CAFs metabolic reprogramming.

Metabolism	Regulated factors		Effects on metabolism	Origin	Reference
	Types	Effects			
Glycolysis	HIF-1α and MCT4	Up-regulation	Increase lactate production and glucose intake	CAFs	(53)
	HK-2, PFKP and PKM2	Up-regulation		PSCs	(49)
	TOMM20 and NQO1	Down-regulation		PSCs	
	LDHA and PKM2	Up-regulation		CAFs	(57)
	miR-21	Up-regulation		CAFs	(58)
Glutamine metabolism	GLS1 and GLUD1	Up-regulation	Promote the production of glutamate and α-ketoglutarate	CAFs	(53)
	NetG1	Up-regulation	Promotes the secretion of glutamine and glutamate	CAFs	(61)
	glutamine synthetase	Up-regulation	Promotes the secretion of glutamine	PSCs	(142)
Alanine metabolism	SLC1A4	Up-regulation	Maintains alanine concentration in TME	PSCs	(65)
Branched-chain amino acid metabolism	BCAT1	Up-regulation	Increases the secretion of BCKAs	CAFs	(68)
Lipid metabolism	FABP4, PLIN1 and PLIN2	Down-regulation	Exhibit the remodeling of the intracellular lipidome	PSCs	(73)
	VLDLR	Up-regulation	Promotes lipoprotein uptake	PSCs	(74)

HIF-1α, hypoxia-inducible factor-1α; MCT4, monocarboxylate transporter 4; CAF, cancer-associated fibroblast; HK-2, hexokinase 2; PFKP, 6-phosphofructokinase; PKM2, pyruvate kinase isozyme type M2; PSC, pancreatic stellate cell; TOMM20, pyruvate kinase isozyme type M2; NQO1, NAD(P)H dehydrogenase [quinone] 1; LDHA, lactate dehydrogenase A; GLS1, glutaminase 1; GLUD1, glutamate dehydrogenase 1; NetG1, Netrin G1; TME, tumor microenvironment; BCAT1, branched-chain amino acid transaminase 1; BCKA, branched-chain α-keto acid; FABP4, fatty acid binding protein 4; PLIN1, perilipin 1; PLIN2, perilipin 2; VLDLR, very-low-density lipoprotein receptor.

fibrosis. In conclusion, CAFs are important targets to explain fibrosis and drug resistance in pancreatic cancer, but further studies on the heterogeneity of CAFs and the mechanisms of crosstalk are still needed to provide more basis for targeting CAFs for therapy.

Author contributions

The manuscript was written by XL, JZ, XW, ZM, CL and QW. XL and XW designed and made the figures. FP and JZ revised the manuscript. FP supported the study. All authors contributed to the article and approved the submitted version.

Funding

The study was supported by National Natural Science Foundation of China (no.82003879 and U19A2010), the Key Project of Science and Technology Department of Sichuan Province (no. 2020YFS0053; 2021YFS0044), and Youth Talent Promotion Project of China Association for Science and Technology (CACM-2020-QNRC1-01) and Project of State Administration of Traditional Chinese Medicine of China (ZYYCXTD-D-202209).

Conflict of interest

The authors declare that the research was conducted in the absence of any commercial or financial relationships that could be construed as a potential conflict of interest.

Publisher's note

References

1. Klein AP. Pancreatic cancer epidemiology: understanding the role of lifestyle and inherited risk factors. *Nat Rev Gastroenterol Hepatol* (2021) 18(7):493–502. doi: 10.1038/s41575-021-00457-x

2. Jungmann F, Kaissis GA, Ziegelmayer S, Harder F, Schilling C, Yen HY, et al. Prediction of tumor cellularity in resectable PDAC from preoperative computed tomography imaging. *Cancers (Basel)* (2021) 13(9):2069. doi: 10.3390/cancers13092069

3. Quoc Lam B, Shrivastava SK, Shrivastava A, Shankar S, Srivastava RK. The impact of obesity and diabetes mellitus on pancreatic cancer: Molecular mechanisms and clinical perspectives. *J Cell Mol Med* (2020) 24(14):7706–16. doi: 10.1111/jcmm.15413

4. Mukherjee AG, Wanjari UR, Gopalakrishnan AV, Bradu P, Sukumar A, Patil M, et al. Implications of cancer stem cells in diabetes and pancreatic cancer. *Life Sci* (2023) 312:121211. doi: 10.1016/j.lfs.2022.121211

5. Andersen DK, Korc M, Petersen GM, Eibl G, Li D, Rickels MR, et al. Diabetes, pancreatogenic diabetes, and pancreatic cancer. *Diabetes* (2017) 66(5):1103–10. doi: 10.2337/db16-1477

6. Mizrahi JD, Surana R, Valle JW, Shroff RT. Pancreatic cancer. *Lancet* (2020) 395 (10242):2008–20. doi: 10.1016/S0140-6736(20)30974-0

7. Jiang S, Fagman JB, Ma Y, Liu J, Vihav C, Engstrom C, et al. A comprehensive review of pancreatic cancer and its therapeutic challenges. *Aging (Albany NY)* (2022) 14 (18):7635–49. doi: 10.18632/aging.204310

8. Wood LD, Canto MI, Jaffee EM, Simeone DM. Pancreatic cancer: Pathogenesis, screening, diagnosis, and treatment. *Gastroenterology* (2022) 163(2):386–402.e381. doi: 10.1053/j.gastro.2022.03.056

9. Affo S, Yu LX, Schwabe RF. The role of cancer-associated fibroblasts and fibrosis in liver cancer. *Annu Rev Pathol* (2017) 12:153–86. doi: 10.1146/annurev-pathol-052016-100322

10. Kinoshita T, Goto T. Molecular mechanisms of pulmonary fibrogenesis and its progression to lung cancer: A review. *Int J Mol Sci* (2019) 20(6):1461. doi: 10.3390/ijms20061461

11. Huang C, Iovanna J, Santofimia-Castaño P. Targeting fibrosis: The bridge that connects pancreatitis and pancreatic cancer. *Int J Mol Sci* (2021) 22(9):4970. doi: 10.3390/ijms22094970

12. Abbas O, Mahalingam M. Desmoplasia: not always a bad thing. *Histopathology* (2011) 58(5):643–59. doi: 10.1111/j.1365-2559.2010.03617.x

13. Weniger M, Honselmann KC, Liss AS. The extracellular matrix and pancreatic cancer: A complex relationship. *Cancers (Basel)* (2018) 10(9):316. doi: 10.3390/cancers10090316

14. Dvorak HF. Tumors: wounds that do not heal-redux. *Cancer Immunol Res* (2015) 3(1):1–11. doi: 10.1158/2326-6066.CIR-14-0209

15. Tracy LE, Minasian RA, Caterson EJ. Extracellular matrix and dermal fibroblast function in the healing wound. *Adv Wound Care (New Rochelle)* (2016) 5(3):119–36. doi: 10.1089/wound.2014.0561

16. McCarroll JA, Naim S, Sharbeen G, Russia N, Lee J, Kavallaris M, et al. Role of pancreatic stellate cells in chemoresistance in pancreatic cancer. *Front Physiol* (2014) 5:141. doi: 10.3389/fphys.2014.00141

17. Feig C, Gopinathan A, Neesse A, Chan DS, Cook N, Tuveson DA. The pancreas cancer microenvironment. *Clin Cancer Res* (2012) 18(16):4266–76. doi: 10.1158/1078-0432.CCR-11-3114

18. Thomas D, Radhakrishnan P. Tumor-stromal crosstalk in pancreatic cancer and tissue fibrosis. *Mol Cancer* (2019) 18(1):14. doi: 10.1186/s12943-018-0927-5

19. Liao Z, Tan ZW, Zhu P, Tan NS. Cancer-associated fibroblasts in tumor microenvironment - accomplices in tumor malignancy. *Cell Immunol* (2019) 343:103729. doi: 10.1016/j.cellimm.2017.12.003

20. Mhaidly R, Mechta-Grigoriou F. Role of cancer-associated fibroblast subpopulations in immune infiltration, as a new means of treatment in cancer. *Immunol Rev* (2021) 302(1):259–72. doi: 10.1111/imr.12978

21. Öhlund D, Handly-Santana A, Biffi G, Elyada E, Almeida AS, Ponz-Sarvise M, et al. Distinct populations of inflammatory fibroblasts and myofibroblasts in pancreatic cancer. *J Exp Med* (2017) 214(3):579–96. doi: 10.1084/jem.20162024

22. Dings MPG, Manoukian P, Waasdorp C, Quik JSE, Strijker M, Lodestijn SC, et al. Serum levels of iCAF-derived osteoglycin predict favorable outcome in pancreatic cancer. *Int J Cancer* (2023) 152(3):511–23. doi: 10.1002/ijc.34276

23. Elyada E, Bolisetty M, Laise P, Flynn WF, Courtois ET, Burkhart RA, et al. Cross-species single-cell analysis of pancreatic ductal adenocarcinoma reveals antigen-presenting cancer-associated fibroblasts. *Cancer Discovery* (2019) 9(8):1102–23. doi: 10.1158/2159-8290.CD-19-0094

24. Wang Y, Liang Y, Xu H, Zhang X, Mao T, Cui J, et al. Single-cell analysis of pancreatic ductal adenocarcinoma identifies a novel fibroblast subtype associated with poor prognosis but better immunotherapy response. *Cell Discovery* (2021) 7(1):36. doi: 10.1038/s41421-021-00271-4

25. Chen K, Wang Q, Li M, Guo H, Liu W, Wang F, et al. Single-cell RNA-seq reveals dynamic change in tumor microenvironment during pancreatic ductal adenocarcinoma malignant progression. *EBioMedicine* (2021) 66:103315. doi: 10.1016/j.ebiom.2021.103315

26. Biffi G, Oni TE, Spielman B, Hao Y, Elyada E, Park Y, et al. IL1-induced JAK/STAT signaling is antagonized by TGFβ to shape CAF heterogeneity in pancreatic ductal adenocarcinoma. *Cancer Discovery* (2019) 9(2):282–301. doi: 10.1158/2159-8290.CD-18-0710

27. Steele NG, Biffi G, Kemp SB, Zhang Y, Drouillard D, Syu L, et al. Inhibition of hedgehog signaling alters fibroblast composition in pancreatic cancer. *Clin Cancer Res* (2021) 27(7):2023–37. doi: 10.1158/1078-0432.CCR-20-3715

28. Hu B, Wu C, Mao H, Gu H, Dong H, Yan J, et al. Subpopulations of cancer-associated fibroblasts link the prognosis and metabolic features of pancreatic ductal adenocarcinoma. *Ann Transl Med* (2022) 10(5):262. doi: 10.21037/atm-22-407

29. Neuzillet C, Tijeras-Raballand A, Ragulan C, Cros J, Patil Y, Martinet M, et al. Inter- and intra-tumoural heterogeneity in cancer-associated fibroblasts of human pancreatic ductal adenocarcinoma. *J Pathol* (2019) 248(1):51–65. doi: 10.1002/path.5224

30. Neuzillet C, Nicolle R, Raffenne J, Tijeras-Raballand A, Brunel A, Astorgues-Xerri L, et al. Periostin- and podoplanin-positive cancer-associated fibroblast subtypes cooperate to shape the inflamed tumor microenvironment in aggressive pancreatic adenocarcinoma. *J Pathol* (2022) 258(4):408–25. doi: 10.1002/path.6011

31. Desbois M, Wang Y. Cancer-associated fibroblasts: Key players in shaping the tumor immune microenvironment. *Immunol Rev* (2021) 302(1):241–58. doi: 10.1111/imr.12982

32. Zheng S, Hu C, Lin H, Li G, Xia R, Zhang X, et al. circCUL2 induces an inflammatory CAF phenotype in pancreatic ductal adenocarcinoma *via* the activation of the MyD88-dependent NF-κB signaling pathway. *J Exp Clin Cancer Res* (2022) 41 (1):71. doi: 10.1186/s13046-021-02237-6

33. Huang H, Wang Z, Zhang Y, Pradhan RN, Ganguly D, Chandra R, et al. Mesothelial cell-derived antigen-presenting cancer-associated fibroblasts induce expansion of regulatory T cells in pancreatic cancer. *Cancer Cell* (2022) 40(6):656–673.e657. doi: 10.1016/j.ccell.2022.04.011

34. Helms EJ, Berry MW, Chaw RC, DuFort CC, Sun D, Onate MK, et al. Mesenchymal lineage heterogeneity underlies nonredundant functions of pancreatic cancer-associated fibroblasts. *Cancer Discovery* (2022) 12(2):484–501. doi: 10.1158/2159-8290.CD-21-0601

35. Watari N, Hotta Y, Mabuchi Y. Morphological studies on a vitamin a-storing cell and its complex with macrophage observed in mouse pancreatic tissues following excess vitamin a administration. *Okajimas Folia Anat Jpn* (1982) 58(4-6):837–58. doi: 10.2535/ofaj1936.58.4-6_837

36. Zhou Y, Zhou J, Sun B, Xu W, Zhong M, Li Y, et al. Vitamin a deficiency causes islet dysfunction by inducing islet stellate cell activation *via* cellular retinol binding protein 1. *Int J Biol Sci* (2020) 16(6):947–56. doi: 10.7150/ijbs.37861

37. Apte MV, Haber PS, Darby SJ, Rodgers SC, McCaughan GW, Korsten MA, et al. Pancreatic stellate cells are activated by proinflammatory cytokines: implications for pancreatic fibrogenesis. *Gut* (1999) 44(4):534–41. doi: 10.1136/gut.44.4.534

38. Xu XF, Liu F, Xin JQ, Fan JW, Wu N, Zhu LJ, et al. Respective roles of the mitogen-activated protein kinase (MAPK) family members in pancreatic stellate cell activation induced by transforming growth factor-β1 (TGF-β1). *Biochem Biophys Res Commun* (2018) 501(2):365–73. doi: 10.1016/j.bbrc.2018.04.176

39. Zheng M, Li H, Sun L, Brigstock DR, Gao R. Interleukin-6 participates in human pancreatic stellate cell activation and collagen I production *via* TGF-β1/Smad pathway. *Cytokine* (2021) 143:155536. doi: 10.1016/j.cyto.2021.155536

40. Ng B, Viswanathan S, Widjaja AA, Lim WW, Shekeran SG, Goh JWT, et al. IL11 activates pancreatic stellate cells and causes pancreatic inflammation, fibrosis and atrophy in a mouse model of pancreatitis. *Int J Mol Sci* (2022) 23(7):3549. doi: 10.3390/ijms23073549

41. Vaupel P, Schmidberger H, Mayer A. The warburg effect: essential part of metabolic reprogramming and central contributor to cancer progression. *Int J Radiat Biol* (2019) 95(7):912–9. doi: 10.1080/09553002.2019.1589653

42. Vaupel P, Multhoff G. Revisiting the warburg effect: historical dogma versus current understanding. *J Physiol* (2021) 599(6):1745–57. doi: 10.1113/JP278810

43. Zhu Y, Li X, Wang L, Hong X, Yang J. Metabolic reprogramming and crosstalk of cancer-related fibroblasts and immune cells in the tumor microenvironment. *Front Endocrinol (Lausanne)* (2022) 13:988295. doi: 10.3389/fendo.2022.988295

44. Nagao A, Kobayashi M, Koyasu S, Chow CCT, Harada H. HIF-1-Dependent reprogramming of glucose metabolic pathway of cancer cells and its therapeutic significance. *Int J Mol Sci* (2019) 20(2:238). doi: 10.3390/ijms20020238

45. Wang GL, Jiang BH, Rue EA, Semenza GL. Hypoxia-inducible factor 1 is a basic-helix-loop-helix-PAS heterodimer regulated by cellular O2 tension. *Proc Natl Acad Sci U.S.A.* (1995) 92(12):5510–4. doi: 10.1073/pnas.92.12.5510

46. Ratcliffe PJ, O'Rourke JF, Maxwell PH, Pugh CW. Oxygen sensing, hypoxia-inducible factor-1 and the regulation of mammalian gene expression. *J Exp Biol* (1998) 201(Pt 8):1153–62. doi: 10.1242/jeb.201.8.1153

47. Capparelli C, Whitaker-Menezes D, Guido C, Balliet R, Pestell TG, Howell A, et al. CTGF drives autophagy, glycolysis and senescence in cancer-associated fibroblasts *via* HIF1 activation, metabolically promoting tumor growth. *Cell Cycle* (2012) 11 (12):2272–84. doi: 10.4161/cc.20717

48. Arcucci A, Ruocco MR, Granato G, Sacco AM, Montagnani S. Cancer: An oxidative crosstalk between solid tumor cells and cancer associated fibroblasts. *BioMed Res Int* (2016) 2016:4502846. doi: 10.1155/2016/4502846

49. Shao S, Qin T, Qian W, Yue Y, Xiao Y, Li X, et al. Positive feedback in cav-1-ROS signalling in PSCs mediates metabolic coupling between PSCs and tumour cells. *J Cell Mol Med* (2020) 24(16):9397–408. doi: 10.1111/jcmm.15596

50. Pavlides S, Whitaker-Menezes D, Castello-Cros R, Flomenberg N, Witkiewicz AK, Frank PG, et al. The reverse warburg effect: aerobic glycolysis in cancer associated fibroblasts and the tumor stroma. *Cell Cycle* (2009) 8(23):3984–4001. doi: 10.4161/cc.8.23.10238

51. Chiarugi P, Cirri P. Metabolic exchanges within tumor microenvironment. *Cancer Lett* (2016) 380(1):272–80. doi: 10.1016/j.canlet.2015.10.027

52. Avagliano A, Granato G, Ruocco MR, Romano V, Belviso I, Carfora A, et al. Metabolic reprogramming of cancer associated fibroblasts: The slavery of stromal fibroblasts. *BioMed Res Int* (2018) 2018:6075403. doi: 10.1155/2018/6075403

53. Knudsen ES, Balaji U, Freinkman E, McCue P, Witkiewicz AK. Unique metabolic features of pancreatic cancer stroma: relevance to the tumor compartment, prognosis, and invasive potential. *Oncotarget* (2016) 7(48):78396–411. doi: 10.18632/oncotarget.11893

54. Kierans SJ, Taylor CT. Regulation of glycolysis by the hypoxia-inducible factor (HIF): implications for cellular physiology. *J Physiol* (2021) 599(1):23–37. doi: 10.1113/JP280572

55. Payen VL, Mina E, Van Hée VF, Porporato PE, Sonveaux P. Monocarboxylate transporters in cancer. *Mol Metab* (2020) 33:48–66. doi: 10.1016/j.molmet.2019.07.006

56. Halestrap AP. The SLC16 gene family - structure, role and regulation in health and disease. *Mol Aspects Med* (2013) 34(2-3):337–49. doi: 10.1016/j.mam.2012.05.003

57. Shan T, Chen S, Chen X, Lin WR, Li W, Ma J, et al. Cancer-associated fibroblasts enhance pancreatic cancer cell invasion by remodeling the metabolic conversion mechanism. *Oncol Rep* (2017) 37(4):1971–9. doi: 10.3892/or.2017.5479

58. Chen S, Chen X, Shan T, Ma J, Lin W, Li W, et al. MiR-21-mediated metabolic alteration of cancer-associated fibroblasts and its effect on pancreatic cancer cell behavior. *Int J Biol Sci* (2018) 14(1):100–10. doi: 10.7150/ijbs.22555

59. Qin C, Yang G, Yang J, Ren B, Wang H, Chen G, et al. Metabolism of pancreatic cancer: paving the way to better anticancer strategies. *Mol Cancer* (2020) 19(1):50. doi: 10.1186/s12943-020-01169-7

60. Son J, Lyssiotis CA, Ying H, Wang X, Hua S, Ligorio M, et al. Glutamine supports pancreatic cancer growth through a KRAS-regulated metabolic pathway. *Nature* (2013) 496(7443):101–5. doi: 10.1038/nature12040

61. Francescone R, Barbosa Vendramini-Costa D, Franco-Barraza J, Wagner J, Muir A, Lau AN, et al. Netrin G1 promotes pancreatic tumorigenesis through cancer-associated fibroblast-driven nutritional support and immunosuppression. *Cancer Discovery* (2021) 11(2):446–79. doi: 10.1158/2159-8290.CD-20-0775

62. Liu H, Zhang H, Liu X, Guo W, Liu Q, Chen L, et al. Pancreatic stellate cells exploit wnt/β-catenin/TCF7-mediated glutamine metabolism to promote pancreatic cancer cells growth. *Cancer Lett* (2022) 555:216040. doi: 10.1016/j.canlet.2022.216040

63. Sousa CM, Biancur DE, Wang X, Halbrook CJ, Sherman MH, Zhang L, et al. Pancreatic stellate cells support tumour metabolism through autophagic alanine secretion. *Nature* (2016) 536(7617):479–83. doi: 10.1038/nature19084

64. Zhang Y, Recouvreux MV, Jung M, Galenkamp KMO, Li Y, Zagnitko O, et al. Macropinocytosis in cancer-associated fibroblasts is dependent on CaMKK2/ARHGEF2 signaling and functions to support tumor and stromal cell fitness. *Cancer Discovery* (2021) 11(7):1808–25. doi: 10.1158/2159-8290.CD-20-0119

65. Parker SJ, Amendola CR, Hollinshead KER, Yu Q, Yamamoto K, Encarnación-Rosado J, et al. Selective alanine transporter utilization creates a targetable metabolic niche in pancreatic cancer. *Cancer Discovery* (2020) 10(7):1018–37. doi: 10.1158/2159-8290.CD-19-0959

66. Sivanand S, Vander Heiden MG. Emerging roles for branched-chain amino acid metabolism in cancer. *Cancer Cell* (2020) 37(2):147–56. doi: 10.1016/j.ccell.2019.12.011

67. Peng H, Wang Y, Luo W. Multifaceted role of branched-chain amino acid metabolism in cancer. *Oncogene* (2020) 39(44):6747–56. doi: 10.1038/s41388-020-01480-z

68. Zhu Z, Achreja A, Meurs N, Animasahun O, Owen S, Mittal A, et al. Tumour-reprogrammed stromal BCAT1 fuels branched-chain ketoacid dependency in stromal-rich PDAC tumours. *Nat Metab* (2020) 2(8):775–92. doi: 10.1038/s42255-020-0226-5

69. Bian X, Liu R, Meng Y, Xing D, Xu D, Lu Z. Lipid metabolism and cancer. *J Exp Med* (2021) 218(1):e20201606. doi: 10.1084/jem.20201606

70. Nardi F, Fitchev P, Franco OE, Ivanisevic J, Scheibler A, Hayward SW, et al. PEDF regulates plasticity of a novel lipid-MTOC axis in prostate cancer-associated fibroblasts. *J Cell Sci* (2018) 131(13):jcs213579. doi: 10.1242/jcs.213579

71. Gong J, Lin Y, Zhang H, Liu C, Cheng Z, Yang X, et al. Reprogramming of lipid metabolism in cancer-associated fibroblasts potentiates migration of colorectal cancer cells. *Cell Death Dis* (2020) 11(4):267. doi: 10.1038/s41419-020-2434-z

72. Hwang SH, Yang Y, Jung JH, Kim Y. Oleic acid from cancer-associated fibroblast promotes cancer cell stemness by stearoyl-CoA desaturase under glucose-deficient condition. *Cancer Cell Int* (2022) 22(1):404. doi: 10.1186/s12935-022-02824-3

73. Auciello FR, Bulusu V, Oon C, Tait-Mulder J, Berry M, Bhattacharyya S, et al. A stromal lysolipid-autotaxin signaling axis promotes pancreatic tumor progression. *Cancer Discovery* (2019) 9(5):617–27. doi: 10.1158/2159-8290.CD-18-1212

74. Yang X, Chen J, Wang J, Ma S, Feng W, Wu Z, et al. Very-low-density lipoprotein receptor-enhanced lipid metabolism in pancreatic stellate cells promotes pancreatic fibrosis. *Immunity* (2022) 55(7):1185–1199.e1188. doi: 10.1016/j.immuni.2022.06.001

75. Chang CH, Pauklin S. Extracellular vesicles in pancreatic cancer progression and therapies. *Cell Death Dis* (2021) 12(11):973. doi: 10.1038/s41419-021-04258-7

76. Urabe F, Kosaka N, Ito K, Kimura T, Egawa S, Ochiya T. Extracellular vesicles as biomarkers and therapeutic targets for cancer. *Am J Physiol Cell Physiol* (2020) 318(1):C29–c39. doi: 10.1152/ajpcell.00280.2019

77. Dai J, Su Y, Zhong S, Cong L, Liu B, Yang J, et al. Exosomes: key players in cancer and potential therapeutic strategy. *Signal Transduct Target Ther* (2020) 5(1):145. doi: 10.1038/s41392-020-00261-0

78. Brosseau C, Colas L, Magnan A, Brouard S. CD9 tetraspanin: A new pathway for the regulation of inflammation? *Front Immunol* (2018) 9:2316. doi: 10.3389/fimmu.2018.02316

79. Nigri J, Leca J, Tubiana SS, Finetti P, Guillaumond F, Martinez S, et al. CD9 mediates the uptake of extracellular vesicles from cancer-associated fibroblasts that promote pancreatic cancer cell aggressiveness. *Sci Signal* (2022) 15(745):eabg8191. doi: 10.1126/scisignal.abg8191

80. Chang WH, Nguyen TT, Hsu CH, Bryant KL, Kim HJ, Ying H, et al. KRAS-dependent cancer cells promote survival by producing exosomes enriched in survivin. *Cancer Lett* (2021) 517:66–77. doi: 10.1016/j.canlet.2021.05.031

81. Masamune A, Yoshida N, Hamada S, Takikawa T, Nabeshima T, Shimosegawa T. Exosomes derived from pancreatic cancer cells induce activation and profibrogenic activities in pancreatic stellate cells. *Biochem Biophys Res Commun* (2018) 495(1):71–7. doi: 10.1016/j.bbrc.2017.10.141

82. Wang HC, Lin YL, Hsu CC, Chao YJ, Hou YC, Chiu TJ, et al. Pancreatic stellate cells activated by mutant KRAS-mediated PAI-1 upregulation foster pancreatic cancer progression *via* IL-8. *Theranostics* (2019) 9(24):7168–83. doi: 10.7150/thno.36830

83. Rossi Sebastiano M, Pozzato C, Saliakoura M, Yang Z, Peng RW, Galiè M, et al. ACSL3-PAI-1 signaling axis mediates tumor-stroma cross-talk promoting pancreatic cancer progression. *Sci Adv* (2020) 6(44):eabb9200. doi: 10.1126/sciadv.abb9200

84. Yu L, Li JJ, Liang XL, Wu H, Liang Z. PSME3 promotes TGFB1 secretion by pancreatic cancer cells to induce pancreatic stellate cell proliferation. *J Cancer* (2019) 10(9):2128–38. doi: 10.7150/jca.30235

85. Heneberg P. Paracrine tumor signaling induces transdifferentiation of surrounding fibroblasts. *Crit Rev Oncol Hematol* (2016) 97:303–11. doi: 10.1016/j.critrevonc.2015.09.008

86. Hu C, Yang J, Su HY, Waldron RT, Zhi M, Li L, et al. Yes-associated protein 1 plays major roles in pancreatic stellate cell activation and fibroinflammatory responses. *Front Physiol* (2019) 10:1467. doi: 10.3389/fphys.2019.01467

87. Tang D, Wu Q, Zhang J, Zhang H, Yuan Z, Xu J, et al. Galectin-1 expression in activated pancreatic satellite cells promotes fibrosis in chronic pancreatitis/pancreatic cancer *via* the TGF-β1/Smad pathway. *Oncol Rep* (2018) 39(3):1347–55. doi: 10.3892/or.2018.6202

88. Orozco CA, Martinez-Bosch N, Guerrero PE, Vinaixa J, Dalotto-Moreno T, Iglesias M, et al. Targeting galectin-1 inhibits pancreatic cancer progression by modulating tumor-stroma crosstalk. *Proc Natl Acad Sci U.S.A.* (2018) 115(16):E3769–e3778. doi: 10.1073/pnas.1722434115

89. Wu X, Qian L, Zhao H, Lei W, Liu Y, Xu X, et al. CXCL12/CXCR4: An amazing challenge and opportunity in the fight against fibrosis. *Ageing Res Rev* (2023) 83:101809. doi: 10.1016/j.arr.2022.101809

90. Bhagat TD, Von Ahrens D, Dawlaty M, Zou Y, Baddour J, Achreja A, et al. Lactate-mediated epigenetic reprogramming regulates formation of human pancreatic cancer-associated fibroblasts. *Elife* (2019) 8:e50663. doi: 10.7554/eLife.50663

91. Wei L, Ye H, Li G, Lu Y, Zhou Q, Zheng S, et al. Cancer-associated fibroblasts promote progression and gemcitabine resistance *via* the SDF-1/SATB-1 pathway in pancreatic cancer. *Cell Death Dis* (2018) 9(11):1065. doi: 10.1038/s41419-018-1104-x

92. Zhao T, Xiao D, Jin F, Sun X, Yu J, Wang H, et al. ESE3-positive PSCs drive pancreatic cancer fibrosis, chemoresistance and poor prognosis *via* tumour-stromal IL-1β/NF-κB/ESE3 signalling axis. *Br J Cancer* (2022) 127(8):1461–72. doi: 10.1038/s41416-022-01927-y

93. Zhang D, Li L, Jiang H, Li Q, Wang-Gillam A, Yu J, et al. Tumor-stroma IL1β-IRAK4 feedforward circuitry drives tumor fibrosis, chemoresistance, and poor prognosis in pancreatic cancer. *Cancer Res* (2018) 78(7):1700–12. doi: 10.1158/0008-5472.CAN-17-1366

94. Cao W, Li J, Yang K, Cao D. An overview of autophagy: Mechanism, regulation and research progress. *Bull Cancer* (2021) 108(3):304–22. doi: 10.1016/j.bulcan.2020.11.004

95. New J, Thomas SM. Autophagy-dependent secretion: mechanism, factors secreted, and disease implications. *Autophagy* (2019) 15(10):1682–93. doi: 10.1080/15548627.2019.1596479

96. Endo S, Nakata K, Ohuchida K, Takesue S, Nakayama H, Abe T, et al. Autophagy is required for activation of pancreatic stellate cells, associated with pancreatic cancer progression and promotes growth of pancreatic tumors in mice. *Gastroenterology* (2017) 152(6):1492–1506.e1424. doi: 10.1053/j.gastro.2017.01.010

97. Jena BC, Das CK, Banerjee I, Bharadwaj D, Majumder R, Das S, et al. TGF-β1 induced autophagy in cancer associated fibroblasts during hypoxia contributes EMT and glycolysis *via* MCT4 upregulation. *Exp Cell Res* (2022) 417(1):113195. doi: 10.1016/j.yexcr.2022.113195

98. Yuan M, Tu B, Li H, Pang H, Zhang N, Fan M, et al. Cancer-associated fibroblasts employ NUFIP1-dependent autophagy to secrete nucleosides and support pancreatic tumor growth. *Nat Cancer* (2022) 3(8):945–60. doi: 10.1038/s43018-022-00426-6

99. Bai J, Liu T, Tu B, Yuan M, Shu Z, Fan M, et al. Autophagy loss impedes cancer-associated fibroblast activation *via* downregulating proline biosynthesis. *Autophagy* (2023) 19(2):632–43. doi: 10.1080/15548627.2022.2093026

100. Geng X, Li L, Luo Y, Yang W, Hu J, Zhao Z, et al. Tumor cell derived lnc-FSD2-31:1 contributes to cancer-associated fibroblasts activation in pancreatic ductal adenocarcinoma progression through extracellular vesicles cargo MiR-4736. *Adv Sci (Weinh)* (2023)2023:e2203324. doi: 10.1002/advs.202203324

101. Piersma B, Hayward MK, Weaver VM. Fibrosis and cancer: A strained relationship. *Biochim Biophys Acta Rev Cancer* (2020) 1873(2):188356. doi: 10.1016/j.bbcan.2020.188356

102. Zhang Z, Zhang H, Shi L, Wang D, Tang D. Heterogeneous cancer-associated fibroblasts: A new perspective for understanding immunosuppression in pancreatic cancer. *Immunology* (2022) 167(1):1–14. doi: 10.1111/imm.13496

103. Tanaka N, Yamada S, Sonohara F, Suenaga M, Hayashi M, Takami H, et al. Clinical implications of lysyl oxidase-like protein 2 expression in pancreatic cancer. *Sci Rep* (2018) 8(1):9846. doi: 10.1038/s41598-018-28253-9

104. Tjomsland V, Pomianowska E, Aasrum M, Sandnes D, Verbeke CS, Gladhaug IP. Profile of MMP and TIMP expression in human pancreatic stellate cells: Regulation by IL-1α and TGFβ and implications for migration of pancreatic cancer cells. *Neoplasia* (2016) 18(7):447–56. doi: 10.1016/j.neo.2016.06.003

105. Kuo TL, Cheng KH, Shan YS, Chen LT, Hung WC. β-catenin-activated autocrine PDGF/Src signaling is a therapeutic target in pancreatic cancer. *Theranostics* (2019) 9(2):324–36. doi: 10.7150/thno.28201

106. Yu Y, Cheng L, Yan B, Zhou C, Qian W, Xiao Y, et al. Overexpression of gremlin 1 by sonic hedgehog signaling promotes pancreatic cancer progression. *Int J Oncol* (2018) 53(6):2445–57. doi: 10.3892/ijo.2018.4573

107. Awaji M, Futakuchi M, Heavican T, Iqbal J, Singh RK. Cancer-associated fibroblasts enhance survival and progression of the aggressive pancreatic tumor *Via* FGF-2 and CXCL8. *Cancer Microenviron* (2019) 12(1):37–46. doi: 10.1007/s12307-019-00223-3

108. Awaji M, Saxena S, Wu L, Prajapati DR, Purohit A, Varney ML, et al. CXCR2 signaling promotes secretory cancer-associated fibroblasts in pancreatic ductal adenocarcinoma. *FASEB J* (2020) 34(7):9405–18. doi: 10.1096/fj.201902990R

109. Pang W, Su J, Wang Y, Feng H, Dai X, Yuan Y, et al. Pancreatic cancer-secreted miR-155 implicates in the conversion from normal fibroblasts to cancer-associated fibroblasts. *Cancer Sci* (2015) 106(10):1362–9. doi: 10.1111/cas.12747

110. Zhang YF, Zhou YZ, Zhang B, Huang SF, Li PP, He XM, et al. Pancreatic cancer-derived exosomes promoted pancreatic stellate cells recruitment by pancreatic cancer. *J Cancer* (2019) 10(18):4397–407. doi: 10.7150/jca.27590

111. Charrier A, Chen R, Chen L, Kemper S, Hattori T, Takigawa M, et al. Connective tissue growth factor (CCN2) and microRNA-21 are components of a positive feedback loop in pancreatic stellate cells (PSC) during chronic pancreatitis and are exported in PSC-derived exosomes. *J Cell Commun Signal* (2014) 8(2):147–56. doi: 10.1007/s12079-014-0220-3

112. Rebours V, Gaujoux S, d'Assignies G, Sauvanet A, Ruszniewski P, Lévy P, et al. Obesity and fatty pancreatic infiltration are risk factors for pancreatic precancerous lesions (PanIN). *Clin Cancer Res* (2015) 21(15):3522–8. doi: 10.1158/1078-0432.CCR-14-2385

113. Yu SY, Luan Y, Dong R, Abazarikia A, Kim SY. Adipose tissue wasting as a determinant of pancreatic cancer-related cachexia. *Cancers (Basel)* (2022) 14(19):4754. doi: 10.3390/cancers14194754

114. Himbert C, Delphan M, Scherer D, Bowers LW, Hursting S, Ulrich CM. Signals from the adipose microenvironment and the obesity-cancer link-a systematic review. *Cancer Prev Res (Phila)* (2017) 10(9):494–506. doi: 10.1158/1940-6207.CAPR-16-0322

115. Lee MJ, Wu Y, Fried SK. Adipose tissue heterogeneity: implication of depot differences in adipose tissue for obesity complications. *Mol Aspects Med* (2013) 34(1):1–11. doi: 10.1016/j.mam.2012.10.001

116. Sagar G, Sah RP, Javeed N, Dutta SK, Smyrk TC, Lau JS, et al. Pathogenesis of pancreatic cancer exosome-induced lipolysis in adipose tissue. *Gut* (2016) 65(7):1165–74. doi: 10.1136/gutjnl-2014-308350

117. Cai Z, Liang Y, Xing C, Wang H, Hu P, Li J, et al. Cancer–associated adipocytes exhibit distinct phenotypes and facilitate tumor progression in pancreatic cancer. *Oncol Rep* (2019) 42(6):2537–49. doi: 10.3892/or.2019.7365

118. Takehara M, Sato Y, Kimura T, Noda K, Miyamoto H, Fujino Y, et al. Cancer-associated adipocytes promote pancreatic cancer progression through SAA1 expression. *Cancer Sci* (2020) 111(8):2883–94. doi: 10.1111/cas.14527

119. Zoico E, Darra E, Rizzatti V, Budui S, Franceschetti G, Mazzali G, et al. Adipocytes WNT5a mediated dedifferentiation: a possible target in pancreatic cancer microenvironment. *Oncotarget* (2016) 7(15):20223–35. doi: 10.18632/oncotarget.7936

120. Okumura T, Ohuchida K, Kibe S, Iwamoto C, Ando Y, Takesue S, et al. Adipose tissue-derived stromal cells are sources of cancer-associated fibroblasts and enhance tumor progression by dense collagen matrix. *Int J Cancer* (2019) 144(6):1401–13. doi: 10.1002/ijc.31775

121. Ganguly K, Cox JL, Ghersi D, Grandgenett PM, Hollingsworth MA, Jain M, et al. Mucin 5AC-mediated CD44/ITGB1 clustering mobilizes adipose-derived mesenchymal stem cells to modulate pancreatic cancer stromal heterogeneity. *Gastroenterology* (2022) 162(7):2032–2046.e2012. doi: 10.1053/j.gastro.2022.02.032

122. Xu PC, You M, Yu SY, Luan Y, Eldani M, Caffrey TC, et al. Visceral adipose tissue remodeling in pancreatic ductal adenocarcinoma cachexia: the role of activin a signaling. *Sci Rep* (2022) 12(1):1659. doi: 10.1038/s41598-022-05660-7

123. Incio J, Liu H, Suboj P, Chin SM, Chen IX, Pinter M, et al. Obesity-induced inflammation and desmoplasia promote pancreatic cancer progression and resistance to chemotherapy. *Cancer Discovery* (2016) 6(8):852–69. doi: 10.1158/2159-8290.CD-15-1177

124. Sahai E, Astsaturov I, Cukierman E, DeNardo DG, Egeblad M, Evans RM, et al. A framework for advancing our understanding of cancer-associated fibroblasts. *Nat Rev Cancer* (2020) 20(3):174–86. doi: 10.1038/s41568-019-0238-1

125. Özdemir BC, Pentcheva-Hoang T, Carstens JL, Zheng X, Wu CC, Simpson TR, et al. Depletion of carcinoma-associated fibroblasts and fibrosis induces immunosuppression and accelerates pancreas cancer with reduced survival. *Cancer Cell* (2014) 25(6):719–34. doi: 10.1016/j.ccr.2014.04.005

126. Rhim AD, Oberstein PE, Thomas DH, Mirek ET, Palermo CF, Sastra SA, et al. Stromal elements act to restrain, rather than support, pancreatic ductal adenocarcinoma. *Cancer Cell* (2014) 25(6):735–47. doi: 10.1016/j.ccr.2014.04.021

127. Schnittert J, Heinrich MA, Kuninty PR, Storm G, Prakash J. Reprogramming tumor stroma using an endogenous lipid lipoxin A4 to treat pancreatic cancer. *Cancer Lett* (2018) 420:247–58. doi: 10.1016/j.canlet.2018.01.072

128. Guan J, Zhang H, Wen Z, Gu Y, Cheng Y, Sun Y, et al. Retinoic acid inhibits pancreatic cancer cell migration and EMT through the downregulation of IL-6 in cancer associated fibroblast cells. *Cancer Lett* (2014) 345(1):132–9. doi: 10.1016/j.canlet.2013.12.006

129. Zhao T, Zhang R, He Q, Zhou H, Song X, Gong T, et al. Partial ligand shielding nanoparticles improve pancreatic ductal adenocarcinoma treatment *via* a multifunctional paradigm for tumor stroma reprogramming. *Acta Biomater* (2022) 145:122–34. doi: 10.1016/j.actbio.2022.03.050

130. Xiao Y, Zhang H, Ma Q, Huang R, Lu J, Liang X, et al. YAP1-mediated pancreatic stellate cell activation inhibits pancreatic cancer cell proliferation. *Cancer Lett* (2019) 462:51–60. doi: 10.1016/j.canlet.2019.07.015

131. Sherman MH, Yu RT, Engle DD, Ding N, Atkins AR, Tiriac H, et al. Vitamin d receptor-mediated stromal reprogramming suppresses pancreatitis and enhances pancreatic cancer therapy. *Cell* (2014) 159(1):80–93. doi: 10.1016/j.cell.2014.08.007

132. Mukai Y, Yamada D, Eguchi H, Iwagami Y, Asaoka T, Noda T, et al. Vitamin d supplementation is a promising therapy for pancreatic ductal adenocarcinoma in conjunction with current chemoradiation therapy. *Ann Surg Oncol* (2018) 25(7):1868–79. doi: 10.1245/s10434-018-6431-8

133. Saison-Ridinger M, DelGiorno KE, Zhang T, Kraus A, French R, Jaquish D, et al. Reprogramming pancreatic stellate cells *via* p53 activation: A putative target for pancreatic cancer therapy. *PloS One* (2017) 12(12):e0189051. doi: 10.1371/journal.pone.0189051

134. Schnittert J, Bansal R, Mardhian DF, van Baarlen J, Östman A, Prakash J. Integrin α11 in pancreatic stellate cells regulates tumor stroma interaction in pancreatic cancer. *FASEB J* (2019) 33(5):6609–21. doi: 10.1096/fj.201802336R

135. Incio J, Suboj P, Chin SM, Vardam-Kaur T, Liu H, Hato T, et al. Metformin reduces desmoplasia in pancreatic cancer by reprogramming stellate cells and tumor-associated macrophages. *PloS One* (2015) 10(12):e0141392. doi: 10.1371/journal.pone.0141392

136. Duan W, Chen K, Jiang Z, Chen X, Sun L, Li J, et al. Desmoplasia suppression by metformin-mediated AMPK activation inhibits pancreatic cancer progression. *Cancer Lett* (2017) 385:225–33. doi: 10.1016/j.canlet.2016.10.019

137. Wu C, Qiu S, Zhu X, Lin H, Li L. OCT1-mediated metformin uptake regulates pancreatic stellate cell activity. *Cell Physiol Biochem* (2018) 47(4):1711–20. doi: 10.1159/000491003

138. Luong T, Cukierman E. Eribulin normalizes pancreatic cancer-associated fibroblasts by simulating selected features of TGFβ inhibition. *BMC Cancer* (2022) 22(1):1255. doi: 10.1186/s12885-022-10330-y

139. Zhang H, Zhu H, Feng J, Zhang Z, Zhang S, Wang Z, et al. Reprogramming of activated pancreatic stellate cells *via* mechanical modulation of transmembrane force-sensitive n-cadherin receptor. *J Mol Biol* (2023) 435(1):167819. doi: 10.1016/j.jmb.2022.167819

140. Chen X, Yu Q, Liu Y, Sheng Q, Shi K, Wang Y, et al. Synergistic cytotoxicity and co-autophagy inhibition in pancreatic tumor cells and cancer-associated fibroblasts by dual functional peptide-modified liposomes. *Acta Biomater* (2019) 99:339–49. doi: 10.1016/j.actbio.2019.09.003

141. Zang S, Huang K, Li J, Ren K, Li T, He X, et al. Metabolic reprogramming by dual-targeting biomimetic nanoparticles for enhanced tumor chemo-immunotherapy. *Acta Biomater* (2022) 148:181–93. doi: 10.1016/j.actbio.2022.05.045

142. Liu H, Zhang H, Liu X, Guo W, Liu Q, Chen L, et al. Pancreatic stellate cells exploit wnt/β-catenin/TCF7-mediated glutamine metabolism to promote pancreatic cancer cells growth. *Cancer Lett* (2023) 555:216040. doi: 10.1016/j.canlet.2022.216040

frontiers | Frontiers in Immunology

TYPE Original Research
PUBLISHED 18 July 2023
DOI 10.3389/fimmu.2023.1154528

OPEN ACCESS

EDITED BY
Denisa Baci,
University of Insubria, Italy

REVIEWED BY
Abhilasha Purohit,
National Institutes of Health (NIH), United States
Jose Manuel Garcia-Manteiga,
San Raffaele Hospital (IRCCS), Italy
Janusz Franco-Barraza,
Chase Cancer Center, United States

*CORRESPONDENCE
Janine T. Erler
janine.erler@bric.ku.dk
Raphael Reuten
raphael.reuten@pharmakol.uni-freiburg.de

†These authors have contributed equally to this work

RECEIVED 30 January 2023
ACCEPTED 30 May 2023
PUBLISHED 18 July 2023

CITATION
Rafaeva M, Jensen ARD, Horton ER, Zornhagen KW, Strøbech JE, Fleischhauer L, Mayorca-Guiliani AE, Nielsen SR, Grønseth DS, Kuś F, Schoof EM, Arnes L, Koch M, Clausen-Schaumann H, Izzi V, Reuten R and Erler JT (2023) Fibroblast-derived matrix models desmoplastic properties and forms a prognostic signature in cancer progression. *Front. Immunol.* 14:1154528. doi: 10.3389/fimmu.2023.1154528

Fibroblast-derived matrix models desmoplastic properties and forms a prognostic signature in cancer progression

Maria Rafaeva[1†], Adina R. D. Jensen[1†], Edward R. Horton[1†], Kamilla W. Zornhagen[1], Jan E. Strøbech[1], Lutz Fleischhauer[2,3], Alejandro E. Mayorca-Guiliani[1], Sebastian R. Nielsen[1], Dina S. Grønseth[1], Filip Kuś[1], Erwin M. Schoof[1,4,5,6], Luis Arnes[1], Manuel Koch[7,8], Hauke Clausen-Schaumann[2,3], Valerio Izzi[9,10,11], Raphael Reuten[1,12,13*] and Janine T. Erler[1*]

[1]Biotech Research and Innovation Centre, University of Copenhagen, Copenhagen, Denmark, [2]Center for Applied Tissue Engineering and Regenerative Medicine-CANTER, Munich University of Applied Sciences, Munich, Germany, [3]Center for NanoScience – CsNS, Ludwig-Maximilians-University Munich, Munich, Germany, [4]Department of Biotechnology and Biomedicine, Technical University of Denmark, Lyngby, Denmark, [5]The Finsen Laboratory, Rigshospitalet, Faculty of Health Sciences, University of Copenhagen, Copenhagen, Denmark, [6]Novo Nordisk Foundation Centre for Stem Cell Biology, DanStem, Faculty of Health Sciences, University of Copenhagen, Copenhagen, Denmark, [7]Center for Biochemistry, Center for Molecular Medicine Cologne (CMMC), Faculty of Medicine and University Hospital Cologne, University of Cologne, Cologne, Germany, [8]Institute for Dental Research and Oral Musculoskeletal Biology, Faculty of Medicine and University Hospital Cologne, University of Cologne, Cologne, Germany, [9]Faculty of Biochemistry and Molecular Medicine, University of Oulu, Oulu, Finland, [10]Faculty of Medicine, University of Oulu, Oulu, Finland, [11]Foundation for the Finnish Cancer Institute, Helsinki, Finland, [12]Institute of Experimental and Clinical Pharmacology and Toxicology, Medical Faculty, University of Freiburg, Freiburg, Germany, [13]Department of Obstetrics and Gynecology, Medical Center, University of Freiburg, Freiburg, Germany

The desmoplastic reaction observed in many cancers is a hallmark of disease progression and prognosis, particularly in breast and pancreatic cancer. Stromal-derived extracellular matrix (ECM) is significantly altered in desmoplasia, and as such plays a critical role in driving cancer progression. Using fibroblast-derived matrices (FDMs), we show that cancer cells have increased growth on cancer associated FDMs, when compared to FDMs derived from non-malignant tissue (normal) fibroblasts. We assess the changes in ECM characteristics from normal to cancer-associated stroma at the primary tumor site. Compositional, structural, and mechanical analyses reveal significant differences, with an increase in abundance of core ECM proteins, coupled with an increase in stiffness and density in cancer-associated FDMs. From compositional changes of FDM, we derived a 36-ECM protein signature, which we show matches in large part with the changes in pancreatic ductal adenocarcinoma (PDAC) tumor and metastases progression. Additionally, this signature also matches at the transcriptomic level in multiple cancer types in patients, prognostic of their survival. Together, our results show relevance of FDMs for cancer modelling and identification of desmoplastic ECM components for further mechanistic studies.

KEYWORDS

extracellular matrix, fibroblasts, mechanics, models, desmoplasia, pancreatic cancer, breast cancer

1 Introduction

The extracellular matrix (ECM) is a protein scaffold to which cells adhere, that provides both biochemical and biophysical cues in order to maintain organ homeostasis and integrity (1). The ECM reveals a vital impact on cancer progression, as cancer cells invade the ECM at the primary tumor and further interact with ECM proteins at different stages of metastasis (2). Secondary to physiological insults, such as wounds, a desmoplastic reaction regularly occurs in cancer (3). Several studies have shown that increased inflammation is a precursor of cancer (4), and tumors are often described as "wounds that do not heal" (5). Such reaction of the cancerous tissue stroma results in overproduction and deposition of ECM concomitant with increased proliferation of myofibroblasts in the tumor microenvironment (TME) and lacks regaining of normal tissue homeostasis (6).

This desmoplastic reaction is a defining feature of breast- and pancreatic cancers and is correlated with poor prognosis (7, 8). In pancreatic adenocarcinoma (PDAC), desmoplasia has largely been attributed to the physical properties of the tumor stroma, that impedes drug delivery, response to radiation, and increases metastasis to other organs, primarily the liver (9). At the primary site in breast cancer, there is also an excessive deposition of the ECM, mainly collagen I, and remodeling, which leads to linearization of the fibers forming 'tracks' for cell migration from the tumor margin (10). This ECM reorganization is usually present at the invasive stage and is used prognostically, with increased observation in the stroma correlating with poor outcome (11, 12). Linearization of the ECM emerges from the cross-linking of fibers with enzymes, primarily lysyl-oxidases (LOX, LOXL1-4) and the physical compacting of the ECM by dividing cells (13) resulting in a denser and stiffer ECM (14). In turn, stiffened matrix boosts β1-integrin activity and thereby focal adhesion formation of the stromal cells in the TME, transforming mechanotransduction into pro-tumorigenic cell signaling responses (15, 16). For instance, transcriptional activation of Yes-associated protein (YAP) with increasing ECM stiffness promotes the proliferation and migration of breast cancer cells upon transduction of signals from the focal adhesions (17, 18). In addition, integrin-independent mechanotransduction was shown to activate the EPHA2/LYN kinase that promotes epithelial to mesenchymal transition (EMT) and subsequently tumor cell invasion in breast cancer (19).

More than 80% of the ECM is produced by stromal cells (20). Cancer-associated fibroblasts (CAFs) are key contributors to the deposition and remodeling of the ECM during cancer progression, in both breast and pancreatic cancer (21, 22). Normal fibroblasts (NFs) and CAFs are commonly used in studies to better understand cancer progression, especially with respect to cancerous transformation and cell-cell communication in the TME (23, 24). However, their contribution to the composition and organization of the ECM and influence of this on cancer cell proliferation has so far not been investigated in detail.

Understanding the specific role of ECM characteristics during cancer progression is becoming increasingly important in order to improve drug efficacy and identify potential therapeutic targets for better patient outcomes. To study the influence of the fibroblast-derived ECM, we utilized fibroblast-derived matrices (FDMs) (25) that resemble the ECM composition detected in decellularized mouse organs (26). Here, we show that although cancer cells equally adhere to the normal and cancerous matrices, they show increased proliferation on CAF FDMs. The CAF FDM composition mimics core changes in desmoplastic metastatic cancer *in vivo*. Strikingly, CAFs assemble denser and stiffer ECM than NFs, structurally resembling tumor matrix. We derive a 36-gene matrisome signature based on CAF ECM, which shows enrichment in multiple cancer types in humans and is prognostic of several cancer types' outcome.

2 Materials and methods

2.1 Cell lines

The 4T1 mouse mammary carcinoma cell line was a kind gift of Fred Miller (Wayne State University). The KPCmT4 murine pancreatic cancer cell line was isolated from PDAC tumor tissue obtained from KrasLSL-G12D/+; Trp53LSL-R172H/+; Pdx1–Cre mice of a pure C57BL/6 background and were gifted by the Tuveson laboratory (Cold Spring Harbor Laboratory, NY, USA) (27). Cell lines were cultured in Dulbecco's modified Eagle medium GlutaMAX (DMEMGlutaMAX; Gibco, Thermo Fisher Scientific, cat. no. 10566016, Grand Island, NY, USA) supplemented with 1% penicillin-streptomycin (PS, 100 U/mL, Gibco, Thermo Fisher Scientific) and 10% fetal bovine serum (FBS, Gibco, Thermo Fisher Scientific). The 4T1-H2B-GFP+ cells were previously generated by stable transfection of 4T1 cells with a pBOS-H2BGFP vector (BD Pharmingen, San Jose, CA, USA) (28). The KPCmT4-zsGreen cells were generated by stable transfection of KPCmT4 cells with pHIV Luc-zsGreen vector (gift from B. Welm, University of Utah, USA, Addgene plasmid no. 39196). Immortalized mCAF1 and mNF1 murine fibroblast cell lines were a kind gift of Erik Sahai (The Francis Crick Institute, London UK), isolated from the mammary tumor, and healthy fat pad of FVB/n MMTV-PyMT mouse line, respectively (23). Cells were cultured in DMEM high glucose (Gibco, Thermo Fisher Scientific) with 10% FBS, 1% Insulin Transferrin Selenium Solution (ITS-G Gibco, Thermo Fisher Scientific) and 1% PS. All cell lines were regularly tested for mycoplasma and maintained at a 37°C, 5% CO2 humidified atmosphere.

2.2 Fibroblast-derived matrices

Fibroblast-derived matrices (FDMs) from the mCAF1 and mNF1 cell lines were generated as previously described (25). Briefly, fibroblasts were seeded on cross-linked gelatin dishes, and treated for 7 days with 50μg/ml ascorbic acid daily. Afterwards, fibroblasts were treated with 20 mM NH_4OH with 0.5% Triton-X-100 for 5 minutes, followed by a gentle wash in PBS. 0.5% sodium deoxycholate (Sigma-Aldrich, D6750-500 mg) was then added for 60 minutes at room temperature, and then removed. The FDMs were washed in PBS and then DNase I (10 μg/ml in PBS) was added for 60 minutes at 37 °C. This protocol was optimized for either a 6-

well plate (volumes 1 ml/well), 12- and 24- well plate (volumes 0.5 ml and 0.25 ml/well) or a 96-well plate (volumes 0.1 ml/well). If not immediately used, they were stored at 4°C in PBS supplemented with 1% PS. For optimizing cell-derived matrix generation and use, reader can further consult with previously published protocols (29–31).

2.3 KPC mouse samples generation

KPC mice (Tg(Pdx1-cre)6TuvKrastm4TyjTrp53tm2Tyj) were imported from The Beatson Institute for Cancer Research (Glasgow, UK) and originally established from Jax stocks #014647, #008180, #008652 in a mixed background (32). Three mice (both sexes) per group were used. As control groups, we used age-matched Pdx1-cre+ mice. KPC mice were used at pancreatic intraepithelial neoplasia (PanIN) stage (3-4 months old), early PDAC tumor stage (4.5 months old) and late tumor stage (5-8 months old). For generating decellularized tissue, pancreas/pancreatic tumors and livers in the same animal were perfused according to previously published protocol (33). For the liver metastases group were selected mice with developed tumor where was observed macroscopic metastasis, resection of area from decellularized livers was performed based on 2 knots of 9-0 suture marking prior decellularization. After perfusion and washes in MQ water samples were resected and snap frozen for further storage at -80°C.

2.4 Intrasplenic KPC injections and sample generation

Female C57BL/6 mice (6–12 weeks old; Taconic, Denmark) were used for intrasplenic injections of KPCmT4 cells at 1 million cells per 50µL of PBS (34). Healthy matched mice were used as a control, 3 mice per group. 20 days post-injection livers were decellularized according to (33) and samples were resected and snap frozen after perfusion washes with MQ water.

2.5 Decellularized tissues for mass spectrometry sample preparation

Decellularized tissue samples were defrosted, and tissues were punched under dissection microscope (Greenough, with two-armed gooseneck; Leica, model no. S6 D) with 2mm punch biopsy tools (Harris Uni-Core) and weighed (tools thoroughly cleaned between samples with methanol). Lysate preparation and digestion was done according to (35) with modifications. Briefly, ~6mg of decellularized tissue pieces were lysed using 30 µl of lysis buffer (consisting of 6 M Guanidinium Hydrochloride, 10 mM TCEP, 40 mM CAA, 50 mM HEPES pH 8.5) in Barocycler 2320EXT (Pressure BioSciences) set to 30 cycles of 45,000 p.s.i., 50 seconds on, 10 seconds off. Samples were boiled at 95 °C for 5 minutes, after which they were sonicated on the 'high' setting for 5 × 30 seconds in a Bioruptor sonication water bath (Diagenode) at 4°C. KPC intrasplenic samples were filtered through Microcon centrifugal unit with 30kDa cut-off (cat. no. Z648086, Millipore). After determining protein concentration with Bradford reagent (cat. no. B6916, Sigma), 20 µg was taken forward for digestion.

Samples were diluted 1:3 with 10% Acetonitrile, 50 mM HEPES pH 8.5, LysC (MS grade, Wako) was added in a 1:50 (enzyme to protein) ratio, and samples were incubated at 37°C for 4 hours. Samples were further diluted to 1:10 with 10% Acetonitrile, 50 mM HEPES pH 8.5, trypsin (MS grade, Promega) was added in a 1:100 (enzyme to protein) ratio and samples were incubated overnight at 37°C. Enzyme activity was quenched by adding 2% trifluoroacetic acid (TFA) to a final concentration of 1%. Prior to mass spectrometry analysis, the peptides were desalted on in-house packed C18 Stage tips. For each sample, 2 discs of C18 material (3M Empore) were packed in a 200µl tip, and the C18 material activated with 40µl of 100% Methanol (HPLC grade, Sigma), then 40µl of 80% Acetonitrile, 0.1% formic acid. The tips were subsequently equilibrated 2 x with 40µl of 1%TFA, 3% Acetonitrile, after which the samples were loaded using centrifugation at 4,000 x rpm. After washing the tips twice with 100µl of 0.1% formic acid, the peptides were eluted into clean 500µl Eppendorf tubes using 40% Acetonitrile, 0.1% formic acid. The eluted peptides were concentrated in an Eppendorf Speedvac, and reconstituted in 1% TFA, 2% Acetonitrile for Mass Spectrometry (MS) analysis.

2.6 FDM mass spectrometry sample preparation

Lysates of the mCAF1 and mNF1 FDMs were collected in biological triplicates. All lysates were washed in 1 x PBS, scraped, and collected. Samples were centrifuged at 8000g for 10 minutes at 4°C. PBS removed, and 20 µL lysis buffer added (6 M Guanidinium Hydrochloride, 10 mM TCEP, 40mM CAA, 100 mM Tris pH8.5). Samples were vortexed and boiled for 5 minutes at 95°C for 5 minutes. Samples were then sonicated using the Bioruptor 5 x 30 seconds on/30 seconds off using maximum setting. Samples were then centrifuged 1 min, 13,000 rpm and snap frozen in liquid nitrogen. Sample preparation and acquisition were then performed as previously described (26).

2.7 Mass spectrometry acquisition and analysis

2.7.1 KPC samples

For each sample, peptides were loaded onto a 2cm C18 trap column (cat. no.164705, Thermo Fisher), connected in-line to a 75 cm C18 reverse-phase analytical column (cat. no. ES805, Thermo EasySpray) using 100% Buffer A (0.1% Formic acid in water) at 750bar, using the Thermo EasyLC 1000 HPLC system, and the column oven operating at 45°C. Peptides were eluted over a 200-minute gradient ranging from 6 to 60% of 80% acetonitrile, 0.1% formic acid at 250 nL/minute, and the Q-Exactive instrument (Thermo Fisher Scientific) was run in a DD-MS2 top10 method.

Full MS spectra were collected at a resolution of 70,000, with an AGC target of 3×10^6 or maximum injection time of 20 milliseconds and a scan range of 300–1750 m/z. The MS2 spectra were obtained at a resolution of 17,500, with an AGC target value of 1×10^6 or maximum injection time of 60 milliseconds, a normalized collision energy of 25 and an intensity threshold of 1.7×10^4. Dynamic exclusion was set to 60 seconds, and ions with a charge state < 2 or unknown were excluded. MS performance was verified for consistency by running complex cell lysate quality control standards, and chromatography was monitored to check for reproducibility.

2.7.2 Analysis of all samples

The raw files were analyzed using Proteome Discoverer 2.4. Label-free quantitation (LFQ) was enabled in the processing and consensus steps, and spectra were matched against the Mus Musculus database obtained from Uniprot. Dynamic modifications were set as Oxidation (M), Deamidation (N, Q) and Acetyl on protein N-termini. Cysteine carbamidomethyl was set as a static modification. All results were filtered to a 1% FDR, and protein quantitation done using the built-in Minora Feature Detector. Normalization was performed in the total peptide amount mode, which sums the peptide group abundances for each sample and determines the maximum for all files, then using it as a normalization factor. At post-processing of the dataset proteins were sorted for identified based on 2 or more unique peptides in addition to be quantified among three biological repeats. Statistical analysis was performed using Limma package of R studio software. LogFC values were calculated as a difference of the means. A linear model was fit to the data, following an empirical Bayes moderated t-test and p-values adjustment for multiple testing with Benjamini-Hochberg method. Proteins were next sorted for 'in silico' defined matrisome (36). For heatmaps generation were used Cluster 3.0 (C Clustering Library 1.59) and visualization was done using Java Tree View (version 1.2.0).

2.8 Second harmonic generation (SHG) imaging of FDMs combined with fluorescence imaging

For imaging FDMs have been deposited as described on glass bottom 24 or 12-well plates (cat. no. P24-1.0-13-F, MatTek) with fibroblast cell number and volumes adjusted to the area of the wells. After staining, FDMs were stored in 1% PS/PBS at +4°C. FDMs were imaged on the inverted Leica SP5-X confocal microscope with a two-photon laser (Spectra-physics, Mai Tai DeepSee model; range 680-1,040nm) adjusted to 880nm and SHG was detected by hybrid detector (at 420-460, Leica, HyD S model). Alexa-488 secondaries were detected simultaneously by PMTs (Leica). We used two different objectives for imaging - lambda blue, 20×, 0.70 numerical aperture (NA) IMM UV; Leica, HCX PL APO model and 40x, 1.3 NA OIL UV; Leica, HCX PL APO CS. SHG imaging stacks were acquired at 512x512 pixels, 100Hz, 1 line averaging with a 2.5um z-step using 40x objective. Antibody staining was acquired at 1024x1024 pixels, 100Hz, 1 line averaging with 2.5µm z-step using 20x objective. For data acquisition, Leica Application Suite (LAS) version 4 microscope software was used.

2.9 Analysis of FDM density and thickness

For analysis of fibrillar collagens density, single planes with the largest presence of the ECM were selected from SHG z-stacks (40x acquired). Brightness of images was equally adjusted, and images were processed in Fiji software with Twombli plugin to measure high density matrix (37). For analysis of FDM thickness, SHG signal was measured across planes of z-stacks (40x acquired) in Fiji software. Number of planes with signal were counted and multiplied by z-step size in order to estimate thickness in µm.

2.10 Indentation-type atomic force microscopy

mNF1 and mCAF1 FDMs were produced as described above in 35 x 10 mm petri dishes (cat. no. 353001, FALCON). Stiffness measurements were carried out using a NanoWizard I AFM (JPK BioAFM Bruker Nano GmbH, Berlin, Germany) in combination with an inverted optical microscope (Axiovert 200, Carl Zeiss Micro Imaging GmbH, Göttingen, Germany). To avoid external disturbance during measurement, the whole setup is placed on an active vibration isolation table (Micro 60, Halcyonics, Göttingen, Germany) inside a self-build 1 m^3 soundproof box. The AFM was used in the indentation mode with pyramidal shaped tips with a radius of around 20 nm and a spring constant of 0.1 N/m. For each cantilever the spring constant and the sensitivity were determined individually using the thermal noise method (38). During measurements, the matrix was immersed in PBS (Biochrom Dulbecco's PBS w/o Mg2 +/Ca2+, pH 7.4, Berlin, Germany). On each obtained matrix 6, force maps of 5 x 5 indentation curves equally distributed in an area of 30 x 30 µm were obtained. Indentations were made up to 1.5 V with a speed of 10 µm/s and calibration was performed after the experiment. The six force map locations were arbitrary chosen. During measurements the cantilever was retracted in vertical direction (z-axis) up to 50 µm and therefore the CellHesion® module (JPK BioAFM Bruker Nano GmbH, Berlin, Germany) was used. The Young's Modulus was extracted by fitting the Hertz-Sneddon model for a pyramidal indenter to the whole approach part of the force-indentation curves, using the JPK Data Processing Software (Version 5.0.96, JPK Instruments).

2.11 FDM staining with antibodies and CNA35 probe

Stored FDMs in 1% PS/PBS at 4°C were brought to room temperature (RT). Next, FDMs were gently washed with PBS following blocking in 3% donkey serum (cat. no.017-000-121, Jackson ImmunoResearch), 1% BSA/PBS solution for 1 hour at RT. After, matrices were gently washed with PBS and covered with primary antibody dilution [1% BSA/PBST (0,05% Tween)]. Primary antibody used: rabbit anti-periostin (polyclonal KR131, provided by M. Koch), rabbit anti-collagen XII (polyclonal KR145, provided by M. Koch), rabbit anti-collagen VIα1C (polyclonal, provided by R. Wagener) at 1:100 dilution. After overnight incubation at 4°C, matrices were gently washed 3x5 minute in PBS-0.2% Tween and then secondary antibody solution has been applied - 1% BSA/PBST with 1:500 donkey anti-

rabbit AlexaFluor488 IgG (H+L) (A-21206, Thermo Fisher Scientific) for 1 hour at RT. Finally, samples were gently washed 3x5 min in PBST and stored in 1% PS/PBS at 4°C until imaging.

FDMs were also stained with in-house produced anti-collagen CNA35-mCherry probe. The probe was produced according to (39) with a few modifications. Briefly, streaked bacterial colony of BL21 (DE3) strain carrying a plasmid pET28a-mCherry-CNA35 (Addgene #61607) was inoculated in 20ml kanamycin (50µg/ml) containing LB medium (4529, SSI Diagnostica) and next day further expanded during overnight culture in 2L NZY Auto-Induction LB medium (1/100) (MB179, NZYtech). After centrifugation, bacterial pellet was lysed in NZY Bacterial Cell Lysis Buffer supplemented with Lysozyme (50mg/ml) and DNase I (2mg/ml) and frozen at -20°C until protein extraction. Cleared from residual cell debris lysate was diluted with 0.5M NaH2PO4 pH 7,6 (1:10) and applied on a washed and equilibrated pre-elution gelatin-sepharose (17-0956-01, GE Healthcare) column connected to elution column with PureCube 100 INDIGO Ni-Agarose (75105, Cube Biotech). After two washes with 10mM Tris, 150mM NaCl (pH = 7.6), elution was performed by loading sequentially 5,10,20,30,60,80,150, 300 mM Imidazol in 20mM Tris, 200mM NaCl (pH = 7.6) solutions. Three last fractions were collected and dialysis of those was performed against 1 x PBS. Protein concentrations were measured in all fractions, probe was protected from light and sterile filtered (Ultrafree-cl gv 0.22um sterile (UFC40GV0S, Millipore) prior being aliquoted and stored at -20°C. For staining, FDMs were incubated with 1µM CNA35-mCherry in PBS at RT overnight and washed with PBS before imaging.

2.12 Cell adhesion and proliferation

Cell adhesion and proliferation assays were performed using 4T1-H2B-GFP and KPCmT4-zsGreen cells. 5000 (in 2% serum DMEM) cells were seeded in high content 96-well imaging plates (Corning, 3340) on wells containing mCAF1 FDMs, mNF1 FDMs or on plastic. Cells were allowed to attach for 1 hour, after which plates for adhesion were fixed in 10% formalin (Formalin solution 10% neutral buffered, Sigma-Aldrich, cat. no. HT501128-4L) (100uL per well) for 10 minutes. To follow proliferation, additional plates were fixed at 1 day and 5 days post-seeding. Cells were permeabilized in 0.2% Triton-X-100 in PBS (Sigma-Aldrich, cat. no. T8787-50 mL) for 2–5 minutes. Next 2×PBS washes were performed, after which DAPI was added at 1 µg/mL for 90 min at room temperature. Plates were then washed 3x5 minutes in PBS, placed in 100 µL PBS and stored at 4°C in the dark until imaging. Imaging was performed on the INCell Analyzer 2200 (GE Healthcare Life Sciences). Images were analyzed using the INCell Analyzer Workstation 1000 software (GE Healthcare Life Sciences). Nuclei were segmented based on the DAPI staining using the Tophat segmentation method. The mean intensity of GFP and DAPI in each nucleus were measured, and the number of GFP positive and DAPI positive cells were counted and compared between conditions. Note: Images in Figure 1A. are acquired from a 24-well plate (cat. no. P24 -1.0-13F, MatTek Corporation) where cell seeding densities were adjusted to the area of the wells and wells were equilibrated with cell culture medium prior seeding. Samples were prepared, fixed and permeabilized as described above after 3 days, stained with DAPI (1 µg/mL) to visualize cell nuclei and AlexaFluor633-phalloidin (1:500; A22284, Thermo Fisher Scientific) to visualize cell bodies for 1 hour at room temperature. Imaging was performed on Leica SP8 confocal microscope with HC Plan-Apochromat 10x/0.40 AI at 1024x1024 pixels resolution, 5 µm z-step.

mNF1 and mCAF1 fibroblasts proliferation was assessed in the following way. 2000 cells were seeded in 96-well plates and cultured under regular conditions for three days (72h). Afterwards, triplicates and background wells measurements were performed 1 hour after incubation with CellTiter 96 Aqueous One Solution Cell Proliferation Assay (Promega, G3580) according to the manufacturers instructions.

2.13 Western blot validation of mNF1/mCAF1 FDMs

FDMs were lysed in 9M Urea with 1% 2-Mercaptoethanol. Lysates were shaken rigorously for 45 minutes at 4°C before 5 minutes of sonication (30 sec. on 30 sec. off). Lysates were boiled for 5 minutes before centrifugation at 15,000 rpm for 15 minutes at 4°C. Protein lysates were resolved on NuPAGE 4 –12% Bis-Tris gels (Thermo Fisher Scientific, cat. no.17080971) and transferred to nitrocellulose membranes. Membrane was stained with Ponceau stain (Supplementary Materials) (Sigma-Aldrich, cat. no. P7170). Membranes were blocked in 5% milk for 1 hour and incubated with primary antibodies overnight at 4°C. Primary antibodies included LOX, Cell Signaling D8F2K (1:1000), Collagen IV Sigma-Aldrich AB756P (1:1000), Collagen XII KR144 (1:1000; provided by M. Koch). The next day, membranes were washed with TBS-Tween and incubated with appropriate HRP-conjugated secondary antibodies for one hour. Immunoblots were visualized on an ImageQuantTM LAS 400 instrument and images were analyzed using ImageJ.

2.14 Desmoplastic signature analysis from human dataset

The long signature used for this study comprises of the following 36 proteins: Col1a1, Col1a2, Col5a2, Col6a1, Col6a2, Col8a1, Col12a1, Col14a1, Col16a1, Dpt, Emilin1, Fn1, Fbn1 Mfap2, Mfap5, Postn, Tgfbi, Thbs1, Thbs2, Thsd4, Tnc, Tsku, Vwa1, Aspn, Adamts2, Bmp1, Cd109, Lox, Loxl2, Mmp19, Serpine1, Timp1, Angptl4 and Crlf1. The short signature comprises 9 of these proteins: Col1a2, Col5a2, Col12a1, Fn1, Mfap5, Postn, Tgfbi, Thbs2, Lox. These proteins were selected based on, LogFC > 1.5, p-value < 0.05).

The entire database from the Celligner/DepMap tool (40) was locally downloaded and the single-sample gene set enrichment value of the desmoplastic fibroblast signature evaluated across 10070 patients from primary tumors of 29 tissues (67 tumor subtypes) using the singscore package (41) in R. Tumor-wise differences were evaluated using one-way ANOVA, followed by Tukey HSD test. ANOVA p-value for all comparisons was $p < 1*10^{-16}$. Matrisome genes were defined in (42) and downloaded from the Matrisome Project portal at http://matrisome.org/. In each test, the entire cohort was scored, and the results presented. Additionally, single genes were scored individually in the same way, results of which are shown in Supplementary Figure 8.

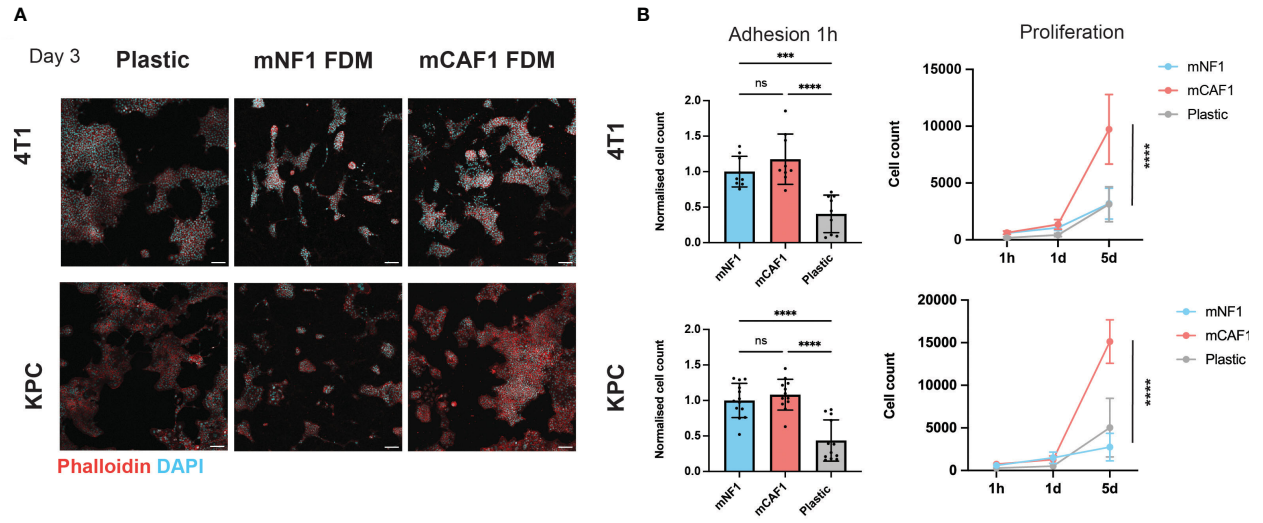

FIGURE 1
CAF FDM promotes breast and pancreatic cancer cells proliferation. **(A)** Representative images of 4T1-H2B-GFP breast cancer and KPCmT4-zsGreen pancreatic cancer cells on plastic, mNF1, and mCAF1 FDMs. Day 3 post-seeding in 2% FBS DMEM. Staining with phalloidin (F-actin) and DAPI (nuclei). **(B)** Adhesion (1 hour) and proliferation (1-5 days) of 4T1-H2B-GFP and KPCmT4-zsGreen cells seeded on plastic, mNF1, mCAF1 FDMs. Normalized or raw cell count based on DAPI and GFP. n=3 repeats. One-way ANOVA test. ns, p-value > 0.05; ***p-value < 0.001, ****p-value < 0.0001. Scale bars 100 µm.

2.15 Analysis and statistics

Statistical analyses other than proteomics datasets were performed in Prism 9 (version 9.4.1). All data was tested for normal distribution, following which the appropriate statistical analysis was performed. Significance was p-value < 0.05 throughout, apart from mass spectrometry data, where it defined as p-value < 0.1 for *in vivo* dataset. Statistical analyses were performed using unpaired t-test, or analysis of variance (ANOVA, where there were multiple comparison groups).

3 Results

3.1 CAF FDM stimulates cancer cells proliferation

For this study, we selected NF (mNF1) and CAF (mCAF1) fibroblasts generated from FVB and PyMT-FVB mice, respectively, which are present in the normal fat pad and late tumor stage. These immortalized and well-characterized cells (23) allowed the generation of sufficient FDMs in a span of 7 days, which is the shortest timeframe described for FDM deposition (25, 29). We probed cancer cell response, adhesion and proliferation, on these matrices versus regular tissue culture plastic (Figure 1A). We chose two cell lines; triple-negative breast cancer cells (4T1) and pancreatic cancer cells (KPCmT4), given these are highly desmoplastic diseases. Firstly, we assessed cell number of the cancer cells upon adhesion to the FDMs and plastic (1 hour post-seeding), which showed no difference between NF and CAF FDMs (Figure 1B). Quantification of the cells at two additional time points (1 day, 5 days) showed that both cell types proliferate more on the CAF FDM comparing to NF. Hence, CAF FDM might instruct the cancer cell proliferative potential.

3.2 CAF FDM structure reflects *in vivo* desmoplastic ECM

In order to investigate whether changes in composition of the cancerous ECM were causing the alterations in proliferation observed, we next characterized the composition of both FDMs by label-free mass spectrometry profiling (Figure 2A). We were able to robustly detect 3392 proteins in total (Supplementary Table 1), from which the matrisome was filtered (in silico defined ECM and related proteins (36)). This led us to identify 151 proteins, further categorized into ECM core (glycoproteins, collagens, and proteoglycans) and associated proteins (ECM-affiliated, ECM regulators, secreted factors). When we compared normalized relative abundance of ECM proteins between CAF and NF, we observed that the abundance of many ECM proteins was significantly increased (adjusted p-value < 0.05) in CAF FDMs (Figure 2A), compared to NF FDMs, where only a couple of ECM proteins (Srpx2, Ctsl) were significantly decreased. Following this finding, we wanted to further evaluate CAF/NF FDM differences. Here, we validated LC-MS/MS findings (Figure 2A) by both immunofluorescence (IF) imaging (Figure 2B) and Western Blot analysis (Figure 2C and Supplementary Figure 3) for selected proteins (periostin, collagen IV, XII, XIV, and lysyl oxidase) in the CAF FDM.

Based on these data, we hypothesized that the ECM produced by CAF versus NF may have altered structure, and we focused on performing label-free second harmonic generation (SHG) imaging (Figure 2D and Supplementary Figure 1A). Single-plane and maximum intensity projection (MIP) image analysis allowed quantification of ECM density. This showed that CAF FDM possesses denser packed collagen fibers (Figure 2E). Using CNA35-mCherry probe, binding fibrillar collagens, we were able to better visualize ECM fibers of the FDMs (Supplementary Figure 1B) showing that CAF FDMs have higher intensity of the

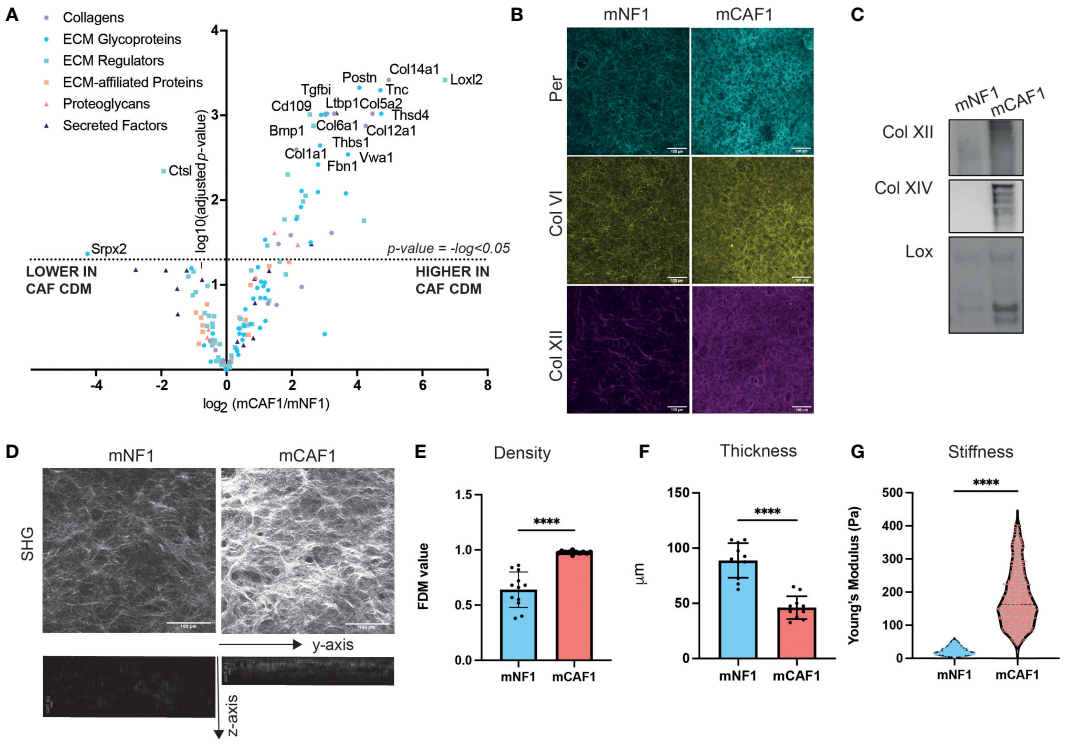

FIGURE 2
CAF FDM is compositionally and structurally different from NF FDM. **(A)** Volcano plot showing ECM composition difference between mCAF1 vs mNF1 FDMs. n= 3 samples per condition. **(B)** Validation of mCAF1 vs mNF1 upregulated proteins (Per - periostin, ColIV - collagen IV, Col XII - -collagen XII) by immunofluorescent staining of FDMs. **(C)** Validation of mCAF1 vs mNF1 upregulated proteins (ColXII, ColXIV - collagen XIV, LOX - lysyl oxidase) by western blotting.**(D)** Representative images of mNF1 and mCAF1 FDMs imaged by second harmonic generation (SHG). Maximum intensity projection and y-z projection. **(E)** mNF1 and mCAF1 FDMs density (based on single plane analysis). n= 3 repeats. **(F)** mNF1 and mCAF1 FDMs thickness (based in y-z projection analysis). n=3 repeats. **(G)** mNF1 and mCAF1 FDMs stiffness based on the atomic force microscopy measurements. n = 5-7 matrices. Unpaired t-test- ****p-value <0.0001. Scale bars 100 um, except z-axis images with 10um scale bar.

collagens staining and indeed increased density of fibers (Supplementary Figures 1C, D). Analysis of stacks through the z-axis of FDMs concluded that CAF FDM is also significantly thinner than NF FDM's (Figure 2F). Thickness was previously shown to positively correlate with the fibroblasts' density (43), which in our model is also reflected in the higher density of NFs nuclei in the depositing FDM layer and NFs increased proliferation rate compared to CAFs (Supplementary Figure 2). These findings highlighted that CAF FDMs contain more ECM proteins and are thinner as well as denser suggesting, a strong change in CAF FDM mechanics. Therefore, we performed atomic force microscopy (AFM) measurements to determine the stiffness of the FDMs. AFM analysis revealed that CAF FDM stiffness is significantly increased compared to NF FDM (Figure 2G). Increased stiffness and density are representative of desmoplastic stroma *in vivo*, therefore, these FDMs present a relevant model for mimicking those differences *in vitro*.

3.3 Composition of mammary CAFs FDM reflects desmoplastic changes in pancreatic cancer

Given this outcome, suggesting a strong pro-fibrotic deposition by mammary CAFs, we hypothesized that these changes could represent desmoplastic changes in other cancer types. As PDAC is known to have a highly desmoplastic primary tumor and metastatic site (liver) (34, 44), we generated a proteomic PDAC dataset in order to further explore desmoplastic ECM composition. Here, we utilized our previously published ISDoT (*In Situ* Decellularization of Tissues) method (45) in order to isolate and enrich native ECM proteins from pancreatic and hepatic tissue during pancreatic cancer progression including pancreatic intraepithelial neoplasia (PanIN) and PDAC stages in the KPC (Tg (Pdx1-cre) 6TuvKras^{tm4Tyj}Trp53^{tm2Tyj}) mouse model. We collected regions from the pancreas of PDAC-developing mice, at PanIN and established tumors stages with early and late formation, as well as from the healthy pancreas of age-matched Pdx-1 Cre mice (Figure 3A). The same approach was performed for the liver, where KPC mice developed spontaneous macrometastases. We also included livers, which developed experimental metastases upon intrasplenic injection, where cancer cells drain into the liver through the splenic vein, mimicking the latter stages of metastasis with vast liver macrometastases (Figure 3A).

These samples were analyzed by label-free LC-MS/MS, and the abundance of ECM proteins between healthy and tumor conditions at each stage was quantified. Here, we detected 5472 proteins across all conditions, of which 210 were core ECM and ECM-associated proteins (filtered in the same way as the mCAF1/mNF1 proteomic

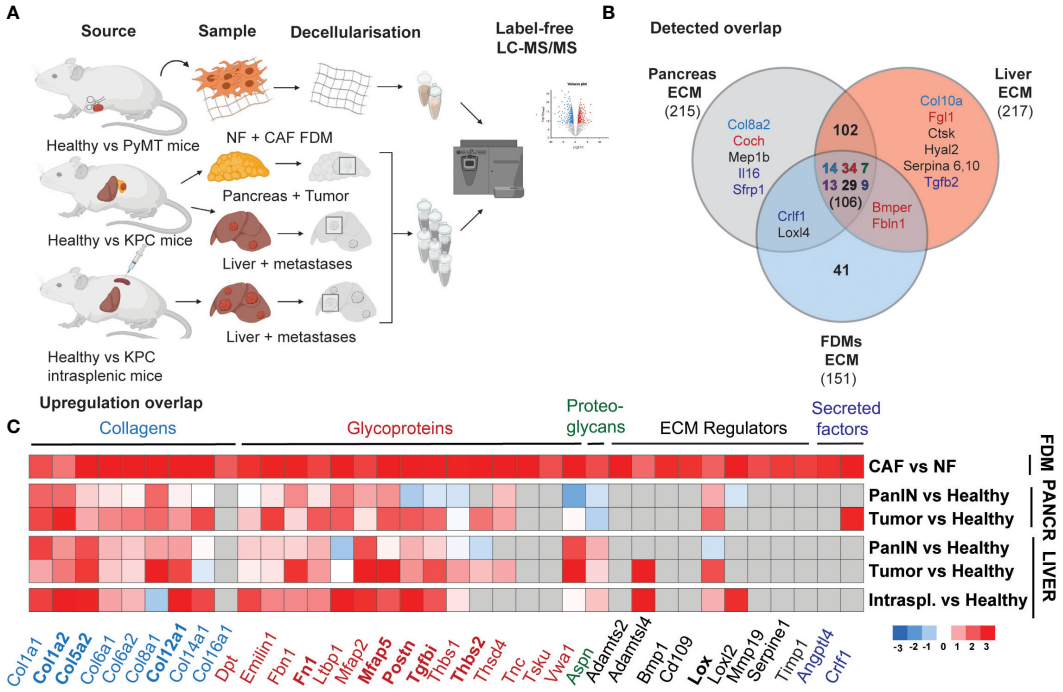

FIGURE 3
Mammary CAFs deposit compositionally complex matrix reflecting desmoplastic changes in primary and metastatic pancreatic cancer. **(A)** Scheme of the mass spectrometry samples generation for mNF1, mCAF1 FDMs dataset and PDAC dataset, including healthy age-matched tissues and tumors, spontaneous liver metastases from PanIN to PDAC stages and healthy livers age-matched with experimental KPC liver metastases. **(B)** Venn diagram showing an overlap in robustly detected proteins between the datasets. Color-coding is used for depicting matrisome categories (Core matrisome: blue – Collagens, red – Glycoproteins, green – Proteoglycans; Matrisome-associated: dark violet – ECM-affiliated, black – ECM regulators, dark blue – Secreted factors). **(C)** Heatmap of the ECM proteins' fold changes significantly upregulated ($p < 0.05$), cutoff logFC >1.59 in mCAF1 vs mNF1 FDMs, compared to the PDAC dataset (tumor conditions vs healthy ones). n=3 samples per group. Grey colored are non-detected proteins. PanIN – pancreatic intraepithelial neoplasia, transition to tumor; Pancreatic tumor presented from the early group. In bold are highlighted genes of the short signature - matched to increasing with progression in the *in vivo* dataset.

data). Comparison between the different stages of PDAC progression (Supplementary Figure 4) allowed identification of 168 significantly upregulated ECM proteins at least in one of the disease stages. These included a number of core matrisome proteins such as collagens (Col1a1, Col1a2, Col5a2, Col8a1, Col12a1) and glycoproteins (Ltbp1, Mfap2, Mfap5), which are upregulated already at the PanIN stage. A few other proteins quantified, such as Postn, Srpx2, Tgfbi, became upregulated during tumor formation, but not at the PanIN stage. We also observed some liver metastasis-specific ECM changes. Vwa1 (Von Willebrand Factor A domain containing 1), for example, was downregulated or unchanged in the pancreas, but significantly upregulated in the liver. As with the CAF/NF proteomics, we also noted an increase in the collagen crosslinking proteins LOX and LOXL2 in tumors and/or metastases. Matching of FDMs dataset with PDAC indicated that most of the proteins were also found *in vivo* (106, all categories) (Figure 3B), while among the top list of altered proteins in CAF vs NF most were also upregulated (Figure 3C) (cut-off LogFC > 1.59, p-value < 0.05; grey – below detection limit in the *in vivo* dataset). This list of 36 genes we defined as a long 'desmoplastic signature' and proteins also gradually upregulated during progression in PDAC, 9 genes, as a short 'desmoplastic signature': Col1a2, Col5a2, Col12a1, Fn1, Mfap5, Postn, Tgfbi, Thbs2, Lox.

3.4 Desmoplastic signature is enriched in multiple cancer types in human and is prognostic of patient survival

We focused on identifying if the murine 'desmoplastic signature' reflects ECM changes in human tumor datasets. The signature genes/proteins were used to define an enrichment score as previously reported (46) from gene expression values of TCGA Pan-Cancer normalized cohort, assessed at both the tumor type and the molecular subtype level.

Results showed a wide difference in enrichment scores, with tumors from the blood [acute myeloid leukemia (AML)] expressing the lowest scores and metaplastic/squamous tumors [breast (BRCA), head and neck (HNSC), pancreatic (PAAD) cancers and sarcoma (SARC)] the highest (Figure 4A). We confirmed these differences at the tumor subtype level, where mesenchymal and immunoreactive subtypes, characterized by large ECM deposition and tissue activation phenomena, topped the landscape of signature enrichment levels. These results are in line with the composition of the signature, that features mostly genes/proteins associated with the ECM, its organization, and TGFβ signaling. The enrichment scores were then divided into quartiles by tumor type and patients in the 1st and 4th quartiles ("low" and "high", respectively) were compared for

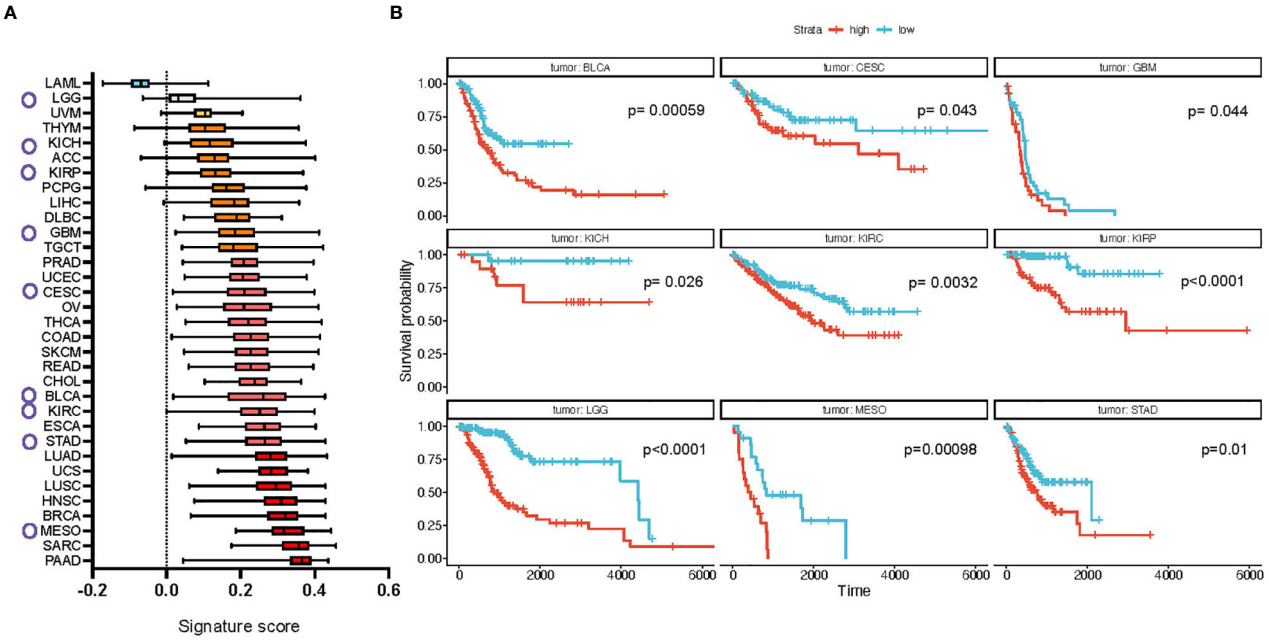

FIGURE 4
Full CAF FDM signature is enriched in multiple cancer types in human and is prognostic of cancer patients' survival. **(A)** Difference in the signature expression score (box plots summarize median with min and max). Circles mark cancer types for which high expression of the signature defines poor survival, shown in b (based on TGCA dataset). **(B)** Kaplan-Meier plots of cancer types which show significantly different probability of patients' survival based on the signature expression. LAML, Acute Myeloid Leukemia; ACC, Adrenocortical carcinoma; BLCA, Bladder Urothelial Carcinoma; LGG, Brain Lower Grade Glioma; BRCA, Breast invasive carcinoma; CESC, Cervical squamous cell carcinoma and endocervical adenocarcinoma; CHOL, Cholangiocarcinoma; COAD, Colon adenocarcinoma; ESCA, Esophageal carcinoma; GBM, Glioblastoma multiforme; HNSC, Head and Neck squamous cell carcinoma; KICH, Kidney Chromophobe; KIRC, Kidney renal clear cell carcinoma; KIRP, Kidney renal papillary cell carcinoma; LIHC, Liver hepatocellular carcinoma; LUAD, Lung adenocarcinoma; LUSC, Lung squamous cell carcinoma; DLBC, Lymphoid Neoplasm Diffuse Large B-cell Lymphoma; MESO, Mesothelioma; OV, Ovarian serous cystadenocarcinoma; PAAD, Pancreatic adenocarcinoma; PCPG, Pheochromocytoma and Paraganglioma; PRAD, Prostate adenocarcinoma; READ, Rectum adenocarcinoma; SARC, Sarcoma; SKCM, Skin Cutaneous Melanoma; STAD, Stomach adenocarcinoma; TGCT, Testicular Germ Cell Tumors; THYM, Thymoma; THCA, Thyroid carcinoma; UCS, Uterine Carcinosarcoma; UCEC, Uterine Corpus Endometrial Carcinoma; UVM, Uveal Melanoma.

overall survival (OS). Results show significant monovariate differences in survival for 9 tumor types (BLCA, CESC, GBM, LGG, KICH, KIRC, KIRP, MESO, STAD (see Figure 4 legend for abbreviations, all p-values < 0.05; Figure 4B), with uveal melanoma (UVM) also being very close to significance (p-value = 0.052) (Supplementary Figure 5). We confirmed that a higher level of signature score in these cancer types positively correlates with the abundance of fibroblasts in the samples (Supplementary Figure 6). Interestingly, in all cases, a higher signature expression was associated with poorer survival and different tumor types from the same organ or system showed similar results (see, e.g., all kidney neoplasms (KICH, KIRC and KIRP) and bladder cancer (BLCA), lung (LUAD, LUSC, MESO), ovarian and cervical cancers (OVCA and CESC), and high- and low-grade gliomas (LGG and GBM). We performed the same analysis for the short signature which showed a relative increase in expression score for most of the cancer types, prominent for ovarian (OV) and colon (COAD) cancers (Supplementary Figure 7A). Survival analysis in addition showed a significant association of the signature expression with poor survival in pancreatic (PAAD) and lung (LUAD) adenocarcinomas (Supplementary Figure 7B).

Compared to 100 random signatures from the rest of the matrisome, which is the largest gene "origin" (ontology) in the signature, we observed that both the 'short' and 'long' signatures obtain much larger scores and much smaller dispersions, strongly suggesting a coordinated and non-random expression of the genes the signatures span across the whole cohort (Supplementary Figures 9A, B). This is also reflected in principal component analysis (PCA) overlaid with binned bidimensional probabilities, showing a clear separation between signature and non-signature genes (Supplementary Figure 9C). More importantly, we have performed Cox Proportional Hazard (CoxPH) analysis for overall survival (OS), disease-specific survival (DSS) and progression-free interval (PFI) evaluating signature scores together with age, sex and tumor type and found that - in all cases - the signature is an independent estimator of survival, both in the pan-cancer cohort and in the tumors previously identified *via* Kaplan-Meier OS analysis (Supplementary Figure 10).

4 Discussion

Desmoplastic reactions at both the primary and secondary site in multiple cancers are a hallmark of disease progression (47, 48), and are characterized by an increased deposition of ECM, altered ECM structure and composition as well as changes in the biophysical properties of the surrounding stroma. These alterations are often associated with poor drug response/delivery and poorer clinical

outcome (49, 50). However, tools to model and study the effect of the native ECM on cancer progression are still lacking. Here, we utilize FDMs generated by NFs and CAFs, and validate FDM relevance to the *in vivo* situation of desmoplastic cancer. Several studies profiled tumors by single-cell RNA sequencing, showing that CAFs are heterogeneous in both breast and pancreatic tumors (51). Importantly, most of those subtypes are still active producers of the ECM (based on Col1 and Col3). Temporally resolved proteomic studies, which more reliably represent deposited ECM over the course of disease progression, are still very limited (20, 52). Our approach of FDM proteomics can be further applied to fill this gap in exploring ECM deposition by the CAF subtypes.

To generate native ECM in a short timeframe *in vitro*, we used immortalized NFs and CAFs densely seeded on cross-linked gelatin-coated plastic. Removal of fibroblasts results in a layer of the ECM with unique composition, structure, and mechanical properties. Our study reveals that CAF FDM structure is much thinner and denser, mechanically stiffer than NF. These parameters potentially depend on both an increase in the crosslinking enzymes (e.g. LOXL2), packaging collagen fibers core ECM components (FACIT collagens - ColXIV, ColXII), and higher contractility of CAFs (23). CAF FDM top compositional changes match desmoplastic PDAC alterations at the primary and metastatic site and they form a gene signature relevant for identifying desmoplastic state among a broad spectrum of human tumors. Our analysis shows that sarcomas, head and neck, mesothelioma, and lung cancers (ductal carcinoma, adenocarcinoma) also possess pronounced desmoplastic ECM changes at the transcriptional level. For some cancer types, stratification based on our signature is prognostic of the overall survival. Surprisingly, those are also 'non-desmoplastic' cancer types with a low signature score (e.g. brain cancers (LGG, GBM) and kidney cancers (KICH, KIRP), suggesting that we potentially lack understanding of which role matrisome plays in their progression. Further experiments, such as evaluation of the non-desmoplastic cancer type cell proliferation on desmoplastic matrices, will shed light on the impact of these stromal changes on either tumor growth, or other parameters driving cancer progression. Interestingly, an earlier study uncovered epigenetic regulation of YAP/TAZ pathway by translocation of JMJD1 histone demethylase in the nucleus on stiffer CAF matrices as a mechanism giving cancer cells a proliferative advantage (53). Other studies so far mainly focused on comparing cancer cell migration on NF versus CAF fibroblast matrices, for instance showing more alignment of the ECM fibers by human prostate and pancreatic CAFs leading to directional migration of cancer cells (54, 55). In this study we did not observe more alignment by CAF indicating tissue or species-specific differences.

We foresee that desmoplastic signature can be a useful tool for identifying patients who could benefit from anti-fibrotic treatment. As some of those targeted treatments were not successful (56), it is critical to consider that pro-fibrotic changes are triggered early on (e.g. in case of PanIN stage in our study), therefore, the stage of disease can be a critical factor for starting the treatment. Further, we need to understand if these ECM components are independent or interdependent in creating desmoplastic response and how preventing their build up can be tuned more effectively, potentially by co-targeting an immune response and CAF heterogeneity. We acknowledge however, that there are limitations when using the TCGA to look at the power of our signature in defining patient outcomes. While different parameters regarding survival are available, there is little information regarding the treatment of these patients and their response, which is a crucial parameter affecting clinical outcome. However, when evaluating signature scores together with age, sex, and tumor type we found that the signature is an independent estimator of survival.

Our datasets also highlight single proteins such as collagen XII, a fibril-associated collagen with interrupted triple helices (FACIT) binding to the surface of collagen fibers and promoting their bundling and compaction. Its presence in the stroma was shown to correlate with epithelial tension mediated by STAT3 signaling in PDAC mouse models (57). Collagen XII was also found to be a prognostic marker of poor patient outcome in colorectal cancer, associated with the myofibroblastic invasive front and liver metastases (58, 59). In breast cancer, its knockdown in CAFs in a cancer cell co-implantation model showed that collagen XII ECM compaction contributes to the metastatic dissemination (52). However, biochemical and structural role of collagen XII, as well as potential therapeutic targeting, remain undefined. This stresses the need for further elucidation of the mechanistic role of ECM components in desmoplasia, and in driving primary tumor progression to metastasis.

5 Conclusions

In summary, our study highlights a desmoplastic signature of 36 ECM genes, the expression of which is prognostic of patient survival in 9 cancers. The proteomic datasets presented here can be further explored to investigate the role of specific ECM proteins in cancer progression, and their potential as therapeutic targets. Our study shows that CAFs can be used *in vitro* to generate complex desmoplastic ECM substrates, and that the difference between 'normal' and desmoplastic ECM matrices stimulates cancer cell proliferation.

Data availability statement

The data presented in the study are deposited in the PRIDE repository, accession number: PXD042342.

Ethics statement

The animal study was reviewed and approved by Danish Inspectorate for Animal Experimentation (permission number #2017-15- 0201-01265).

Author contributions

Project was conceived by JE, AJ, EH. *In vitro* assays were performed by MR, AJ, EH, FK, DG. Mass spectrometry was

performed by MR, ES and analyzed by EH and MR. KPC mice were bred and maintained by MR and LA. *In vivo* work and sample collection were performed by AM-G, SN, KZ. Imaging and FDM image-based characterization was performed by MR. FDM stiffness measurements were performed by LF and HC-S. Western blotting was performed by JS. Signature score and survival analysis in patient datasets were performed by VI. Manuscript was written by AJ, MR, RR, and JE. Project was supervised by RR and JE. All authors contributed to the article and approved the submitted version.

Funding

This work was supported by a PhD fellowship from the Lundbeck Foundation (MR: R286-2018-621), the Danish Council for Independent Research YDUN grant (AJ; 1084181001), the European Research Council (MR, AJ, EH, JS, AM-G, SN, RR, JE: ERC-2015-CoG-682881-MATRICAN), the Danish Cancer Society (SN: R167-A10618; EH: R204-A12445; RR: R204-A12454), the European Molecular Biology Organization (EH: ALTF 922-2016), a Novo Nordisk Foundation Hallas Møller Stipend (JE), and the German Cancer Aid (RR). LF and HC-S acknowledge funding from the Bavarian State Ministry for Science and Art through the Research Focus "Angewandte Photonik" and the Bavarian Academic Forum (BayWISS)—Doctoral Consortium "Health Research". The Cancer Society of Finland (VI: 63-6445) (VI). The funder was not involved in the study design, collection, analysis, interpretation of data, the writing of this article or the decision to submit it for publication.

Acknowledgments

We thank core facilities of the University of Copenhagen, especially Elin J Pietras (High Throughput Screening (HTS) Facility) and Nynne Christensen (the Center for Advanced Bioimaging (CAB)) for training and assistance with the imaging. We thank all members of the Erler group for project discussions. We are grateful to Linbu Liao and Kyoung Jae Won for the bioinformatic support. We thank Manuel Koch and Raimund Wagener (University of Cologne, Germany) for providing the antibodies. We thank Jennifer P.Morton and Owen J Sansom (The Beatson Institute for Cancer Research, UK) for providing the Pdx-Cre+ and KPC mice. We would like to mention that the scheme in within Figure 3 was created with BioRender.com.

Conflict of interest

The authors declare that the research was conducted in the absence of any commercial or financial relationships that could be construed as a potential conflict of interest.

Publisher's note

Supplementary material

The Supplementary Material for this article can be found online at: https://www.frontiersin.org/articles/10.3389/fimmu.2023.1154528/full#supplementary-material

References

1. Cox TR, Erler JT. Remodeling and homeostasis of the extracellular matrix: implications for fibrotic diseases and cancer. *DMM Dis Models Mech* (2011) 4:165–78. doi: 10.1242/dmm.004077

2. Winkler J, Abisoye-Ogunniyan A, Metcalf KJ, Werb Z. Concepts of extracellular matrix remodelling in tumour progression and metastasis. *Nat Commun* (2020) 11:1–19. doi: 10.1038/s41467-020-18794-x

3. Pandol S, Edderkaoui M, Gukovsky I, Lugea A, Gukovskaya A. Desmoplasia of pancreatic ductal adenocarcinoma. *Clin Gastroenterol Hepatol* (2009) 7:44–47. doi: 10.1016/J.CGH.2009.07.039

4. Coussens LM, Werb Z. Inflammation and cancer. *Nature* (2002) 420:860–7. doi: 10.1038/NATURE01322

5. Deyell M, Garris CS, Laughney AM. Cancer metastasis as a non-healing wound. *Br J Cancer* (2021) 124:1491–502. doi: 10.1038/s41416-021-01309-w

6. Yen TW, Aardal NP, Bronner MP, Thorning DR, Savard CE, Lee SP, et al. Myofibroblasts are responsible for the desmoplastic reaction surrounding human pancreatic carcinomas. *Surgery* (2002) 131:129–34. doi: 10.1067/MSY.2002.119192

7. Ilic M, Ilic I. Epidemiology of pancreatic cancer. *World J Gastroenterol* (2016) 22:9694–705. doi: 10.3748/WJG.V22.I44.9694

8. Soysal SD, Tzankov A, Muenst SE. Role of the tumor microenvironment in breast cancer. *Pathobiology* (2015) 82:142–52. doi: 10.1159/000430499

9. Weniger M, Honselmann KC, Liss AS. The extracellular matrix and pancreatic cancer: a complex relationship. *Cancers (Basel)* (2018) 10. doi: 10.3390/cancers10090316

10. Lee JY, Chang JK, Dominguez AA, Lee H-P, Nam S, Chang J, et al. YAP-independent mechanotransduction drives breast cancer progression. *Nat Commun* (2019) 10:1848. doi: 10.1038/s41467-019-09755-0

11. Conklin MW, Eickhoff JC, Riching KM, Pehlke CA, Eliceiri KW, Provenzano PP, et al. Aligned collagen is a prognostic signature for survival in human breast carcinoma. *Am J Pathol* (2011) 178:1221. doi: 10.1016/J.AJPATH.2010.11.076

12. Drifka CR, Loeffler AG, Mathewson K, Keikhosravi A, Eickhoff JC, Liu Y, et al. Highly aligned stromal collagen is a negative prognostic factor following pancreatic ductal adenocarcinoma resection. *Oncotarget* (2016) 7:76197–213. doi: 10.18632/ONCOTARGET.12772

13. Provenzano PP, Inman DR, Eliceiri KW, Knittel JG, Yan L, Rueden CT, et al. Collagen density promotes mammary tumor initiation and progression. *BMC Med* (2008) 6:1–15. doi: 10.1186/1741-7015-6-11

14. Levental KR, Yu H, Kass L, Lakins JN, Egeblad M, Erler JT, et al. Matrix crosslinking forces tumor progression by enhancing integrin signaling. *Cell* (2009) 139:891–906. doi: 10.1016/j.cell.2009.10.027

15. Egeblad M, Rasch MG, Weaver VM. Dynamic interplay between the collagen scaffold and tumor evolution. *Curr Opin Cell Biol* (2010) 22:697–706. doi: 10.1016/J.CEB.2010.08.015

16. Hamidi H, Ivaska J. Every step of the way: integrins in cancer progression and metastasis. *Nat Rev Cancer* (2018) 18:533–48. doi: 10.1038/S41568-018-0038-Z

17. Chen W, Park S, Patel C, Bai Y, Henary K, Raha A, et al. The migration of metastatic breast cancer cells is regulated by matrix stiffness *via* YAP signalling. (2017). doi: 10.1016/j.heliyon.2021.e06252

18. Shen J, Cao B, Wang Y, Ma C, Zeng Z, Liu L, et al. Hippo component YAP promotes focal adhesion and tumour aggressiveness *via* transcriptionally activating THBS1/FAK signalling in breast cancer. *J Exp Clin Cancer Res* (2018) 37. doi: 10.1186/S13046-018-0850-Z

19. Fattet L, Jung HY, Matsumoto MW, Aubol BE, Kumar A, Adams JA, et al. Matrix rigidity controls epithelial-mesenchymal plasticity and tumor metastasis *via* a mechanoresponsive EPHA2/LYN complex. *Dev Cell* (2020) 54:302–316.e7. doi: 10.1016/J.DEVCEL.2020.05.031

20. Tian C, Clauser KR, Öhlund D, Rickelt S, Huang Y, Gupta M, et al. Proteomic analyses of ECM during pancreatic ductal adenocarcinoma progression reveal different contributions by tumor and stromal cells. *Proc Natl Acad Sci* (2019) 116:19609–18. doi: 10.1073/pnas.1908626116

21. Santi A, Kugeratski FG, Zanivan S. Cancer associated fibroblasts: the architects of stroma remodeling. *Proteomics* (2018) 18. doi: 10.1002/PMIC.201700167

22. von Ahrens D, Bhagat TD, Nagrath D, Maitra A, Verma A. The role of stromal cancer-associated fibroblasts in pancreatic cancer. *J Hematol Oncol* (2017) 10. doi: 10.1186/S13045-017-0448-5

23. Calvo F, Ege N, Grande-Garcia A, Hooper S, Jenkins RP, Chaudhry SI, et al. Mechanotransduction and YAP-dependent matrix remodelling is required for the generation and maintenance of cancer-associated fibroblasts. *Nat Cell Biol* (2013) 15:637–46. doi: 10.1038/ncb2756

24. Wu F, Yang J, Liu J, Wang Y, Mu J, Zeng Q, et al. Signaling pathways in cancer-associated fibroblasts and targeted therapy for cancer. *Signal Transduction Targeted Ther* (2021) 6:1–35. doi: 10.1038/s41392-021-00641-0

25. Kaukonen R, Jacquemet G, Hamidi H, Ivaska J. Cell-derived matrices for studying cell proliferation and directional migration in a complex 3D microenvironment. *Nat Protoc* (2017) 12:2376–90. doi: 10.1038/nprot.2017.107

26. Jensen ARD, Horton ER, Blicher LH, Pietras EJ, Steinhauer C, Reuten R, et al. Organ-specific, fibroblast-derived matrix as a tool for studying breast cancer metastasis. *Cancers* (2021) 13:3331. doi: 10.3390/CANCERS13133331

27. Boj SF, Hwang C, Baker LA, Chio IIC, Engle DD, Corbo V, et al. Organoid models of human and mouse ductal pancreatic cancer. *Cell* (2015) 160:324–38. doi: 10.1016/j.cell.2014.12.021

28. Cox TR, Bird D, Baker A-M, Barker HE, Ho MW-Y, Lang G, Erler JT. LOX-mediated collagen crosslinking is responsible for fibrosis-enhanced metastasis. *Cancer Res* (2013) 73:1721. doi: 10.1158/0008-5472.CAN-12-2233

29. Franco-Barraza J, Beacham DA, Amatangelo MD, Cukierman E. Preparation of extracellular matrices produced by cultured and primary fibroblasts. *Curr Protoc Cell Biol* (2016) 71:10. doi: 10.1002/CPCB.2

30. Franco-Barraza J, Raghavan KS, Luong T, Cukierman E. Engineering clinically-relevant human fibroblastic cell-derived extracellular matrices. *Methods Cell Biol* (2020) 156:109–60. doi: 10.1016/BS.MCB.2019.11.014

31. Godeau AL, Delanoë-Ayari H, Riveline D. Generation of fluorescent cell-derived-matrix to study 3D cell migration. *Methods Cell Biol* (2020) 156:185–203. doi: 10.1016/BS.MCB.2019.11.013

32. Hingorani SR, Wang L, Multani AS, Combs C, Deramaudt TB, Hruban RH, et al. Trp53R172H and KrasG12D cooperate to promote chromosomal instability and widely metastatic pancreatic ductal adenocarcinoma in mice. *Cancer Cell* (2005) 7:469–83. doi: 10.1016/j.ccr.2005.04.023

33. Mayorca-Guiliani AE, Willacy O, Madsen CD, Rafaeva M, Elisabeth Heumüller S, Bock F, et al. Decellularization and antibody staining of mouse tissues to map native extracellular matrix structures in 3D. *Nat Protoc* (2019) 14:3395–425. doi: 10.1038/S41596-019-0225-8

34. Nielsen SR, Quaranta V, Linford A, Emeagi P, Rainer C, Santos A, et al. Macrophage-secreted granulin supports pancreatic cancer metastasis by inducing liver fibrosis. *Nat Cell Biol* (2016) 18:549–60. doi: 10.1038/ncb3340

35. Kulak NA, Pichler G, Paron I, Nagaraj N, Mann M. Minimal, encapsulated proteomic-sample processing applied to copy-number estimation in eukaryotic cells. *Nat Methods* (2014) 11:319–24. doi: 10.1038/nmeth.2834

36. Naba A, Clauser KR, Hoersch S, Liu H, Carr SA, Hynes RO. The matrisome: in silico definition and *in vivo* characterization by proteomics of normal and tumor extracellular matrices. *Mol Cell Proteomics* (2012) 11. doi: 10.1074/mcp.M111.014647

37. Wershof E, Park D, Jenkins RP, Barry DJ, Sahai E, Bates PA. Matrix feedback enables diverse higher-order patterning of the extracellular matrix. *PloS Comput Biol* (2019) 15:e1007251. doi: 10.1371/journal.pcbi.1007251

38. Butt H-J, Jaschke M. Calculation of thermal noise in atomic force microscopy. *Nanotechnology* (1995) 6:1. doi: 10.1088/0957-4484/6/1/001

39. Aper SJA, van Spreeuwel ACC, van Turnhout MC, van der Linden AJ, Pieters PA, van der Zon NLL. Colorful protein-based fluorescent probes for collagen imaging. *PLoS One* (2014) 9:e114983. doi: 10.1371/journal.pone.0114983

40. Warren A, Chen Y, Jones A, Shibue T, Hahn WC, Boehm JS, et al. Global computational alignment of tumor and cell line transcriptional profiles. *Nat Commun* (2021) 12:1–12. doi: 10.1038/s41467-020-20294-x

41. Foroutan M, Bhuva DD, Lyu R, Horan K, Cursons J, Davis MJ. Single sample scoring of molecular phenotypes. *BMC Bioinf* (2018) 19:1–10. doi: 10.1186/S12859-018-2435-4/FIGURES/2

42. Naba A, Clauser KR, Ding H, Whittaker CA, Carr SA, Hynes RO. The extracellular matrix: tools and insights for the "omics" era. *Matrix Biol* (2016) 49:10–24. doi: 10.1016/J.MATBIO.2015.06.003

43. Amatangelo MD, Bassi DE, Klein-Szanto AJP, Cukierman E. Stroma-derived three-dimensional matrices are necessary and sufficient to promote desmoplastic differentiation of normal fibroblasts. *Am J Pathol* (2005) 167:475–88. doi: 10.1016/S0002-9440(10)62991-4

44. Lee JW, Komar CA, Bengsch F, Graham K, Beatty GL. Genetically engineered mouse models of pancreatic cancer: the KPC model (LSL-KrasG12D/+;LSL-Trp53R172H/+;Pdx-1-Cre), its variants, and their application in immuno-oncology drug discovery. *Curr Protoc Pharmacol* (2016) 2016:14. doi: 10.1002/cpph.2

45. Mayorca-Guiliani AE, Madsen CD, Cox TR, Horton ER, Venning FA, Erler JT. ISDoT: *in situ* decellularization of tissues for high-resolution imaging and proteomic analysis of native extracellular matrix. *Nat Med* (2017) 23:890–8. doi: 10.1038/nm.4352

46. Bhuva DD, Cursons J, Davis MJ. Stable gene expression for normalisation and single-sample scoring. *Nucleic Acids Res* (2020) 48:e113–3. doi: 10.1093/NAR/GKAA802

47. Rafaeva M, Erler JT. Framing cancer progression: influence of the organ- and tumour-specific matrisome. *FEBS J* (2020) 287. doi: 10.1111/febs.15223

48. Cox TR. The matrix in cancer. *Nat Rev Cancer* (2021) 21:217–38. doi: 10.1038/S41568-020-00329-7

49. Xu S, Xu H, Wang W, Li S, Li H, Li T, et al. The role of collagen in cancer: from bench to bedside. *J Trans Med* (2019) 17:1–22. doi: 10.1186/S12967-019-2058-1

50. Piersma B, Hayward MK, Weaver VM. Fibrosis and cancer: a strained relationship. *Biochim Biophys Acta Rev Cancer* (2020) 1873. doi: 10.1016/J.BBCAN.2020.188356

51. Sebastian A, Hum NR, Martin KA, Gilmore SF, Peran I, Byers SW, et al. Single-cell transcriptomic analysis of tumor-derived fibroblasts and normal tissue-resident fibroblasts reveals fibroblast heterogeneity in breast cancer. *Cancers* (2020) 12:1307. doi: 10.3390/CANCERS12051307

52. Papanicolaou M, Parker AL, Yam M, Filipe EC, Wu SZ, Chitty JL, et al. Temporal profiling of the breast tumour microenvironment reveals collagen XII as a driver of metastasis. *Nat Commun* (2022) 13. doi: 10.1038/S41467-022-32255-7

53. Kaukonen R, Mai A, Georgiadou M, Saari M, De Franceschi N, Betz T, et al. Normal stroma suppresses cancer cell proliferation *via* mechanosensitive regulation of JMJD1a-mediated transcription. *Nat Commun* (2016) 7:12237. doi: 10.1038/ncomms12237

54. Erdogan B, Ao M, White LM, Means AL, Brewer BM, Yang L, et al. Cancer-associated fibroblasts promote directional cancer cell migration by aligning fibronectin. *J Cell Biol* (2017) 216:3799. doi: 10.1083/JCB.201704053

55. Lee H-O, Mullins SR, Franco-Barraza J, Valianou M, Cukierman E, Cheng JD. FAP-overexpressing fibroblasts produce an extracellular matrix that enhances invasive velocity and directionality of pancreatic cancer cells. *BMC Cancer* (2011) 11:1–13. doi: 10.1186/1471-2407-11-245

56. Hauge A, Rofstad EK. Antifibrotic therapy to normalize the tumor microenvironment. *J Trans Med* (2020) 18:1–11. doi: 10.1186/S12967-020-02376-Y

57. Laklai H, Miroshnikova YA, Pickup MW, Collisson EA, Kim GE, Barrett AS, et al. Genotype tunes pancreatic ductal adenocarcinoma tissue tension to induce matricellular fibrosis and tumor progression. *Nat Med* (2016) 22:497–505. doi: 10.1038/nm.4082

58. Karagiannis GS, Petraki C, Prassas I, Saraon P, Musrap N, Dimitromanolakis A, et al. Proteomic signatures of the desmoplastic invasion front reveal collagen type XII as a marker of myofibroblastic differentiation during colorectal cancer metastasis. *Oncotarget* (2012) 3:267–85. doi: 10.18632/oncotarget.451

59. van Huizen NA, Coebergh van den Braak RRJ, Doukas M, Dekker LJM, IJzermans JNM, Luider TM. Up-regulation of collagen proteins in colorectal liver metastasis compared with normal liver tissue. *J Biol Chem* (2019) 294:281–9. doi: 10.1074/JBC.RA118.005087

Frontiers in Immunology

Explores novel approaches and diagnoses to treat immune disorders.

The official journal of the International Union of Immunological Societies (IUIS) and the most cited in its field, leading the way for research across basic, translational and clinical immunology.

Discover the latest Research Topics

See more →

Frontiers

Avenue du Tribunal-Fédéral 34
1005 Lausanne, Switzerland
frontiersin.org

Contact us

+41 (0)21 510 17 00
frontiersin.org/about/contact